Electrocatalysing CO_2 Conversion to Value-added Products using Metal Oxides and Metal-Salen Complexes

Thesis Submitted in Partial Fulfilment of the Requirements
for the Award of the Degree of

DOCTOR OF PHILOSOPHY

by

PAULOMI BOSE

Centre for the Environment
Indian Institute of Technology Guwahati
Assam-781039, INDIA

April 2021

भारतीय प्रौद्योगिकी संस्थान गुवाहाटी
Indian Institute of Technology Guwahati

This thesis is dedicated to my beloved parents and my dear husband who have always been a source of motivation and stamina to pursue my higher studies and face the prospects of life with a great zeal and fervor

भारतीय प्रौद्योगिकी संस्थान गुवाहाटी
Indian Institute of Technology Guwahati

Centre for the Environment
Indian Institute of Technology Guwahati
Guwahati -781 039
Assam, India

DECLARATION

I, hereby declare that the content embodied in this thesis entitled "**Electrocatalysing CO_2 Conversion to Value-added Products using Metal Oxides and Metal-Salen Complexes**" is the result of investigations carried out by me at the in the Indian Institute of Technology Guwahati, Guwahati – 781 039, Assam, under the supervision of Prof. Chandan Mukherjee, Department of Chemistry, IIT Guwahati, and Prof. Animes K Golder, Department of Chemical Engineering, IIT Guwahati, and is submitted to the Indian Institute of Technology Guwahati, for the award of the degree of Doctor of Philosophy.

In keeping with the general practice of reporting scientific observations, due acknowledgements have been made wherever the work described is based on the findings of other investigators.

Paulomi Bose
Roll No. 146152005
Centre for the Environment
Indian Institute of Technology Guwahati

भारतीय प्रौद्योगिकी संस्थान गुवाहाटी
Indian Institute of Technology Guwahati

Centre for the Environment
Indian Institute of Technology Guwahati
Guwahati -781 039
Assam, India

CERTIFICATE

This is to certify that the thesis entitled "**Electrocatalysing CO_2 Conversion to Value-added Products using Metal Oxides and Metal-Salen Complexes**", being submitted by **Ms. Paulomi Bose**, to the Indian Institute of Technology Guwahati, India, for the degree of Doctor of Philosophy, has been carried out by her under our guidance and supervision and this work has not been submitted elsewhere for the award of any degree.

Dr. Chandan Mukherjee
(Thesis Supervisor)
Professor
Department of Chemistry
Indian Institute of Technology Guwahati
Guwahati-781 039
Assam, India

Dr. Animes K Golder
(Thesis Supervsior)
Professor
Department of Chemical Engineering
Indian Institute of Technology Guwahati
Guwahati- 781 039
Assam, India

भारतीय प्रौद्योगिकी संस्थान गुवाहाटी
Indian Institute of Technology Guwahati

Acknowledgement

Life is like a hilly terrain where climbing up is tough and falling down is quite easy. It is not only the hard work that you put into but also the guidance and backing of elders & well-wishers, that can turn impossible into possible. As a doctoral student, it was a dream come true when I joined IIT Guwahati. In all these years that I have spent at IITG, it has shaped me what I am today. It was nearly impossible to accomplish my doctoral studies without the help and inspiration extended by a lot of personalities.

Words cannot always do the justification of translating my feelings into reality but it can be sensed when I execute my deepest gratitude and profound respect for my supervisors Prof. Chandan Mukherjee and Prof. Animes Kumar Golder for their erudite supervision, thoughtful planning, unmatchable co-operation and plenteous inspiration during the course of my PhD studies. Their stupendous ability in planning the project and the astounding reasoning capabilities made me fortunate enough to work on a completely unfamiliar area of research. I shall appreciate their level of tolerance to consistently rectify any kind of errors with astute discussions and debates during my research work and propelled me in the right direction.

I feel honoured to express my gratitude to my doctoral committee members, Prof. Subhendu Sekhar Bag, Prof. Chandan Das, and Prof. Lal Mohan Kundu, for their interest in my work and productive inputs from time to time that helped me a lot to improve my quality of research. I must thank Prof. Utpal Bora, Head of the Centre for the Environment, for his constant encouragement, advice till date and all research facilities which helped me to keep moving on and accomplish the work in appropriate time. I also take the opportunity to thank all the previous Heads of Centre for the Environment Prof. Mihir Kumar Purkait, Prof. Gopal Das and Prof. Vikash Kumar Dubey for their help and support during my PhD tenure. I am deeply indebted to Prof. Gopal Das, Head of the Chemistry Department (IITG), and Prof. Anugrah Singh, Head of the Chemical Engineering Department (IITG), for allowing me to avail various facilities in their respective departments.

My sincere thanks go to all the official and technical staffs of the Department of Chemical Engineering and Department of Chemistry of IIT Guwahati for allowing me to access all the Laboratory, and research facilities. I am also thankful to all the technical and non-technical staff of Centre for the Environment (Dr. Deepmoni Deka, Mr. Partha P. Bakal, Mr. Kaustubh Rakshit, Mr. Rajiv Gogoi and Mr. Mridul Das) for helping me in all possible ways and made themselves available when in need. Help extended by Central Instruments Facility of IIT Guwahati in providing me with some of the world-class instrumentation facilities is deeply accredited without which this work would not have been possible.

I sincerely thank my lab seniors, Dr. Manas Kumar Mondal, Dr Vedika Pukhan, Dr. Venkatanarasimha Rao Chelli, and Dr. Raj Kumar Das for sharing their experiences and helping in various lab activities and gruelling discussions which helped a lot in better understanding of the subject. I would like to express my special thanks and immense gratitude to my senior Dr. Surya Singh who always supported me in my research work and guided me through the tough times. In particular, profound gratitude must be expressed to Dr. Papu Kumar Naik, Dr. Visva Bharati Barua, Dr. D Narendra Naik, Dr. Pallab das and Dr. Basudhrity Banerjee for their well wishes and their constant support in my journey in IIT Guwahati. A special thanks to Dr. Neha Singh, Mr. Rishabh Saxena, Ms. Ila Verma,

Ms. Jinat Aktar. Ms. Nibedita Ghosh and Mr. Jayakrishnan for their constant love, support and guidance for all these years. My lab mates (Mr. Prasenjit Sarkar, Ms. Riya Mallik, Ms. Sumana Nath, Ms. Devipriya Gogoi, Mr. Ravi, Mr. Chandra Bhan, Mr. Joy Patar, Mr. Anirban Chowdhury) and all the juniors of Centre for the Environment deserves a special mention here for being nice, loving, and understanding friends. The most important "chai times" (tea breaks) with them made me refreshed and boosted my efficiency in carrying out my research.

This long journey would not have completed without the blessings, endless love, and support from my family. I dedicate my every accomplishment to my father (Shri Tapan Kumar Bose), my mother (Smt. Jhanjha Bose) and my in laws. Their constant blessings, support and sacrifice for me every single day made my life cheerful. My uncle Dr. Anupam Mitra needs a special mention as he was the one who instilled in me the zeal to go for my PhD. I feel the luckiest person for having such a lovely family.

A special section in my acknowledgement must be dedicated exclusively for my darling husband (Mr. Smruti Ranjan Dash) He has always inspired me with his way to approach any challenging circumstances, and surely, for making every small occasion so special for me. I especially thank him for tolerating me even in times of severe frustration, and for being my most supportive friend. Without your support, I am damn sure that it would have been impossible for me to complete my PhD.

Above all, I thank the Almighty God, for bestowing me with the wonderful life and appropriate environment in which I could flourish and enhance my vistas of learning. I thank Maa Kamakhya, Lord Jagannath and Maa Durga for giving me the power to rise whenever I tumble. I thank almighty for blessing me with a lovely family and a bunch of well-wishers and friends.

Finally, I would like to thank our frontline health workers and policy makers taking important decisions in pursuit of making our life calmer during this global pandemic of CoVID-19.

Paulomi Bose
Centre for the Environment
IIT Guwahati
March 2021

Abstract

Carbon dioxide (CO_2) is essential for the survival of living organisms. It exists as a tiny fraction of the total carbon inventory in the atmosphere and the continuous industrial development primarily has increased the level of CO_2 in the atmospheric gases. CO_2 is increased by 43.3% from 280 to 416.3 ppm over the past 60 years, which is about 66 ppm higher than the safety limit. This rise in CO_2 causes an increase in global temperature by 1-2°C. With this context, this thesis focuses to look for a suitable technology to convert CO_2 into valuable products. Among all the CO_2 reduction processes, electrochemical reduction of CO_2 (ERC) is carried out either in aqueous or non-aqueous electrolytes saturated with CO_2 or directly using different metal and its derivatives as catalysts within a short span of reaction time. CO_2 can be converted into CO, acids, alcohols, hydrocarbons, etc. During the electrolysis, O_2 gas is also generated at the CE side, which can be trapped and utilized for further application. Thus in this thesis, we have focused on finding suitable catalysts for reducing CO_2 into valuable by-products. In particular, in the first part of the thesis, we have synthesized selected transition (Cu and Ni) and post-transition (Pb) metal oxides and checked their role in ERC. Then in the second part, salen metal complexes of the same metals were synthesized and compared their role with their corresponding metal oxides in ERC.

At the beginning of the thesis, the selected transition and post-transition metal oxides (Cu, Ni and Pb) were synthesized. The Cu_2O and NiO nanoparticles were synthesized in a chemical route and ascorbic acid was used as a reducing agent. In 100 mL distilled water in two beakers, 3 mM $Cu(NO_3)_2$ and 3 mM $NiCl_2 \cdot 6H_2O$ was prepared in which 3 mmol sodium citrate was added in each of them and prepared a solution. 250 mM of NaOH (20 mL) was added dropwise to each of them and kept on stirring for 15 mins. During that time a color change was observed (from blue to sky blue for Cu_2O and green to dark green for NiO) due to the formation of $Cu(OH)_2$ and $Ni(OH)_2$ respectively. After that, 150 mM of ascorbic acid was added dropwise in each of them until the color was changed to light yellow for Cu_2O and black for the NiO nanoparticle solution. After that, both the solution was washed with ethanol and water (1:1) for 3 times and the precipitate was collected. Cu_2O powder was used after drying in the oven. To prepare NiO nanopowder, the collected precipitate was then dried and then the powder was kept in a muffle furnace for 3 h at 300ºC and the final NiO powder (black in color) was prepared. The PbO nanocatalyst was prepared by mixing (100 mL) of 0.1 mol, $Pb(NO_3)_2$ (precursor) solution and 0.1 mol urea (stabilizing agent) and kept in a magnetic stirrer. In that mixture, 1M, NaOH (approx. 200 µL) was added to adjust the pH (9.5). After that, the solution was heated at 90ºC for 30 mins constantly in that magnetic stirrer (150 rpm). Gradually, the color of the solution was changed from a clear solution to white color. The solution was naturally cooled and washed and the precipitate was dried in the oven properly at 80ºC for 4 h. Then the dried filtrate (now pale yellowish color) was kept in a muffle furnace for 2 h at 400ºC to obtain the lead oxide nanopowder (brick red). After that, the nanocatalysts were characterized using XRD, FETEM, FTIR, and EDX techniques.

After that, the electrochemical analysis was conducted using the synthesized catalysts. A custom made H-type reactor was designed for electrochemical analysis throughout the experiments with a capacity of 150 mL of each electrolyte chamber. At first, the synthesized catalyst is coated on the graphite plate and used as the WE. The platinum wire was used as the CE and Ag/AgCl saturated with 3 M KCl was used as the reference electrode (RE). The electrolyte medium was 0.5 M aqueous $KHCO_3$ solution (each

catholyte and anolyte of 120 mL). N_2 gas (99.99% purity) was bubbled for 15 to 20 mins to purge out dissolved O_2 from the electrolyte solution before each experiment. CO_2 gas (99.99% purity) was then bubbled for ~ 45 mins with 10 mL.min^{-1} flow rate, which brought down pH of the solution from 8.5 to 7.0 with CO_2 saturation. The effects of fundamental electro-parameters were studied through linear sweep voltammetry, cyclic voltammetry and constant-potential analysis. The entire ERC reactions were conducted at 25°C and atmospheric pressure. The same experimental protocol was used throughout the doctoral work. The catalyst ink was prepared by dispersing the metal oxides electrocatalysts in isopropyl alcohol and then with Nafion binder and used as the (WE). The nanoparticle coated electrode was then fixed in our custom made H-type electrolyzer with CE and RE and at first LSV analysis was conducted.

In the case of Cu_2O and PbO, the current density is higher in the CO_2 environment than the inert gas environment which confirms the activity of the catalyst. In the case of NiO electrocatalyst, the observation was the exact opposite which confirms that the catalyst is not active in reducing CO_2 in our system. To confirm further constant potential analysis was conducted at five different electrode potentials with all the electrocatalysts. The Cu_2O electrocatalyst was active for the formation of HCOOH mainly with a trace amount of CH_3OH at the higher potential. 22% FE was found at −1.80 V vs. Ag/AgCl, for HCOOH production. Whereas, a very low amount of CH_3OH (3.5% of FE) was observed at −2.00 V vs. Ag/AgCl. In the constant-potential analysis also it was found that the NiO as electrocatalyst produced only H_2 and was inactive in able to reducing CO_2. The PbO electrocatalysts were able to produce HCOOH from CO_2 at five different electrode potential and a maximum of 23% FE was achieved. Using the three metal oxide catalysts, the hydrogen evolution (HER) is very high which affects the CO_2 reduction Thus, to increase the FE of value-added by-products and reduce the HER, the salen metal complexes (M = Cu, Ni and Pb) were synthesized and used in ERC.

In the next part, salen ligand metal complexes were synthesized. Salen ligand **1** ($H_2L^{NO_2}$) was synthesized from the reaction of 4-Nitro-*o*-phenylenediamine and salicylaldehyde in 1:6 ratios. After that, ligand $H_2L^{NO}{}_2$ (1.81 g; 5 mmol) was mixed with $Na_2S{\bullet}H_2O$ (0.78 g; 10 mmol) in EtOH (15 mL) solution to produce salen ligand **2** ($H_2L^{NH}{}_2$). Then salen ligand **2** was further mixed with $CuCl_2{\bullet}2H_2O$ and $NiCl_2{\bullet}6H_2O$ in CH_3CN solution in which triethylamine (0.2 mL) was added dropwise fixing in a magnetic stirrer. After 6 h of reaction at 30°C, the precipitate was filtered, washed and collected as the desired $Cu^{II}(L^{NH}{}_2)$ complex ($C_{20}H_{15}N_3O_2Cu$; **1**) and $Ni^{II}(L^{NH}{}_2)$ complex ($C_{20}H_{15}N_3O_2Ni$; **2**) respectively. Salen ligand **1** and **2** was further mixed with $Pb(NO_3)_2$ in 1:1 ratio in EtOH solution (9 mL) in presence of Et_3N to synthesize $Pb^{II}L^{NO}{}_2$ complex ($C_{20}H_{13}N_3O_4Pb$; **3**) and $Pb^{II}L^{NH}{}_2$ complex ($C_{20}H_{15}N_3O_2Pb$; **4**) respectively. Then the metal complexes were characterized using FTIR, NMR, HR-MS, C, H and N analysis. After that, the metal complexes were used as electrocatalysts in electrocatalysing CO_2 conversion process in our system.

Complex **1** was surface-coated over the graphite plate in an H-type electrolyzer. Formic acid (21.20 µmol/FE 2.14%) was detected as the sole product at −1.20 V. In addition to the production of formic acid (28.5 µmol; FE of 2%), C_2 products; acetic acid (16.70 µmol; FE 5.96%) and acetaldehyde (13.9 µmol; FE 6.20%) formed at −1.40 V. The five different CO_2-reduced products; acetic acid, formic acid, methanol, ethanol and acetaldehyde were detected at E_{cat} = −1.60 V. A maximum amount of 36% FE was achieved at −1.80 V vs. Ag/AgCl for 60 mins of reaction (Fig. 2). The production of HCOOH was 64 µmol after 60 mins with 4.5% FE at −1.80 V. The acetic acid formation was 39 µmol

(FE 11.14%) at 60 mins of ERC. The production of formic and acetic acid was notably higher than methanol, ethanol, and acetaldehyde. Methanol/ethanol/acetaldehyde production was reached to 26/18/20 after 60 mins at this potential. The corresponding FE was 5.50/7.70/7.10% after 60 mins, respectively. The cumulative production was 112 μmol (FE 27.92%), 167 μmol (36%), and 130 μmol (FE 28.29%) at 60 mins at −1.60 V, −1.80 V and −2.00 V, respectively using complex **1** electrocatalyst. The highest selectivity (SE) was achieved for the formation of non-alcoholic CO_2-reduced products such as CH_3COOH (SE 21%) and HCOOH (SE 35%). Whereas, complex **2** effectively reduced CO_2 to C_1 (HCOOH, CH_3OH) and C_2 (C_2H_5OH) products also in that same system. Initially, HCOOH was formed which was further reduced to CH_3OH and C_2H_5OH in a $6e^-$ and $12e^-$ transfer pathway. Overall current efficiency of 49% was recorded for the formation of alcohols at −1.80 V vs. Ag/AgCl in aqueous media (ERC time 1 h, pH 7.0 and $KHCO_3$ 0.5 M). The effect of attached anchoring amine group was further reestablished by examining the CO_2 reduction-efficiency of the similar Cu^{II} and Ni^{II} complex and without having the tethered –NH_2 group. No reduction products were observed for this case buttressed the importance of the anchoring group with the electrodes during the electrochemical reduction.

At the end the two Pb(II)-salen complexes (**3** = [$Pb^{II}(L^{NO_2})$], **4** = [$Pb^{II}(L^{NH_2})$]) as the catalysts were deposited on to graphite electrodes with the help of Nafion binder to fabricate working electrodes. The complexes were different in terms of ligand backbone-containing functional groups. In complex **3** and **4**, a -NO_2 and an –NH_2 functional groups were present at the parent ligand unit respectively. ERC by complex **3** and **4** coated graphite electrode as electrocatalysts, provided majorly C_2 products. While CH_3CH_2OH was formed as the single C_2 product with FE = 57% and SE = 66% in the presence of complex **3**. A mixture of C_2 products; acetic acid (CH_3COOH, FE = 36%; SE = 54%), acetaldehyde (CH_3CHO, FE = 12%; SE = 14%) and CH_3OH (FE = 12%; SE = 14%); with total FE = 68% was realized using complex **4** as the electrocatalyst material. The anchoring free $Pb^{II}L$ complex generated only C_1 products, formic acid (HCOOH, FE = 7%; SE = 41%) and methanol (CH_3OH, FE = 27%; SE = 59%) at −1.80 V vs. Ag/AgCl. Thus, the presence of functional groups facilitated C-C coupling between the pertinent intermediates. The role of the parent ligand was to stabilize *COOH intermediate species on to the electrode surface *via* *COOH(O)-to-phenyl(π) interactions for the successive reduction as implied by the formation of only HCOOH as the CO_2-reduced product in the presence of PbO as the electrocatalyst. In this way, the metal oxides and metal complexes were synthesized and compared their role in ERC to produce various by-products.

Keywords: Electrocatalysts; Electrochemical reduction of CO_2; Metal oxides; Salen metal complexes; C_1 (CH_3OH, HCOOH) and C_2 (CH_3COOH, C_2H_5OH) products formation.

भारतीय प्रौद्योगिकी संस्थान गुवाहाटी
Indian Institute of Technology Guwahati

Table of Contents

List of Table Captions

List of Figure Captions

भारतीय प्रौद्योगिकी संस्थान गुवाहाटी
Indian Institute of Technology Guwahati

List of Scheme Captions

List of Symbols

A	Area (cm^2)
amu	Atomic mass unit
Avg	Average
B	magnetic field
cm	centimeter
d	doublet
E°	equilibrium potential (V)
Exp	experimental
F	Faraday constant ($C \cdot mol^{-1}$)
h	hour
I	current density ($mA \cdot cm^{-2}$)
K	kelvin
M	molar
mL	mililiter
m/z	mass per charge
n	number of moles of a particular product (mol)
nm	nanometer
q	quartet
Q	total charge passed during the experiment (C)
S	singlet
Sim	simulated
T	temperature (°C)
V	potential or voltage (V)
z	number of moles of electrons required for formation of 1 mole of a reaction product
θ	diffraction angle (°)
λ	wavelength of X-rays (cm)
υ	potential scan rate ($V.s^{-1}$)

List of Abbreviations

AR	Assessment report
CH_3CN	Acetonitrile
CH_3OH	Methanol
C_2H_5OH	Ethanol
CH_3CHO	Acetaldehyde
CO_{ad}	Adsorbed carbon monoxide
CV	Cyclic voltammetry
DMF	Dimethyl formamide
DMSO	Dimethyl sulfoxide
EDX	Energy dispersive X-ray spectroscopy
EIA	Energy information administration
EPR	Electron paramagnetic resonance
ERC	Electrochemical reduction of CO_2
Et_3N	Trimethylamine
EtOH	Ethanol
ESI-MS	Electrospray ionization mass spectroscopy
FCC	Face centered cubic
FESEM	Field emission scanning electron microscope
FETEM	Field emission transmission electron microscope
FID	Flame ionization detector
FTIR	Fourier transform infrared
GHG	Greenhouse gases
HER	Hydrogen evolution reaction
HR-MS	High resolution mass spectroscopy
IEA	International energy agency
IEO	International energy outlook
IFFT	Inverse Fast Fourier Transform
IPCC	Intergovernmental panel on climate change
IUPAC	International union of pure and applied chemistry
KBr	potassium bromide
LSV	Linear sweep voltammetry
NHE	Normal hydrogen electrode

NMR	Nuclear magnetic resonance
NRC	National research council
Ppm	Parts per million
RHE	Reversible hydrogen electrode
SAED	Selected Area (electron) Diffraction
SHE	Standard hydrogen electrode
$TBAPF_6$	Tetrabutylammonium hexafluorophosphate
TCD	Thermal conductivity detector
XRD	X-ray diffractometer

CHAPTER 1

Introduction

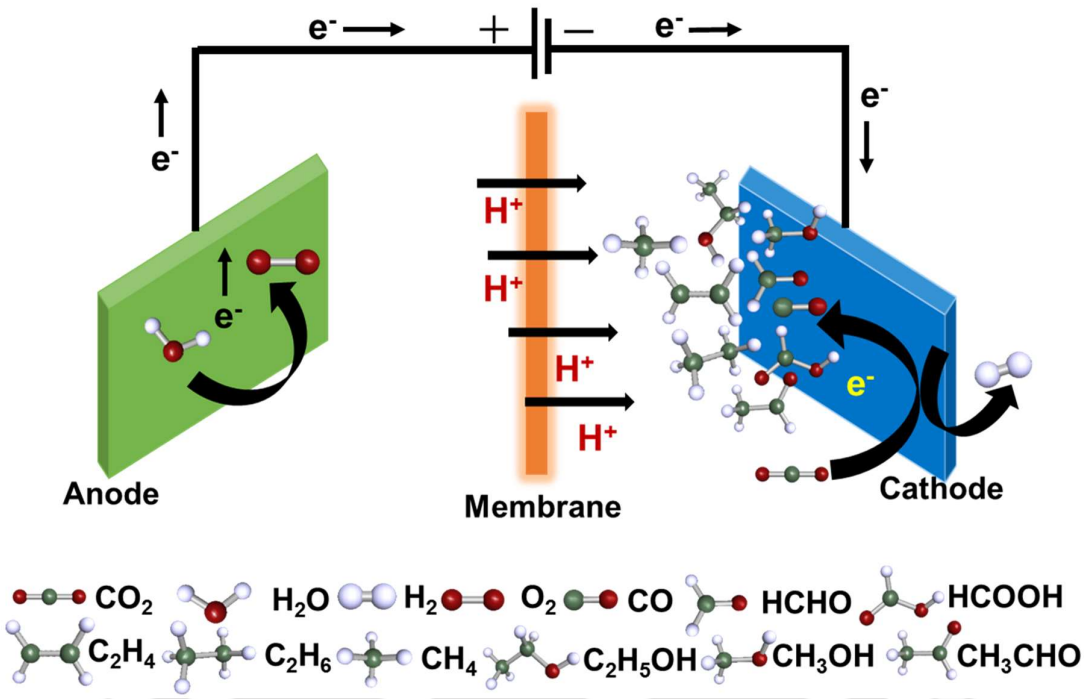

1.1 Overview

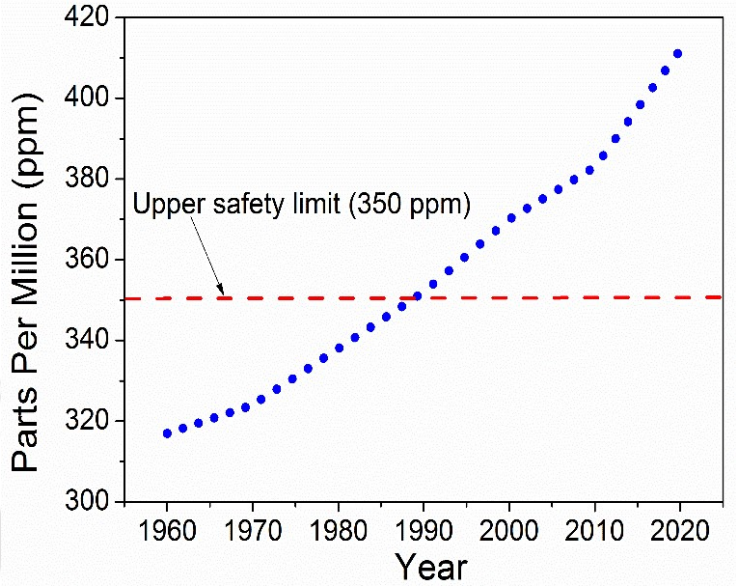

Figure 1.1: Global CO_2 data from the Mauna Loa Observatory between the timespan 1960 to 2020.

Carbon dioxide (CO_2) is very important for the survival of living organisms on the earth. It exists as a trace gas i.e., 0.03% by volume (300 ppm). Though it's a tiny fraction of the total carbon inventory; it makes an enormous impact on the life on the earth. Plants consume carbon dioxide from the air and uptake water to produce glucose in the presence of sunlight. Glucose is utilized by the rest of the biota and again returns to the environment through respiration or the demise of the living bodies. The total carbon is transferred from one form to another through a cycle known as the carbon cycle and remains constant. Nowadays rapid urbanization, industrial development, and various anthropogenic activities such as deforestation, burning of fossil fuels, transportation, etc., increases the amount of CO_2 in the atmosphere. Fossil fuels are the world's primary energy source and energy production from fossil fuels is very cheap. Fossil fuel accounts for more than 65% of usage for power generation. During the combustion of fossil fuels, various gases like methane,

nitrous oxide, other halocarbons, and CO_2 generally evolve. However, if there is more inflow of CO_2 into the atmosphere, then it leads to an increased amount of carbon balance in the atmosphere. The increased CO_2 level cannot be absorbed by the forest fauna of the earth and thus the carbon cycle is disrupted. Generally, atmospheric CO_2 absorbs the infrared radiation and trap the heat to maintain the earth's temperature. The excess CO_2 gas and the tiny carbon particles produced by incomplete burning behaves like a reflective glass and trap the sun's energy and thus increases the temperature. This effect is known as the greenhouse effect and the gases that are responsible for trapping the heat are known as greenhouse gases. Thus, the excess carbon dioxide increases the average temperature of the atmosphere, which is known as global warming which finally causes dangerous climate change.

There is an increase in atmospheric temperature by 1-2°C for the elevation of CO_2 level by about 100 ppm in the years from 1960 to 2010 (Daiyan et al., 2017). According to the literature survey, the upper safety limit of the CO_2 level is 350 ppm (Hansen et al., 2008). The level of CO_2 was increased by 43.3% from 280 to 416.27 ppm over the past 60 years. The data observed from the year 1960 to 2020, recorded by Mona Loa Observatory is depicted in Fig. 1.1. The CO_2 level and recent CO_2 concentration are higher than the upper safety limit. Therefore, it is necessary to reutilize carbon dioxide or store it by employing an alternative approach. This phenomenon is known as carbon sequestration. These valuable products can be used as green fuels which reduces pollution.

1.2 Environmental consequences of CO_2 (global scenario)

Fossil fuel is the most used energy source (85%) in various sectors. Industrial development and other anthropogenic activities (which use fossil fuels) increase the amount of CO_2 in nature which causes global warming. Among all the anthropogenic greenhouse gases (GHGs), CO_2 has occupied 77% of all the GHGs. Though the CO_2 has a global

warming potential (GWP) of 1 which is far lower than the other potential GHGs such as N_2O (GWP 298) and CH_4 (GWP 25), the amount of CO_2 in the atmosphere is higher than these two gases (US Energy Information Administration/ Emissions of Greenhouse Gases in the United States 2009). Not only that, but the intense use of conventional fuels also decreases its stock as well as increases the global energy demand. These make non-conventional sources of energy a necessity of the hour. This problem starts with the increasing human demand which is more than nature's regenerative capacity. Recent data illustrates that human biota needs a minimum of 1.5 planets like earth to satisfy its need. UN projections implicate that humans will require two earth to support its existence by 2030.

The problem starts with the industrial revolution in the year 1750. The emission from the industries and the transportation sector creates a huge impact on society. Various greenhouse gases and other toxic components released by the industries and the transportation sectors induce pollution. Among all the sources of gaseous CO_2, 57% is directly coming from the industries and the transportation sector which is powered by conventional fossil fuels. Flue gases and smoke released by the industries comprised of CO_2 thus have a large impact on global warming. After the industrial revolution started in the year 1758, the CO_2 emission was very low about 11 million metric tons initially. It was increased to 1198 million metric tons in 100 years (in 1888). After that, there was a sharp rise and the amount increased to 1000 times higher and reached 12848 million metric tons in the year 1968. The rise of the CO_2 emission after this period was very sharp and reached 36 billion metric tons globally (IEA Statistics 2019).

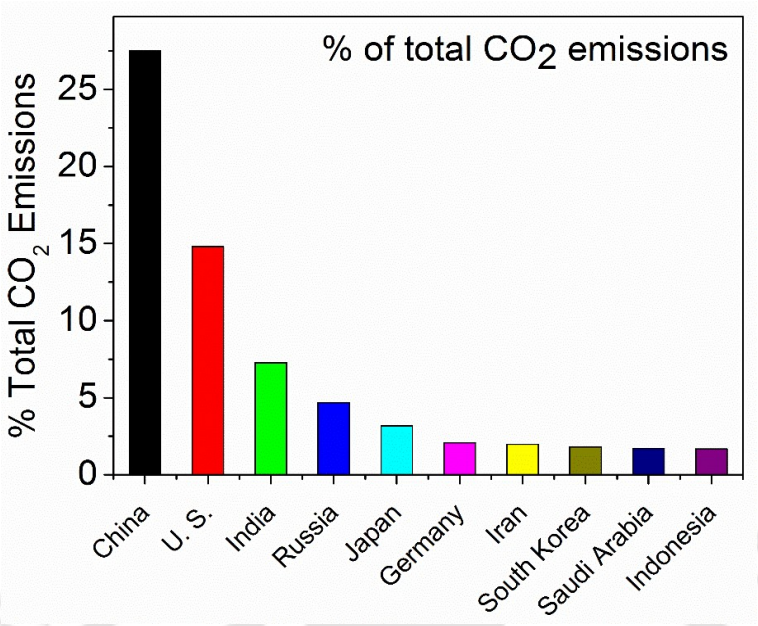

Figure 1.2: Recent percentage of the CO_2 emission data by various countries up to 2020 (IEA Statistics 2020).

In Fig. 1.2, the recent data of the percentage of CO_2 emissions from the various country is recorded. The maximum share of CO_2 emission is coming from China and then from the U.S.A. India (3rd largest) being a developing country, also has an enormous impact on the global CO_2 emission (IEA Statistics 2020). India also has a huge contribution to the increase in global CO_2 emissions and it is estimated to flourish in the upcoming years because of many reasons. There is an increase in urbanization and various other anthropogenic activities, rapid growth in vehicular usage, and continuous use of fossil fuels. That is why the emission rate of CO_2 is increasing day by day in India (Singh and Singh 2009). The IPCC recently released the 4th assessment report (AR-4) which described that the temperature of the earth is rising and it is due to the increase in anthropogenic activities around the world (IPCC 2007). Again in 2014, a 5th assessment report was passed stating that a rise in temperature (3.7-4.8°C) will occur within 2100 because of the increasing GHG emission (IPCC 2014). Thus, to reduce the increasing pollution level and energy crisis,

reduction of GHG is necessary. This frightening occurrence attracted many researchers to find solutions to this problem.

In 1992, a set of protocols were proposed at the Rio Earth Summit in June. It was proposed that the emission of the various greenhouse gases will be reduced so that the impact on global climate change can be resolved. After that, the Kyoto Protocol came into force in 1997, which described that the GHGs are the main reason behind climate change. Thus, this protocol limits the emission of all the GHGs including CO_2. After that, the Paris Agreement also came into force in December 2015 to fight against climate change. In this agreement, it was decided to use green energy sources to reduce the GHG emission and thus lessen the global temperature. Though the reduction of the GHG emission (by 5%) within a stipulated time (within 2012) than the previously reported GHG emission (in 1992) was not achieved. Anthropogenic activities still produce 30 billion tons of CO_2 every year (NRC 2010). Not only that, the rigorous use of fossil fuel for the development of mankind reduces the amount of stored energy (fossil fuels) also. Thus, the reduction of the use of conventional energy sources as well as the use of renewable energy is necessary for future development purposes.

1.3 Requisite for CO_2 utilization and conversion

The rate of use of conventional fuels for industrial development purposes is gradually increasing day by day. Another significant threat includes increment in the use of vehicles which assist in the depletion of conventional fossil fuels. Although, fossil fuels are not renewable and the rate of formation is far slower than its consumption. The available renewable resources are very few. Thus, on one side where the world is suffering from the fear of climate change, fossil fuel depletion has also been identified as a future challenge. Over the next 25 years, it is the transportation sector where the demand for liquid fuels will increase more rapidly than in any other sector and the increase will come from the

developing non-OECD (Organization for Economic Co-operation and Development) countries (e.g. India). The utilization among the developed OECD countries will remain comparatively unchanged. The reason for more growth of energy consumption in non-OECD countries is because of the demands for personal travel increase with the increase in urbanization and personal incomes (International Energy Outlook 2019).

Thus it is clear that the energy requirement is continuously increasing and putting a lot of pressure on conventional energy resources. But since fossil fuels are limited and also responsible for environmental issues, alternative energy sources need to be explored for sustainable energy supply. Three possible ways can be achieved to deal with this problem.

1. At first to reduce the dependency on the consumption of fossil fuels.
2. Not only that, the use of renewable fuels will emit lesser CO_2 than conventional methods. During the utilization of CO_2, various other products (fuels and hydrocarbons) can be generated which can be reused as the alternative to fossil fuels.
3. This will reduce the emission of CO_2 as well as the other GHGs. CO_2 is a potent greenhouse gas and thus the reduction of CO_2 will reduce the global warming effect.

1.4 Various processes of CO_2 conversion towards the generation of value-added products

A large amount of CO_2 is generated from various anthropogenic activities and increase its level in the environment and causes global warming. The extensive use and exploitation of fossil fuels, increasing rate of pollution have inspired many scientists to convert CO_2 into value-added products (C_1: CH_4, CO, HCHO, CH_3OH and HCOOH, etc.;

and C_2: CH_3CHO, CH_3CH_2OH, C_2H_6, and C_2H_4, etc.). People have started using CO_2 as a feedstock a long time back for its conversion to various industrially relevant products. CO_2 can be utilized directly as a solvent or working fluid in various sectors or can be reduced to various chemicals and fuels. To reduce and reuse the gaseous CO_2 four main methods such as chemical, biological, electrochemical, and photochemical methods can be used traditionally (Sakakura et al., 2007).

1.4.1 Chemical process of CO_2 conversion

Chemical reaction-based strategies include washing with alkaline solutions, multi-walled carbon nanotubes and amine coated activated carbon. CO_2 can be converted into different industrially relevant products. It can be chemically converted to useful products through Sabatier reaction, Fischer-Tropsch synthesis, urea formation, carbonate, bicarbonate, and a variety of other products (Sakakura et al., 2007; Song and Pan 2004). During the Sabatier's reaction, a mixture of CO_2 and H_2 is converted into CH_4 and H_2O at a very high temperature (300-400°C) in the presence of a Ni catalyst (Miao et al., 2016). Other metal such as ruthenium (Ru), rhodium (Rh) also makes a better catalyst for this type of exothermic reaction (Eqn. 1.1).

$$CO_2 + 4H_2 \rightarrow CH_4 + 2H_2O \qquad (1.1)$$

Another process of chemical conversion of CO_2 is Fischer-Tropsch synthesis. This process involves two steps. In the first step, partial oxidation of the coal or natural gas takes place into carbon-monoxide (CO). After that, CO and hydrogen are converted to liquid hydrocarbons at an elevated temperature in the presence of Fe catalysts. Several transition metals such as cobalt, ruthenium, and nickel also can be used as the catalyst during this synthesis process (Khodakov et al., 2007) (Eqns. 1.2 to 1.3).

$$2C + 1/2\ O_2 + H_2O \rightarrow 2CO + H_2 \qquad (1.2)$$

$$nCO + 2nH_2 \rightarrow C_nH_{2n} + nH_2O \quad (1.3)$$

There are many other chemical conversions of CO_2 conversion as well. CO_2 can be used in dimethyl carbonate (DMC) synthesis instead of phosgene and chlorine through an environmentally friendly route. This process lowers the phosgene utilization (The US uses 1.2 million tons' phosgene per year) (Aresta, 1997). There is an emergence of using alternative energy resources to fulfill the demand of the increasing population. Tri reforming of methane from using CO_2 is one of them (Song and Pan 2004). In 1995, a group of researchers performed selective dehydrogenation of ethylbenzene using CO_2 gas as a diluent and oxidant. CO_2, being a mild oxidant can produce active oxygen species on a variety of catalyst surfaces. Adjunction of lithium nitrate (20-30 mol%) increases the catalytic activity. It produces styrene and CO, H_2 as byproducts using an activated carbon-supported iron catalyst (Sugino et al., 1995).

1.4.2 Biological process of CO_2 conversion

Biological CO_2 conversion can be a good option because of its small negative impact on the earth. The light energy is converted to chemical energy by utilizing CO_2 and water. In this process plants at first, takes CO_2 to produce carbohydrates (mainly glucose) as a form of energy and store the carbon by reducing CO_2. After that, the other complex carbohydrates (sucrose, starch, glycogen, etc.) can be synthesized (Eqn. 1.4).

$$6CO_2 + 6H_2O + \text{energy} \rightarrow C_6H_{12}O_6 + 6O_2 \quad (1.4)$$

Mostly, all varieties of plants can produce carbohydrates from CO_2. Microalgae are also often used on an industrial-scale to treat the wastewater and form energy (waste to energy). Algae cultivation in wastewater has become very famous as it can use the nutrients present in the wastewater and use the atmospheric CO_2 to produce glucose. After the treatment process, the microalgal biomass is used for producing different value-added

products like renewable fuels which are known as transesterification (Jajesniak et al., 2014). The mass transfer of CO_2 is a vital parameter to identify the CO_2 removal efficiency of algae. Hulatt and coworkers discussed the total mass transfer of the energy return during the CO_2 sequestration by algae within a photobioreactor (Hulatt and Thomas, 2011). In a study by Kumar and coworkers, *Chlorella Sorokiniana* was used for CO_2 sequestration from flue gas in the oil industry. The highest amount of CO_2 reduced at the inlet was 4.1% (Kumar et al., 2014). The study by Jiang and his group investigated the effect of flue gas components (NO, SO_2 and CO_2) on *Scenedesmus dimorphous*. The maximum amount of CO_2, NO, and SO_2 concentrations were tolerated by the *S. dimorphous* were 20%, 500 ppm, and 100 ppm, respectively and the maximum CO_2 utilized efficiency was 75.61% (Jiang et al., 2013).

Chiu and his group investigated the bioremediation performance of a CO_2 and thermotolerant mutant microalgal strain Chlorella sp. MTF-7. At first, flue gas was purged into a photobioreactor (50 L) directly from a steel plant coke oven. With intermittent aeration, the CO_2 removal efficiency reached 60% (Chiu et al., 2011). A study by Li and his research group presented a comparison of the cellular components of *Scenedesmus Raciborskii* WZKMT (protein, total sugar, chlorophyll, starch, and lipid) with purged flue gas. The strain attained 53.16% and 66.76% starch and sugar contents respectively; which indicates the potential for bioethanol production during CO_2 sequestration (Li et al., 2015).

But after extracting the useful products, the discarded dead biomasses may have some unhealthy effects on the environment. The rest part of the dead biomasses can contain other pollutants (ex: heavy metals which are not easily biodegradable) that harm the environment. Biochemical degradation followed by geochemical maturation of plant materials produces coal under specific environmental conditions. Direct CO_2 conversion to C_1 substances through a biochemical process for long-term storage is a very new and

promising approach (Mahajan et al., 2000; Beecy et al., 2001). Direct underground injection of CO_2 into the ocean also can store CO_2 but can affect marine life in the long run.

1.4.3 Electrochemical process for CO_2 conversion

Electrochemical reduction of CO_2 (ERC) is an alternative to the other methods of carbon dioxide reuse which converts CO_2 to useful chemicals within a very short time (Ma et al., 2009; Taniguchi 1989). CO_2 is a linear molecule with a C=O bond energy of about 750 $kJ.mol^{-1}$ (Zhang et al., 2018). Thus, this process requires a high amount of energy. In the first step of CO_2 reduction, changing in its geometry from linear CO_2 to bent CO_2 anion radical ($\bullet CO_2^-$) requires huge energy (−1.90 V vs. standard hydrogen electrode; SHE) (Azuma et al., 1989; Lim et al., 2014). A significant amount of activation potential is required to start the reduction process. Metals and their derivatives can gain or lose electrons easily and thus, act as electrocatalysts during the conversion process. An electrochemical cell fabricated with a semi-porous membrane between the working and counter electrode side can be used as a reactor. CO_2 is purged in the one side where it gets converted to valuable products in the presence of the proton comes from the other half of the reactor passing through the membrane. Electrochemical reduction of CO_2 is carried out either in aqueous or non-aqueous electrolyte solutions saturated with CO_2 or directly as a gas at different metal or metal derivative catalysts.

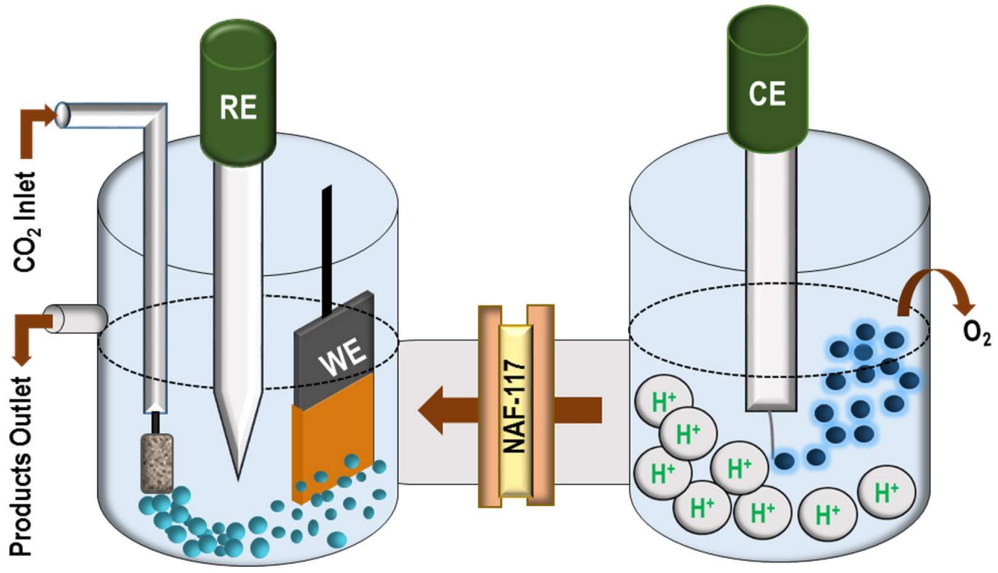

Figure 1.3: Schematic representation of the custom-made H-type divided electrochemical cell, WE = Working electrode, CE = Counter electrode, and RE = reference electrode.

Normally, an H-type cell is used as the electrochemical reactor in which the working and counter electrode chambers are is separated with a proton exchange membrane. At the counter electrode side, H_2O is used as the proton source and H_2O splits into H^+ and OH^-. Two molecules of H_2O splits into $2H^+$ and $2OH^-$ and is a two-electron process. The protons are transferred to the working electrode side and in presence of $2e^-$, CO_2 is reduced to CO or HCOOH. After that, the CO_2 is further reduced to various products and as a result, many useful products can be produced. During the electrolysis, O_2 gas is also generated in the counter electrode side. Thus, during ERC in the presence of a natural source (H_2O) and electrochemical energy, CO_2 can be converted into useful chemicals. The design of an electrochemical cell is shown in Fig. 1.3. A few important overall reactions are as follows (Eqns. 1.5 to 1.12) (Dixit and Majumder 2018; Hao and Shi, 2018).

$$CO_2 + 6H^+ + 6e^- \rightarrow CH_3OH + H_2O,\ E^0 = -0.38\ V\ vs.\ SHE \quad (1.5)$$

$$2CO_2 + 12H^+ + 12e^- \rightarrow C_2H_5OH + 3H_2O,\ E^0 = -0.33\ V\ vs.\ SHE \quad (1.6)$$

$$CO_2 + 2H^+ + 2e^- \rightarrow HCOOH,\ E^0 = -0.61\ V\ vs.\ SHE \quad (1.7)$$

$$CO_2 + 2H^+ + 2e^- \rightarrow CO + H_2O,\ E^0 = -0.52\ V\ vs.\ SHE \quad (1.8)$$

$$CO_2 + 4H^+ + 4e^- \rightarrow HCHO,\ E^0 = -0.51\ V\ vs.\ SHE \quad (1.9)$$

$$CO_2 + 8H^+ + 8e^- \rightarrow CH_4 + 2H_2O,\ E^0 = -0.24\ V\ vs.\ SHE \quad (1.10)$$

$$2CO_2 + 8H^+ + 8e^- \rightarrow CH_3COOH + 2H_2O,\ E^0 = -0.35\ V\ vs.\ SHE \quad (1.11)$$

$$2CO_2 + 12H^+ + 12e^- \rightarrow C_2H_4 + 4H_2O,\ E^0 = -0.34\ V\ vs.\ SHE \quad (1.12)$$

1.4.4 Processes of electrochemical CO_2 reduction and scope of work

ERC reduction processes are merited with several advantages. It can produce value-added products such as hydrocarbons (CH_4, C_2H_4, and C_2H_6, etc.), alcohols (CH_3OH, C_2H_5OH), acids (HCOOH, CH_3COOH), and some amount of CO and H_2 as byproducts. The process requires water as a proton source and converts and stores energy in the form of value-added chemicals (Centi et al., 2013; Dixit and Majumder 2018; Hu et al., 2013; Jhong et al., 2013). The process suffers from large activation potential. Otherwise, it would have been one of the most favourable operations as this process could curb harmful emissions and audible pollution. The major advantages of ERC processes include:

i. Atmospheric CO_2 can be used as the CO_2 feedstock in ERC, and thus it could decrease CO_2 concentration and hence lessens global warming.

ii. Various useful chemicals such as hydrocarbons, alcohols, etc. can be obtained and reused.

iii. Can store the energy in terms of product formation, and thus reduces the dependency on fossil fuels and minimize pollution.

iv. Only, electrical energy is used as the energy source and water is used as the H^+ source.

v. Product formation occurs within very little time at ambient temperature and pressure.

vi. Scaling up the electrochemical reactor is easy, and after the completion of the ERC reaction, no harmful chemical has remained, and the total process is pollution-free.

The CO_2 reduction products such as alcohols and hydrocarbons can be reused as a form of fuel (instead of the conventional fossil fuel). The acids also can be used as laboratory chemicals or useful chemicals in various industries. The combination of produced CO and H_2 also can be used as Syn-gas in various sectors. Thus, the ERC process not only reduces the viable pollution by reducing CO_2 into various products but also reuses them as an alternative source of required energy. That is why scientists have taken the ERC process seriously and it has gained interest from many. Various electrocatalysts are commercially available which can reduce CO_2. Metals and various metal derivatives are extensively used in the ERC. Among the metals, Pb, Hg, In, Sn, Cd, and Ti mostly produce formate or formic acid (HCOOH) under various experimental conditions. Whereas, Au, Ni, Ag, Zn, Pd, and Ga usually produces carbon monoxide (CO). The oxides of metals such as Cu_2O, NiO, ZnO, CO_3O_4, PbO_2, RuO_2 can reduce CO_2 to CO, HCOOH, and CH_3OH mainly (Albo et al., 2017; Aljabour et al., 2018; Bashir et al., 2015; Chen et al., 2017). Copper metal (Cu) and various modifications over Cu metals mostly produce hydrocarbons and alcohols (Albo et al., 2015; Furuya et al., 1997; Hori et al., 1985). Oxides of Cu were tested for ERC in 0.1 M $KHCO_3$ and 0.1 M $CsHCO_3$ in different applied potentials. At −1.00 V vs. RHE, the selectivity of C_2 products reached 70%, and the selectivity of C_1 products observed was

only 3% when the electrolyte is 0.1 M $CsHCO_3$. In 0.1 M $KHCO_3$ solution, the selectivity of C_2 products decreased to 56% using the same catalyst (Lum et al., 2017).

A Cu-Zn catalyst was also reported for the production of C_2H_5OH (10.44%) in the $NaHCO_3$ solution (Riyanto et al., 2018). Hazarika and Manna (2019) also reported selective production of CH_3OH (FE of 47.5%) with CH_4, C_2H_4, and CO using Cu_2O nanocatalyst as a cathode in $KHCO_3$ solution. Recently in 2019, Zarandi et al. (2019) used copper nanofoam as an electrocatalyst and 1-butyl-3-methyl-imidazolium bromide (BMIMB) as cocatalyst in 0.1 M $KHCO_3$ solution and reported a 46% improvement in terms of FE for the production of C_2H_5OH (FE 49%), $HCOO^-$ (FE 19%), and CH_4 (FE 9.6%). In 2020, a group of scientists introduced Cu nanoparticles supported on N-doped porous carbon (Cu/NPC) in ERC and produced C_2H_5OH (FE 64.6) and C_3H_7OH and (FE 8.7 %) at −1.05 V vs. RHE (Han et al., 2020). The forbidden cost of noble metal catalysts also limits their application in ERC. Thus, metal complexes have also been introduced in ERC and they can catalyze ERC for the production of a variety of acids, hydrocarbons, and alcohols with a high FE (Weng et al., 2018). Even the electrolyte solution also has an important role in governing electrocatalysis (Dunwell et al., 2017).

There are plenty of metal and metal oxide catalysts are available for the CO_2 reduction reaction. One of the main obstacles is the continuous hydrogen evolution reaction (HER) with CO_2-reduced products during ERC reactions. Some metals are selective towards HER than ERC. Thus, it is difficult to get a selective product with high FE. Not only that, most of the catalysts were reported for only HCOOH or CO production which needs only 2 electron reduction. So, the synthesis of a new class of catalysts can reduce FE of HER and can produce C_1 as well as C_2 products. Cu-based catalysts are mostly reported for hydrocarbons and alcohol production. Thus, it is important to include not only copper

but also some other metal oxides and metal complex catalysts that can produce hydrocarbons as well as alcohols in ERC.

In Chapter 2, a brief description is given regarding the role of the electrolyte solution on the product selectivity in the ERC reaction. In Chapters 4 to 7, the role of three metal oxides (M = Cu, Ni and Pb) and their corresponding metal complexes (salen ligand complexes) are described in detail. The role of various metals, metal oxides, metal complexes, and other metal derivative catalysts, product formation, and corresponding FE in the ERC reaction is explained. The specific advantages and disadvantages are also outlined in the pertinent sections/chapters.

References

Albo, J., Alvarez-Guerra, M., Castaño, P., and Irabien, A., 2015. "Towards the Electrochemical Conversion of Carbon Dioxide into Methanol." *Green Chemistry,* 17, 2304-2324.

Albo, J., Beobide, G., Castaño, P., and Irabien, A., 2017. "Methanol Electrosynthesis from CO_2 at Cu_2O/ZnO Prompted by Pyridine-Based Aqueous Solutions." *Journal of CO_2 Utilization,* 18, 164-172.

Aljabour, A., Coskun, H., Apaydin, D. H., Ozel, F., Hassel, A.W., Stadler, P., Sariciftci, N. S., and Kus, M., 2018. "Nanofibrous Cobalt Oxide for Electrocatalysis of CO_2 Reduction to Carbon Monoxide and Formate in an Acetonitrile-Water Electrolyte Solution." *Applied Catalysis B: Environmental,* 229, 163-170.

Aresta, M., and Quaranta, E., 1997. "Carbon dioxide: A substitute for phosgene." *Chemtech*, 27, 32-40.

Azuma, M., Hashimoto, K., Hiramoto, M., Watanabe, M., and Sakata, T., 1989. "Carbon Dioxide Reduction at Low Temperature on Various Metal Electrodes." *Journal of Electroanalytical Chemistry,* 260, 441-445.

Bashir, S. M., Hossain S.S., Rahman, S., Ahmed, S., and Hossain M. M., 2015. "NiO/MWCNT Catalysts for Electrochemical Reduction of CO_2." *Electrocatalysis,* 6, 544-553.

Beecy, D., 2001. "The role of carbon sequestration in a national carbon management strategy." *Am. Chem. Soc. Div. Fuel Chem. Prepr*., 46, 38-44.

Centi, G., Quadrelli, A. E., and Perathoner, S., 2013. "Catalysis for CO_2 Conversion: A Key Technology for Rapid Introduction of Renewable Energy in the Value Chain of Chemical Industries." *Energy and Environmental Science,* 6, 1711-1731.

Chen, L., Li, F., Bentley, C. L., Horne, M., Bond, A. M., and Zhang, J., 2017.

"Electrochemical Reduction of CO_2 with an Oxide-Derived Lead Nano-Coralline Electrode in Dimcarb." *ChemElectroChem,* 4, 1402-1410.

Chiu, S. Y., Kao, C. Y., Huang, T. T., Lin, C. J., Ong, S. C., Chen, C. D., Chang, J. S., and Lin, C.S., 2011. "Microalgal Biomass Production and On-Site Bioremediation of Carbon Dioxide, Nitrogen Oxide and Sulfur Dioxide from Flue Gas Using Chlorella Sp. Cultures." *Bioresource Technology,* 102, 9135-9142.

Daiyan, R., Lu, X., Ng, Y. H., and Amal, R., 2017. "Liquid Hydrocarbon Production from CO_2: Recent Development in Metal-Based Electrocatalysis." *ChemSusChem,* 10, 4342-4358.

Dixit, R. J., and Majumder, C. B., 2018. "CO_2 Capture and Electro-Conversion into Valuable Organic Products: A Batch and Continuous Study." *Journal of CO_2 Utilization,* 26, 80-92.

Dunwell, M., Lu, Q., Heyes, J. M., Rosen, J., Chen, J. G., Yan, Y., Jiao, F., and Xu, B., 2017. "The Central Role of Bicarbonate in the Electrochemical Reduction of Carbon Dioxide on Gold." *Journal of the American Chemical Society,* 139, 3774-3783.

Furuya, N., Yamazaki, T., and Shibata, M., 1997. "High-Performance Ru-Pd Catalysts for CO_2 Reduction at Gas-Diffusion Electrodes." *Journal of Electroanalytical Chemistry,* 431, 39-41.

Han, H., Noh, Y., Kim , Y., Park, S., Yoon, W., Jang, D., Choi, S. M., and Kim, W. B., 2020. "Selective Electrochemical CO_2 Conversion to Multicarbon Alcohols on Highly Efficient N-Doped Porous Carbon-Supported Cu Catalysts." *Green Chemistry,* 22, 71-84.

Hazarika, J., and Manna, M. S., 2019. "Electrochemical Reduction of CO_2 to Methanol with Synthesized Cu_2O Nanocatalyst: Study of the Selectivity." *Electrochimica Acta,* 328, 1-9.

Hansen, J., Sato, M., Kharecha, P., Beerling, D., Berner, R., Delmotte, V. M., Pagani, M., Raymo, M., Royer, D. L., and Zachos, J. C., 2008. "Target Atmospheric CO_2: Where Should Humanity Aim?" *The Open Atmospheric Science Journal*, *2*, 217-231.

Hao, J., and Shi, W., 2018. "Transition metal (Mo, Fe, Co, and Ni)-based catalysts for electrochemical CO_2 reduction." *Cuihua Xuebao/Chinese Journal of Catalysis*, *39*, 1157-1166.

Hori, Y., Kikuchi, K., and Suzuki, S., 1985. " Production of CO and CH_4 in Electrochemical Reduction of CO_2 At Metal Electrodes in Aqueous Hydrogencarbonate Solution." *Chemistry Letters,* 14, 1695-1698.

Hu, B., Guild, C., and Steven L. Suib. S. L., 2013. "Thermal, Electrochemical, and Photochemical Conversion of CO_2 to Fuels and Value-Added Products." *Journal of CO_2 Utilization,* 1, 18-27.

Hulatt, C. J., and Thomas, D. N., 2011. "Productivity, Carbon Dioxide Uptake and Net Energy Return of Microalgal Bubble Column Photobioreactors." *Bioresource Technology,* 102, 5775-5787.

IEA (2019), *World Energy Statistics 2019*, IEA, Paris (https://www.iea.org/reports/world-energy-statistics-2019).

IEA (2020), *Global Energy Review 2020*, IEA, Paris (https://www.iea.org/reports/global-energy-review-2020).

International Energy Outlook Report (2019), U.S. Energy Information Administration, IEO 2019.

IPCC (2007) Fourth Assessment Report (AR4), IPCC website (http://www.ipcc.ch/).

IPCC (2014) Fifth Assessment Report (AR5), IPCC website (http://www.ipcc.ch/).

Jajesniak, P., Ali, H. E. M. O., and Wong, T. S., 2014. "Carbon Dioxide Capture and Utilization Using Biological Systems: Opportunities and Challenges." *Journal of*

Bioprocessing and Biotechniques, 4, 1-15.

Jhong, H. R. M., Ma, S., and Kenis, P. J., 2013. "Electrochemical Conversion of CO_2 to Useful Chemicals: Current Status, Remaining Challenges, and Future Opportunities." *Current Opinion in Chemical Engineering,* 2, 191-199.

Jiang, Y., Zhang, W., Wang, J., Chen, Y., Shen, S., and Liu, T., 2013. "Utilization of Simulated Flue Gas for Cultivation of Scenedesmus Dimorphus." *Bioresource Technology,* 128, 359-64.

Khodakov, A. Y., Chu, W., and Fongarland, P., 2007. "Advances in the Development of Novel Cobalt Fischer-Tropsch Catalysts for Synthesis of Long-Chain Hydrocarbons and Clean Fuels." *Chemical Reviews,* 107, 1692-1744.

Kumar, K., Banerjee, D., and Das, D., 2014. "Carbon Dioxide Sequestration from Industrial Flue Gas by Chlorella Sorokiniana." *Bioresource Technology,* 152, 225-233.

Li, X-K., Xu, J-L., Guo, Y., Zhou, W-Z., and Yuan, Z-Y., 2015. "Effects of Simulated Flue Gas on Components of Scenedesmus Raciborskii WZKMT." *Bioresource Technology,* 190, 339-344.

Lim, R. J., Xie, M., Sk, M. A., Lee, J-M., Fisher, A., Wang, X., and Lim, K. H., 2014. "A Review on the Electrochemical Reduction of CO_2 in Fuel Cells, Metal Electrodes and Molecular Catalysts." *Catalysis Today,* 233, 169-180.

Lum, Y., Yue, B., Lobaccaro, P., Bell, A. T., and Ager, J. W., 2017. "Optimizing C-C Coupling on Oxide-Derived Copper Catalysts for Electrochemical CO_2 Reduction." *Journal of Physical Chemistry C,* 121, 14191-14203.

Ma, J., Sun, N., Zhang, X., Zhao, N., Xiao, F., Wei, W., and Sun, Y., 2009. "A Short Review of Catalysis for CO_2 Conversion." *Catalysis Today,* 148, 22-31.

Mahajan, D., Song, C., and Scaroni, A.W., 2000. "Micro-reactor study on catalytic reduction of CO_2 into liquid fuels: simulating reactions under geologic formation

conditions." *Am. Chem. Soc. Div. Petrol. Chem. Prepr*., 45, 113-117.

Miao, Bi., Ma, S. S. K., Wang, X., Su, H., and Chan, S. H., 2016. "Catalysis Mechanisms of CO_2 and CO Methanation." *Catalysis Science and Technology,* 6, 4048-4058.

NRC (2010), Advancing the science of climate change, National Research Council, The National Academics Press, Washington DC, USA.

Riyanto, Ramadan, S., Fariduddin, S., Aminudin, A. R., and Hayatri, A. K., 2018. "Conversion of Carbon Dioxide into Ethanol by Electrochemical Synthesis Method Using Cu-Zn Electrode." *IOP Conference Series: Materials Science and Engineering,* 288, 1-9.

Sakakura, T., Choi, J. C., and Yasuda, H., 2007. "Transformation of Carbon Dioxide." *Chemical Reviews,* 107, 2365-2387.

Singh, B. R., and Singh, O., 2008. "A Study on Sustainable Energy Sources and Its Conversion Systems towards Development of an Efficient Zero Pollution Novel Air Turbine to Use as Prime-Mover to the Light Vehicle." In *ASME International Mechanical Engineering Congress and Exposition, Proceedings*, Vol. 8, Paper No. IMECE2008-66803, 371-378.

Song, C., and Pan, W., 2004. "Tri-Reforming of Methane: A Novel Concept for Catalytic Production of Industrially Useful Synthesis Gas with Desired H_2/CO Ratios." *Catalysis Today,* 98, 463-484.

Sugino, M., Shimada, H., Turuda, T., Miura, H., Ikenaga, N., and Suzuki, T., 1995. "Oxidative Dehydrogenation of Ethylbenzene with Carbon Dioxide." *Applied Catalysis A, General,* 121, 125-137.

Taniguchi, Isao. 1989. "*Electrochemical and Photoelectrochemical Reduction of Carbon Dioxide*." In: Bockris *et al*. (ed.) 'Modern Aspects of Electrochemistry No. 20', Ch. 1, Springer, NewYork, pp. 327-400.

US Energy Information Administration. 2009. "Emissions of Greenhouse Gases in the United States in 2009." *Independent Statistics and Analysis,* March 2011, 1-78.

Weng, Z., Wu, Y., Wang, M., Jiang, J., Yang, K., Huo, S., Wang, X-F., Ma, Q., Brudvig,G. W., Batista, V. S., Liang, Y., Feng, Z., and Wang, H., 2018. "Active Sites of Copper-Complex Catalytic Materials for Electrochemical Carbon Dioxide Reduction." *Nature Communications,* 9, 1-9.

Zarandi, R. F., Rezaei, B., Ghaziaskar, H. S., and Ensafi. A. A., 2019. "Electrochemical Reduction of CO_2 to Ethanol Using Copper Nanofoam Electrode and 1-Butyl-3-Methyl-Imidazolium Bromide as the Homogeneous Co-Catalyst." *Journal of Environmental Chemical Engineering,* 7, 1-7.

Zhang, W., Hu, Y., Ma, L., Zhu, G., Wang, Y., Xue, X., Chen, R., Yang, S., and Jin, Z., 2018. "Progress and Perspective of Electrocatalytic CO_2 Reduction for Renewable Carbonaceous Fuels and Chemicals." *Advanced Science,* 5, 1-24.

This page is intentionally left blank

CHAPTER 2

Literature Review

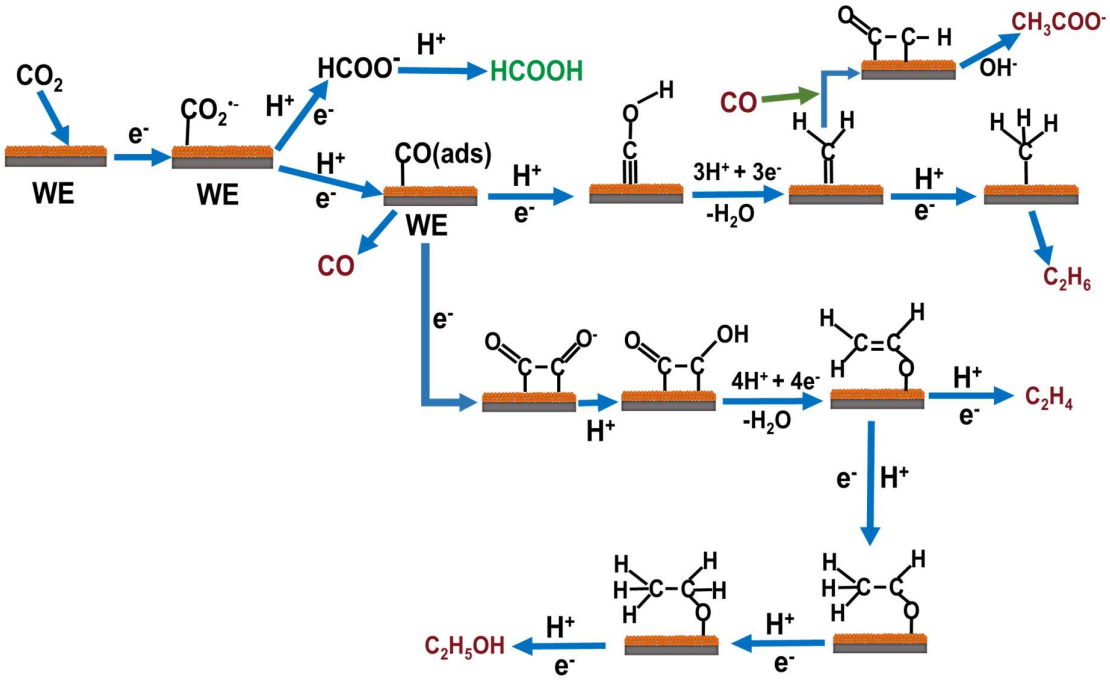

2.1 Electrochemical tools to study the CO_2 reduction process

The excessive growth of industrial development has increased the amount of CO_2 gas around the World. This causes an increase in global temperature and depletion in the stock of conventional energy resources. This danger has encouraged many scientists to look for a way to efficiently reduce gaseous CO_2. There are various processes of CO_2 reduction such as chemical, biological, biochemical, electrochemical, etc. which were already discussed in chapter 1. Thus, in this chapter, the various factors are elaborated that govern the electrochemical procedure. The role of various electrocatalysts, electrolyte solution, and the process parameters are described in this section. The electrochemical reduction of CO_2 is a growing research field as this process reduces pollution and stores the energy in the form of a chemical bond. Not only that, but the energy density generated from the renewable fuels produced from CO_2 conversion is higher than the previously used energy storage systems (fossil fuels). The most common problems of this research are the stability of the molecule, selective product formation during reduction, reusability of the electrocatalysts, continuous hydrogen production, etc. CO_2 is very stable and the first step of the CO_2 electro reduction is to activating the gaseous CO_2. This needs huge energy and that is −1.90 V vs. standard hydrogen potential (SHE) (Costentin et al., 2013; Schouten et al., 2011). Production of hydrogen at the working electrode outlet is another main drawback in the ERC system. In the electrochemical environment, H_2 production has an almost similar type of reduction potential as CO_2. Thus a huge amount of energy for the CO_2 electrochemical reduction is utilized in the H_2 formation (Ohya et al., 2009). This reduces the faradaic efficiency of the CO_2 electrochemical reduction. The selective and single product formation is also another disadvantage in this process. Many catalysts can selectively produce HCOOH and CO only, but the selective production of the hydrocarbons and alcohol are still elusive.

In the electrochemical reduction of CO_2 various hydrocarbons and oxygenates are formed. During the reaction, formic acid is the easily produced reduction product from CO_2 as the addition of two hydrogen atoms is preferably less complicated as there is also no need to break the C-O bond. After that, the other products can be generated depending on the catalysts and other factors. Thus, tuning in the experimental conditions, electrocatalysts, and electrolytic solutions are essential to make the reaction selective towards a particular product. Theoretical calculations have been pursued to understand the mechanism and the various intermediates generated during the formation of various CO_2 reduced products *via* multiple proton and electron additions. In Scheme 2.1, a proposed mechanism for various proton insertion reactions during ERC is shown (Ma et al., 2016; Ren et al., 2018; Zheng et al., 2019).

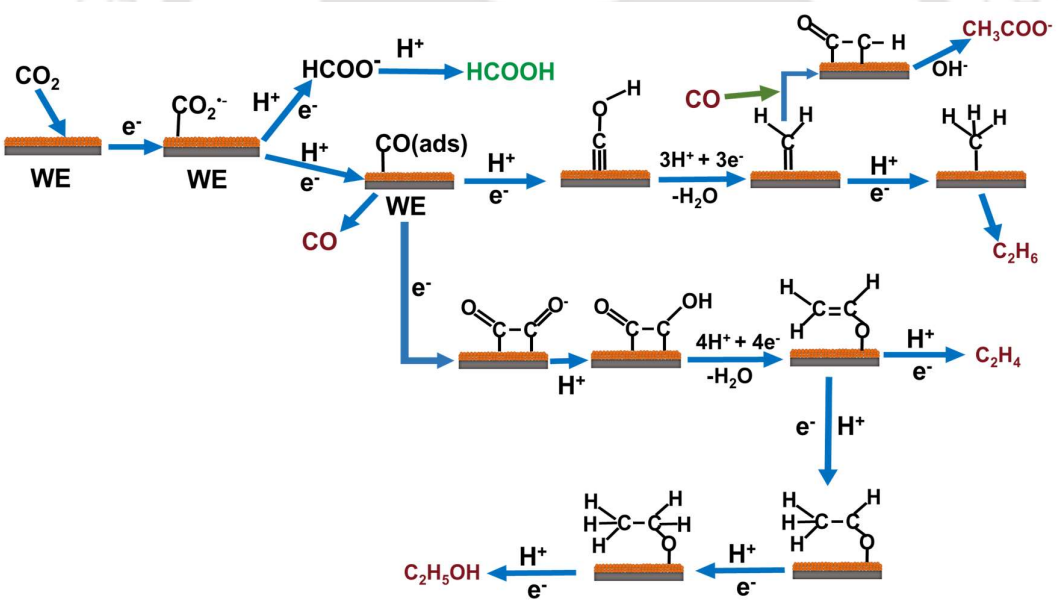

Scheme 2.1: Proposed pathway for various ERC product formation.

2.2 Solution chemistry in the electrochemical reduction of CO_2

Carbon dioxide is soluble in water and other organic solvents. Most of the experiments were done in aqueous bicarbonate solutions by scientists worldwide. Initially,

the pH of the 0.5 M bicarbonate solution was 8.5. During the experiment of CO_2 reduction, the gaseous CO_2 is bubbled for at least 45 minutes to get a proper CO_2 saturated electrolyte (pH 7.0). The electroactive state of the soluble CO_2 is H_2CO_3 which is present within pH 2 to 8.5. At high pH (≥ 8.5), a less electroactive species CO_3^{2-} is abundant in a solution (Tan et al., 1995). At very low pH, H_2 production is more feasible than the CO_2 reduction and thus the neutral pH is set for the reduction. The choice of cation and anion also affects the selectivity of the production. The H_2 evolution was favorable with the sequence of Li^+> Na^+>Cs^+>K^+. The hydrogen gas formation is least among all alkali metals in the presence of K^+ of $KHCO_3$ (Murata and Hori, 1991). Not only that, but the product selectivity is also affected by the concentration of the bicarbonate. The cathodic reduction of CO_2, CO, and H_2O produce OH^- during the production of HCOOH releases OH^- (Eqns 2.1 to 2.4).

$$CO_2 + 6H_2O + 8e^- \rightarrow CH_4 + 8OH^- \quad (2.1)$$

$$CO + 5H_2O + 6e^- \rightarrow CH_4 + 6OH^- \quad (2.2)$$

$$2H_2O + 2e^- \rightarrow H_2 + 2\,OH^- \quad (2.3)$$

$$CO_2 + H_2O + 2e^- \rightarrow HCOO^- + OH^- \quad (2.4)$$

The OH^- produced by the CO_2, is continuously neutralized by the HCO_3^- of the bicarbonate. Thus, the higher concentration of the bicarbonate also helps in product formation (Murata and Hori, 1991; Ogura, 2013; Yano et al., 2004). At a high pressure of gaseous CO_2 saturated conditions (60 atm) the formation of hydrocarbons was increased in 0.1 M $KHCO_3$ electrolyte (Kudo et al., 1993). In 0.5M H_2SO_4 solution iron metal as electrocatalyst (Fe/C catalysts) produces CH_4, HCHO, C_2H_6, C_2H_5OH at 25°C, and 1 atm pressure during ERC (Pérez-Rodríguez et al., 2011). In 2013, a group of scientists used $KHCO_3$ as the electrolytic solution and various metals as electrodes. Among them, Rh, Pt, Ni produces CO and formic acid under 30 atm pressure of CO_2 and they also claimed that

the hydrogen evolution is more at 1 atm pressure. So when the amount of CO_2 has increased the generation of formic acid, and CO was more than the H_2 evolution reaction (HER) (Thorson et al., 2013).

The CO_2 gas is less soluble in an aqueous solvent (4 times lower) than in a methanol solution. In methanol electrolyte solution, the oxides of Cu metal (Cu_2O and CuO) can selectively reduce CO_2 to mostly ethylene and then various other hydrocarbons (Ohya et al., 2009). That is why methanol is used to absorb CO_2 in industries which is known as the rectisol method. ERC can also take place at low temperatures because at low temperatures the solubility in methanol increases. The products can be methane, CO, and ethylene. However, the production of ethylene was lower in methanol solution than when aqueous $KHCO_3$ was used as the electrolytic solution according to Mizuno and his team (Mizuno et al., 1995). Some researchers have varied the concentration of CO_2 in the methanol system for ERC. A high concentration of CO_2 is beneficial for its mass transfer (Saeki et al., 1995). At $CO_2 + CH_3OH$ electrolyte, the FE of hydrocarbon formation using a Ni electrode reached 23.5% with 200 $mA.cm^{-2}$ partial current density. But in an aqueous system H_2 is the major product using the same electrode. The solubility of the gaseous CO_2 is more in methanol than in an aqueous system and thus the reduction rate increases (Saeki et al., 1996). CSOH/methanol also can be used as electrolytes with Cu electrodes where methane can be formed. Using this electrolyte solution also the hydrogen evolution reaction can be reduced to 23% (Kaneco et al., 1999). CO_2 is more soluble in clathrate hydrates electrolyte than in aqueous solutions. For example, 170 L of CO_2 gas can be trapped in 1 L of clathrate hydrates which is two orders of magnitude greater than the solubility of CO_2 in water. Clathrate hydrates as the electrolyte can reduce the production of hydrogen gas formation. The presence of clathrate hydrates helped in the production of carbon monoxide. The

faradaic efficiency of CO and methane increased when clathrates are present (Deciccio et al., 2015).

Solid polymers also can be used as the electrolyte in the ERC reaction. These systems produce mostly gaseous products from CO_2. A copper/Nafion electrode was used as the WE and reported 20% of FE for hydrocarbon production at −2.00 V vs. saturated calomel electrode (SCE). The increase in negative potential and the increase in proton concentration in the counter solution cause a decrease in FE of ERC products due to an increase in proton reduction. Similarly, if the proton concentration decreases to alkaline pH, the hydrocarbon production decreases due to a lower percentage of the proton (Dewulf and Bard, 1988). Using Cu-based cation and anion exchange membranes used as solid polymer electrolytes, the FE of the production of hydrocarbons can reach up to 19 to 27% (Komatsu et al., 1995). SPEEK and Nafion membrane can be used as electrocatalysts. This process was very exciting because it was successful in the lower alkaline solution also. This process was free from undesired hydrogen production (Aeshala et al., 2012). It is also proved that an anionic solid electrolyte is more favorable than a cationic solid electrolyte (Aeshala et al., 2013).

Though scientists have used many non-aqueous electrolytes, the aqueous medium provides better results towards the formation of hydrocarbons than the non-aqueous medium (Scibioh and Viswanathan, 2004). In 2010 a group of researchers claimed that using Ag as electrocatalyst and with decreasing temperature the formation of carbon monoxide increases and the formation of H_2 decreases. They also stated that, at a low concentration of the aqueous electrolyte, CO formation increases (Lee et al., 2010). In ERC, with the decreasing pH, the reduction rate decreases because of the increase in H^+ ions in the solution results in hydrogen gas production. That is why it is more favorable to use alkali electrolytes to avoid hydrogen evolution. Some researchers produced a model using

the product formation ratio and the solution pH. Bumroongsakulsawat and Kelsall (2014) proposed more than one intermediates (protonation states of CO_2) during the formation of CO from CO_2. Those intermediates can produce CO or HCOOH with higher value of protonation states of CO_2.

2.3 Effect of metal electrodes in ERC

In the ERC process, several metal electrocatalysts were used as the cathode to produce various products by many scientists. Metals as an electrocatalyst can reduce CO_2 into CO, hydrocarbons, alcohols, and acids, etc. Noble metals such as Ru, Pd, Pt, Ir, Ag, Au, transition metals such as Co, Cu, Ni, Zn, Ti, and main group metals such as In, Sn, Pb can be used as electrocatalysts to reduce CO_2. Pb, Hg, In, Sn, Cd, and Ti mostly produce formate or formic acid (HCOOH) under various experimental conditions whereas, Au, Ag, Zn, Pd, and Ga usually produces carbon monoxide (CO). Copper metal (Cu) and various modifications over Cu metals mostly produce hydrocarbons and alcohols (Albo et al., 2015; Furuya et al., 1997; Hori et al., 1985). Ag and Au are well known for their ability to reduce CO_2 into CO in $KHCO_3$ (Hori et al., 1985; Zhou et al., 2014). Pt gas diffusion electrode was able to produce CH_4 (27.9% FE) as the main product and CO (3%), C_2H_6 (0.10%), C_2H_4 (0.46%), HCOOH (8.8%) and C_2H_5OH (1.9%) as minor products at −1.82 V vs. Ag/AgCl (Hara et al., 1997).

However, the use of noble metals in catalyzing various reaction in a large scale is not possible because of its high cost. Thus, the scientists have chosen the earth abundant transition and main group metals also for their low cost in ERC. Hydrocarbons (especially CH_4) has always been a better choice as fuels in various sectors than the already used fossil fuels. Most of the transition metals were reported either for the formation of CO, HCOOH, or trace amount of CH_4 only. To form the C-C bond and produce C_2 products (hydrocarbons and alcohols) are the most challenging task. Cu metal and its derivatives are reported as

electrocatalysts for hydrocarbon production (Gonçalves et al., 2010; Y. Hori et al., 2005; Kuhl et al., 2012; Lee and Tak, 2001; Saeki et al., 1996; Yano et al., 2004). The production of hydrocarbons depends upon various factors. In 1986, Hori and his group claimed that the temperature harms the formation of the product. CH_4 formation efficiency is highest (65%) at 0°C which decreases with an increase in temperature (0% at 40°C). But, C_2H_4 formation rises with an increase in temperature. The presence of longer-lived intermediates is the key reason behind the higher FE of CH_4 at a lower temperature (Hori et al., 1986). Metal loaded gas diffusion electrode can increase the product formation efficiency than the metal foil electrodes. The surface contact between the metal and the electrode material increases the interaction between these two and thus rises the productivity (Mahmood et al., 1987). Cu is the most widely used electrocatalyst for hydrocarbon and alcohol formation but the poisoning of the metal surface limits its application on a large scale (Hori et al., 2005). The adsorption of some species such as graphite, coming from the CO_{ad} may be the reason for metal surface poisoning. Cu metal has a high affinity to bind with oxygen which induces the various organic products to contaminate it during the reaction (Lee and Tak, 2001).

The main group metals such as Pb, Sn, Bi, and In were also reported for their catalytic activity for the reduction of CO_2 to HCOOH only (Baruch et al., 2015; Dimeglio and Rosenthal 2013; Narayanan et al., 2011; Prakash et al., 2013; Subramanian et al., 2007) Using Pb, Hg and In electrodes, the Faraday efficiency of formation of HCOOH increases with the increasing pressure of CO_2. The Pb cathode in the $KHCO_3$ system showed a better result in terms of FE (95%) and current densities (Köleli and Balun, 2004). In 0.5 M $KHCO_3$ and 0.5 M K_2CO_3 electrolyte solution, Pb and Sn electrode as electrocatalysts produce the only formate as the reduction product. The Pb/$KHCO_3$ system showed a better result in terms of FE and current densities (Koleii et al., 2003). However, the Sn gas

diffusion electrode has better efficacy in ERC than the metallic Sn surface. In 2009, Innocent and his co-workers reported formate with a high FE (65 to 90%) using lead as the working electrode in NaOH electrolyte (0.5 $M.L^{-1}$) (Innocent et al., 2009). In a mixture of 0.45 M $KHCO_3$ and 0.5 M KCl catholyte solution, the Pb plate as cathode reduces CO_2 to formate (Alvarez-guerra et al., 2012). In K_2SO_4 electrolyte anodized indium metal is catalytically active for the production of formate at −1.40 V vs. saturated calomel electrode (SCE) (Detweiler et al., 2014). The recent reports of ERC on the metallic surfaces are depicted in Table 2.1.

Table 2.1: Selected reports on electrochemical reduction of CO_2 using various metals.

Electrocatalyst used	**Electrolyte**	**Experimental parameters**	**Main products (Faradaic efficiency, %)**	**References**
Cu	0.1 M $KHCO_3$	−1.10 V vs. RHE	CH_4 (1.7%), HCOOH (8.7%), C_2H_5OH (12%) and C_2H_4 (51%)	Kim and Palmore, 2020
Dendritic bismuth	0.1 M $KHCO_3$	−0.70 V vs. RHE	HCOOH (95%)	Piao et al., 2019
Cu_2O-deposited carbon black	Methanol	−1.90 V vs. Ag quasi reversible electrode (Q.R.E)	CH_4 (26.9%) and C_2H_4 (13.4%)	Uemoto et al., 2019
Fe–N–C catalysts	0.1 M $KHCO_3$	−0.60 V vs. RHE	CO (85%)	Leonard et al., 2018
Au-Pt	0.1 M $KHCO_3$	−0.65 V vs. RHE	CO (45%)	Ma et al., 2017
Ag-CeO_x/C	0.1 M $KHCO_3$	−0.89 V vs. RHE	CO (92.6%)	Gao et al., 2017
Carbon nanotube decorated with Pt electrode	0.1 M $KHCO_3$	Superficial CO_2	HCOOH (59-89%), CO (3-11%), CH_3OH (0-1.9 %), CH_4 (2-33%)	Jiménez et al., 2017
Cu foil	0.1 M $KHCO_3$	−1.20 V vs. RHE	CH_4, CO (97%), C_2H_4	Kumar et al., 2016a
Cu mesocrystals	0.1 M $KHCO_3$	−0.99 V vs. RHE	CH_4 (1.5%), C_2H_4 (27.2%)	Chen et al., 2015
$Pd_xPt_{(100-x)}$/C nanoparticle	0.5 M H_2SO_4	−0.40 V vs. RHE	HCOOH (88%)	Kortlever et al., 2015
Cu nanocube electrocatalysts	0.1 M $KHCO_3$	−0.60 V vs. RHE	C_2H_4	Roberts et al., 2015

2.4 Effect of oxides of metals as electrocatalysts

The oxide of metals was also used as an electrocatalyst in ERC by many researchers. Oxides of metals have a higher CO_2 adsorption capability than pure metals and are more stable than their metal counterparts. The use of pure copper metal and its derivatives have always been advantageous because of its ability to produce hydrocarbons. Cu metal has a high affinity to bind with oxygen that is why the organic products can easily contaminate it during the reaction (Lee and Tak, 2001). The oxide form of copper is more favorable for hydrocarbon production than the pure metal. Not only that, but Cu_2O also has a greater affinity to adsorb CO than metallic Cu which finally helps in achieving higher FEs. The main reason behind this is the heat of adsorption of CO (it describes the amount of energy is released when produced CO is adsorbed onto the catalytic surface) gas over the Cu_2O surface is higher than the metallic Cu surface. Cu_2O can reduce CO_2 to $\bullet CO_2^-$ intermediate at lower overpotential than metallic Cu (Li and Kanan, 2012). Adsorption of the produced CO on the surface of the electrode and interaction of it with the atomic hydrogen at the reaction surface helps in the formation of hydrocarbons (Terunuma et al., 1997). Air oxidized Cu foil, anodized copper foil, and electrodeposited Cu_2O thin films were used as electrocatalyst in a 0.5 M $KHCO_3$ electrolyte solution by Le and his group in ERC. They stated that the Cu(I) species is selective towards CH_3OH formation and in their study, the CH_3OH formation was highest (43 $\mu mol.cm^{-2}.h^{-1}$ with 38% FE) using Cu oxide which is much higher than the other two electrocatalysts (air oxidized Cu foil and anodized copper foil) (Le et al., 2011). Copper (I) halide also has a higher affinity to adsorb CO than the metallic Cu and produces intermediate CH_{rad} which leads to the production of C_2H_4 (Yano et al., 2004).

In addition to oxides of Cu, other metal oxides such as NiO, ZnO, CO_3O_4, PbO_2, and RuO_2 can reduce CO_2. Co-precipitated $Cu/ZnO/Al_2O_3$ catalysts at high pressure (350

bars) reduce CO_2 above 95% and produce CH_3OH (selectivity>98%). It can further produce alkenes (42%) and alkane (85%) with modified experimental conditions (Bansode and Urakawa, 2014). In 2015, Bashir and his team introduced NiO based carbon nanotube which can reduce CO_2 to CO (FE 35.2%) at −1.70 V vs. NHE in sodium bicarbonate solution (Bashir et al., 2015). Ultrathin Co_3O_4 produces $HCOO^-$ with 60% FE in the 0.1 M $KHCO_3$ solution at −0.88 V vs. SCE (Gao et al., 2016). In 2013, a group of researchers deposited Cu nanocluster over single-crystal ZnO powder and was used as an electrocatalyst in an aqueous bicarbonate solution. The Cu/ZnO electrocatalyst was able to produce various products such as CO, CH_4, C_2H_4, $HCOO^-$, CH_3OH, C_2H_5OH, CH_3COO^- and trace amount of C_3H_7OH also in −1.40 V vs. Ag/AgCl (Andrews et al., 2013). Lead oxide is also well known for its ability to reduce CO_2 to HCOOH mainly. Electrochemically synthesized Pb_2O was able to reduce CO_2 to HCOOH (60% FE) at −2.00 V vs. SHE in the $KHCO_3$ solution (Yadav and Purkait, 2015). Sometimes the surface modification of the oxide surface provides better performance in terms of better product formation and FE. A group of researchers modified Pt metal surface with RuO_2/TiO_2 and compare their role with RuO_2/TiO_2 composite electrode in ERC. The modified composite electrode showed better performance for CH_3OH production (61% FE) than the RuO_2/TiO_2 composite (40% FE) (Qu et al., 2005). The recent reports of ERC on the metal oxides surfaces are shown in Table 2.2.

Table 2.2: Selected reports on electrochemical reduction of CO_2 using various metal oxides.

Electrocatalyst used	Electrolyte	Experimental parameters	Main products (Faradaic efficiency, %)	References
nBuLi-Bi	1.0 M $KHCO_3$	−0.77 V vs. RHE	$HCOO^-$ (97%)	Fan et al., 2020
$Cu(OH)_2$	0.1 M $NaHCO_3$	−1.60 V vs. Ag/AgCl	C_2H_4 (25%) and C_2H_5OH (5%)	Iijima et al., 2019
CuO nanoparticles	0.5 M $KHCO_3$	−1.05 V vs. RHE	C_2H_4 (70%)	Kim et al., 2019
CO_3O_4	0.1 M $TBAPF_6$ in ACN solution	−1.50 V vs. NHE	CO (65%) and HCOOH (27%)	Aljabour et al., 2018
Commercial PbO_2	$[Bzmim]BF_4$	−2.30 V vs. Ag/Ag^+	HCOOH (95%)	Wu et al., 2018
Cu/TiO_2	0.2 M KI	−0.75 V vs. RHE	C_2H_5OH (43.6%)	Yuan et al., 2018
Cu	0.1 M $KHCO_3$	−1.80 V vs. Ag/AgCl	C_2H_4 (60%)	Baturina et al., 2017
Au-CeOx /C	0.1 M $KHCO_3$	−0.89 V vs. RHE	CO (89.1%)	Gao et al., 2017
Oxide derive (OD)-Pb	distillable ionic liquid solution	−1.84 V vs. $Cc^{0/+}$ (where Cc^+ = cobaltocenium)	CO (10%), and $HCOO^-$ (62%)	Chen et al., 2017
CO_3O_4	0.1 M $KHCO_3$	−0.87 V vs. SCE	CO and $HCOO^-$ up to 10 and 80%	Gao et al., 2017
Cu_2O-MWCNTs	0.5 M $NaHCO_3$	−0.80 V vs. Ag/AgCl	CH_3OH (38%)	Malik et al., 2016
RuO_2	Aqueous electrolyte	−0.43 V vs. RHE	HCOOH, CH_3OH, CO, and CH_4	Karamad et al., 2015
OD-Pb	0.5 M $NaHCO_3$	−1.00 to −0.75 V vs. RHE	$HCOO^-$ (~100%)	Lee and Kanan, 2015
Cu_2O films	0.1 M $KHCO_3$	−0.99 V vs. RHE	C_2H_4 (34-39%), C_2H_5OH (9-16%), CH_4 (<1)	Ren et al., 2015

2.5 Metal complexes as electrocatalysts

Metal catalysts are easily available but the metal catalyst can easily get poisoned, produces mainly one or two products with a low FE. Not only that, but many of the noble metals also has a high cost. Thus, the researchers have modified the metals into various complexes which can reduce this difficulty for ERC. The complexes can produce various reduced products (hydrocarbons, alcohols, and acids) with higher FE than pure metals (Lieske et al., 2018). The metal complexes can be designed easily by choosing any suitable

ligand and metal centre. Not only that, but the incorporation of electron-withdrawing or electron-donating groups in the metal complexes can also enhance the efficiency of the complexes as well as decrease the reduction potential (García et al., 2014). A detailed review on the metal complexes, their activity, production of CO, hydrocarbons, and alcohols, and the probable mechanism of the production of gaseous and liquid fuels are detailed by many groups of researchers (Benson et al., 2009; Elgrishi et al., 2017; Feng et al., 2017; Inglis et al., 2012; Kumar et al., 2016b; Laitar et al., 2005; Louis et al., 2019).

At first, hexa-aza-macrocycles was derived from the condensation of 1, 10-phenanthroline, and then Co(II) complex was synthesized and the complex was used as an electrocatalyst in the ERC. CO and HCOOH were detected as the reduction product in DMF/TBAP electrolyte solution (Isaacs et al., 2003). In acidic acetonitrile solution, [Pd(triphos)(solvent)]$(BF_4)_2$ complex as electrocatalyst produces CO from CO_2 (Dubois 1997; Dubois et al., 1991). In 2015, Issacs and his team used poly-M-aminophthalocyanines (M = Co, Ni, and Fe) in ERC. They claimed that the centre metal atom was responsible for the product formation selectivity. Ni metal complex was able to produce HCHO and HCOOH, whereas the copolymer was selective for HCOOH. The Fe polymer was reported for HCHO and H_2 production only (Isaacs et al., 2005). $Ni(cyclam)^{2+}$ and $Ni_2(biscyclam)^{4+}$ were also reported for their ability to selectively produce CO from CO_2 (Beley et al., 1986; Collin et al., 1988). Carbon supported, nitrogen-based organometallic silver catalysts are active in the field of ERC. They show almost similar results with Ag metal having a low loading of metal. Faradaic efficiency for the production of CO is above 90%. An addition of amine ligand to Ag/C, the partial current density for CO increases in 1 M KOH solution (Tornow et al., 2012). Several cobalt porphyrins (CoP) have been used to produce CO from CO_2 by photochemical, radiation chemical, and electrochemical methods in aqueous and organic solvents. The $Co^{I}P$ state is stable at high

pH but is shorter-lived in neutral and acidic solutions. One-electron reduction of $Co^{I}P$ leads to the formation of an intermediate species and which is the active state of reduction of CO_2 (Behar et al., 1998). In 2017, Co–phthalocyanine molecules modified carbon nanotubes in a 0.5 M $KHCO_3$ solution exhibited a higher FE (>95%) but the product was only C_1 (CO) and not C_2 (Zhang et al., 2017).

C_2 product formation was also observed using metal complexes. A triangular rhodium complex selectively produced oxalate and formate at −1.50 V vs. SCE in CH_3CN solution (Kushi et al., 1994). In 0.5 M KCl solution, crystalline copper(II) phthalocyanine catalyst produced C_2H_4 (FE 25%) selectively (Kusama et al., 2017). In CH_3OH + 0.1% solution of $KHCO_3$ in 0.05 M Bu_4NBF_4 electrolyte solution, an electropolymerized tetraamino-substituted copper monophthalocyanine (poly^{NH_2}PcCu) was also reported for their ability to reduce CO_2 into CO (FE 5-9%), CH_4 (FE 0-0.5%) and HCOOMe (30-40%) (Magdesieva et al., 2002). At −0.98 V vs. RHE, copper(II) porphyrin complex produced CH_4 and C_2H_4 (total FE 47%) in 0.5 M $KHCO_3$ solution. A multilayer porphyrins/polyoxotungstate electrode was introduced in ERC in a 0.1 M $NaClO_4$ solution. Among them Ni(II)TRP]$^{5+}$ was reported for CO and HCOOH, Mn(II)TRP]$^{5+,}$ and Zn(II)TRP]$^{5+}$ was reported for the production of HCOOH and methanol (García et al., 2014). In potassium chloride electrolyte, a pyridine derivative, [PYD]@Cu–Pt electrocatalyst reduces the CO_2 and produces CH_3OH, HCOOH, and C_2H_5OH (Yang et al., 2016). In 2017, dihydropyridines (DHPs) were also reported for the production of $HCOO^-$ and CH_3OH 0.1 M $LiClO_4$ in CH_3CN/H_2O electrolyte (Giesbrecht and Herbert, 2017). A Ru(II) polypyridyl carbene complex was coated over N doped porous carbon which was used as electrocatalysts in the $KHCO_3$ solution. A FE of 21 to 27% was achieved for C_2H_5OH production and FE of 7.1 to 12.5% was achieved for CH_3COO^- production at −0.87 to −1.07 V (vs. normal hydrogen electrode) (Liu et al., 2019). In 2019, a group of

researchers claimed that the cobalt phthalocyanine electrocatalyst at first reduces CO_2 to CO. CO is then act as a reactant to produce CH_3OH (Boutin et al., 2019).

Cu and Ni salen complex was introduced in direct electrochemical CO_2 reduction (DERC) by Singh et al. (2015) which can reduce the activation potential of the CO_2 reduction reaction. They claimed that during the process, the metals are reduced from M^{+2} to M^{+1} and form a complex with CO_2^- radical compound. The M^{+1} again goes back to its oxidation state M^{+2}; thus reduce CO_2. They also claimed that the anchoring group plays a significant role in the formation of C_1 and C_2 hydrocarbons (Singh et al., 2015). In another study, a Cu–porphyrin (PorCu) complex with a built-in -OH group was reported to exhibit better catalytic activity compared to its -OH free $PorCH_3Cu$ complex congener in ERC in $KHCO_3$ electrolyte at various applied potentials (Weng et al., 2016). The active state of CO_2 reduction is the M^{+1} state. Thus the onset potential of the CO_2 reduction solely dependent on the conversion between the M^{+2} to the M^{+1} state (Shen et al., 2015). The recent reports of ERC on the metal complexes are shown in Table 2.3.

Table 2.3: Reports on electrochemical reduction of CO_2 using various metal complexes during 2015-2020.

Electrocatalyst used	Electrolyte	Experimental parameters	Main products (Faradaic efficiency, %)	References
Fac-[Re(bpy)(CO)$_3$Cl] ([Re-Cl]) complex	CO_2-saturated KOH and K_2CO_3 solution	−0.68 V vs. RHE	CO (90%)	Sato et al., 2020
CoPc complex	0.1 M $KHCO_3$	−0.80 V vs. RHE	CO (99%)	Xia et al., 2020
Pd/NbN complex	0.5 M $NaHCO_3$	−0.60 V vs. RHE	CO (38.4%)	Liu et al., 2020
Cobalt phthalocyanine complex	0.5 M $NaHCO_3$	−0.92 V vs. RHE	CO (95%)	Wang et al., 2019
Ru(II) poly-pyridyl carbene complex	0.5 M $KHCO_3$	−0.87 V to −1.07 V vs. NHE	C_2H_5OH (21-27.5%) and CH_3COO^- (7.1-12.5%)	Liu et al., 2019
CoPc-CN complex	1 M KOH	−0.49 V vs. RHE	CO (100%)	Iijima et al., 2019
Di-nuclear Ni complex	Acetonitrile solution	−1.16 V vs. NHE	CO (95%)	Cao et al., 2018
Copper(II) phthalocyanine	0.5 M $KHCO_3$	−1.06 V vs. RHE	CH_4 (66%)	Weng et al., 2018
Cu-C_3N_4 complex	0.1 M $KHCO_3$	25°C	CO, CH_3OH, HCOOH, and C_2H_4	Jiao et al., 2017
[Mn^+(cyclam)Cl_n] (M = Ni^{2+} and Co^{3+})	$BMImBF_4$	−1.40 V vs. Ag/AgCl	CO (95.2% for Ni and 85.9% for Co)	Honores et al., 2017
Cobalt porphyrin	0.1 M $HClO_3$	25°C	CO, CH_4, H_2, HCOOH, CH_3OH	Shen et al., 2015

2.6 Other metal derivatives as electrocatalyst in ERC

Other metal derivatives can be metal carbides, sulfides, alloy, composites, mesh and bimetals, etc. which are not that much familiar in the field of ERC. An electrodeposited Cu metal on Ni was used in ERC in an H-type reactor in 0.500 M $KHCO_3$ in water with CH_3OH electrolyte solution. CH_4, C_2H_4, HCOOH, and CO were produced from the reduction of CO_2 (Kaneco et al., 2007). Cu electrodes were modified using electrodeposits and introduced in ERC which selectively produced CH_4 and C_2H_4 (Gonçalves et al., 2010). Au oxide derived Au nanoparticles can reduce CO_2 at lower overpotential (140 mV). Polycrystalline Au and conventionally prepared Au nanoparticles need more overpotential

(200 mV) than this catalyst and are active for a very short time. Production of the $CO_2^{\bullet-}$ intermediate increases the activity of the catalyst (Chen et al., 2012). Using Au nanoparticle in aqueous $KHCO_3$ solution reduction of CO_2 to CO is possible. Between various particles sizes of NP, 8 nm AuNP results in better performance. Intermediate COOH* formation is the reason for the better performance of the ERC reaction (Zhu et al., 2013). Cu nanoflower (NF) catalyst, derived from CuO NFS with a unique 3D chrysanthemum-like structure can reduce CO_2 at low overpotential than Cu (400 mV lower). The faradaic efficiency of H_2 production can be reduced by 25%. The surface deposited amorphous carbon was seen and catalytic activity protocol was derived (Xie et al., 2014). Cu-Au alloy can act as electrocatalysts in the CO_2 reduction in an aqueous 0.5 M $KHCO_3$ solution. It was seen from linear sweep voltammogram the activity of the catalyst. The selectivity and the formation of the products (CH_3OH and C_2H_5OH) solely depend upon the compositions of the catalyst (Jia et al., 2014).

The particle size of the nanoparticles has a great role during the reduction reactions. The lesser size of the particle assists in a higher amount of product generation. Cu-NP below 5 nm gives a better result for the formation of hydrocarbons (CH_4 and C_2H_4) (Reske et al., 2014). Another study also shows a similar result was using 3.7 nm particle-sized Pd-NP showed 91.2% faradaic efficiency for the production of CO where the 10.3 nm Pd-NP exhibited only 5.8% faradaic efficiency (Gao et al., 2015). Gd_2O_3 nanoparticles were reported for the production of CO in 0.1 M TBAH/CH_3CN electrolyte solution (Behnamfar 2015). In 0.1 M $KHCO_3$ solution Cu_2O films were reported for the production of C_2H_4 (FE 34-39%), C_2H_5OH (FE 9-16%) and CH_4 (FE<1%) at −0.99 V vs. RHE, 25°C, 1 atm (Ren et al., 2015). In 0.2 M KI electrolyte solution, Cu nanoparticles were also reported for C_2H_5OH (FE 35%), C_3H_7OH (FE 5%) production during ERC (Chi et al., 2014). A Cu-Au alloy as electrocatalyst reported for the production of CH_3OH which is 19 times greater

than the Cu plate as an electrocatalyst. The FE of production of C_2H_5OH was also increased by 12% in a phosphate-buffered solution as electrolyte (Jia et al., 2014). Metallic silver surfaces as electrocatalyst reported CH_4, HCOOH, CH_3OH, C_2H_5OH in 0.1 M $KHCO_3$ electrolyte solution (Hatsukade et al., 2014). A bimetallic Pd-Pt nanoparticle selectively produced HCOOH (FE 90%) in phosphate buffer solution (Kortlever et al., 2015). Cu mesocrystal catalysts were also selective towards C_2H_4 formation during ERC in 0.1 M $KHCO_3$ (Chen et al., 2015). In 2016, a porous hollow fiber copper electrode (three-dimensional geometry) was reported for their ability to produce CO (FE 85%) (Kas et al., 2016). A boron and nitrogen co-doped nanodiamond was reported for their selectivity towards ethanol production with FE 93.2% at −1.00 V vs. RHE by a group of researchers (Liu et al., 2017). In 2017, copper nanoparticles on carbon nanotubes were used as a cathode which produced CH_3COOH during ERC. A carbon-based selectivity of 56% and 7000 h^{-1} of Turnover number (TOF) was achieved for CH_3COOH. The other products observed were HCOOH and CH_3OH (Genovese et al., 2017). Whereas, A Cu/TiO_2 showed a FE of 27.4% for C_2H_5OH production which is almost 10 fold higher than Cu-NP as electrocatalyst at the same experimental conditions (Yuan et al., 2017). Recently a group of scientists synthesized a 3D dendritic copper-cuprous oxide composite by reduction of the electrodeposited copper complex. Then they introduced the composite in ERC and produced C_2H_5OH and CH_3COOH (total FE 80%) (Zhu et al., 2019).

2.7 Scope of improvement

In the electrochemical reduction of carbon dioxide (ERC), electro-catalysts play an important role in the harvesting of several useful products. The discussion over electro-catalysts in ERC reveals that there are enough possibilities for syngas (CO + H_2), hydrocarbons, and alcoholic products formation. However, there are various challenges to

overcome for the development of this process. The major obstacle is to minimize the competitive hydrogen evolution reaction which is one of the important causes for the underperformance of CO_2 reduction. Another requirement is to improve the selectivity of the catalysts towards the alcohols and hydrocarbons formation for which more focus should be devoted to optimizing the ERC process parameters as well as modification of the catalysts. Energy consumption for carrying out the process needs to be minimized and it requires the development of electro-catalysts which can lessen the overpotential to make the system energy efficient. The development of hydrocarbons is rather difficult as it includes breaking of the C-O bond. To overcome the overpotential issues and production of both C_1 as well as C_2 products, the use of metal complexes can be advocated. Usually copper metal and its derivative assistances in C_1 as well as C_2 product formation. Metal complexes also can be tuned in an efficient way which can also result in hydrocarbon and alcohol formation.

From the library of literature, we are aware of the fact that there is a prerequisite to research on producing renewable fuels to meet the ever-increasing energy demands and reduce the load on the consumption of fossil fuels. Therefore, the primary objective of this thesis work is to devise a greener process to produce those fuels. To further explore the process, designing a new class of electro-catalysts is essential. Production of gaseous and liquid fuels at lower over-potential with greater Faradaic efficiency is limited in the field of ERC. There is an emergence to investigate the role of metals and their derivatives to achieve these targets. Therefore, the following objectives are taken into considerations.

2.8 Objectives of the work

1. To fabricate divided electrochemical cells for ERCs of CO_2 using proton exchange membrane and derive fundamental electrochemical and process parameters for the formation of specific chemicals.

2. To synthesize selected transition and main group metal oxides (Cu, Ni and Pb) and Investigate their catalytic-role in ERC in an aqueous bicarbonate medium.
3. To synthesize Cu-salen [$Cu^{II}(L^{NH_2})$] metal complex (**1**), Ni-salen [$Ni^{II}(L^{NH_2})$] metal complex (**2**) and Pb-salen metal complexes ([$Pb^{II}(L^{NO_2})$] complex (**3**), and [$Pb^{II}(L^{NH_2})$] complex (**4**)) with various functional/anchoring groups in the ligand backbone and understand their role in ERC forming acids and alcohols.

References

Aeshala, L. M., Rahman, S. U., and Verma. A., 2012. "Effect of Solid Polymer Electrolyte on Electrochemical Reduction of CO_2." *Separation and Purification Technology,* 94, 131-37.

Aeshala, L. M., Rahman, S. U., and Verma. A., 2013. "Effect of Cationic and Anionic Solid Polymer Electrolyte on Direct Electrochemical Reduction of Gaseous CO_2 to Fuel." *Journal of CO_2 Utilization,* 3-4, 49-55.

Albo, J., Alvarez-Guerra, M., Castaño, P., and Irabien A., 2015. "Towards the Electrochemical Conversion of Carbon Dioxide into Methanol." *Green Chemistry*, 17, 2304-2324.

Aljabour, A., Coskun, H., Apaydin, D. H., Ozel, F., Hassel, A.W., Stadle, P., Sariciftc, N. S., and Kus, M., 2018. "Nanofibrous Cobalt Oxide for Electrocatalysis of CO_2 Reduction to Carbon Monoxide and Formate in an Acetonitrile-Water Electrolyte Solution." *Applied Catalysis B: Environmental,* 229, 163-170.

Alvarez-guerra, M., Quintanilla, S., and Irabien. A., 2012. "Conversion of Carbon Dioxide into Formate Using a Continuous Electrochemical Reduction Process in a Lead Cathode." *Chemical Engineering Journal,* 207-208, 278-284.

Andrews, E., Ren, M., Wang, F., Zhang, Z., Sprunger, P., Kurtz, R., and Flake, J., 2013. "Electrochemical Reduction of CO_2 at Cu Nanocluster/$(10\bar{1}0)$ ZnO Electrodes." *Journal of The Electrochemical Society,* 160, H841-846.

Bansode, A., and Urakawa, A., 2014. "Towards Full One-Pass Conversion of Carbon Dioxide to Methanol and Methanol-Derived Products." *Journal of Catalysis*, 309, 66-70.

Baruch, M. F, Pander III, J. E., James L White, J. L., and Bocarsly, A. B., 2015. "Mechanistic Insights into the Reduction of CO_2 on Tin Electrodes Using in Situ ATR-

IR Spectroscopy." *ACS Catalysis,* 5, 3148-3156.

Bashir, S. M., Hossain, S. S., Rahman, S., Ahmed, S., and Hossain, M. M., 2015. "NiO/MWCNT Catalysts for Electrochemical Reduction of CO_2." *Electrocatalysis,* 6, 44-53.

Baturina, O., Qin, L., Feng, X., Dyatkin, Boris, D., Xiahan, S., Raymond, U., Todd, B., and Yury, G., 2017. "Effect of Nanostructured Carbon Support on Copper Electrocatalytic Activity toward CO_2 Electroreduction to Hydrocarbon Fuels." Catalysis Today, 288, 2-10.

Behar, D., Dhanasekaran, T., Neta, P., Hosten, C. M., Ejeh, D., Hambright, P., and Fujita, E., 1998. "Cobalt Porphyrin Catalyzed Reduction of CO_2. Radiation Chemical, Photochemical, and Electrochemical Studies." *Journal of Physical Chemistry A,* 102, 2870-2877.

Behnamfar, M. T., 2015. "Preparation of Gd_2O_3 Nanoparticles from a New Precursor and Their Catalytic Activity for Electrochemical Reduction of CO_2 to CO." *Journal of Particle Science and Technology,* 1, 21-30.

Beley, M., Collin, J. P., Ruppert, R., and Sauvage, J. P., 1986. "Electrocatalytic Reduction of CO_2 by Ni Cyclam^{2+} in Water: Study of the Factors Affecting the Efficiency and the Selectivity of the Process." *Journal of the American Chemical Society*, 108, 461-67.

Benson, E. E., Clifford P. K., Sathrum, A. J. and Smieja, J. M., 2009. "Electrocatalytic and Homogeneous Approaches to Conversion of CO_2 to Liquid Fuels." *Chemical Society Reviews,* 38, 89-99.

Boutin, E., Wang, N., Lin, J. C., Mesnage, M., Mendoza, D., Lassalle-Kaiser, B., Hahn, C., Jaramillo, T. F., and Robert, M., 2019. "Aqueous Electrochemical Reduction of Carbon Dioxide and Carbon Monoxide into Methanol with Cobalt Phthalocyanine."

Angewandte Chemie-International Edition, 58, 16172-16176.

Bumroongsakulsawat, P., and Kelsall, G. H., 2014. "Effect of Solution pH on CO: Formate Formation Rates during Electrochemical Reduction of Aqueous CO_2 at Sn Cathodes." *Electrochimica Acta,* 141, 216-225.

Cao, L-M., Huang, H-H., Wang, J-W., Zhong, D-C., and Lu, T-B., 2018. "The Synergistic Catalysis Effect within a Dinuclear Nickel Complex for Efficient and Selective Electrocatalytic Reduction of CO_2 to CO." *Green Chemistry*, 20, 798-803.

Chen, C. S., Handoko, A. D., Wan, J. H., Liang, M., Ren, D., and Yeo, B. S., 2015. "Stable and Selective Electrochemical Reduction of Carbon Dioxide to Ethylene on Copper Mesocrystals." *Catalysis Science and Technology,* 5, 161-168.

Chen, L., Li, F., Bentley, C. L., Horne, M., Bond, A. M., and Zhang, J., 2017. "Electrochemical Reduction of CO_2 with an Oxide-Derived Lead Nano-Coralline Electrode in Dimcarb." *ChemElectroChem*, 4, 1402-1410.

Chen, Y., Li, C. W., and Kanan, M. W., 2012. "Aqueous CO_2 Reduction at Very Low Overpotential on Oxide-Derived Au Nanoparticles." *Journal of the American Chemical Society*, 134, 19969-19972.

Chi, D., Hengpan, Y., Yanfang, D., Ting, L., Guojiao, S., Huan, W., and Jiaxing, L., 2014. "Morphology-Controlled CuO Nanoparticles for Electroreduction of CO_2 to Ethanol." *RSC Advances,* 4, 37329-37332.

Collin, J. P., Jouaiti, A., and Sauvage, J. P., 1988. "Electrocatalytic Properties of $Ni(Cyclam)^{2+}$ and $Ni^2(Biscyclam)^{4+}$ with respect to CO_2 and H_2O Reduction." *Inorganic Chemistry,* 27, 1986-1990.

Costentin, C., Robert, M., and Savéant, J. M., 2013. "Catalysis of the Electrochemical Reduction of Carbon Dioxide." *Chemical Society Reviews,* 42, 2423-2436.

Dewulf, D. W., and Bard, A, J., 1988. "The Electrochemical Reduction of CO_2 to CH_4 and

C_2H_4 at Cu/Nafion electrodes (solid polymer electrolyte structures)." *Catalysis Letters,* 1, 73-79.

Deciccio, D., Ahn, S. T., Sen, S., Schunk, S., Palmore, G. T. R., and Rose-Petruck, C., 2015. "Electrochemical Reduction of CO_2 with Clathrate Hydrate Electrolytes and Copper Foam Electrodes." *Electrochemistry Communications,* 52, 13-16.

Detweiler, Z. M, White, J. L., Bernasek, S, L., and Bocarsly. A. B., 2014. "Anodized Indium Metal Electrodes for Enhanced Carbon Dioxide Reduction in Aqueous Electrolyte." *Langmuir,* 30, 7593-7600.

Dimeglio, J. L., and Rosenthal, J., 2013. "Selective Conversion of CO_2 to CO with High Efficiency Using an Inexpensive Bismuth-Based Electrocatalyst." *Journal of the American Chemical Society,* 135, 8798-8801.

Dubois, D. L., 1997. "Development of Transition Metal Phosphine Complexes as Electrocatalysts for CO_2 and CO Reduction." *Comments on Inorganic Chemistry,* 19, 307-325.

DuBois, D. L., Miedaner, A., and Haltiwanger, R, C., 1991. "Electrochemical Reduction of CO_2 Catalyzed by [Pd(Triphosphine)(Solvent)]$(BF_4)_2$ Complexes: Synthetic and Mechanistic Studies." *Journal of the American Chemical Society,* 113, 8753-8764.

Elgrishi, N., Chambers, M. B., Wang, X., and Fontecave, M., 2017. "Molecular Polypyridine-Based Metal Complexes as Catalysts for the Reduction of CO_2." *Chemical Society Reviews,* 46, 761-796.

Fan, L., Xia, C., Zhu, P., Lu, Y., and Wang, H., 2020. "Electrochemical CO_2 Reduction to High-Concentration Pure Formic Acid Solutions in an All-Solid-State Reactor." *Nature Communications,* 11, 1-9.

Feng, D. M., Zhu, Y-P., Chen, P., and Ma. T-Y., 2017. "Recent Advances in Transition-Metal-Mediated Electrocatalytic CO_2 Reduction: From Homogeneous to

Heterogeneous Systems." *Catalysts,* 7, 1-18.

Furuya, N., Yamazaki, T., and Shibata, M., 1997. "High-Performance Ru-Pd Catalysts for CO_2 Reduction at Gas-Diffusion Electrodes." *Journal of Electroanalytical Chemistry,* 431, 39-41.

Gao, D., Zhou, H., Wang, J., Miao, S., Yang, F., Wang, G., Wang, J., and Bao, X., 2015. "Size-Dependent Electrocatalytic Reduction of CO_2 over Pd Nanoparticles." *journal of American Chemical Society,* 137, 4288-4291.

Gao, D., Zhang, Y., Zhou, Z., Cai, F., Zhao, X., Huang, W., Li, Y., Zhu, J., Liu, P., Yang, F., Wang, G., and Bao, B., 2017. "Enhancing CO_2 Electroreduction with the Metal-Oxide Interface." *Journal of the American Chemical Society,* 139, 5652-5655.

Gao, S., Lin, Y., Jiao, X., Sun, Y., Luo, Q., Zhang, W., Li, D., Yang, J., and Xie, Y., 2016. "Partially Oxidized Atomic Cobalt Layers for Carbon Dioxide Electroreduction to Liquid Fuel." *Nature,* 529, 68-71.

Gao, S., Sun, Z., Liu, W., Jiao, X., Zu, X., Hu, Q., Sun, Y., Yao, T., Zhang, W., Wei, S., and Xie, Y., 2017. "Atomic Layer Confined Vacancies for Atomic-Level Insights into Carbon Dioxide Electroreduction." *Nature Communications,* 8, 1-7.

García, M., Aguirre, M. J., Canzi, G., Kubiak, C. P., Ohlbaum, M., and Isaacs, M., 2014. "Electro and Photoelectrochemical Reduction of Carbon Dioxide on Multimetallic Porphyrins/Polyoxotungstate Modified Electrodes." *Electrochimica Acta,* 115, 146-154.

Genovese, C., Ampelli, C., Perathoner, S., and Centi, G., 2017. "Mechanism of C-C Bond Formation in the Electrocatalytic Reduction of CO_2 to Acetic Acid. A Challenging Reaction to Use Renewable Energy with Chemistry." *Green Chemistry,* 19, 2406-2415.

Giesbrecht, P. K., and Herbert. D. E., 2017. "Electrochemical Reduction of Carbon Dioxide

to Methanol in the Presence of Benzannulated Dihydropyridine Additives." *ACS Energy Letters,* 2, 549-555.

Gonçalves, M. R. Gomes, A., Condeço, J., Fernandes, R., Pardal, T., Sequeira, C. A. C., and Branco , J. B., 2010. "Selective Electrochemical Conversion of CO_2 to C_2 Hydrocarbons." *Energy Conversion and Management,* 51, 30-32.

Hara, K., Sonoyama, N., and Sakata, T., 1997. "Electrocatalytic Fischer-Tropsch Reactions. Formation of Hydrocarbons and Oxygen-Containing Compounds from CO on a Pt Gas Diffusion Electrode." *Bulletin of the Chemical Society of Japan,* 70, 745-754.

Hatsukade, T., Kuhl, K. P., Cave, E. R., Abram, D. N., and Jaramillo, J. N., 2014. "Insights into the Electrocatalytic Reduction of CO_2 on Metallic Silver Surfaces." *Physical Chemistry Chemical Physics,* 16, 13814-13819.

Honores, J., Quezada, D., García, M., Calfumán, K., Muen, J. P., Aguirre, M. J., Arévalo, M.C., and Isaacs, M., 2017. "Carbon Neutral Electrochemical Conversion of Carbon Dioxide Mediated by [M: N +(Cyclam)Cln] (M = Ni^{2+} and Co^{3+}) on Mercury Free Electrodes and Ionic Liquids as Reaction Media." *Green Chemistry* 19, 1155-1162.

Hori, Y., Konishi, H., Futamura, T., Murata, A., Koga, O., Sakurai, H., and Oguma, K., 2005. "Deactivation of Copper Electrode in Electrochemical Reduction of CO_2." *Electrochimica Acta,* 50, 5354-5369.

Hori, Yoshio, Kikuchi, K., Akira Murata, A., and Suzuki, S., 1986. "Production of Methane and Ethylene in Electrochemical Reduction of Carbon Dioxide At Copper Electrode in Aqueous Hydrogencarbonate Solution." *Chemistry Letters,* 15, 897-898.

Hori, Yoshio, Kikuchi, K., Akira Murata, A., and Suzuki, S., 1985. "Production of CO and CH_4 in Electrochemical Reduction of CO_2 At Metal Electrodes in Aqueous Hydrogencarbonate Solution." *Chemistry Letters* 14, 1695-1698.

Iijima, Go., Inomata, T., Yamaguchi, H., Ito, M., and Masuda, H., 2019. "Role of a Hydroxide Layer on Cu Electrodes in Electrochemical CO_2 Reduction." *ACS Catalysis,* 9, 6305-6319.

Inglis, J. L., MacLean, B. J., Pryce, M. T., and Vos. J. G., 2012. "Electrocatalytic Pathways towards Sustainable Fuel Production from Water and CO_2." *Coordination Chemistry Reviews,* 256, 2571-2600.

Innocent, B., Liaigre, D., Pasquier, D., Ropital, F., Le´ger, J. M., and Kokoh, K. B., 2009. "Electro-Reduction of Carbon Dioxide to Formate on Lead Electrode in Aqueous Medium." *journal of applied Electrochemistry,* 39, 227-232.

Isaacs, M., Armijo, F., Ramırez, G., Trollund, E., Biaggio, S. R., Costamagna, J., and Aguirre M. J., 2005. "Electrochemical Reduction of CO_2 Mediated by Poly-M-Aminophthalocyanines (M = Co, Ni, Fe): Poly-Co-Tetraaminophthalocyanine, a Selective Catalyst." *Journal of Molecular Catalysis A: Chemical*, 229, 249-257.

Isaacs, M., Canales, J. C., Riquelme, A., Lucero, M., Aguirre, M. J., and Costamagna, J., 2003. "Contribution of the Ligand to the Electroreduction of CO_2 Catalyzed by a Cobalt(II) Macrocyclic Complex." *Journal of Coordination Chemistry*, 56, 1193-1201.

Jia, F., Yu, X., and Zhang, L., 2014. "Enhanced Selectivity for the Electrochemical Reduction of CO_2 to Alcohols in Aqueous Solution with Nanostructured Cu e Au Alloy as Catalyst." *Journal of Power Sources,* 252, 85-89.

Jiao, Y., Zheng, Y., Chen, P., Jaroniec, M., and Qiao, S-Z., 2017. "Molecular Scaffolding Strategy with Synergistic Active Centers to Facilitate Electrocatalytic CO_2 Reduction to Hydrocarbon/Alcohol." *Journal of the American Chemical Society*, 139, 18093-18100.

Jiménez, C., García, J., Camarillo, R., Martínez, F., and Rincón, J., 2017. "Electrochemical

CO_2 Reduction to Fuels Using Pt/CNT Catalysts Synthesized in Supercritical Medium." *Energy and Fuels,* 31, 3038-3046.

Kaneco, S., Iiba, K., Hiei, N., Ohta, K., Mizuno, T., and Suzuki, T., 1999. "Electrochemical Reduction of Carbon Dioxide to Ethylene with High Faradaic Efficiency at a Cu Electrode in CsOH/Methanol." *Electrochimica Acta*, *44*, 4701–4706.

Kaneco, S., Sakaguchi, Y., Katsumata, H., Suzuki, T., and Ohta, K., 2007. "Cu-Deposited Nickel Electrode for the Electrochemical Conversion of CO_2 in Water/Methanol Mixture Media." *Bulletin of the Catalysis Society of India,* 6, 74-82.

Karamad, M., Hansen, H. A., Rossmeisl, J., and Nørskov, J. K., 2015. "Mechanistic Pathway in the Electrochemical Reduction of CO_2 on RuO_2." *ACS Catalysis,* 5, 4075-4081.

Kas, R., Hummadi, K. K., Kortlever, R., Wit, P., Milbrat, A., Luiten-Olieman, M. W. J., Benes, N. E., Koper, M. T. M., and Mul, G., 2016. "Three-Dimensional Porous Hollow Fibre Copper Electrodes for Efficient and High-Rate Electrochemical Carbon Dioxide Reduction." *Nature Communications*, 7, 1-7.

Kim, J., Choi, W., Park, J. W., Kim, C., Kim, M., and Song, H., 2019. "Branched Copper Oxide Nanoparticles Induce Highly Selective Ethylene Production by Electrochemical Carbon Dioxide Reduction." *Journal of the American Chemical Society,* 141, 6986-6994.

Kim, T., and Palmore, G. T. R., 2020. "A Scalable Method for Preparing Cu Electrocatalysts That Convert CO_2 into $C2^+$ Products." *Nature Communications,* 11, 1-11.

Koleii, F., Atilan, T., Palamut, N., Gizir, A. M., Aydin, R., and Hamann, C. H., 2003. Electrochemical reduction of CO_2 at Pb and Sn electrodes in a fixed-bed reactor in aqueous K_2CO_3 and $KHCO_3$ media. *Journal of Applied Electrochemistry*, *33*, 447-

450.

Köleli, F., and Balun, D., 2004. "Reduction of CO_2 under High Pressure and High Temperature on Pb-Granule Electrodes in a Fixed-Bed Reactor in Aqueous Medium." *Applied Catalysis A: General*, 274, 237-242.

Komatsu, S., Tanaka, M., Okumura, A., and Kungi, A., 1995. "Preparation of Cu-Solid Polymer Electrolyte Composite Electrodes and Application to Gas-Phase Electrochemical Reduction of CO_2." *Electrochimica Acta,* 40, 745-753.

Kortlever, R., Peters, I., Koper, S., and Koper, M. T. M., 2015. "Electrochemical CO_2 Reduction to Formic Acid at Low Overpotential and with High Faradaic Efficiency on Carbon-Supported Bimetallic Pd-Pt Nanoparticles." *ACS Catalysis,* 5, 3916-3923.

Kudo, A., Nakagawa, S., Tsuneta, A., and Sakata, T., 1993. "Electrochemical Reduction of High Pressure CO on Ni Electrodes." *Journal of The Electrochemical Society,* 140, 1541.

Kuhl, K. P., Cave, E. R., Abram, D. N., and Jaramillo, T. F., 2012. "New Insights into the Electrochemical Reduction of Carbon Dioxide on Metallic Copper Surfaces." *Energy and Environmental Science,* 5, 7050-7059.

Kumar, B., Brian, J. P., Atla, V., Kumari, S., Bertram, K. A., White, R. T., and Spurgeon, J. M., 2016a. "Controlling the Product Syngas H_2:CO Ratio through Pulsed-Bias Electrochemical Reduction of CO_2 on Copper." *ACS Catalysis,* 6, 4739-4745.

Kumar, B., Brian, J. P., Atla, V., Kumari, S., Bertram, K. A., White, R. T., and Spurgeon, J. M., 2016b. "New Trends in the Development of Heterogeneous Catalysts for Electrochemical CO_2 Reduction." *Catalysis Today,* 270, 19-30.

Kusama, S., Saito, T., Hashiba, H., Sakai, A., and Yotsuhashi, S., 2017. "Crystalline Copper(II) Phthalocyanine Catalysts for Electrochemical Reduction of Carbon Dioxide in Aqueous Media." *ACS Catalysis,* 7, 8382-8385.

Kushi, Y., Hirotaka, N., Takanori, N., Kiyoshi, I., and Koji, T., 1994. "Oxalate Formation in Electrochemical CO_2 Reduction Catalyzed by Rhodium-Sulfur Cluster." *Chemistry Letters,* 23, 2175-2178.

Laitar D.S., Muller P., and Sadighi J.P., 2005. "Efficient Homogeneous Catalysis in the Reduction of CO_2 to CO. " *Journal of American Chemical Society*, 127, 17196-17197.

Le, M., Ren, M., Zhang, Z., Sprunger, P. T., Kurtz, R. L. and Flake, J. C., 2011. "Electrochemical Reduction of CO_2 to CH_3OH at Copper Oxide Surfaces." *Journal of The Electrochemical Society,* 158, E45-E49.

Lee, C. H., and Kanan. M.W., 2015. "Controlling H^+ vs. CO_2 Reduction Selectivity on Pb Electrodes." *ACS Catalysis,* 5, 465-469.

Lee, J., and Tak. Y., 2001. "Electrocatalytic Activity of Cu Electrode in Electroreduction of CO_2." *Electrochimica Acta,* 46, 3015-3022.

Lee, S-W, Lee, J. K., Lee, K. H., and Lim, J. H., 2010. "Electrochemical Reduction of CO and H_2 from Carbon Dioxide in Aqua-Solution." *Current Applied Physics,* 10, S51-S54.

Leonard, N., Ju, W., Sinev, I., Steinberg, J., Luo, F., Varela, A. S., Cuenya, B. R., Strasser, P., 2018. "The Chemical Identity, State and Structure of Catalytically Active Centers during the Electrochemical CO_2 Reduction on Porous Fe-Nitrogen-Carbon (Fe-N-C) Materials." *Chemical Science,* 9, 5064-5073.

Li, C. W., and Kanan, M. W., 2012. "CO_2 Reduction at Low Overpotential on Cu Electrodes Resulting from the Reduction of Thick Cu_2O Films." *journal of American Chemical Society*, 134, 10-13.

Lieske, L. E., Rheingold, A. L., and Machan, C. W., 2018. "Electrochemical Reduction of Carbon Dioxide with a Molecular Polypyridyl Nickel Complex." *Sustainable Energy and Fuels,* 2, 1269-1277.

Liu, Y., Zhang, Y., Cheng, K., Quan, X., Fan, X., Su, Y., Chen, S., Zhao, H., Zhang, Y., Yu, H., and Hoffmann, M. R., 2017. "Selective Electrochemical Reduction of Carbon Dioxide to Ethanol on a Boron- and Nitrogen-Co-Doped Nanodiamond." *Angewandte Chemie,* 129, 15813-15817.

Liu, Y., Fan, X., Nayak, A., Wang, Y., Shan, B., Quan, X., and Meyer, T. J., 2019. "Steering CO_2 Electroreduction toward Ethanol Production by a Surface-Bound Ru Polypyridyl Carbene Catalyst on N-Doped Porous Carbon." *Proceedings of the National Academy of Sciences of the United States of America,* 116, 26353-26358.

Liu, Y., Tian, D., Biswas, A. N., Xie, Z., Hwang, S., Lee, J, H., Meng, H and Chen, J. G., 2020. "Transition Metal Nitrides as Promising Catalyst Supports for Tuning CO/H_2 Syngas Production from Electrochemical CO_2 Reduction." *Angewandte Chemie - International Edition*, 59, 11345-11348.

Louis, H., Akakuru, O. U., Monday, P., and Funmilayo, O. O., 2019. "A Review on the State-of-the-Art Advances for CO_2 Electro-Chemical Reduction Using Metal Complex Molecular Catalysts." *Ecletica Quimica,* 44, 11-39.

Ma, M., Hansen, H. A., Valenti, M., Wang, Z., Cao, A., Dong, M., and Smith, W. A., 2017. "Electrochemical Reduction of CO_2 on Compositionally Variant Au-Pt Bimetallic Thin Films." *Nano Energy,* 42, 51-57.

Ma, S., Sadakiyo, M., Luo, R., Heima, M., Yamauchi, M., and Kenis, P. J. A., 2016. "One-step electrosynthesis of ethylene and ethanol from CO_2 in an alkaline electrolyzer." *Journal of Power Sources*, *301*, 219-228.

Magdesieva, T. V., Zhukov, I. V., Kravchuk, D. N., Semenikhin, O. N., Tomilova, L. G., and Butin, K. P., 2002. "Electrocatalytic CO_2 Reduction in Methanol Catalyzed by Mono-, Di-, and Electropolymerized Phthalocyanine Complexes." *Russian Chemical Bulletin*, 51, 805-812.

Malik, M. I., Malaibari, Z. O., Atieh, M., and Abussaud, B., 2016. "Electrochemical Reduction of CO_2 to Methanol over MWCNTs Impregnated with Cu_2O." *Chemical Engineering Science,* 152, 468-477.

Mahmood, M. N., Masheder, D., and Harty, C. J., 1987. "Use of Gas-Diffusion Electrodes for High-Rate Electrochemical Reduction of Carbon Dioxide. II. Reduction at Metal Phthalocyanine-Impregnated Electrodes." *Journal of Applied Electrochemistry,* 17, 1223-1227.

Mizuno, T., Naitoh, A., and Ohta, K., 1995. "Electrochemical Reduction of CO_2 in Methanol at −30°C." *Journal of Electroanalytical Chemistry,* 391, 199-201.

Murata, A., and Hori, Y., 1991. "Product Selectivity Affected by Cationic Species in Electrochemical Reduction of CO_2 and CO at a Cu Electrode." *Bulletin of the Chemical Society of Japan*, 64, 123-127.

Narayanan, S. R., Haines, B., Soler, J., and Valdez. T. I., 2011. "Electrochemical Conversion of Carbon Dioxide to Formate in Alkaline Polymer Electrolyte Membrane Cells." *Journal of The Electrochemical Society,* 158, A167-A173.

Ogura, K., 2013. "Electrochemical Reduction of Carbon Dioxide to Ethylene: Mechanistic Approach." *Journal of CO_2 Utilization,* 1, 43-49.

Ohya, S., Kaneco, S., Katsumata, H., Suzuki, T., and Ohta, K., 2009. "Electrochemical Reduction of CO_2 in Methanol with Aid of CuO and Cu_2O." *Catalysis Today,* 148, 329-334.

Pérez-Rodríguez, S., Garc´ıa, G., Calvillo, L., Celorrio, V., Pastor, E., and Lazaro, M. J., 2011. "Carbon-Supported Fe Catalysts for CO_2 Electroreduction to High-Added Value Products: A DEMS Study: Effect of the Functionalization of the Support." *International Journal of Electrochemistry*, 2011, 1-13.

Piao, G., Yoon, S. H., Han, D. S., and Park, H., 2019. "Ion-Enhanced Conversion of CO_2

into Formate on Porous Dendritic Bismuth Electrodes with High Efficiency and Durability." *ChemSusChem,* 13, 698-706.

Prakash, G. K. S., Viva, F. A., and George A Olah. G. A., 2013. "Electrochemical Reduction of CO_2 over Sn-NaFion coated Electrode for a Fuel-Cell-like Device." *Journal of Power Sources,* 223, 68-73.

Qu, J., Zhang, X., Wang, Y., and Xie, C., 2005. "Electrochemical Reduction of CO_2 on RuO_2/TiO_2 Nanotubes Composite Modified Pt Electrode." *Electrochimica Acta,* 50, 3576-3580.

Ren, D., Deng, Y., Handoko, A. D., Chen, C, S., Malkhandi, S., and Yeo, B. S., 2015. "Selective Electrochemical Reduction of Carbon Dioxide to Ethylene and Ethanol on Copper(I) Oxide Catalysts." *ACS Catalysis,* 5, 2814-2821.

Ren, D., Fong, J., and Yeo, B. S., 2018. "The effects of currents and potentials on the selectivities of copper toward carbon dioxide electroreduction." *Nature Communications*, *9*, 1-8.

Reske, R., Mistry, H., Behafarid, F., Cuenya, B. R., and Strasser, P., 2014. "Particle Size Effects in the Catalytic Electroreduction of CO_2 on Cu Nanoparticles." *journal of American Chemical Society,* 138, 6978-6986.

Roberts, F. S., Kuhl, K. P., and Nilsson, A., 2015. "High Selectivity for Ethylene from Carbon Dioxide Reduction over Copper Nanocube Electrocatalysts." *Angewandte Chemie-International Edition,* 54, 5179-5182.

Saeki, T., Hashimoto, K., Kimura, N., Omata, K., and Fujishima, A., 1995. "Electrochemical Reduction of CO_2 with High Current Density in a CO_2-Methanol Medium." *Journal of Physical Chemistry,* 99, 8440-8446.

Saeki, T., Hashimoto, K., Kimura, N., Omata, K., and Fujishima, A., 1996. "Electrochemical Reduction of CO_2 with High Current Density in a CO_2^+ Methanol

Medium II. CO Formation Promoted by Tetrabutylammonium Cation." *Journal of Electroanalytical Chemistry,* 404, 299-302.

Sato, S., McNicholas, B. J., and Grubbs. R. H., 2020. "Aqueous Electrocatalytic CO_2 Reduction Using Metal Complexes Dispersed in Polymer Ion Gels." *Chemical Communications,* 56, 4440-4443.

Schouten, K. J.P. Kwon, Y., Van der Ham, C. J. M., Qin, Z., and Koper, M. T. M., 2011. "A New Mechanism for the Selectivity to C_1 and C_2 Species in the Electrochemical Reduction of Carbon Dioxide on Copper Electrodes." *Chemical Science,* 2, 1902-1909.

Scibioh M.A. and Viswanathan B., 2004. "Electrochemical reduction of carbon dioxide: A status report." *Proceedings of Indian National Science Academy*, 70 A, 407-462.

Shen, J., Kortlever, R., Kas, R., Birdja, Y. Y., Diaz-morales, O., Kwon, Y., Ledezma-yanez, I., Schouten, K. J. P., Mul, G., and Koper, M. T. M., 2015. "Electrocatalytic Reduction of Carbon Dioxide to Carbon Monoxide and Methane at an Immobilized Cobalt Protoporphyrin ring." *Nature Communications,* 6, 1-8.

Singh, S., Phukan, B., and Verma, A., 2015. "Salen Ligand Complexes as Electrocatalysts for Direct Electrochemical Reduction of Gaseous." *RSC Advances,* 5, 3581-3589.

Subramanian, K., Asokan, K., Jeevarathinam, D., and Chandrasekaran. M., 2007. "Electrochemical Membrane Reactor for the Reduction of Carbon dioxide to Formate." *Journal of Applied Electrochemistry,* 37, 255-260.

Thorson, M. R., Siil, K. I., and Kenis, P, J. A., 2013. "Effect of Cations on the Electrochemical Conversion of CO_2 to CO." *Journal of the Electrochemical Society,* 160, F69-F74.

Tan, T. A., Yusuf, S. Y., and Fazara, M. A. U., 1995. "Eelectrochemical Reduction of Carbon Dioxide into Formate." *Journal of Engineering Science and Technology,* 36,

625-628.

Terunuma Y., Saitoh A., and Momose Y., 1997. "Relationship between Hydrocarbon Production in the Electrochemical Reduction of CO_2 and the Characteristics of the Cu Electrode." *Journal of Electroanalytical Chemistry*, 434, 69-75.

Tornow, C. E., Thorson, M. R., Ma, S., Gewirth, A. A., and Kenis, P. J. A., 2012. "Nitrogen-Based Catalysts for the Electrochemical Reduction of CO_2 to CO." *Journal of the American Chemical Society,* 134, 19520-19523.

Uemoto, N., Furukawa, M., Tateishi, I., and Katsumata, H., 2019. "Electrochemical Carbon Dioxide Reduction in Methanol at Cu and Cu_2O-Deposited Carbon Black Electrodes." *ChemEngineering,* 3, 1-10.

Wang, M., Torbensen, K., Salvatore, D., Ren, S., Joulié, D., Dumoulin, F., Mendoza, D., Lassalle-Kaiser, B., Işci, U., Berlinguette, C, P., and Robert, M., 2019. "CO_2 Electrochemical Catalytic Reduction with a Highly Active Cobalt Phthalocyanine." *Nature Communications,* 10, 1-8.

Weng, Z., Jianbing, J., Wu, Y., Wu, Z., Guo, X., Guo, X., Materna, K. L., Liu, W., Batista, V. S., Brudvig, G. W., and Wang, H., 2016. "Electrochemical CO_2 Reduction to Hydrocarbons on a Heterogeneous Molecular Cu Catalyst in Aqueous Solution." *Journal of the American Chemical Society,* 138, 8076-8079.

Weng, Z., Wu, Y., Wang, M., Jiang, J., Yang, K., Huo, S., Wang, X-F., Ma, Q., Brudvig, G. W., Batista, V. S., Liang, Y., Feng, Z., and Wang, H., 2018. "Active Sites of Copper-Complex Catalytic Materials for Electrochemical Carbon Dioxide Reduction." *Nature Communications,* 9, 1-9.

Wu, H., Song, J., Xie, C., Hu, Y., and Han., B., 2018. "Highly Efficient Electrochemical Reduction of CO_2 into Formic Acid over Lead Dioxide in an Ionic Liquid-Catholyte Mixture." *Green Chemistry,* 20, 1765-1769.

Xia, Y., Kashtanov, S., Yu, P., Chang, L., Feng, K., Zhong, J., Guo, J., and Sun, X., 2020. "Identification of Dual-Active Sites in Cobalt Phthalocyanine for Electrochemical Carbon Dioxide Reduction." *Nano Energy,* 67, 104163.

Xie, J-F., Huang, Y-X., Li, W-W., Song, X-N., Xiong, L., and Yu, H-Q., 2014. "Electrochimica Acta Efficient Electrochemical CO_2 Reduction on a Unique Chrysanthemum-like Cu Nano flower Electrode and Direct Observation of Carbon Deposite." *Electrochimica Acta,* 139, 137-144.

Yadav, V. S. K., and Purkait, M. K., 2015. "Synthesis of Pb_2O Electrocatalyst and Its Application in the Electrochemical Reduction of CO_2 to HCOOH in Various Electrolytes." *RSC Advances,* 5, 40414-40421.

Yang, H. P., Yue, Y. N., Qin, S., Wang, H., and Lu, J-X., 2016. "Selective Electrochemical Reduction of CO_2 to Different Alcohol Products by an Organically Doped Alloy Catalyst." *Green Chemistry,* 18, 3216-3220.

Yano, H., Tanaka, T., Nakayama, M., and Ogura, K., 2004. "Selective Electrochemical Reduction of CO_2 to Ethylene at a Three-Phase Interface on Copper(I) Halide-Confined Cu-Mesh Electrodes in Acidic Solutions of Potassium Halides." *Journal of Electroanalytical Chemistry,* 565, 287-293.

Yuan, J., Guo, R-R., Zeng, S., Wang, H., and Lu, J-X., 2017. "Electroreduction of CO_2 into Ethanol over an Active Catalyst: Copper Supported on Titania." *Catalysts,* 7, 1-10.

Yuan, J., Yang, M-P., Hu, Q-L., Li, S-M., Wang, H., and Lu, J-X., 2018. "Cu/TiO_2 Nanoparticles Modified Nitrogen-Doped Graphene as a Highly Efficient Catalyst for the Selective Electroreduction of CO_2 to Different Alcohols." *Journal of CO_2 Utilization*, 24, 334-340.

Zhang, X., Wu, Z., Zhang, X., Li, L., Li, Y., Xu, H., Li, X., Yu, X., Zhang, Z., Liang, Y., and Wang, H., 2017. "Highly Selective and Active CO_2 Reduction Electrocatalysts

Based on Cobalt Phthalocyanine/Carbon Nanotube Hybrid Structures." *Nature Communications,* 8, 1-8.

Zheng, Y., Vasileff, A., Zhou, X., Jiao, Y., Jaroniec, M., and Qiao, S. Z., 2019. "Understanding the Roadmap for Electrochemical Reduction of CO_2 to Multi-Carbon Oxygenates and Hydrocarbons on Copper-Based Catalysts."*Journal of the American Chemical Society*, *141*, 7646-7659.

Zhou, Feng., Liu, S., Yang, B., Wang, P., Alshammari, A. S., and Deng, Y., 2014. "Highly Selective Electrocatalytic Reduction of Carbon Dioxide to Carbon Monoxide on Silver Electrode with Aqueous Ionic Liquids." *Electrochemistry Communications,* 46, 103-116.

Zhu, Q., Sun, X., Yang, D., Ma, J., Kang, X., Zheng, L., Zhang, J., Wu, Z., and Han, B., 2019. "Carbon Dioxide Electroreduction to C_2 Products over Copper-Cuprous Oxide Derived from Electrosynthesized Copper Complex." *Nature Communications,* 10, 1-11.

Zhu, W., Michalsky, R., Metin, O., Lv, H., Guo, S., Wright, C. J., Sun, X., Peterson, A. A., Sun, S., 2013. "Monodisperse Au Nanoparticles for Selective Electrocatalytic Reduction of CO_2 to CO." *Journal of the American Chemical Society*, 135, 16833-16836.

CHAPTER 3

Materials and Methodology

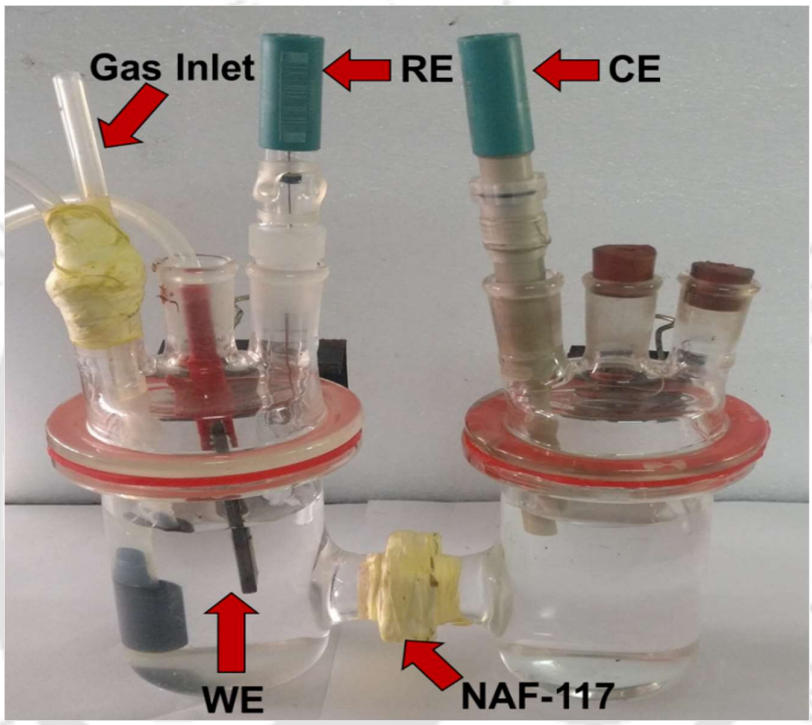

3.1 Materials and analytical reagents

All the chemicals employed in this study were of analytical grades and used without further purification unless otherwise mentioned. The chemicals and any other reagents used for specific applications are detailed below. 4-nitro-o-phenylenediamine (98%) was obtained from Sigma Aldrich, Bangalore, India. $CuCl_2•2H_2O$, $NiCl_2•6H_2O$, $Pb(NO_3)_2$, $Cu(NO_3)_2•3H_2O$, KBr (IR grade), $KHCO_3$, CH_3CN (HPLC grade), C_2H_5OH (HPLC grade), CH_3CHO (HPLC grade), CH_3COOH (HPLC grade), DMF (EMSURE), HCOOH (purity 98-100%), $C_6H_8O_6$ (reagent grade), CH_3OH (GC grade), NaOH (reagent grade), CH_4N_2O (reagent grade), $Na_3C_6H_5O_7$ (reagent grade), and Et_3N (reagent grade) were supplied by Merck, Mumbai, India. Nafion dispersion (5% w/w dispersion) in water and 1-propanol and Nafion membrane (Nafion-117) were procured from Alfa Aesar, Haverhill, USA. An iso-molded graphite plate (GM 10, particle size: 0.0102 mm, porosity: 12% of volume, resistivity: 0.55×10^{-3} $\Omega.inch^{-1}$), was procured from GraphiteStore.com, Inc., USA. Deionized water was synthesized in the laboratory with a resistance of ≥ 18.2 mΩ.cm, Millipore, USA was employed for preparing all the solutions and reagents used in this study. Milli-Q water (model: Elix 3) was used to prepare all the solutions.

3.2 Fabrication of electrodes, and ERC reactor

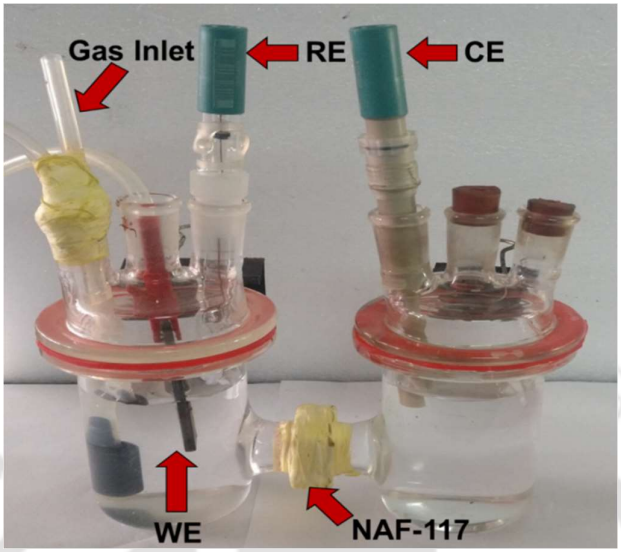

Figure 3.1: Schematic representation of the custom-made H-type divided electrochemical cell, WE = Working electrode, CE = Counter electrode, and RE = Reference electrode.

The ERC reactions were conducted in a custom-made 150 mL volume H-type reactor using a three-electrode assembly system (Fig. 3.1). The electrode assembly was consisting of a graphite plate (bare or functionalized with catalysts, 4 cm^2: 2 cm × 2 cm) as the working electrode (WE) and Ag/AgCl saturated with 3M KCl as the reference electrode (RE). A platinum wire (ϕ 2 mm) was fixed as the counter electrode (CE). The electrocatalyst solution was prepared by dissolving synthesized metal complexes in DMF along with Nafion dispersion (5% w/w) and sonicated for 15 mins. The catalyst ink was coated by brush-coating (3 times) over the graphite electrode (2 cm × 2 cm: 4 cm^2) and dried overnight. It is referred to as a catalyst/graphite electrode. This procedure was repeated thrice, and an average catalyst coverage on the WE was about 2 $mg.cm^{-2}$ with a uniform dispersity of the metal complexes (Singh et al., 2015). The metal oxide electrocatalysts were mixed with Nafion dispersion (5% w/w) with isopropyl alcohol in 1:5 ratios and sonicated for 45 minutes to get a mixture (Yadav and Purkait, 2016). The catalyst

solution was coated on the working electrode and then dried in the oven at 80°C to get the final WE (Fig. 3.2).

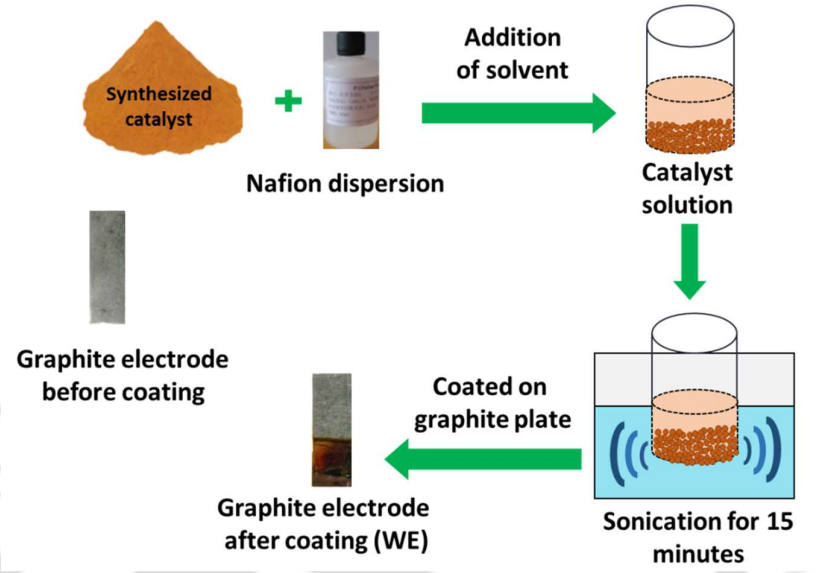

Figure 3.2: Schematic diagrams of preparation of catalyst solution coated working electrode.

In the custom-made H-type reactor, a gap of 1 cm was kept between the WE and RE (Fig. 3.1). CE was positioned in the second chamber at 3 cm apart from the WE. The experiments were carried out in an aqueous bicarbonate solution saturated with gaseous CO_2 (99.99%) (each catholyte and anolyte of 120 mL). Hydrogen gas formation is least in the presence of $KHCO_3$; thus $KHCO_3$ was used as an electrolyte (Hori, 2008; Murata and Hori, 1991). N_2 gas (99.99%) was purged for 15 min through the $KHCO_3$ solution to remove air from the solution. The experiments were then carried out in a 0.5 M $KHCO_3$ solution saturated with gaseous CO_2 at a flow rate of 10 mL.min^{-1} until (~45 min). The pH of the saturated solution reached 7.0. The experiments were performed at room temperature (25°C). Then linear sweep voltammetry (LSV) and cyclic voltammetry (CV) data were recorded to identify the activity of the metal complex and metal oxide electrocatalysts and then chronoamperometry was performed at the reduction potential found in LSV.

After the completion of the voltammetric tests, a constant-potential analysis was performed and the products formed were analyzed following the above procedure. In these experiments, the same H-type electrochemical reactor with 120 mL of 0.5 M $KHCO_3$ solution in each compartment was employed. The gas sample was collected from the headspace, and the liquid sample was collected from the vicinity of the WE. The chronoamperometry data was recorded with a pulse of 5 s and the sample was analyzed by GC. The liquid sample was analyzed using a flame ionization detector (FID) (Agilent DB-WAXetr, GC column (30 m length, 0.25 mm ID, and 0.25 μm film) with a detector temperature of 270°C and injector temperature of 250°C. The oven temperature was maintained at 40°C for 5 min and then ramped at 5°C min^{-1} up to 130°C with argon as carrier gas (flow rate of 2 $mL.min^{-1}$) (Sharp, 2001). The gas sample was analyzed in a TCD detector and Carboxen-1000 column. The oven temperature was maintained at 100°C for 10 min and the detector temperature was fixed at 190°C with an injector temperature of 150°C.

3.3 Electrocatalyst characterization techniques

Various characterization techniques were selected for the characterization of the catalysts such as; nuclear magnetic resonance (NMR) spectroscopy, Fourier transform infrared (FTIR) spectroscopy, high-resolution mass spectrometry (HR-MS), CHN analyzer, electron spin resonance spectroscopy (ESR), X-ray diffraction (XRD) studies, field emission scanning electron microscopy (FESEM), transmission electron microscopy (TEM), energy-dispersive X-ray Spectroscopy (EDX), and atomic absorption spectroscopy. The electrocatalysts were further analyzed to check its activity in the electrochemical environment using linear sweep voltammetry (LSV) and cyclic voltammetry (CV) method. After that, the qualitative analysis was conducted with

chronoamperometry (CA) study (constant-potential analysis) and product analysis was conducted using gas chromatography.

3.3.1 Nuclear magnetic resonance (NMR) spectroscopy

Nuclear magnetic resonance (NMR) spectroscopy is an analytical technique used extensively for determining the structure of organic compounds. The nuclei have a spin and they are electrically charged in most cases and have magnetic properties. When an external magnetic field is applied, a higher energy state opposes it and the lower energy state gets aligned. This creates an energy difference between these two spin states and this barrier depends on the external magnetic field. The differential energy between the excited and the ground level nucleus acts as a potential of energy transfer in the form of a specific wavelength corresponding to the applied radiofrequency range. The same range of frequency is emitted when the spin comes back to its base energy. In this work, 1H-NMR was analyzed. During the analysis, samples were solubilized in $CDCl_3$ and placed in an NMR tube. For the analysis of synthesized ligand, a nuclear magnetic resonance spectrometer (make: Bruker, model: ASCEND 600) has been used. The applied external magnetic field corresponded to the precession frequency of 600 MHz.

3.3.2 Fourier transform infrared (FTIR) spectroscopy

The FTIR spectroscopy is conducted to get the infrared absorption spectrum of emission or absorption of solid, liquid, or gaseous samples. During the analysis, some amount of the infrared radiation is absorbed by the sample and the rest amount of radiation is transmitted. A spectrum is thus generated and recorded. In this experiments, the FTIR analysis was done for solid samples only. During the sample analysis, 1-3 mg of sample is mixed properly with at around 10-15 mg of KBr and then mixed properly to produce a pellet. At first, a background spectrum is taken and the percentage of the transmittance is observed by comparing the background spectrum and the sample spectrum. The FTIR

analysis of electrocatalysts was conducted in a Fourier transform infrared spectrometer of Perkin Elmer (model: Spectrum two) to detect many of the functional groups present in the synthesized electrocatalysts. The transmission spectra of the electrocatalysts were recorded in the spectral range of 400-4000 cm^{-1}.

3.3.3 High-resolution mass spectrometry (HR-MS)

Mass spectrometry is an analytical technique that is used to detect the chemical identity or the structure of various molecules. During the analysis, the samples are transformed into gaseous ions by bombarding it with electrons. These will help the molecules either become charged or break into charged ions which can then be detected with the use of a magnetic field according to their mass to charge ratio and finally provide peaks. In this study, the mass spectra of the dissolve compounds were taken. The samples were at first solubilized in an appropriate solvent and then were injected in the mass analyzer. The mass of the synthesized ligand was obtained through the high-resolution mass spectrometer (make: Agilent, model: 6520). The mobile phase used during the HR-MS analysis was a mixture of 0.1% formic acid and acetonitrile. The obtained peaks were used to identify the exact molecular mass of the sample.

3.3.4 CHN analyzer

A CHN Analyzer is an instrument that can detect the percentage of carbon, hydrogen, and nitrogen concentration in a particular sample. This analysis is done by combusting the sample in the presence of oxygen. In the combustion process, carbon is converted to carbon dioxide; hydrogen to water; nitrogen to nitrogen gas to oxides of nitrogen and sulphur to sulphur dioxide, and finally detected by a gas chromatography system. The gas chromatography separates the elements and produces a respective peak from which the amount of C, H, and N present in the sample can be determined. This indirectly helps in the determination of the mass of an unknown sample. During the

analysis, 4-5 mg sample is taken, dried properly and it is then combusted in the presence of oxygen which involves the complete and instantaneous oxidation of the sample by the "flash combustion" method. Then the products are separated in GC using a respective chromatographic column and detected in a TCD detector. The CHN analysis was done in an elemental analyzer (make: Thermo Finnigan, model: FLASH EA 1112).

3.3.5 X-ray diffraction (XRD)

X-ray diffraction analysis is an analytical technique that is used to identify the phase of the crystalline material and used to identify the information of its on unit cells. X-ray diffraction results from the constructive interference between X-rays and electrons of the sample material. X-rays generated from a cathode ray tube are filtered and monochromatic radiation is produced which is then assimilated to concentrate before pointing on the sample. The diffraction occurs only when Bragg's law is satisfied with the constructive interference from planes with spacing d (Eqn. 3.1).

$$n\lambda = 2d \sin\theta \qquad (3.1)$$

Where λ is the wavelength, d is the spacing between the two crystal planes, and θ is the Bragg's angle, which is the angle between the incident and reflected beam. After that, the diffracted X-rays are then detected, processed, and recorded. This phenomenon helps to identify the substance and the nanocatalysts were characterized using this method. In a sample holder, 20 mg of dried sample was placed and then the XRD patterns were recorded between 20 and 80° 2θ angle. The X-ray diffraction analysis was conducted in an advanced X-ray diffractometer (make: Bruker, model: D8 Advance) with λ = 0.15406 nm of CuKα radiation at 5° per min scan rate.

3.3.6 Energy-dispersive X-ray (EDX) spectroscopy

Energy-dispersive X-ray spectroscopy is an analytical technique used for the elemental analysis or chemical characterization of a sample. In this spectroscopy, a beam of X-rays is focused and penetrates on the sample and after interacting with it the X-rays are emitted. The emitted X-rays are then detected with the energy dispersive detector. During the EDX analysis, the preparation of the sample is very simple. The EDX data of the electrocatalysts were taken as well as the coated electrode also. The electrocatalysts were mixed with appropriate solvents and sonicated to make complete homogenized dispersion. Then a glass slide was cropped into a small piece and covered with aluminum foil in which the mixture was drop cast. This was directly kept on the stub after fixing a conductive carbon tape. The coated electrode was also cut into small pieces and fixed on the carbon tape over the metal stub. The EDX spectra of the electrocatalysts were obtained using a scanning electron microscope (make: Zeiss, model: Sigma).

3.3.7 Field emission scanning electron microscopy (FESEM)

A FESEM is used to visualize very small topographic details of the surface. Researchers in applying this technique to observe structures that may be as small as 1 nanometer. A field emission cathode is used to produce a high electron energy beam in FESEM. Surface morphologies of the synthesized electrocatalysts were studied using this analytical method. FESEM can magnify the samples higher than the 10 KX range. At first, the synthesized electrocatalysts were dispersed properly in an appropriate solvent and sonicated to make complete homogenized dispersion. A glass slide covered with aluminum foil was used as the base in which a drop of the prepared solution was poured and dried in the oven. After drying the glass slide it was then kept on the metal stub covered with a conductive carbon tape in field emission scanning electron microscope (make: Zeiss, model: Sigma).

3.3.8 Field emission transmission electron microscopy (FETEM)

In transmission electron microscopy also the morphological and topographic details of a sample are recorded. In FETEM, the electron beam is projected on the sample and the transmitted electrons from the samples are then used to generate two-dimensional images. In the case of FETEM, as the electrons pass through inside the samples, it produces better information than FESEM. The sample was prepared by dispersing the sample in an appropriate solvent. Then the sample was drop cast over a TEM grid (made up of copper). Then the sample was dried in the oven and then the grid was put in the sample holder and the TEM analysis was done (make: JEOL, model: JEM 2100F).

3.3.9 Atomic absorption spectroscopy (AAS)

Atomic absorption spectroscopy is a spectroscopic method that determines the percentage of chemical elements using the absorption of optical radiation (light) by the free atoms in those elements in a gaseous state. At first, the molecules are exposed to a high temperature in a flame or graphite furnace. This is done using an atomizer and the role of it is to separate the particles into various individual molecules and then into atoms. The free atoms generated in the atomizer can absorb the radiation at a specific frequency and thus makes transitions to higher electronic energy levels. The concentration is then calculated from the amount of absorption. In this work, the concentration of metal ions present in the electrolyte after the ERC reaction was determined using this spectroscopy (make: Varian, model: AA240FS). The calibration curve was obtained in the range of 1 to 10 $mg.L^{-1}$ for all metal ions separately, and calibration samples were prepared each time before the analysis. Air-acetylene gas at a flow rate of 400 $L.h^{-1}$ for drying and 150 $L.h^{-1}$ for sheathing were purged. The specific metal hollow cathode lamps were used during analysis.

3.4 Fundamental process parameters govern the ERC process

In this experiments, a conventional three-electrode assembly system was used. In the system, an electrode is an electrical conductor through which current flows. The Ag/AgCl saturated with 3 M KCl was used as the reference electrode (RE) and Pt wire was used as the counter electrode (CE). A graphite plate coated with electrocatalyst was used as the working electrode (WE). In this system, the electrochemical cell consists of these three electrodes and a divided H-type cell separated with a membrane. On one side of the H-type chamber, the working electrode and reference electrode is placed and on the other side, the counter electrode is placed. The various process parameters can be studied in the field of ERC are linear sweep voltammetry, cyclic voltammetry (CV), and chronoamperometry analysis (constant-potential analysis). These three analyses were conducted to test the activity of the catalysts in ERC using a Potentiostat (make: Metrohm, model: PGSTAT 302N).

3.4.1 Cyclic voltammetry (CV)

To receive preliminary information about an electrochemical process cyclic voltammetry (CV) is the most common method. CV method measures the current flowing through the WE, where the applied potential is measured against the RE. The potentiostat controls the voltage. The potential is continuously changing with the function of time. The potential is swept linearly at a constant rate between two limiting potentials. After the set potential is reached in a CV experiment, the working electrode's potential is ramped in the opposite direction to return to its initial potential. The same sweep is commonly chosen for a forward and reverse sweep. The current corresponding to the different potential is recorded. For the anodic scan where the potential is increasing the current has a positive sign and for the cathodic scan, the current has a negative sign. The peak obtained is the characteristic of the electrode reaction. The cyclic voltammetry is generally used to study

the electrochemical properties of a molecule adsorbed on the electrode or of an analyte (gas or liquid) dissolved in the solution. In this study, the CO_2 gas was purged in the electrolyte solution and acted as the analyte. The complexes were solubilized in the solution and acted as an analyte in the other experiments and the CV data of the complexes were taken. The only limitation is that it is not good for quantitative analysis for the electrochemical nucleation process. The cyclic voltammetry was conducted at first to know the preliminary observations and then the quantitative observations were made.

In a redox system, the redox reactions can be stated as $O + ne^- \leftrightarrow R$. Where, O and R is considered as the oxidized and reduced species when n numbers of electrons are transferred. A redox reaction can be considered as reversible when the transfer rate of electrons is the same, the process is reversible. In a reversible process, the anodic and the cathodic peak separation is 59/n mV in which n is the number of electrons transferred in the oxidation as well as a reduction process. With the increase in scan rate, the current density was also increased because of the higher analyte (CO_2) influx towards the electrode. The peak current density is directly proportional to the square root of the scan rate for a free diffusing system. Under the irreversible process, the reaction is $O + ne^- \rightarrow R$. In such a case, the system does not remain in an equilibrium.

3.4.2 Linear sweep voltammetry (LSV)

Linear sweep voltammetry is similar to CV technique where it is dealing with one side of the CV graph (either the cathode or the anode). That is why potential is fixed from a lower limit to an upper limit of either side of the CV graph and current flows linearly with time. It provides useful information about the rate of the electrochemical process. The time taken to sweep the range can be altered by changing the potential scan rate. The applied potential varies linearly with time; therefore, the scan rate is defined as the slope ($V.s^{-1}$).

In this study, the CO_2 gas was saturated in the electrolyte and performed as an analyte and the LSV data was taken.

3.4.3 Chronoamperometry (constant-potential) analysis

It is generally used for the qualitative analysis of the electrochemical process. The details about the electrochemical reaction are studied using this process. Current can be measured versus time as a response to the potential pulse. The recorded current can be analyzed, and nature can be determined from the variations with time. The total current observed in the system is a combination of faradaic and nonfaradaic current. The Faradaic current is generated because of the electron transfer and the interaction between the electroactive species during the reaction. From the cyclic voltammetry and LSV, the potential of the reduction or oxidation of the ERC reaction was identified. That potential is fixed in the chronoamperometry process and conducted for 1 h to know the details of the experiment. During the reduction reaction, the total charge is measured by concerning the electron transfer during the reaction which is proportional to the amount of the product formed. In any electrochemical system, the experimental potential is always higher than the original equilibrium potential for a particular reduction reaction. The difference between these two is known as over-potential which forms due to the activation polarization, concentration polarization, ohmic polarization, etc. Thus, to design a catalyst that reduces the activation overpotential and increases the FE is very important.

3.4.4 Faradaic efficiency (FE)

To understand completely the activity of the electrocatalysts and the products obtained during the reaction there is an emergence to know the amount of product formation and charge transferred during the particular reaction. Chronoamperometry provides the details of the electrical charge transferred during the experiment and GC analyses the amount of the product formed. Current efficiency or the Faradaic efficiency

(FE) helps to determine the efficacy of the charge transfer for a particular reaction. The FE can be calculated by determining the charge passes to produce a particular product during the conversion concerning the total charge passed during the experiment (Kuhl et al., 2012). The formula to calculate the FE is detailed in Eqn. 3.2.

$$\text{Faradaic efficiency (FE)} = \frac{nFz}{Q} \tag{3.2}$$

Where, n = number of moles of a particular product (mol),

F = Faraday constant ($C.mol^{-1}$),

Z = number of electrons involved for 1 mol of a particular product,

Q = Total charge passed during the experiment (C).

3.4.5 Selectivity (SE)

The selectivity is defined as the amount of desired product to the amount of total CO_2 reduction products obtained (based on the carbon content) during the reaction. The carbon-based selectivity (Eqn. 3.3) of ERC is calculated from the ratio of the desired chemical formed to the amount of total CO_2 reduction products obtained during the reaction (Ogura et al., 2004; Yang et al., 2019).

$$\text{Selectivity (SE, \%)} = \frac{\%\,i \times n}{\Sigma(\%\,i \times n)} \times 100 \tag{3.3}$$

Where, i describes a carbon-containing reduced product formed during the ERC and n is the number of carbon present in that carbon-containing reduced product.

3.4.6 Turnover number (TON) and the Turnover frequency (TOF)

The turnover number (TON) and the turnover frequency (TOF) for the ERC employing complexes-coated electrodes were calculated using (Eqn. 3.4) and (Eqn. 3.5). The larger the value of TOF of a catalyst, the more active is the catalyst (Shen et al., 2015).

$$\text{TOF} = \frac{(\text{FE for the product formation}) \times \left(\frac{\text{Current density}}{\text{nF}}\right)}{\text{number of catalyst per cm}^2} \quad (3.4)$$

$$\text{Turnover number (TON, } s^{-1}) = (\text{TOF}) \times (\text{time}) \quad (3.5)$$

References

Hori, Y., 2008. "Electrochemical CO_2 reduction on metal electrodes," In: Vayenas *et al.* (ed.) 'Modern Aspects of Electrochemistry', No. 42, Ch. 3, Springer, New York, pp. 89-189.

Kuhl, K. P., Cave, E. R., Abram, D. N., and Jaramillo, T. F., 2012. "New Insights into the Electrochemical Reduction of Carbon Dioxide on Metallic Copper Surfaces." *Energy and Environmental Science,* 5, 7050-7059.

Murata A., and Hori, Y., 1991. "Product Selectivity Affected by Cationic Species in Electrochemical Reduction of CO_2 and CO at a Cu Electrode." *Bulletin of the Chemical Society of Japan,* 64, 123-127.

Ogura K., Yano H., and Tanaka T., 2004. "Selective Formation of Ethylene from CO_2 by Catalytic Electrolysis at a Three-phase Interface." *Catalysis Today*, *98*, 515-521.

Sharp, M. E. E., 2001. "A Comprehensive Screen for Volatile Organic Compounds in Biological Fluids." *Journal of Analytical Toxicology*, *25*, 631-636.

Shen, J., Kortlever, R., Kas, R., Birdja, Y. Y., Diaz-morales, O., Kwon, Y., Ledezma-Yanez, I., Schouten, K. J. P., Mul, G., and Koper, M. T. M., 2015. "Electrocatalytic Reduction of Carbon Dioxide to Carbon Monoxide and Methane at an Immobilized Cobalt Protoporphyrin." *Nature Communications*, *6*, 1-8.

Singh S., Mukherjee C., and Verma A., 2015. "Development of Catalytic Activity Protocol for Electrochemical Reduction of Carbon Dioxide to Value Added Products." *Clean Technologies and Environmental Policy*, *17*, 533-540.

Yadav V. S. K., and Purkait M. K., 2016. "Simultaneous CO_2 Reduction and Dye (Crystal

Violet) Removal Electrochemically on Sn and Zn Electrocatalysts Using Co_3O_4 Anode." *Energy and Fuels*, *30*, 3340-3346.

Yang, C., Mu, R., Wang, G., Song, J., Tian, H., Zhao, Z. J., and Gong, J., 2019. "Hydroxyl-mediated Ethanol Selectivity of CO_2 Hydrogenation." *Chemical Science*, *10*, 3161-3167.

CHAPTER 4

Investigation on Cu, Ni and Pb Oxides for Electrocatalysing CO_2 Conversion to Value-added Products

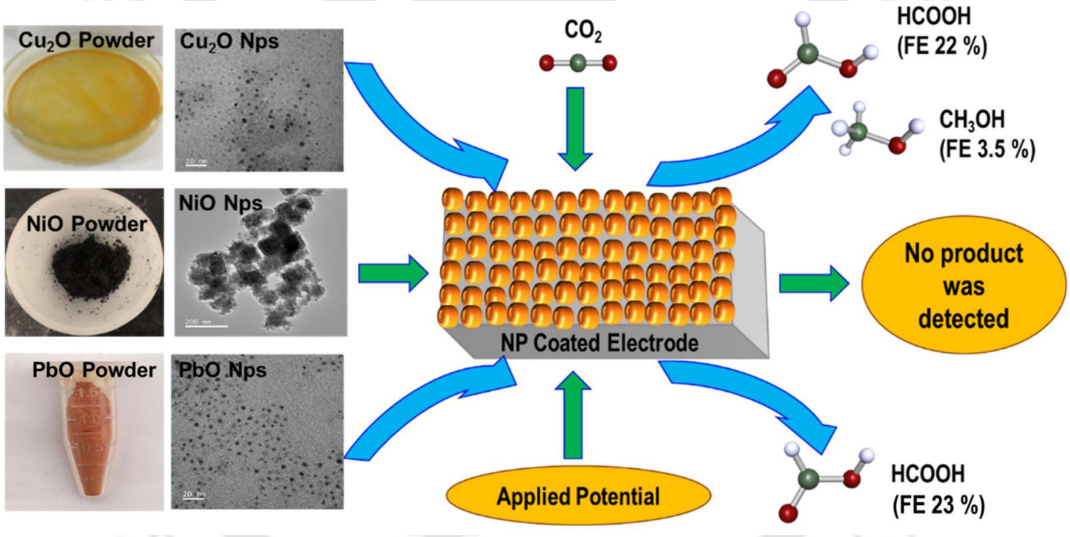

4.1 Background of the work

The electrocatalysing CO_2 reduction (ERC) is the most promising field for its capability to reuse the waste for storing renewable energy. The most important factors of the ERC are the electrolyte solution and the electrocatalysts. ERC is carried out in electrolytes saturated with CO_2 using different metals and their derivatives as catalysts within a short span of reaction time. Metals electrocatalysts, such as Au, Ag, Cu, Zn, Sn, In, Pb, etc., have been reported for the production of mostly HCOOH, CO, and trace amounts of C_2H_4 and CH_4 as minor products (Hori et al., 1993). Among all the transition metals, Cu and its derivatives have been reported for the production of hydrocarbons (C_1 and C_2), but their FE was low (Deciccio et al., 2015; Kaneco et al., 1999). Ni electrocatalysts have generally been used for the ERC of CO_2 to either HCOOH and CO with low FE or hardly reduce CO_2 (Arana et al., 1994; Hara et al., 1995; Maria D. Salazar-Villalpando, 2011). However, the metal surface can easily get contaminated by the adsorbed CO (Lee and Tak, 2001). The oxides are better catalysts than their metal counterparts because of their better CO_2 adsorption properties and are more stable (Li and Kanan 2012). Thus, in this chapter, metal oxides were selected and their role in ERC is elaborated.

4.2 Synthesis of metal oxides

Two transitions (Cu and Ni) and one main group (Pb) metal oxides were synthesized and they were used as electrocatalysts. The synthesized catalysts were coated on the graphite plate and used as WE. The platinum wire was used as the counter electrode (CE) and Ag/AgCl saturated with 3 M KCl was used as the reference electrode (RE). The electrolyte medium was 0.5 M aqueous $KHCO_3$ solution (each catholyte and anolyte of 120 mL). The cell set up described in chapter 3 was used in all the electrochemical analysis.

4.2.1 Preparation of Cu_2O electrocatalyst

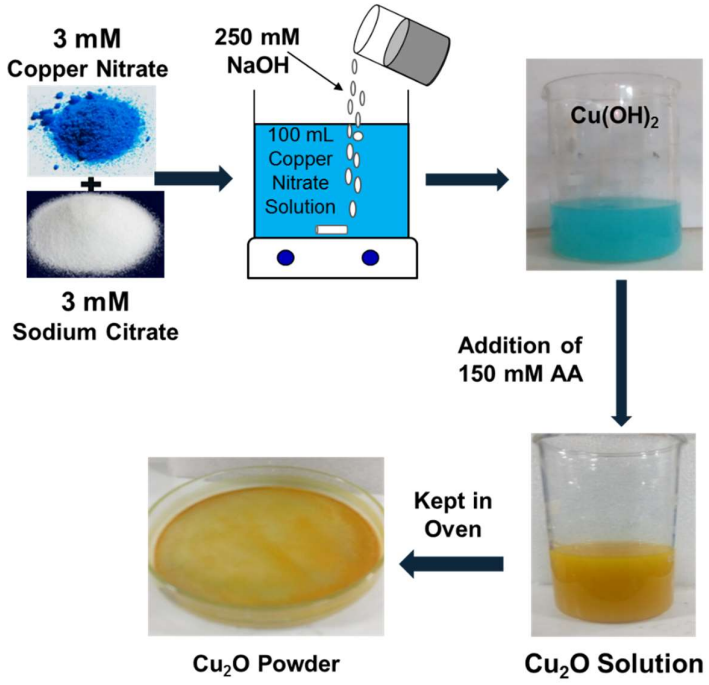

Scheme 4.1: Schematic representation of Cu_2O nanoparticle synthesis.

In 100 mL distilled water, 3 mM $Cu(NO_3)_2$ as a precursor solution was prepared and kept in a magnetic stirrer. In that precursor solution, 3 mmol sodium citrate was added as a capping agent. 250 mM of NaOH (20 mL) was added dropwise into the solution and the stirring was continued for 15 minutes at 500 rpm to increase the pH of the solution to 9.5. A sharp color change was observed during that time duration. The dark blue color of the precursor solution was changed into light sky blue. The color change was observed due to the formation of $Cu(OH)_2$ solution. After that, 150 mM of ascorbic acid (AA) about 10 mL was added dropwise into that mixture within a span of 3 to 4 min as a reducing agent until the color was changed to light yellow (Cu_2O nanoparticle solution) (Scheme 4.1). All the experiments were carried out at room temperature (Arshadi-rastabi et al., 2015; Bhosale and Bhanage 2016). After that, the solution was washed at least four times with ethanol-water (1:1) and then again with pure distilled water (3 times). The washing was done using

a centrifuge at 5000 rpm for 10 min, each time re-dispersing the precipitate with fresh washing solution or deionized water. Then the solution was filtered and the filtrate was dried and collected as Cu_2O nanopowder.

4.2.2 Preparation of NiO electrocatalyst

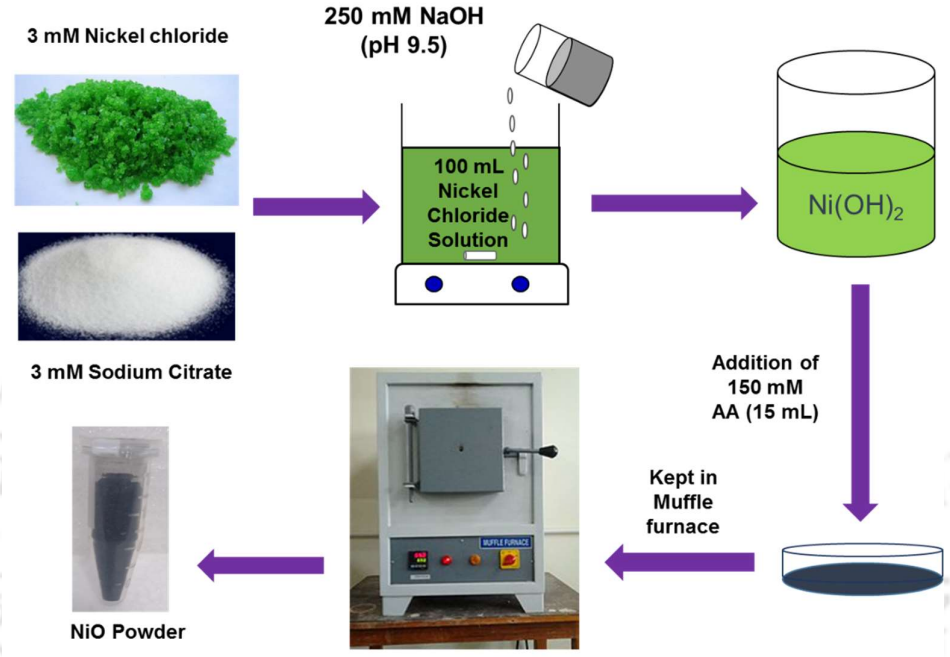

Scheme 4.2: Schematic representation of NiO nanoparticle synthesis.

During the synthesis of NiO nanoparticle, the same synthesis procedure was followed as Scheme 4.1. In this process, 3 mM of $NiCl_2 \cdot 6H_2O$ was used as the precursor solution in 100 mL of distilled water. A dark green color was observed after the addition of 3 mM of sodium citrate. The solution was fixed in a magnetic stirrer (150 rpm) and heated at 90°C for 30 mins constantly. After that, to increase the pH of the solution (9.5), 20 mL of 250 mM of NaOH was added to that mixture to produce $Ni(OH)_2$ as intermediate. The color of the solution was then changed from a dark green color to whitish green color [$Ni(OH)_2$]. To reduce the intermediate, 15 mL AA was added to that solution (150 mM) and kept for stirring for 1 h until a black color was observed. After that, the black color solution was collected, washed with ethanol and water (1:1) for 4 times to remove all the impurities

(using a centrifuge at 5000 rpm for 10 min each time). Again, the solution was washed with pure distilled water three times and filtered. Then, the collected precipitate (black color) was kept in the oven for drying and after that kept in a muffle furnace for 3 h at 300°C in presence of air and the final NiO powder (black) was prepared (Scheme 4.2) (Channu et al., 2012; El-kemary and Nagy, 2013).

4.2.3 Preparation of PbO electrocatalyst

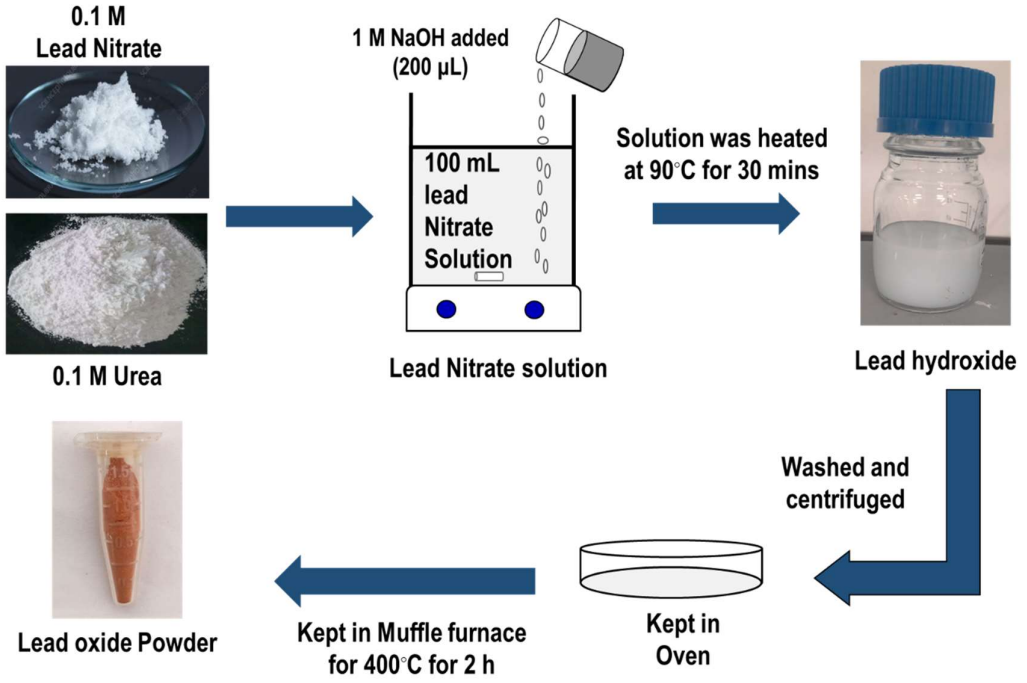

Scheme 4.3: Schematic representation of PbO nanoparticle synthesis.

The PbO nanocatalyst was prepared by a modified method described by Li and his workers (Li et al., 2005). Briefly, a mixture (100 mL) of 0.1 M, $Pb(NO_3)_2$ (precursor) solution, and 0.1 M urea (stabilizing agent) were kept in a magnetic stirrer. In that mixture, 1 M NaOH (approx. 200 µL) was added to adjust the pH of the solution to 9.5. After that, the solution was heated at 90°C for 30 mins constantly in that magnetic stirrer (150 rpm). Gradually, the color of the solution was changed from a clear solution to white color and in the end, the white color precipitate was formed. The solution was naturally cooled to

room temperature and the precipitate was filtered and washed 3 times with ethanol and water (1:1 ratio) followed by profuse washing with de-ionized water (3 times). The washing procedure was the same as sections 4.2.1 and 4.2.2. After washing, the cleaned precipitate was dried in the oven properly at 80°C for 4 h. Then the dried precipitate (now pale yellowish colour) was kept in a muffle furnace for 2 h at 400°C to obtain the lead oxide nanopowder (brick red) (Scheme 4.3) (Kannan et al., 2014; Li et al., 2005).

4.3 Results and Discussion

The metal oxide electrocatalysts were characterized by FETEM, XRD, EDX analysis, and FTIR spectroscopy. All the electrochemical analysis was conducted using Potentiostat (Autolab PGSTAT 302N).

4.3.1 FETEM, XRD, FTIR, and EDX analysis of Cu_2O nanoparticle

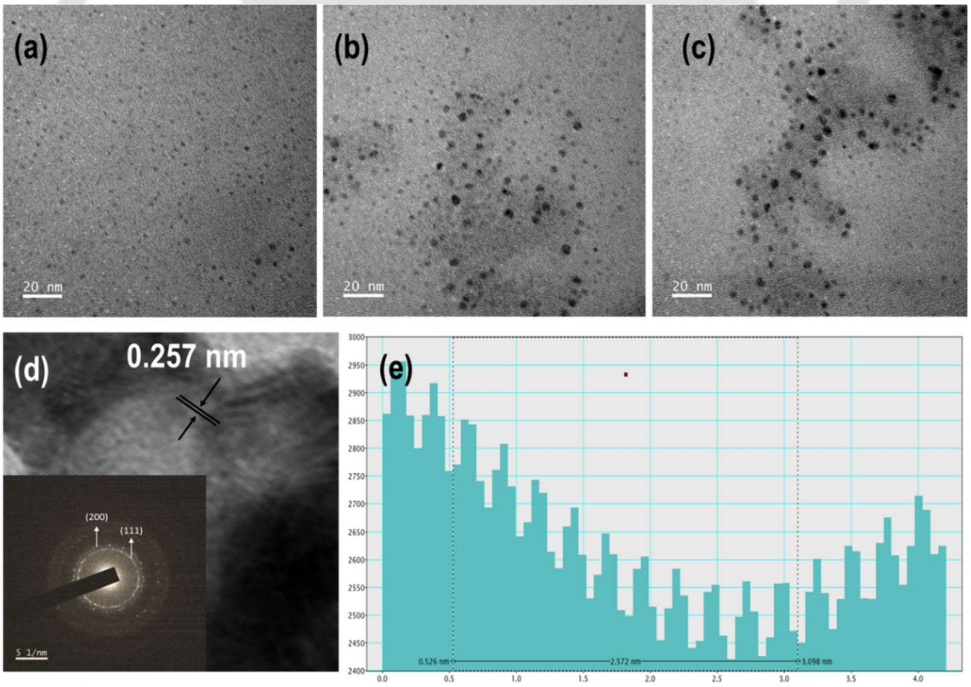

Figure 4.1: (a, b, c) FETEM, (d) HRTEM image, and (e) corresponding IFFT profile of synthesized Cu_2O nanoparticle.

The FETEM (Fig. 4.1) analysis was performed using synthesized Cu_2O nanoparticle. The results obtained from the analysis indicate that particles were properly dispersed and spherical. The average size of the Cu_2O nanoparticle observed from FETEM images is 4 nm (Figs. 4.1a, 4.1b, 4.1c). The particles observed in the TEM analysis are highly crystalline and the interplanar spacing was found 0.25 nm was for the (111) plane of Cu crystals (Fig. 4.1d) (Liu et al., 2011). The selected area (electron) diffraction (SAED) micrographs are explained in Fig. 4.1d (inset). The SAED rings were found from the diffraction of the (200) and the (111) planes respectively (Kumar et al., 2020). The IFFT (inverse first Fourier transform) image further clarifies the crystallinity of the synthesized material and confirms the d-spacing of each crystalline layer as a space between two peaks (Fig. 4.1e). The TEM, HRTEM analysis confirmed the successful synthesis of the Cu_2O nanoparticles.

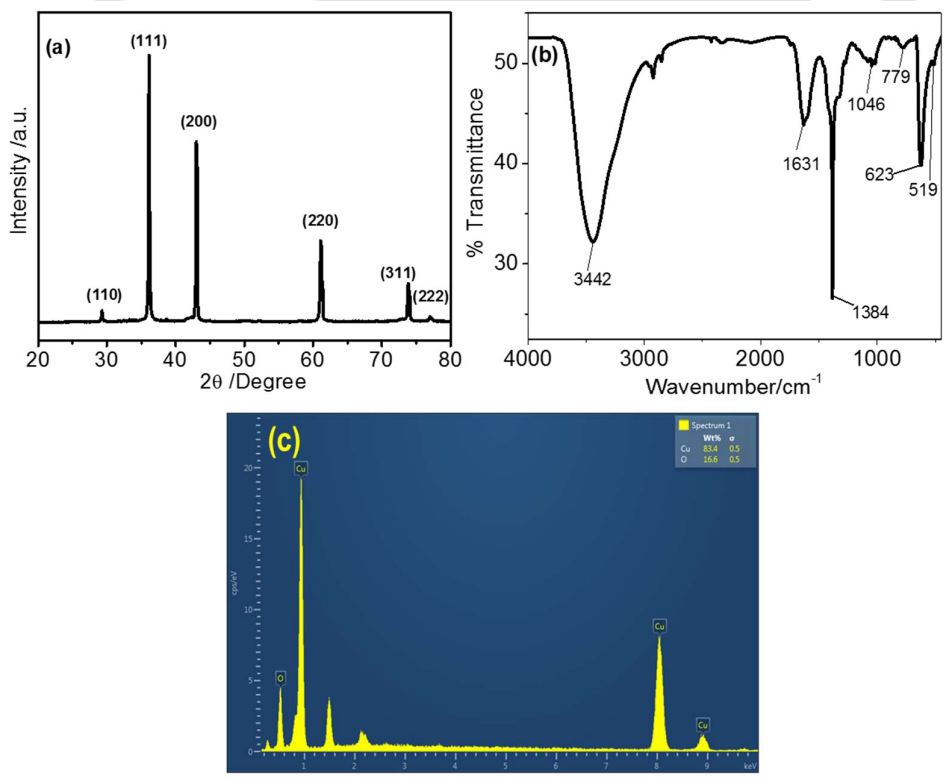

Figure 4.2: (a) XRD, (b) FTIR, and (c) EDX analysis of synthesized Cu_2O nanoparticle.

In the XRD analysis the dominant peaks at 29, 36, 43, 61, 74 and 77° 2θ angles were the characteristics for Cu_2O crystal for the diffraction from the (110), (111), (200), (220), (311), and (222) planes respectively (Fig. 4.2a) (Arshadi-rastabi et al., 2015). The XRD analysis was matched from the JCPDS card no: 78-2076 for Cu_2O nanoparticle. The peak around 3442 cm^{-1} on the FTIR spectrum is related to the O-H stretching. The absorption at 1619 cm^{-1} attributed to hydroxyl groups. The absorption bands at 1323 cm^{-1} are assigned to the -OH bending vibrations, which prove the presence of the -COOH groups. As shown in Fig. 4.2b, the absorption bands at 1270 cm^{-1} are due to the C-O stretching vibration. While the strong band in 623 cm^{-1} vibrations of copper (I)-O (Cu_2O) agrees with the previous literature (Chen et al., 2013). EDX analysis was also conducted to check the desired elements in the catalyst. In the EDX analysis of the sample, Cu metal along with oxygen was observed which confirmed the successful synthesis of the Cu_2O catalyst. The absence of undesired species was also rechecked using this procedure (Fig. 4.2c). The above information confirmed the formation of pure Cu_2O nanoparticles (Fig. 4.2).

4.3.2 FETEM, XRD, FTIR, and EDX analysis of NiO nanoparticle

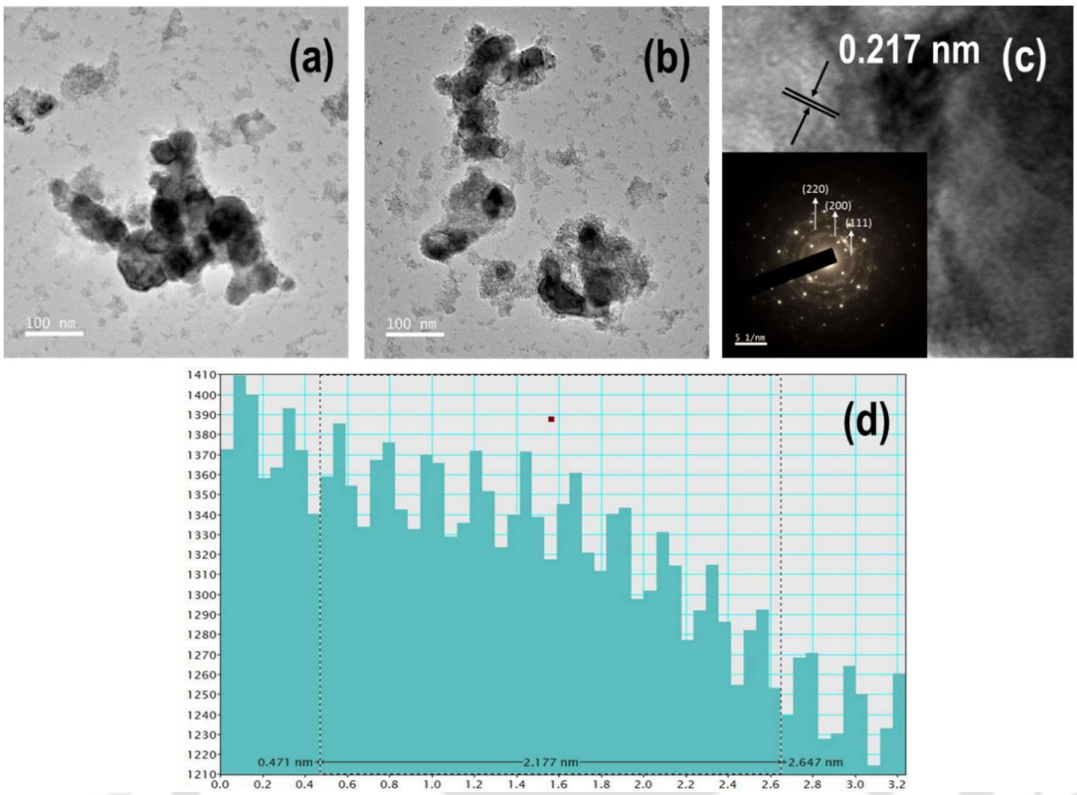

Figure 4.3: (a, b) FETEM, (c) HRTEM image, (c) SAED micrographs, and (d) corresponding IFFT profile of synthesized NiO nanoparticle.

The FETEM, HRTEM image, and corresponding IFFT profile of synthesized NiO nanoparticle are depicted in Fig. 4.3. The results obtained from the FETEM analysis indicate that particles were spherical and some nanoclusters were formed due to the agglomeration which is very common in the case of NiO nanoparticles (Kalaie et al., 2016; Nik Roselina and Azizan 2012). The average size of the NiO nanoparticle observed from FETEM images is 80 nm (Figs. 4.3a and 4.3b). The particles observed in the TEM analysis are highly crystalline and the interplanar spacing was found 0.21 nm (Fig. 4.3c) was for the (200) plane and further confirmed by IFFT images (Fig. 4.3d) (Liu, et al., 2017). The SAED rings were found from the diffraction of the (220), (200), and the (111) planes

respectively (Sharma et al., 2013). The HRTEM and IFFT profile indicated a successful synthesis of NiO nanoparticle.

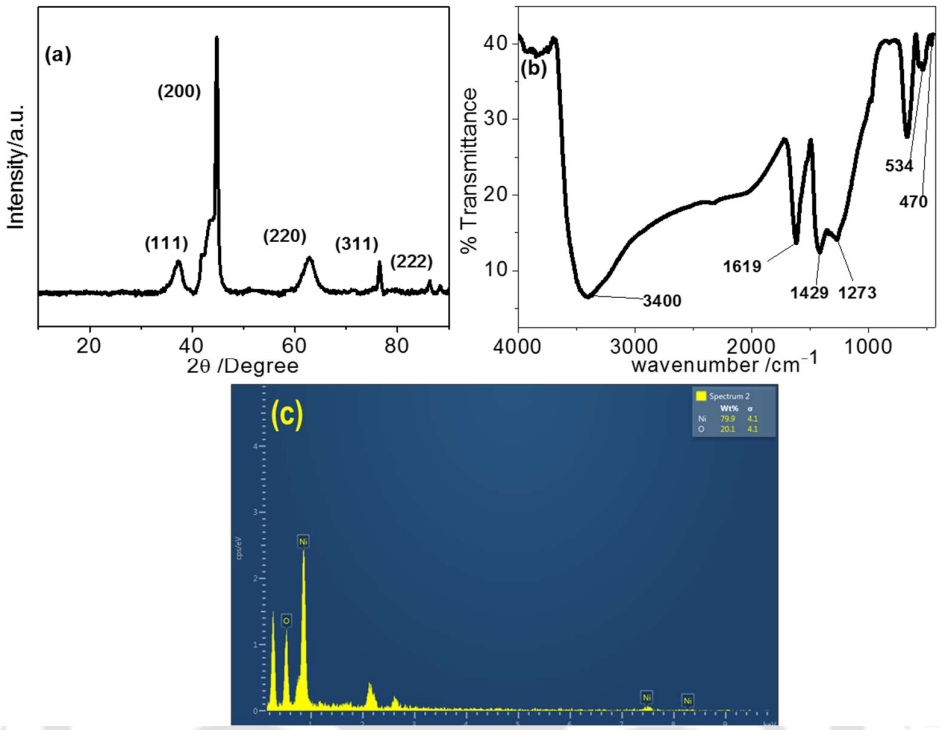

Figure 4.4: (a) XRD, (b) FTIR, and (c) EDX analysis of synthesized NiO nanoparticle.

The XRD analysis of the nanoparticle was conducted to check the pure NiO synthesis. The dominant peaks at 37, 44, 63, 76, and 86° 2θ angles were the characteristics for NiO crystal for the diffraction from the (111), (200), (220), (311), and (222) planes respectively Fig. 4.4a (Rahdar et al., 2015).(Rahdar et al., 2015) These values were matched with the ICDD database (JCPDS card no: 1010095) of NiO and thus confirms the successful synthesis of the nanoparticles. The FTIR analysis of the NiO nanoparticle produced a peak around 3400 cm^{-1}, which is related to the O-H stretching. The absorption at 1619 cm^{-1} attributed to hydroxyl groups. The absorption bands at 1429 cm^{-1} and 1273 cm^{-1} indicates the existence of carbonates of the capping agent. As shown in Fig. 4.4b, the absorption bands at 470 and 534 cm^{-1} are associated with the Ni-O vibration bond and the

absorption band at 674 cm^{-1} is assigned to Ni-O-H stretching band. The above information confirmed the formation of pure NiO nanoparticles (Fig. 4.4b) (El-kemary and Nagy, 2013). The EDX analysis confirmed the presence of Ni and O ions in the nanoparticle powder. The EDX spectra obtained NiO are shown in Fig. 4.4c.

4.3.3 FETEM, XRD, FTIR, and EDX analysis of PbO nanoparticle

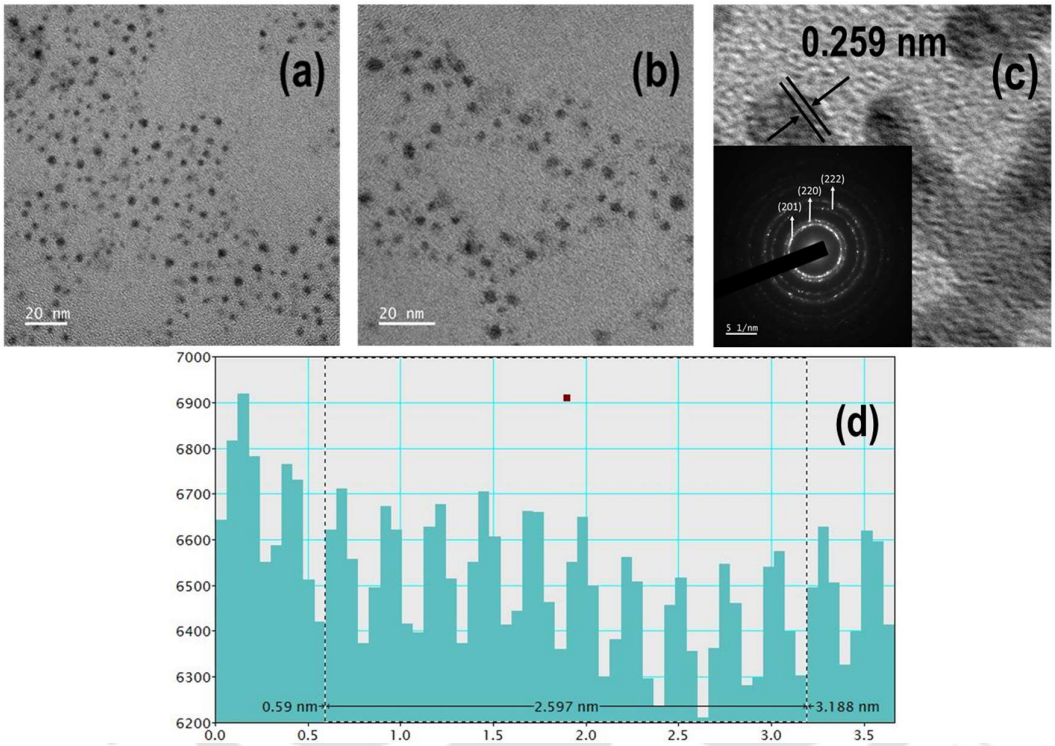

Figure 4.5: (a, b) FETEM image, (c) HRTEM, and (d) corresponding IFFT profile of synthesized PbO catalyst.

The FETEM, HRTEM image, and corresponding IFFT profile of synthesized PbO nanoparticle are depicted in Fig. 4.5. The results obtained from the FETEM analysis indicate that particles were spherical and well dispersed. The average particle size of the nanoparticles was 4 nm from the TEM analysis. The particles observed in the TEM analysis are polycrystalline and the interplanar spacing was found 0.26 nm was for the (200) plane further confirmed by IFFT images (Figs. 4.5c and 4.5d) (Zou et al., 2014). The SAED

micrographs are explained in Fig. 4.5c. The SAED rings were found from the diffraction of the (220), (200), and the (111) planes respectively (Cattley et al., 2010). The HRTEM and IFFT profile of PbO was matched from the previous literature and confirmed the successful synthesis of this catalyst.

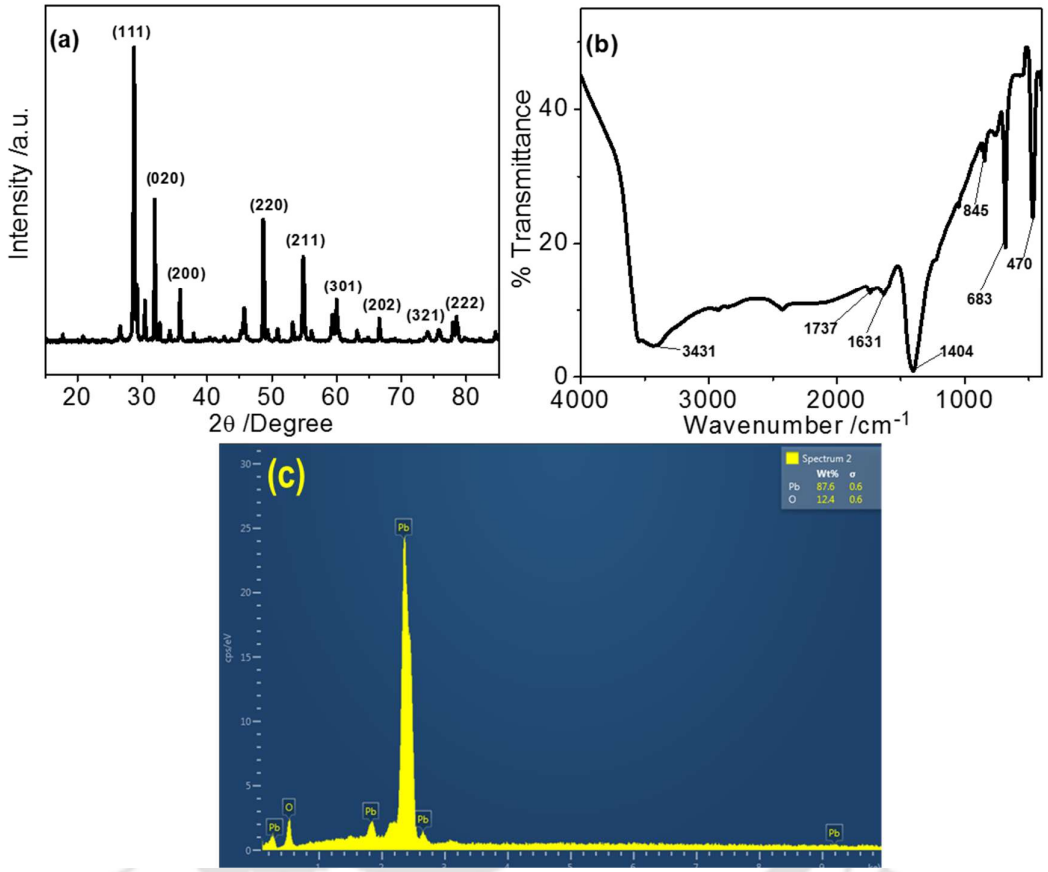

Figure 4.6: (a) XRD, (b) FTIR, and (c) EDX analysis of synthesized PbO nanoparticle.

In the XRD analysis the dominant peaks at 28.7, 31.9, 35.84, 42.74, 45.6, 45.78,48.6, 59.3, 59.9, 66.5, 73.7, 75.8, 77.9, 78.5° 2θ angles were the characteristics for PbO crystal for the diffraction from the (101), (110), (002), (102), (200), (112), (211), (202), (103), (220), (301), (310), (311) and (114) planes respectively (Fig. 4.6a) (Kannan et al., 2014). These values were matched with the ICDD database ((JCPDS card no: 38-1477) of PbO which confirms the successful synthesis of the catalyst. FTIR analysis was also performed by PbO nanocatalyst. The peak around 3431 cm^{-1} on the FTIR spectrum is

related to the O-H bond. The weak band at 1737 cm^{-1} is observed due to the C=O stretching. The absorption at 1631 cm^{-1} attributed to hydroxyl groups. These bands are found because of the capping agents on the particle surfaces. The strong and intense peaks around 1404 cm^{-1} are due to OH bending vibration in adsorbed water. A sharp peak around 683 cm^{-1} represents the asymmetric bending vibration of the Pb-O-Pb bond. Absorption peak around 470 cm^{-1} related to Pb-O stretching vibration (Fig. 4.6b) (Arulmozhi and Mythili, 2013). EDX analysis was also conducted to check the desired elements in the catalyst. In the EDX analysis of the sample, Pb metal along with oxygen was observed which confirmed the successful synthesis of the PbO catalyst. The absence of undesired species was also rechecked using this procedure (Fig. 4.6c).

4.3.4 Voltammetric analysis during ERC using metal oxide electrocatalysts

To know the role of metal oxide electrocatalysts in ERC of CO_2, the linear sweep voltammetry was conducted from 0 to −2.20 V vs. Ag/AgCl at a scan rate of 30 $mV.s^{-1}$. The analysis was conducted in a 0.5 M $KHCO_3$ solution by saturating the CO_2 gas for ~45 mins. At first, the electrolyte solution was purged with N_2 gas to remove any dissolved O_2 from the solution, and then the LSV data was taken. Then the CO_2 was purged until the pH of the solution was changed from 8.5 to 7.0 (~45 min) and again LSV was conducted. In the aqueous system, the reduction potential of CO_2 and hydrogen evolution are similar. The onset potential of hydrogen evolution reaction (HER) is at −0.70 V vs. SHE (Uchida et al., 2017). Thus, in the aqueous medium, the generated cell current in the ERC was not only for the CO_2 reduction but also for H_2 gas generation. Therefore, it is really difficult to distinguish from the LSV whether the peak observed is for the ERC or the HER. Thus, most of the finest ERC peak doesn't appear, and the higher current density is considered as the preliminary observation of a catalyst to be active in ERC (Hori, 2008). In the linear sweep voltammogram of Cu_2O catalyst in the inert atmosphere, the current observed was

only due to the H_2 evolution reaction. A higher current density was observed in the CO_2 saturated electrolyte medium. In the CO_2 saturated medium, the current observed was due to the combined effect of CO_2 reduction and H_2 production activity. Thus, the higher current density observed in the CO_2 saturated medium confirmed the Cu_2O electrocatalyst is active towards the electrochemical CO_2 reduction activity (Fig. 4.7a). After that, the chronoamperometry study was conducted to identify the products.

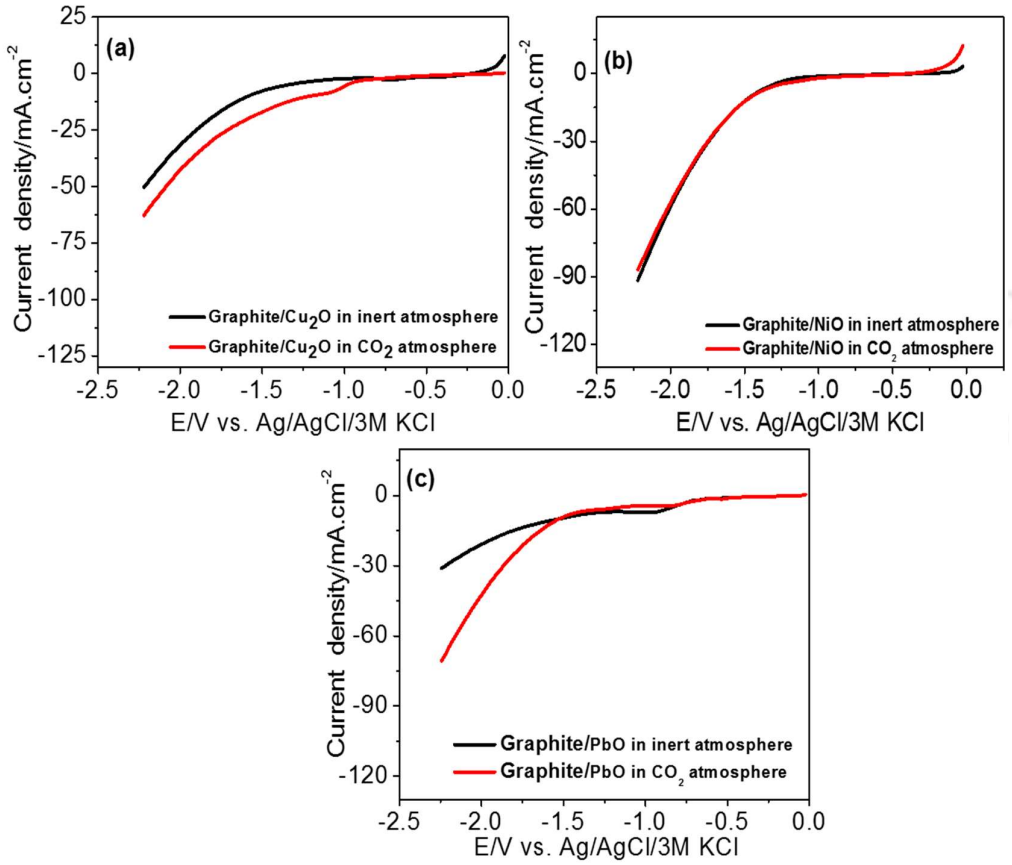

Figure 4.7: Linear sweep voltammetry of reduction of CO_2 by sweeping from 0 to −2.20 V vs. Ag/AgCl at inert and CO_2 saturated environment at a scan rate of 30 mV.s^{-1} using (a) Cu_2O, (b) NiO, and PbO (c) electrocatalysts. Experimental condition: Electrolyte 0.5 M $KHCO_3$, catholyte and analyte 120 mL each, pH 7.0, and CO_2 bubbling rate 10 mL.min^{-1} with ~45 min initial pre-saturation time.

In the LSV analysis using NiO electrocatalyst, a slightly higher current density was observed in the inert atmosphere. No change was seen in the current density after introducing CO_2 in the electrolyte solution (Fig. 4.7b). This analysis does not indicate the catalyst is active in reducing CO_2 which was further confirmed by chronoamperometry analysis at various electrode potential. The NiO electrocatalyst was active in proton reduction (hydrogen evolution) only in both environments (inert as well as CO_2) (Karamad et al., 2015). In the qualitative analysis (LSV) using PbO electrocatalyst, the potential is varied from 0 to −2.20 V vs. Ag/AgCl. A higher current density was observed in the CO_2 saturated atmosphere than the inert atmosphere which confirms the ability of the catalyst to reduce CO_2 (Fig. 4.7c). Later, the chronoamperometry analysis was conducted to confirm the preliminary analysis.

4.3.5 Products formation and FE during ERC using Cu_2O electrocatalysts

The Cu_2O electrocatalyst was active for the formation of HCOOH mainly with a trace amount of CH_3OH at higher potentials in this study. The production FE is negligible at a lower potential of less than −1.40 V. At −1.40 V, the amount of HCOOH production was 136 µmol with 15% FE. The amount of HCOOH production was 249 µmol with 20% FE at −1.60 V. The FE of HCOOH production was highest at −1.80 V (22%) with a 325 µmol production. The amount of production is highest (343 µmol with 20.42% FE) at −2.00 V vs. Ag/AgCl. The trace amount of CH_3OH was detected at higher potential, 20 µmol was detected at −2.00 V vs. Ag/AgCl (3.5% FE) (Fig. 4.8). Cu-based stepped alloys surfaces produce CH_3OH with CH_4 over the C_2 products (Hirunsit et al., 2015; Le et al., 2011). According to a group of scientists, the tetrahedral structure of the Cu_2O surface (111) is favourable for CH_3OH production (Wu et al., 2005). According to Kumar and his coworkers also, the Cu(I) sate is the active site for methanol production (Kumar et al., 2016). In 2019, Hazarika et al. also reported the CH_3OH production selectively at higher

potential (Hazarika and Manna, 2019). Though in this study, the CH_3OH selectivity (5.3%) is very much lower than HCOOH (SE 94.6%) (Fig. 4.8c). At a higher potential above −2.00 V, the H_2 evolution increases which adversely affects the CO_2 reduction activity. At −2.20 V, the HCOOH and CH_3OH production FE remains at 15.38 and 2.6% respectively. After this potential, the CO_2 reduction product formation FE declines and reaches less than 5%. The production of H_2 was 690/833/981/1098/1450 µmol with FE of 62/63/64.9/65.39/72% at −1.40, −1.60, −1.80, −2.00 and at −2.20 V vs. Ag/AgCl respectively.

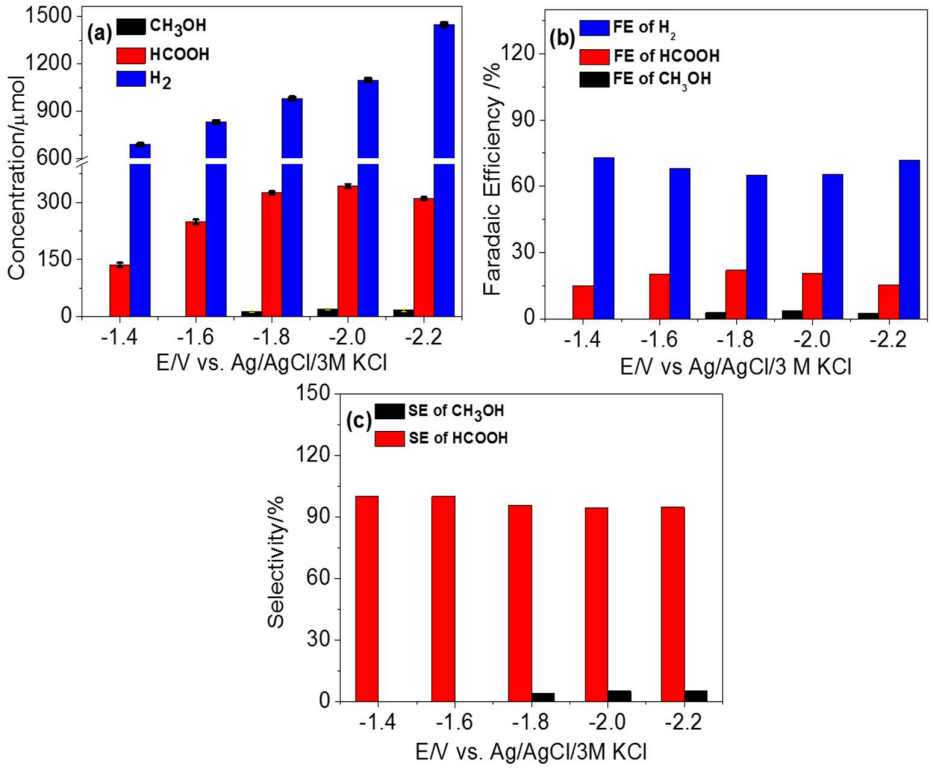

Figure 4.8: (a) Amount of product formation, (b) corresponding FE, and (c) SE using Cu_2O electrocatalyst. Experimental condition: Electrolyte 0.5 M $KHCO_3$, catholyte, and anolyte 120 mL each, pH 7.0, and CO_2 bubbling rate 10 mL.min^{-1} with ~45 min initial pre-saturation time.

The TON and the TOF were also calculated for the Cu_2O electrocatalyst. In the case of Cu_2O electrocatalyst, at the lower potential, the TOF for ERC products was low, and

then again at a higher potential above −2.00 V the TOF and TON decreases. The lowest TON (720) and TOF (0.2 s^{-1}) was found at −1.40 V. At −1.60 V also, the TOF (0.49 s^{-1}) and TON (1764) was increased slightly. At −1.80 V, a sharp increase was observed in the TON and TOF. For HCOOH the TOF and TON observed was 2412 and 0.67 s^{-1} respectively (Table 4.1). The TOF for CH_3OH production was 0.082 s^{-1} and the TON was 295 at that potential. The calculated TOF and TON were highest at −2.00 V vs. Ag/AgCl. Using Cu_2O as the catalyst-material in this system, at −2.00 V, TON = 2484, and TOF 0.7 s^{-1} for HCOOH was found. The TOF and TON of HCOOH production were almost similar at −1.80 and −2.00 V. The TOF for CH_3OH production was 0.119 s^{-1} and the TON was 428 at −2.00 V (Table 4.1). The TOF for CH_3OH production was 0.106 s^{-1} and the TON was 382 at −2.20 V. The higher is the TON value, the more active is the catalyst. Thus, it can be concluded that the optimum potential for CO_2 reduction varies from −1.80 V and −2.00 V using Cu_2O electrocatalyst in this study.

Table 4.1: Calculated TOF and TON using Cu_2O electrocatalyst at 0.5 M $KHCO_3$, pH 7.0/ NAF/Graphite plate.

Potential Applied (V vs. Ag/AgCl)	TOF of HCOOH (s^{-1})	TON of HCOOH	TOF of CH_3OH (s^{-1})	TON of CH_3OH
−1.40	0.2	720		-
−1.60	0.49	1764		-
−1.80	0.67	2412	0.082	295
−2.00	0.69	2484	0.119	428
−2.20	0.63	2268	0.106	382

Various materials such as metals, complexes of metals, and oxides of metals have already been studied earlier in ERC. Transition metals were reported previously for their

catalytic activity for the production of CO, HCOOH, oxalic acid, and sometimes methane and methanol (Feaster et al., 2017). Among all the metals, Cu could catalyze ERC to hydrocarbons such as CH_4 (FE 27%) and C_2H_4 (FE 19.9%) in CH_3COOK/methanol electrolyte at −3.00 V vs. Ag/AgCl (Kaneco et al., 1999). However, the Cu metal surface has a high affinity to bind with these organic compounds which adversely affect the efficiency of ERC (Lee and Tak, 2001). Thus, scientists have used various derivatives of Cu for ERC of CO_2. Cu metal and its derivatives have been reported for their ability to produce not only hydrocarbons but also various alcohols (CH_3OH, C_2H_5OH, etc.). CuNPs (10-15 nm), were synthesized from Cu nanowires and then impregnated over carbon nanotubes (Cu NPs/CNTs) by a group of researchers. This catalyst was then implemented in ERC and results in a threefold higher HCOOH and CH_3OH formation, in comparison with the so-called wet impregnation method for Cu NPs/CNTs synthesis (Marepally et al., 2017). A group of scientists have shown that the Cu halides can catalyze ERC to ethylene, mediated through the formation of CO and methylene radical, with a superior FE and selectivity in aqueous KBr solution (Yano et al., 2004). Though, the Cu-based catalysts have been reported for a variety of products (hydrocarbons and alcohols), in this system mainly HCOOH and CH_3OH was found as CO_2 reduced product.

In ERC, the CO_2 molecule is first reduced to CO(ad) which is then converted to hydrocarbons through proton insertion reactions (Schouten et al., 2011). This phenomenon has inspired many scientists to synthesize such Cu-based catalysts for the production of hydrocarbons (mediated by the reduction of CO). The CO_2 gas can easily get adsorbed to metal oxide surface and thus the performance depends upon the heat of adsorption on the surface and at first, produces CO. The H_2 gas can be easily produced from the protons and considered as a by-product in ERC. C_1 and C_2 products such as hydrocarbons and alcohols can be generated from the interaction between the adsorbed CO and the H_2 produced. The

heat of adsorption of CO_2 on the Cu_2O site is higher than metallic Cu and thus the Cu_2O surface is more favourable for CO adsorption (Terunuma et al., 1997). In this study, CO was not detected (maybe was not in a measurable value), which may be a reason for not detecting the other higher-order hydrocarbons or alcohols.

4.3.6 Products formation and FE during ERC using NiO electrocatalysts

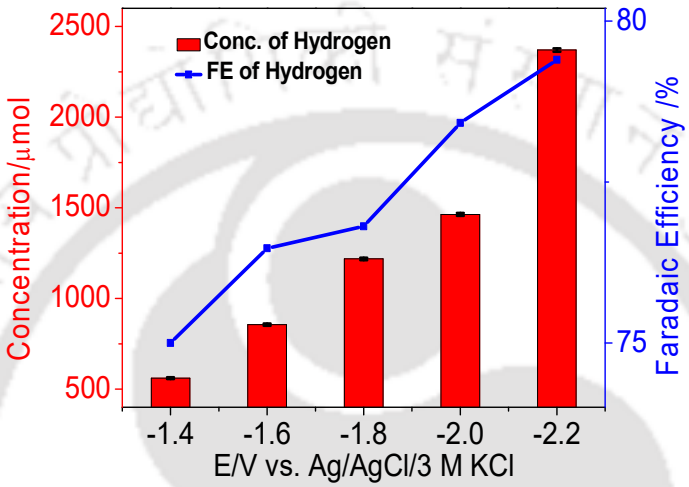

Figure 4.9: Amount of hydrogen evolution and corresponding FE using NiO electrocatalyst. Experimental condition: Electrolyte 0.5 M $KHCO_3$, catholyte, and anolyte 120 mL each, pH 7.0, and CO_2 bubbling rate 10 $mL.min^{-1}$ with ~45 min initial pre-saturation time.

NiO was inactive in reducing CO_2 to any kind of CO_2 reduced products at various applied potentials in this system. Only H_2 was detected as the sole gaseous product and this is the effect of proton reduction only. This study reconfirms the LSV analysis using NiO electrocatalyst. The amount of H_2 production was 550/856/1218/1463/2370 µmol with FE of 75/76.47/76.81/78.42/79.4% at −1.40, −1.60, −1.80, −2.00 and −2.20 V vs. Ag/AgCl respectively (Fig. 4.9). The CO_2 adsorption is very low at the NiO surface (32.53 $µmol.g^{-1}$) (Razali et al., 2017). Generally, the NiO surface is more favourable for proton adsorption and selective for hydrogen evolution mainly and hardly produces any carbon-based

products (Karamad et al., 2015; Nakagawa et al., 1991; Pérez-Rodríguez et al., 2011). In this study also, it produces H_2 only at various electrode potentials. This phenomenon also can be one of the possible reasons for not producing any CO_2 reduced products using NiO as electrocatalysts.

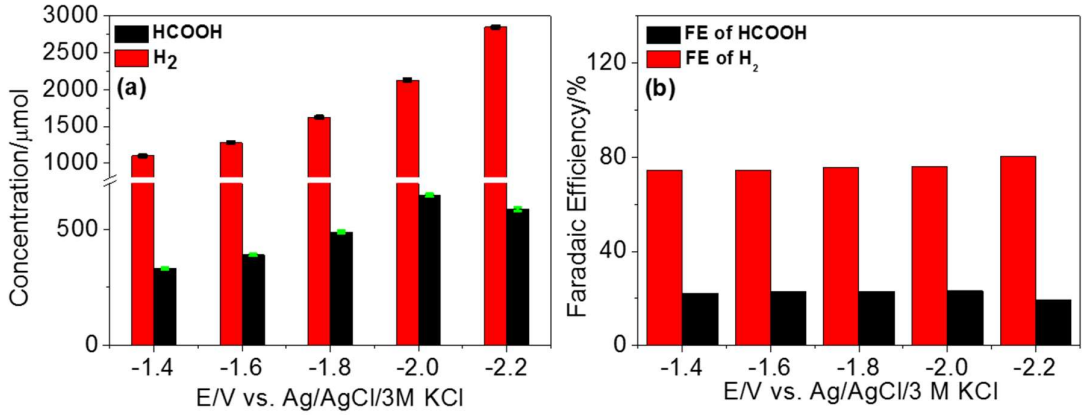

Figure 4.10: (a) Amount of product formation, and (b) corresponding FE using PbO electrocatalyst. Experimental condition: Electrolyte 0.5 M $KHCO_3$, catholyte, and anolyte 120 mL each, pH 7.0, and CO_2 bubbling rate 10 $mL.min^{-1}$ with ~45 min initial pre-saturation time.

4.3.7 Products formation and FE during ERC using PbO electrocatalysts

After the successful completion of preliminary analysis, the potential was varied at five different electrode potentials using PbO electrocatalyst also. The higher current density observed in the CO_2 saturated environment than the inert environment initially confirms that the PbO catalyst can reduce CO_2. Only HCOOH was detected as the lone reduction product during the reduction of CO_2 using lead oxide catalysts at various electrode potentials in this study. In 0.5 M $KHCO_3$ electrolyte solution, Pb cathode is reported for only HCOOH (Koleii et al., 2003). In $KHCO_3$ (0.45 M) + KCl (0.5 M) catholyte solution also, Pb plate as cathode reduces CO_2 to formate (Alvarez-guerra et al., 2012). At −1.40 V

vs. Ag/AgCl, the detectable amount of HCOOH (331 µmol) was found with 22% FE. The amount of HCOOH production was 392 µmol with 22.8% FE at −1.60 V. The amount of HCOOH production was highest at −2.00 V vs. Ag/AgCl with 650 µmol with 23% FE (Fig. 4.10). The product formation decreases above −2.20 V vs. Ag/AgCl and the H_2 production also increases.

The amount of H_2 production was 1100/1277/1624/2131/2849 µmol with FE of 74/74.4/75.6/76/80.37% at −1.40, −1.60, −1.80, −2.00 and at −2.20 V vs. Ag/AgCl respectively. Though lead-based electrodes were used in various aqueous medium, better FEs can be achieved in bicarbonate mediums (Mahmood et al., 1987). According to Kolelii and his group workers also, the Pb/$KHCO_3$ system showed a better result in terms of FE and current densities (Kolelii et al., 2003). The TON and the TOF were also calculated for the PbO electrocatalyst. The TOF and TON increase with increasing potential and highest at −2.20 V vs. Ag/AgCl. Using PbO as the catalyst-material in this system, at −2.20 V, TON = 7668, and TOF 2.13 s^{-1} for HCOOH was found. The lowest TON (3672) and TOF (1.02) was observed at −1.40 V. At −1.80 V, the TON and TOF was observed was 5472 and 1.52 s^{-1} respectively (Table 4.2).

Table 4.2: Calculated TOF and TON using PbO electrocatalyst at 0.5 M $KHCO_3$, pH 7.0/ NAF/Graphite plate.

Potential Applied (V vs. Ag/AgCl)	**TOF of HCOOH (s^{-1})**	**TON of HCOOH**
−1.40	1.02	3672
−1.60	1.18	4248
−1.80	1.52	5472
−2.00	2.01	7236
−2.20	2.13	7668

The main group metals such as lead, tin, bismuth, and indium were also reported for their catalytic activity to produce formic acid from ERC (Baruch et al., 2015; Prakash et al., 2013). In this study, the lead oxide electrode also reported HCOOH production. Commercial PbO_2 can reduce CO_2 to HCOOH in ionic liquid catholyte solution. A FE of 95% was achieved using PbO_2 at −2.30 V vs. Ag/Ag^+ reference electrode (Wu et al., 2018). Oxide derived Pb electrode also delivers better FE than polycrystalline Pb surfaces for the production of CO_2 to formate (Lee and Kanan, 2015). The catalytic systems with the efficiency of producing highly desirable C_{1+} products (C_{1+} stands for the molecule with more than one carbon atom) using metallic lead/lead oxides or lead complexes are not familiar.

Normally metal oxides are basic whereas CO_2 acts as a lewis acid. Thus, there will always be an attraction between them which helps the CO_2 molecule adsorb on the metal oxide surface easily. A similar case happens in the case of PbO as an electrocatalyst also. The role of the working electrode (PbO coated graphite electrode) in ERC is to provide an electron to adsorbed CO_2 on the surface to produce CO_2 radical anion. At the CE (Pt wire) side, the water splits into H^+ and OH^-. The protons are continuously transferred into the WE chamber through the proton exchange membrane (Nafion-117) from the CE side. In presence of proton coming from the CE side, the CO_2 radical anion can produce formate after some internal rearrangements. Then the produced formate can again take H^+ and generates HCOOH and in this way, PbO can take part in CO_2 electroreduction (Albo et al., 2015; Wang et al., 2014). It was noticed that the catalysts were selective towards the formation of HCOOH using mainly Cu_2O and PbO. PbO was almost 100% selective towards HCOOH production at various electrode potentials. Cu_2O was less selective towards CH_3OH production (4%) at −1.80 V vs. Ag/AgCl. The SE was increased with the rise in electrode potentials (5.3% at −2.20 V vs. Ag/AgCl) using Cu_2O as an electrocatalyst.

HCOOH production was almost 100% at various other potentials using Cu_2O (Fig. 4.8c). NiO was inactive in reducing CO_2 and produces only H_2. A comparison among various metal oxide catalysts in ERC used in recent years is provided in Table 4.3.

Table 4.3: Recent reports on electrochemical reduction of CO_2 using various metal oxides and comparing their role with the catalysts reported in this study.

Electrocatalyst	Electrolyte	Experimental conditions	Main products (FE %)	References
PbO	CO_2-saturated [Bmim]BF_4 (0.5 M)	−2.30 V vs. Ag/Ag^+	CO (60%)	Huang et al., 2020
Cu_2O/CuO	0.5 M $KHCO_3$	−1.30 vs. Ag/AgCl	CH_3OH (6.46%)	Roy et al., 2020
CuO	0.5 M $KHCO_3$	−0.65 V vs. RHE	CO (16.6%)	Devi et al., 2019
PbO_2	[Emim]BF_4-MeCN-H_2O	−2.30 V vs. Ag/Ag^+	CO (3.5%)	Wu et al., 2018
Oxide-derived Pb	Dimcarb	1.84 V vs. Cc^+ / 0 (Cc^+ = cobaltocenium)	CO (11.6)	Chen, et al., 2017
CO_3O_4	0.1 M $KHCO_3$	−0.87 V vs. SCE	CO and $HCOO^-$ up to 10 and 80%	Gao et al., 2017
Gd_2O_3 nanoparticles/GC	0.1 M TBAH/CH_3CN	25°C, 1 atm	CO	Behnamfar, 2015
Cu_2O films	0.1 M $KHCO_3$	−0.99 V vs. RHE	C_2H_4 (34-39%), C_2H_5OH (9-16%), CH_4 (<1)	Ren et al., 2015
ZnO/Cu nanoclusters	0.1 M $KHCO_3$	−1.20 V vs. SHE	CO (5.4%), CH_4 (1.8%), C_2H_4 (10%), CH_3OH (2.8%), C_2H_5OH (10%), $HCOO^-$ (8%)	Andrews et al., 2013
Cu_2O powder	**0.5 M $KHCO_3$**	**−2.00 V vs. Ag/AgCl**	**HCOOH (22%), CH_3OH (3.5%)**	**This work**
NiO Powder	**0.5 M $KHCO_3$**	**--**	**--**	
PbO Powder	**0.5 M $KHCO_3$**	**−2.00 V vs. Ag/AgCl**	**HCOOH (23%)**	

4.4 Electrode Characterization

The electrode characterization was done after the successful coating of the catalyst over the electrode surface. The EDX analysis of the coated electrode was conducted to

check the fabricated catalysts on the graphite plate. The stability of the electrode was also checked conducting electrochemical (150 cycle CV) analysis.

4.4.1 EDX analysis of the coated electrode surface

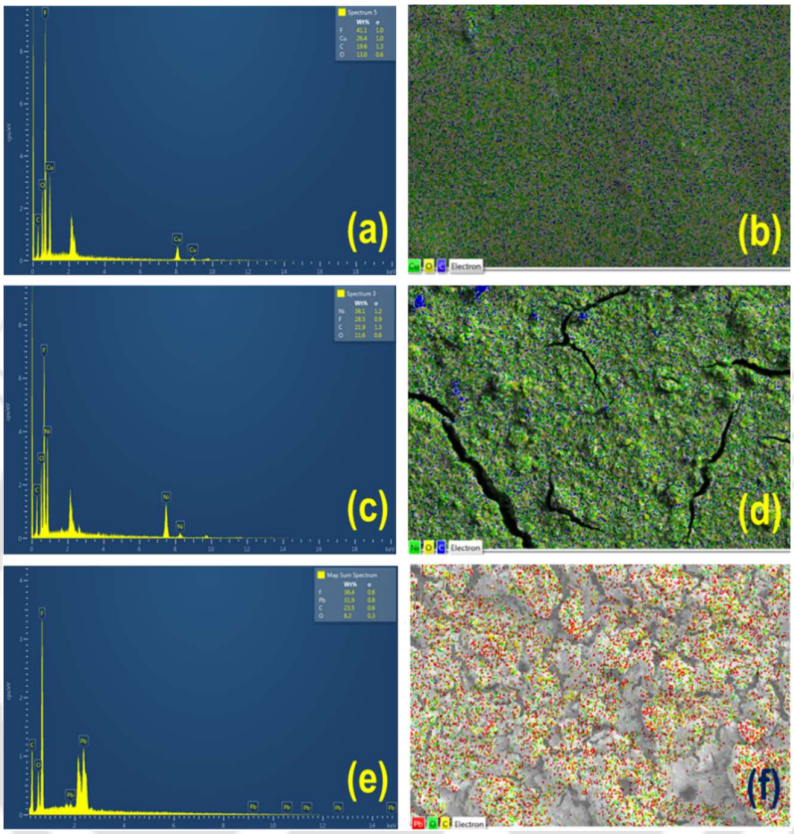

Figure 4.11: Morphology and EDX analysis of metal oxide electrocatalysts. (a) EDX micrograph of the WE after Cu_2O coating: Elemental distribution, (b) Corresponding image mapping showing Cu surface coverage on the WE (green dots) after catalyst coating, (c) EDX micrograph of the WE after NiO coating: Elemental distribution, (d) Corresponding image mapping showing Ni surface coverage on the WE (green dots) after catalyst coating, (e) EDX micrograph of the WE after PbO coating: Elemental distribution and (f) Corresponding image mapping showing Pb surface coverage on the WE (red dots) after catalyst coating.

The EDX analysis was already completed to confirm the catalyst synthesis and described in the results and discussion section (Section 4.3.1 to 4.3.3). After that, the electrocatalysts were fabricated on the graphite plate and then a small portion was scratched from the graphite surface and again EDX analysis was conducted. The surface of the Cu_2O coated electrode contains Cu (26%) O (13%), F (4%) and C (19%) ions (Fig. 4.11a). The NiO nanocomposite contained about 38% Ni, 11% O, 28% F, and 21% C respectively (Fig. 4.11c). In the corresponding image mapping analysis, the distribution of the Cu and Ni metals is shown (green dots) (Figs. 4.11b and 4.11d). In the Figs. 4.11e and 4.11f, the EDX analysis and corresponding mapping of the PbO electrocatalyst (31% Pb, 8.2% O, 36% F, and 23% C) on the graphite plate are displayed. This analysis confirms the successful coating of the electrocatalysts on the electrode surface.

4.4.2 Electrode stability

After the successful completion of the quantification processes, the cyclic voltammetric analysis using the same electrocatalyst coated electrodes were conducted. The process was the same as the linear sweep analysis. At first, N_2 was purged in 0.5 M $KHCO_3$ electrolyte solution and then again CO_2 gas was purged. Then the CV data was taken by sweeping 0 to −2.30 V vs. Ag/AgCl at a scan rate of 30 $mV.s^{-1}$ using the three electrocatalysts for up to the 150th cycle. The current density observed in the 3rd and the 150th cycle was almost similar for the electrocatalysts. Using Cu_2O electrocatalyst the current density was 3% lesser than the 3rd cycle. In the case of NiO electrocatalyst, the current density reduced was only 0.12% and for PbO it was 1.8% only (Fig. 4.12). The difference in current density between the 3rd time and the 150th time is negligible. Thus it can be stated that the catalyst coated electrode is stable up to the 150th cycle in CO_2 saturated medium and are reusable. It also can be stated that the catalyst coating is also

stable up to 150th time CV analysis which confirms the successful coating of the electrocatalysts.

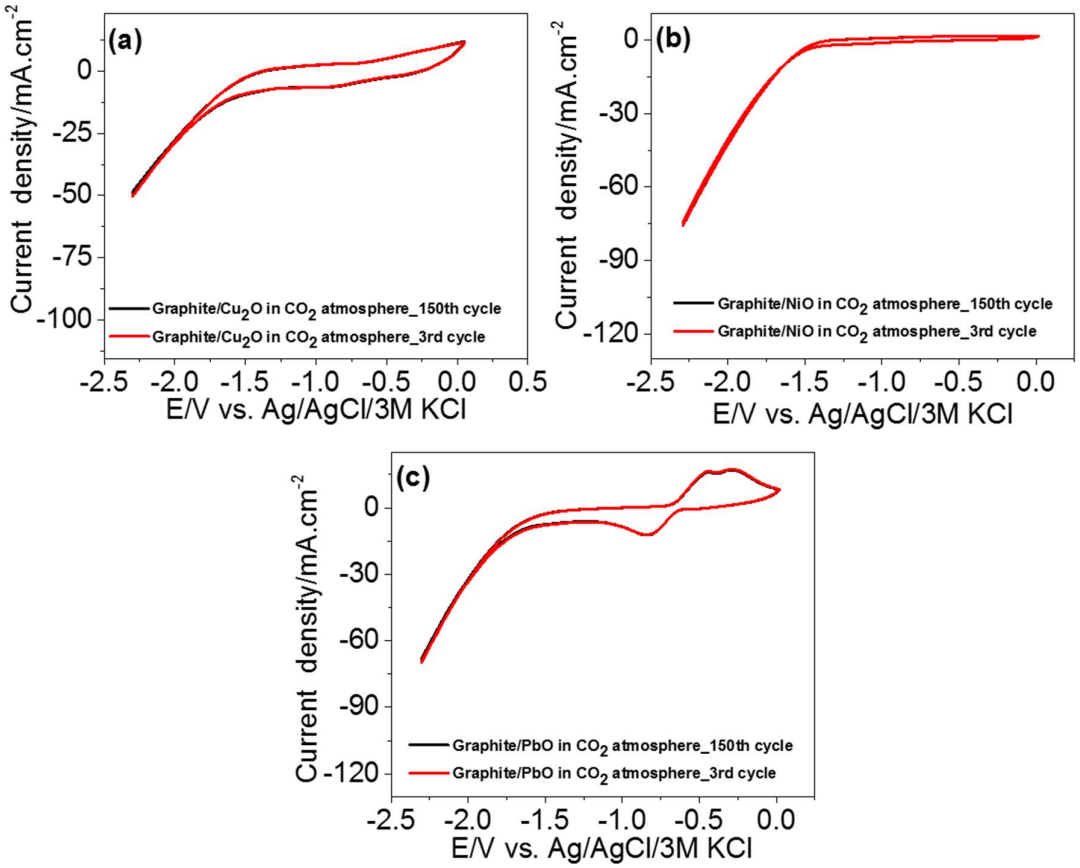

Figure 4.12: Cyclic voltammetry of reduction of CO_2 by sweeping from 0 to −2.30 V vs. Ag/AgCl at CO_2 saturated environment 150 times at a scan rate of 30 $mV.s^{-1}$ using (a) Cu_2O, (b) NiO, and (c) PbO electrocatalysts. Experimental condition: Electrolyte 0.5 M $KHCO_3$, catholyte, and anolyte 120 mL each, pH 7.0, and CO_2 bubbling rate 10 $mL.min^{-1}$ with ~45 min initial pre-saturation time.

4.5 Reaction kinetics

CO_2 molecule is highly stable and difficult to activate. In the present study, the Cu_2O electrocatalyst was active for the formation of mainly HCOOH with a trace amount of CH_3OH. The NiO electrocatalyst was inactive in ERC and was not able to reduce CO_2.

The PbO electrocatalysts were able to produce HCOOH from CO_2 at five different electrode potentials. Moreover, the observed FE was quite less, and the total FE achieved was below 25%. This decreased performance of electrocatalysts can occur due to various reasons.

The activation of CO_2 with one electron transfer from the catalyst to the lowest unoccupied molecular orbital of CO_2 to form radial anion is the most energetically demanding and likely key step. CO_2 adsorption on the catalyst surface can allow for both heterogeneous electrons transfer and CO_2 species stabilization due to the decreased LUMO level of CO_2 as the molecule bends. Depending on the operating conditions, the type of reductant, the number and potential of the charge carriers involved in the reduction reaction, and the number and potential of the charge carriers involved in the reduction reaction, the distribution is determined by the multiple electron-proton transfer steps described below. CO is created by two electrons and proton transfers that occur in the intermediates of $*CO_2$ and *COOH and is regarded as the key intermediate in the formation of a C_2 product. In the metal oxide surfaces, there are mainly four steps are involved in reducing CO_2. The very first step is to adsorption of the gaseous CO_2 molecule onto the catalysts (metal and metal oxides) surface. The heat of adsorption of the CO_2 molecule differs for different metal surfaces and hence affects the reduction process. The second step is the activation of the molecule (CO_2 to CO_2 radical) (Scheme 4.4). After the activation process, the CO_2 radical anion undergoes a proton insertion and reduction process and thus produces HCOOH at first (Scheme 4.5). Then the radical anion can go further for multiple proton insertion and produce CHO radical and then can produce CH_3OH from that (Scheme 2.1, Chapter 2) (Albo et al., 2015). In this way, other by-products will also be generated further with multiple proton addition and reduction reaction. The last step is the desorption of that products from the catalyst coated WE (Scheme 4.4). The inefficient desorption process

from the electrode surface adversely affects the electrode surface and thus reduces the active surface area as well as the electrolyte diffusion etc. These problems not only reduce the FE of CO_2 reduced products but also increases the efficiency of H_2 evolution (Hao and Shi, 2018).

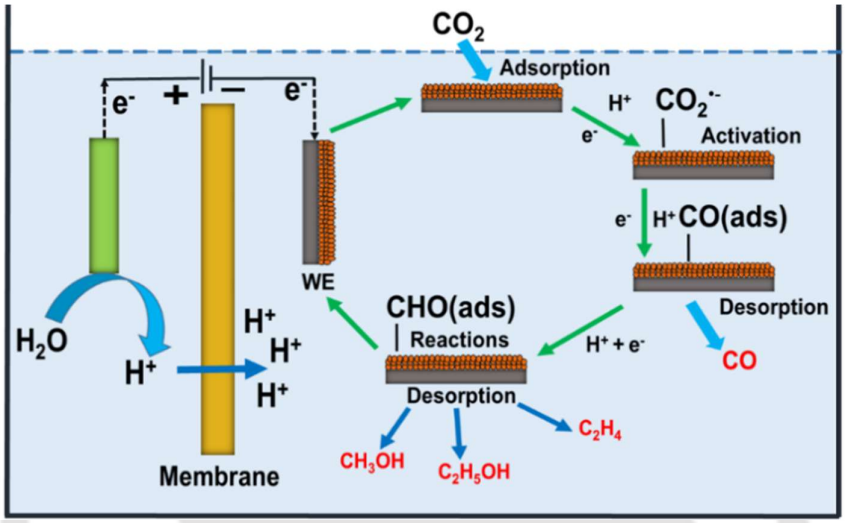

Scheme 4.4: Proposed mechanism and the major steps of ERC reactions in metal and metal oxide surfaces (Hao and Shi, 2018; Hatsukade et al., 2014).

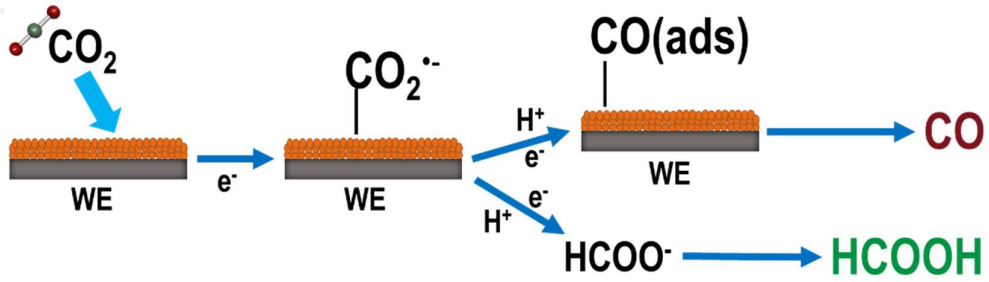

Scheme 4.5: Probable mechanism for CO and HCOOH production from ERC (Albo et al., 2015).

In this system, a comparatively large electrochemical reactor was used (already discussed in chapter 3) and thus the hydrogen gas evolution was always competitive with ERC reactions. Not only that, there was always a competition between the H_2O and the CO_2 molecule to adsorb on the catalyst surface. Metal complexes act differently than metal

oxides in presence of CO_2 in an electrochemical system. The central metal atom of the transition metal complexes is reduced to M^{+1} from its M^{+2} state and form a complex with CO_2^- radical compound. Thus, conversion between the M^{+2} to the M^{+1} state is the key factor for the activation of the CO_2 molecule. The intermediate M^{+1} again go back to its previous state M^{+2}, and thus reduces CO_2. In this way, the problem of the poisoning of the electrode material can be resolved (Shen et al., 2015). Concerning these things in mind, metal complexes (with increased FE in terms of CO_2 reduced products) were introduced of the same transition and main group metals discussed here and elaborated in chapters 5, 6, and 7.

References

Albo, J., Alvarez-guerra, M., Castaño, P., and Irabien, A., 2015. "Towards the Electrochemical Conversion of Carbon Dioxide into Methanol." *Green Chemistry*, *17*, 2304-2324.

Alvarez-guerra, M., Quintanilla, S., and Irabien, A., 2012. "Conversion of Carbon Dioxide into Formate using a Continuous Electrochemical Reduction Process in a Lead Cathode." *Chemical Engineering Journal*, *207-208*, 278-284.

Andrews, E., Ren, M., Wang, F., Zhang, Z., Sprunger, P., Kurtz, R., and Flake, J., 2013. "Electrochemical Reduction of CO_2 at Cu Nanocluster/$(10\bar{1}0)$ ZnO Electrodes." *Journal of The Electrochemical Society*, *160*, H841-H846.

Arana, C., Keshavarz, M., Potts, K. T., and Abruña, H. D., 1994. "Electrocatalytic Reduction of CO_2 and O_2 with Electropolymerized Films of Vinyl-terpyridine Complexes of Fe, Ni and Co." *Inorganica Chimica Acta*, *225*, 285-295.

Arshadi-rastabi, S., Moghaddam, J., & Eskandarian, M. R., 2015. "Synthesis, Characterization and Stability of Cu_2O Nanoparticles Produced via Supersaturation Method Considering Operational Parameters Effect." *Journal of Industrial and Engineering Chemistry*, *22*, 34-40.

Arulmozhi, K. T., and Mythili, N., 2013. "Studies on the Chemical Synthesis and Characterization of Lead Oxide Nanoparticles with Different Organic Capping Agents." *AIP Advances 3*, 122122, 1-9.

Baruch, M. F., Pander III, J. E., White, J. L., and Bocarsly, A. B., 2015. "Mechanistic Insights into the Reduction of CO_2 on Tin Electrodes using in Situ ATR-IR Spectroscopy." *ACS Catalysis*, *5*, 3148-3156.

Behnamfar, M. T., 2015. "Preparation of Gd_2O_3 Nanoparticles from a New Precursor and their Catalytic Activity for Electrochemical Reduction of CO_2 to CO." *Particle*

Science and Technology, *3*, 21-30.

Bhosale, M. A., and Bhanage, B. M., 2016. "A Simple Approach for Sonochemical Synthesis of Cu_2O Nanoparticles with High Catalytic Properties." *Advanced Powder Technology*, *27*, 238-244.

Cattley, C. A., Stavrinadis, A., Beal, R., Moghal, J., Cook, A. G., Grant, P. S., Smith, J. M., Assender, H., and Watt, A. A. R., 2010. "Colloidal Synthesis of Lead Oxide Nanocrystals for Photovoltaics." *Chemical Communications*, *46*, 2802-2804.

Channu, V. S. R., Holze, R., and Rambabu, B., 2012. "Synthesis and Characterization of NiO Nanoparticles for Electrochemical Applications." *Colloids and Surfaces A: Physicochemical and Engineering Aspects*, *414*, 204-208.

Chen, C., Xu, H., Xu, L., Zhang, F., Dong, J., and Wang, H., 2013. "One-pot Synthesis of Homogeneous Core-shell Cu_2O Films with Nanoparticle-Composed Multishells and Their Photocatalytic Properties." *RSC Advances*, *3*, 25010-25018.

Chen, L., Li, F., Bentley, C. L., Horne, M., Bond, A. M., and Zhang, J., 2017. "Electrochemical Reduction of CO_2 with an Oxide-Derived Lead Nano-Coralline Electrode in Dimcarb." *ChemElectroChem,* 4, 1402-1410.

Deciccio, D., Ahn, S. T., Sen, S., Schunk, F., Palmore, G. T. R., and Rose-Petruck, C., 2015. "Electrochemical Reduction of CO_2 with Clathrate Hydrate Electrolytes and Copper Foam Electrodes." *Electrochemistry Communications*, *52*, 13-16.

Devi, P., Malik, K., Arora, E., Bhattacharya, S., Kalendra, V., Lakshmi, K. V, Verma, A., Singh, J. P., 2019. "Selective electrochemical reduction of CO_2 to CO." *Catalysis Science & Technology*, *9*, 5339-5349.

El-kemary, M., Nagy, N., and El-Mehasseb, I., 2013. "Materials Science in Semiconductor Processing Nickel oxide nanoparticles : Synthesis and spectral studies of interactions with glucose." *Materials Science in Semiconductor Processing*, *16*, 1747-1752.

Feaster, J. T., Shi, C., Cave, E. R., Hatsukade, T., Abram, D. N., Kuhl, K. P., Hahn, C., Nørskov, J. K., and Jaramillo, T. F., 2017. "Understanding Selectivity for the Electrochemical Reduction of Carbon Dioxide to Formic Acid and Carbon Monoxide on Metal Electrodes." *ACS Catalysis*, *7*, 4822−4827.

Gao, S., Sun, Z., Liu, W., Jiao, X., Zu, X., Hu, Q., Sun, Y., Yao, T., Zhang, W., Wei, S., and Xie, Y., 2017. "Atomic layer confined vacancies for atomic-level insights into carbon dioxide electroreduction." *Nature Communications*, *8*, 1-9.

Hao, J., and Shi, W., 2018. "Transition metal (Mo, Fe, Co, and Ni) based catalysts for electrochemical CO_2 reduction." *Cuihua Xuebao/Chinese Journal of Catalysis*, *39*, 1157-1166.

Hara, K., Kudo, A., and Sakata, T., 1995. "Electrochemical reduction of carbon dioxide under high pressure on various electrodes in an aqueous electrolyte." *Journal of Electroanalytical Chemistry*, *391*, 141-147.

Hatsukade, T., Kuhl, K. P., Cave, E. R., Abram, D. N., and Jaramillo, T. F., 2014. "Insights into the electrocatalytic reduction of CO_2 on metallic silver surfaces." *Phys. Chem. Chem. Phys.*, *16*, 13814-13819.

Hazarika, J., and Manna, M. S., 2019. "Electrochemical reduction of CO_2 to methanol with synthesized Cu_2O nanocatalyst: Study of the selectivity." *Electrochimica Acta*, *328*, 1-9.

Hirunsit, P., Soodsawang, W., and Limtrakul, J., 2015. "CO_2 electrochemical reduction to methane and methanol on copper-based alloys: Theoretical insight." *Journal of Physical Chemistry C*, *119*, 8238-8249.

Hori, Y., Wakebe, H., Tsukamoto, T., and Koga, O., 1993. "Electrocatalytic process of CO selectivity in electrochemical reduction of CO_2 at metal electrodes in aqueous media." *Electrochimica Acta*, *39*, 1833-1839.

Hori, Y., 2008. "Electrochemical CO_2 reduction on metal electrodes," In Vayenas *et al.* (ed.) 'Modern Aspects of Electrochemistry', No. 42, Ch. 3, Springer, New York, pp. 89-189.

Huang, X., Song, J., Wu, H., Xie, C., Hua, M., and Hu, Y., 2020. "Ordered-Mesoporous-Carbon-Confined Pb / PbO Composites : Superior Electrocatalysts for CO_2 Reduction." *ChemSusChem*, *13*, 6346-6352.

Kalaie, M. R., Youzbashi, A. A., Meshkot, M. A., and Hosseini-Nasab, F., 2016. "Preparation and characterization of superparamagnetic nickel oxide particles by chemical route." *Applied Nanoscience*, *6*, 789-795.

Kaneco, S., Iiba, K., Ohta, K., and Mizuno, T., 1999. "Electrochemical reduction of carbon dioxide on copper in methanol with various potassium supporting electrolytes at low temperature." *Journal of Solid State Electrochemistry*, *3*, 424-428.

Kannan, K., Muthuraman, G., and Moon, I. S., 2014. "Controlled synthesis of highly spherical nano-PbO_2 particles and their characterization." *Materials Letters*, *123*, 19-22.

Karamad, M., Hansen, H. A., Rossmeisl, J., and Nørskov, J. K., 2015. "Mechanistic Pathway in the Electrochemical Reduction of CO_2 on RuO_2." *ACS Catalysis*, *5*, 4075-4081.

Koleii, F., Atilan, T., Palamut, N., Gizir, A. M., Aydin, R., and Hamann, C. H., 2003. "Electrochemical reduction of CO_2 at Pb and Sn electrodes in a fixed-bed reactor in aqueous K_2CO_3 and $KHCO_3$ media." *Journal of Applied Electrochemistry*, *33*, 447-450.

Kumar, Bijandra, Brian, J. P., Atla, V., Kumari, S., Bertram, K. A., White, R. T., and Spurgeon, J. M., 2016. "New trends in the development of heterogeneous catalysts for electrochemical CO_2 reduction." *Catalysis Today*, *270*, 19-38.

Kumar, B., Smita, K., Debut, A., and Cumbal, L., 2020. "Andean sacha inchi (*Plukenetia Volubilis* L.) Leaf-mediated synthesis of Cu_2O nanoparticles: A low-cost approach." *Bioengineering*, *7*, 1-10.

Le, M., Ren, M., Zhang, Z., Sprunger, P. T., Kurtz, R. L., and Flake, J. C., 2011. "Electrochemical Reduction of CO_2 to CH_3OH at Copper Oxide Surfaces." *Journal of The Electrochemical Society*, *158*, E45-E49.

Lee, C. H., and Kanan, M. W., 2015. "Controlling H^+ vs. CO_2 Reduction Selectivity on Pb Electrodes." *ACS Catalysis*, *5*, 465-469.

Lee, J., and Tak, Y., 2001. "Electrocatalytic activity of Cu electrode in electroreduction of CO_2." *Electrochimica Acta*, *46*, 3015-3022.

Li, C. W., and Kanan, M. W., 2012. "CO_2 Reduction at Low Overpotential on Cu Electrodes Resulting from the Reduction of Thick Cu_2O Films." 134, 7231-7234.

Li, S., Yang, W., Chen, M., Gao, J., Kang, J., and Qi, Y., 2005. "Preparation of PbO nanoparticles by microwave irradiation and their application to Pb(II)-selective electrode based on cellulose acetate." *Materials Chemistry and Physics*, *90*, 262-269.

Liu, D., Li, D., and Yang, D., 2017. "Size-dependent magnetic properties of branchlike nickel oxide nanocrystals." *AIP Advances*, *7*, 1-8.

Liu, G., He, F., Li, X., Wang, S., Li, L., Zuo, G., Huang, Y., and Wan, Y., 2011. "Three-dimensional cuprous oxide microtube lattices with high catalytic activity templated by bacterial cellulose nanofibers." *Journal of Materials Chemistry*, *21*, 10637-10640.

Mahmood, M. N., Masheder, D., Harty, C. J., 1987. "Use of gas-diffusion electrodes for high-rate electrochemical reduction of carbon dioxide. I. Reduction at lead, indium and tin impregnated electrodes."*17*, 1159-1170.

Marepally, B. C., Ampelli, C., Genovese, C., Tavella, F., Veyre, L., Quadrelli, E. A., Perathoner, S., and Centi, G., 2017. "Role of small Cu nanoparticles in the behavior

of nanocarbon-based electrodes for the electrocatalytic reduction of CO_2." *Journal of CO_2 Utilization*, *21*, 534-542.

Maria D. Salazar-Villalpando., 2011. "Effect of Electrolyte on the Electrochemical Reduction of CO_2." *ECS Transactions*, *33*, 77-88.

Nakagawa, S., Kudo, A., Azuma, M., and Sakata, T., 1991. "Effect of pressure on the electrochemical reduction of CO_2 on Group VIII metal electrodes." *Journal of Electroanalytical Chemistry*, *308*, 339-343.

Nik Roselina, N. R., and Azizan, A., 2012. "Ni nanoparticles: Study of particles formation and agglomeration." *Procedia Engineering*, *41*, 1620-1626.

Prakash, G. K. S., Viva, F. A., and Olah, G. A., 2013. "Electrochemical reduction of CO_2 over Sn-Na fi on Ò coated electrode for a fuel-cell-like device." *Journal of Power Sources*, *223*, 68-73.

Rahdar, A., Aliahmad, M., and Azizi, Y., 2015. "NiO Nanoparticles : Synthesis and Characterization." *Journal of Nanostructures*, *5*, 145-151.

Razali, M. H., Osman, U. M., Rozaini, M. Z. H. M., and Yusoff, M., 2017. "CO_2 adsorption study on NiO and Pr_2O_3-NiO catalyst synthesis using simple sol-gel method." *Oriental Journal of Chemistry*, *33*, 1864-1870.

Ren, D., Fong, J., and Yeo, B. S., 2018. "The effects of currents and potentials on the selectivities of copper toward carbon dioxide electroreduction. " *Nature Communications*, *9*, 1-8.

Roy, A., Jadhav, H. S., and Gil Seo, J., 2020. "Cu_2O/CuO Electrocatalyst for Electrochemical Reduction of Carbon Dioxide to Methanol." *Electroanalysis*, *32*, 1-9.

Schouten, K. J. P., Kwon, Y., Van Der Ham, C. J. M., Qin, Z., and Koper, M. T. M., 2011. "A new mechanism for the selectivity to C_1 and C_2 species in the electrochemical

reduction of carbon dioxide on copper electrodes." *Chemical Science*, *2*, 1902-1909.

Sharma, S. K., Bahadur, J., Patil, P. N., Maheshwari, P., Mukherjee, S., Sudarshan, K., Mazumder, S., and Pujari, P. K., 2013. "Revealing the nano-level molecular packing in chitosan-NiO nanocomposite by using positron annihilation spectroscopy and small-angle X-ray scattering." *ChemPhysChem*, *14*, 1055-1062.

Shen, J., Kortlever, R., Kas, R., Birdja, Y. Y., Diaz-morales, O., Kwon, Y., Ledezma-Yanez, I., Schouten, K. J. P., Mul, G., and Koper, M. T. M., 2015. "Electrocatalytic reduction of carbon dioxide to carbon monoxide and methane at an immobilized cobalt protoporphyrin." *Nature Communications*, *6*, 1-8.

Terunuma, Y., Saitoh, A., and Momose, Y., 1997. "Relationship between hydrocarbon production in the electrochemical reduction of CO_2 and the characteristics of the Cu electrode." *Journal of Electroanalytical Chemistry*, *434*, 69-75.

Uchida, T., Sasaki, Y., Ikeshoji, T., and Osawa, M., 2017. "4, 4′-Bipyridine as a molecular catalyst for electrochemical hydrogen production." *Electrochimica Acta*, *248*, 585-592.

Wang, S. J., Zhang, H., Shao, L. M., Liu, S. M., and He, P. J., 2014. "Thermochemical reaction mechanism of lead oxide with poly(vinyl chloride) in waste thermal treatment." *Chemosphere*, *117*, 353-359.

Wu, H., Song, J., Xie, C., Hu, Y., and Han, B., 2018. "Highly efficient electrochemical reduction of CO_2 into formic acid over lead dioxide in an ionic liquid-catholyte mixture." *Green Chemistry*, *20*, 1765-1769.

Wu, J. C. S., Lin, H. M., and Lai, C. L., 2005. "Photoreduction of CO_2 to methanol using optical-fiber photoreactor." *Applied Catalysis A: General*, *296*, 194-200.

Yano, H., Tanaka, T., Nakayama, M., and Ogura, K., 2004. "Selective electrochemical reduction of CO_2 to ethylene at a three-phase interface on copper(I) halide-confined

Cu-mesh electrodes in acidic solutions of potassium halides." *Journal of Electroanalytical Chemistry*, *565*, 287-293.

Zou, S., Liu, J., Kobayashi, H., Hu, X., Xiao, L., and Fan, J., 2014. "A new reaction between common compounds: Lead oxide reacts with formaldehyde." *Chemical Communications*, *50*, 6316-6318.

CHAPTER 5

Cu(II)-Salen Complexes as Electrocatalysts for CO_2 Reduction

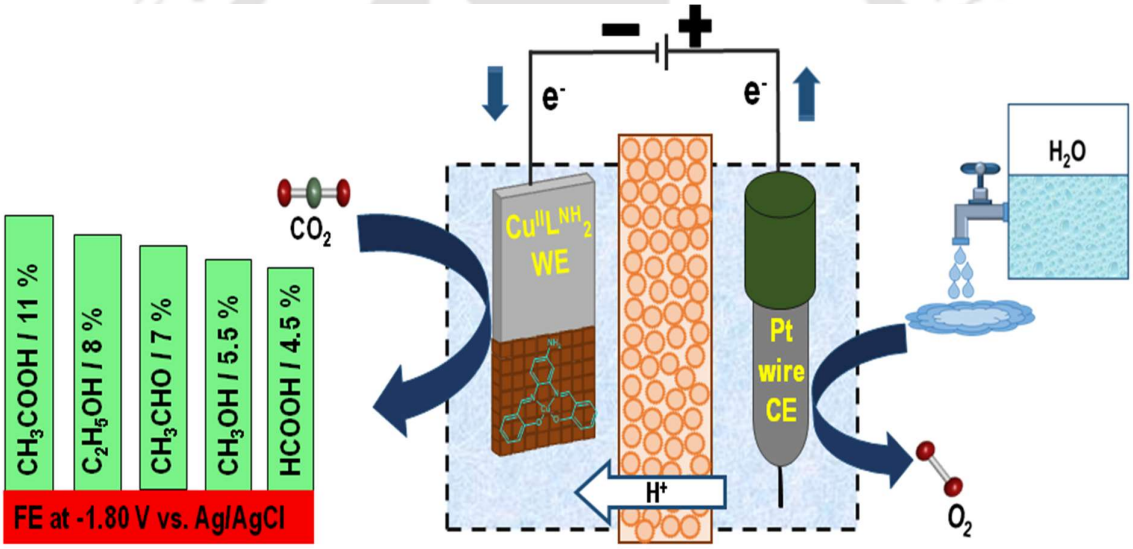

5.1 Background of the work

In the previous chapter (4), the role of metal oxides in ERC was examined. In this chapter, a four-coordinate Cu(II) salen complex {[$Cu^{II}(L^{NH_2})$]; **1**} of the tetradentate $H_2L^{NH_2}$ ligand was introduced through a metalation reaction in the presence of Et_3N. Salen ligand-based complexes are already studied by many researchers for their ability to catalyze various chemical reactions (Cohen and Coates, 2006; Cozzi, 2004). A bifunctional Co salen complex containing acidic and basic sites exhibits excellent ability to capture CO_2 (Gambarotta et al., 1982). Not only that, salen was chosen as the ligand backbone of the complex because: (i) it forms thermodynamically stable metal complexes, and (ii) in metal-salen complexes, the metal ion resides over the salen coordination unit that would render easy access to CO_2 molecules. An anchoring group (-NH_2) was attached in the ligand backbone to examine its ability to facilitate the electron transfer process during multielectron ERC to value-added product formation. The synthesized complex (**1**) acted as an electrocatalyst for the CO_2 conversion towards C_1 and C_2 products by activating the stable C-O bond. Complex **1** showed a better catalytic performance in terms of FE (35%) and product formation. The CO_2-reduced products were obtained as HCOOH>CH_3COOH>CH_3OH>C_2H_5OH, which were formed through multiple-electrons transfer (2 e^- to 12 e^-) proton-insertion reactions. Complex **1**, at −1.80 V vs. Ag/AgCl exhibited high selectivity towards the production of C_2 products (C_2H_5OH and CH_3COOH) with a high FE. The catalytic activity of the Cu(II) complex was enhanced by the presence of the terminal -NH_2 anchoring-group in the ligand backbone. The fact was confirmed by electrocatalytic CO_2 conversion experiments in the presence of [Cu^{II}(L)] complex as the electrocatalyst, which did not contain the anchoring group in the salen ligand structure.

5.2 Synthesis of salen ligand $H_2L^{NH_2}$ and corresponding complex 1: $[Cu^{II}(L^{NH_2})]$

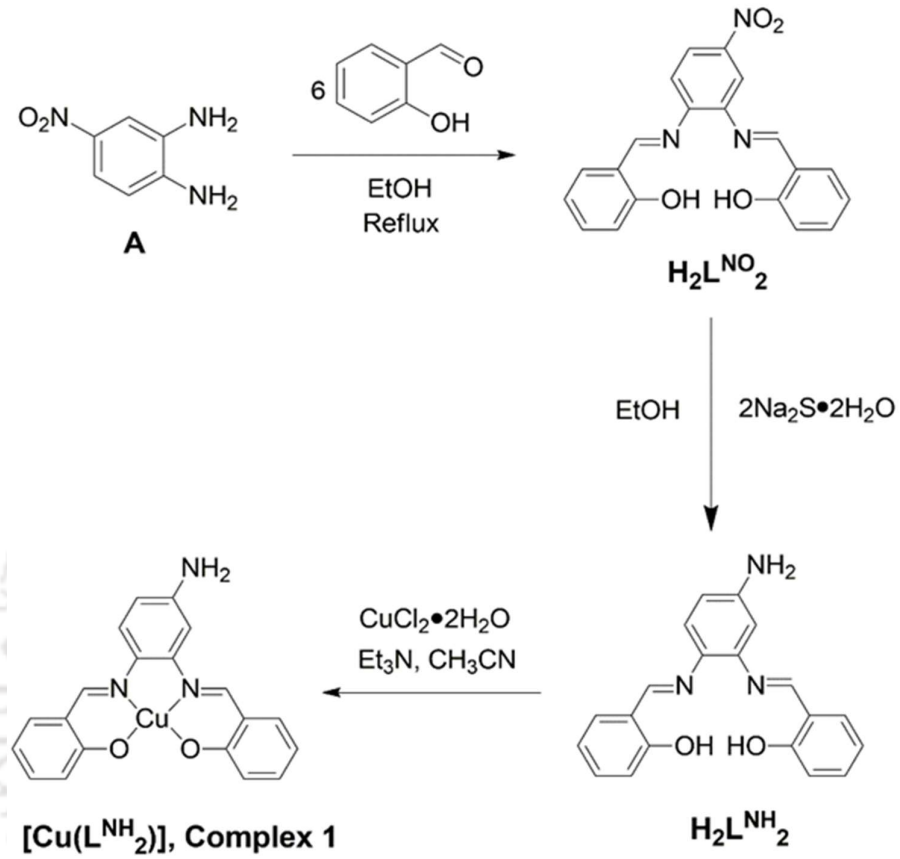

Scheme 5.1. Schematized steps for the synthesis route of Cu(II) complex (**1**).

Salen ligand $H_2L^{NO_2}$ was synthesized from the reaction of compound **A** (1.53 g; 10 mmol) and salicyldehyde (7.32 g; 60 mmol) in 1:6 ratio (w/w) as reported previously (Singh et al., 2015). After that, ligand $H_2L^{NO_2}$ (1.81 g; 5 mmol) was mixed with $Na_2S•H_2O$ (0.78 g; 10 mmol) in EtOH (15 mL). The suspension was stirred under refluxing condition for 10 mins to get a homogeneous solution. Then the reaction solution was cooled and kept at 0°C for 4 h. During the time, a yellow colour precipitate appeared which was collected by filtration and then washed thoroughly with EtOH and dried under air to get expected ligand $H_2L^{NH_2}$; $C_{20}H_{17}N_3O_2$; (Yield: 0.68 g, 41%) (Scheme 5.1).

Salen ligand $H_2L^{NH_2}$ (0.163 g; 0.5 mmol) was then mixed with $CuCl_2 \cdot 2H_2O$ (0.086 g; 0.5 mmol) in CH_3CN (8 mL) solution. In that mixture triethylamine (0.2 mL) was added dropwise and the mixture was stirred properly for 6 h at 30°C. A color change was observed from yellow to brown, and after 6 h of stirring the precipitate was collected. The precipitate was filtered, washed with CH_3CN, and kept for drying. Then the desired $[Cu^{II}(L^{NH_2})]$ complex ($C_{20}H_{15}N_3O_2Cu$; **1**) was obtained (Scheme 5.1). Yield: 0.143 g, 73%.

5.3 Results and Discussion

5.3.1 Ligand and metal complex characterization

The synthesized ligand was characterized using NMR and FTIR spectroscopy and ESI-MS analysis. The metal complex was characterized by FTIR spectroscopy, Mass, and CHN analysis. All the electrochemical analysis was conducted using Potentiostat.

5.3.1.1 Nuclear magnetic resonance spectrum of $H_2L^{NH_2}$ ligand

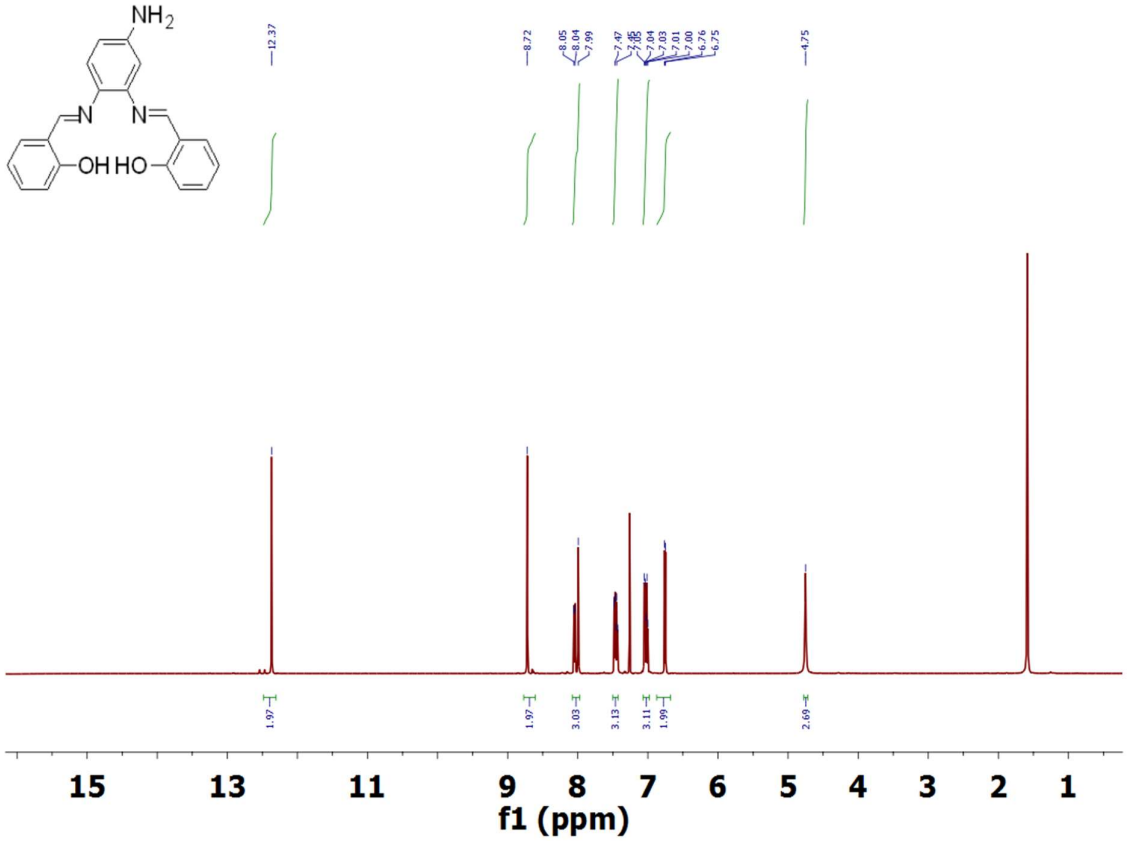

Figure 5.1: ^{1}H NMR spectrum of synthesized ligand $H_2L^{NH_2}$ (in $CDCl_3$).

The NMR spectrum was recorded by solubilizing 8 mg of the ligand sample in $CDCl_3$ solution. The obtained NMR spectrum of $H_2L^{NH_2}$ ligand is shown in Fig. 5.1. In Fig 5.1, the peaks observed in the NMR spectrum was the hydrogen atoms present in the ligand. ^{1}H NMR ($CDCl_3$, 600 MHz): δ 4.75(s, 2H), 6.75 (d, J = 6 Hz, 1H), 6.76 (d, J = 6 Hz, 1H), 7.00-7.05 (m, 3H), 7.43-7.48 (m, 3H), 7.99-8.05 (t, 3H), 8.72 (s, 2H), 12.37 (s, 2H). The H atoms in the hydroxyl groups are reflected at the position of 12.37 ppm and the others are attached with carbon atoms present in the ligand.

5.3.1.2 Mass analysis of $H_2L^{NH_2}$ ligand and corresponding complex 1

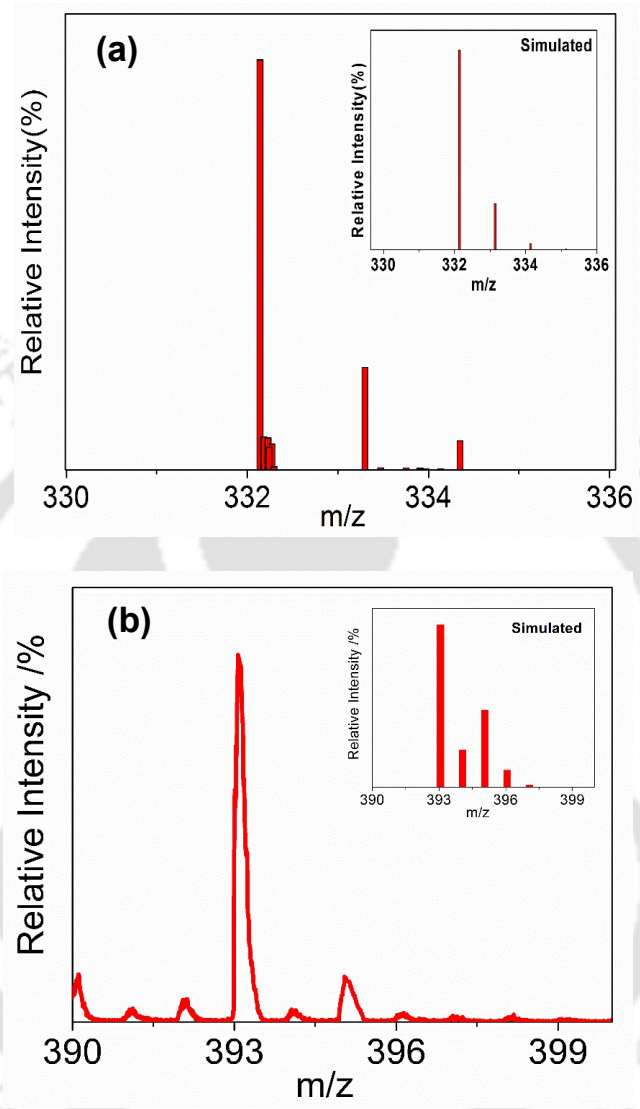

Figure 5.2: Experimental and simulated mass spectrum of synthesized ligand (a) $H_2L^{NH_2}$ [$C_{20}H_{17}N_3O_2$ + H], and (b) complex **1** [$C_{20}H_{15}N_3O_2Cu$ + H].

High-resolution mass spectrum (HR-MS) analysis in positive mode on ligand appeared at 332.16 amu [$C_{20}H_{17}N_3O_2$ + H] (Fig. 5.2a). The theoretically calculated weight value of the ligand was 332.14. The almost similar values of the calculated and the experimental analysis revealed the successful synthesis of the ligand. Electrospray

ionization mass spectrum (ESI-MS) analysis in positive mode on complex **1** appeared at 393.08 amu and the theoretically calculated values were 393.05 (Fig. 5.2b). The peak corroborated to the composition $C_{20}H_{16}N_3O_2Cu$ was established by isotope pattern distribution. The composition corresponded to [M + H]; where M is the molecular composition of the expected complex **1**. Thus, mass spectrum analysis was congruous with the formation of the complex.

5.3.1.3 FTIR spectra of $H_2L^{NH_2}$ ligand and corresponding complex 1

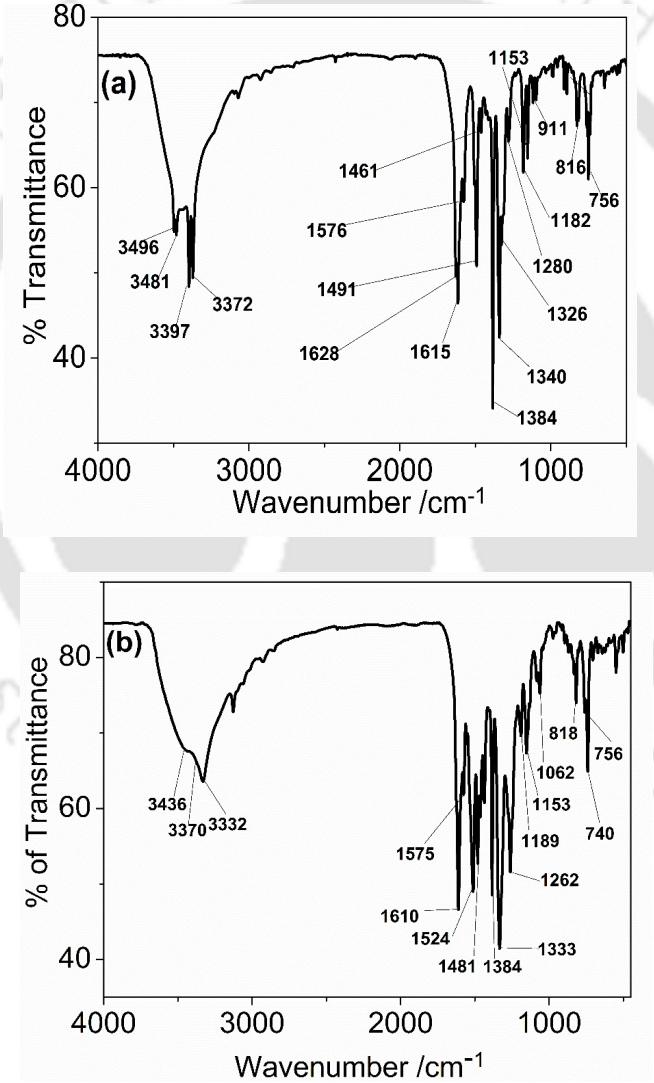

Figure 5.3: FTIR spectra of (a) ligand $H_2L^{NH_2}$ and (b) corresponding complex **1**.

The FTIR spectrum of $H_2L^{NH_2}$ ligand was observed at characterized peaks at 3496, 3481, 3397, 3372, 1576, 1615, 1491, 1340, 1280, 1182, 911, 816 and 756 cm^{-1}. In the FTIR spectrum of ligand $H_2L^{NH_2}$, two bands for ν(O-H) stretches of the two -OH groups appeared at 3496 and 3481 cm^{-1} (Fig. 5.3a). The asymmetric and symmetric ν(N-H) stretches for the $-NH_2$ group were found at 3397 and 3372 cm^{-1}, respectively. Similar to two -OH stretches, two different ν(C=N) stretches appeared at 1628 and 1615 cm^{-1}. These features reflected the fact that the two salen units were from two different chemical environments. The position of the anchoring $-NH_2$ group relative to the imine group (ortho- and meta-) was responsible for such a dissimilar chemical environment. The FTIR spectrum of complex **1** was observed at characterized peaks at 3436, 3370, 3332, 1610, 1575, 1333, 1262, 1189, 1153, 1062, 818, 756 and at 740 cm^{-1}. In the FTIR spectrum of the corresponding Cu(II) complex, ν(N-H) stretches of the $-NH_2$ anchoring-group observed at 3370 and 3332 cm^{-1} (Fig. 5.3b). The aldamine C=N stretch was found at 1610 cm^{-1}. The asymmetric ν(C=C) stretch for the phenyl systems was observed at 1575 cm^{-1}. The shift in the peaks was observed in complex **1** than the ligand proves the successful synthesis of it.

5.3.1.4 X-band EPR spectrum of complex 1

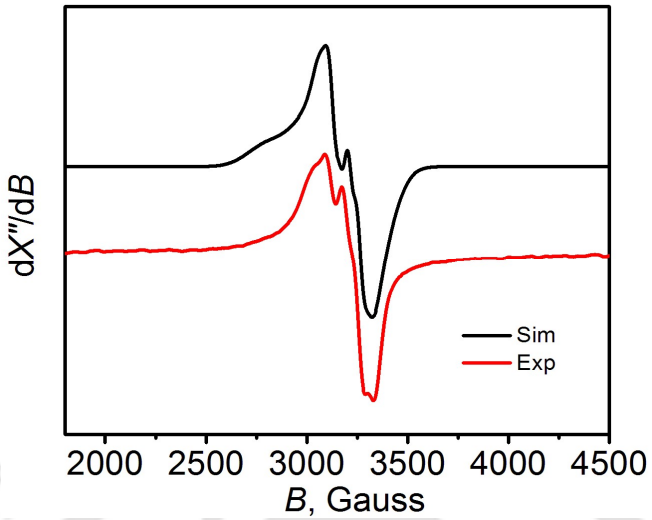

Figure 5.4: X-band EPR spectrum of complex **1** in DMF solution measured at room temperature, X-band microwave frequency (GHz): 9.43, microwave power: 0.995 mW, modulation frequency = 100 kHz, and amplitude = 70 G.

Complex **1** was paramagnetic in nature. The presence of Cu(II)-centered unpaired electron was consolidated by X-band EPR measurement at 25°C. The experimental X-band EPR spectrum of complex **1** along its simulated spectrum is shown in Fig. 5.4. The experimentally obtained spectrum was satisfactorily simulated with the following parameters: $g_1 = g_2 = 2.11$; $g_3 = 2.20$; Cu (A_1, A_2, A_3) = (37, 57, 183) × 10^{-4}.cm^{-1}. $g_3 > g_1 = g_2 > g_e = 2.0003$ and $A_3 > A_2 > A_1$ values indicated an axial four-coordinate system with the existence of the unpaired electron at the $3d_{x^2-y^2}$ orbital of the central Cu (II) ion (Bennur et al., 2001).

5.3.1.5 CHN analysis of complex 1

The elemental analysis (CHN) of complex **1** was conducted to establish the elemental formula. Two molecules of acetonitrile and five molecules of lattice bound water were found in the experimentally calculated value of complex **1**. Thus, the theoretically calculated percentage of C, H, and N were 51.05, 5.54, and 12.41%. The experimental

composition was found is % C 51.09; % H 5.71; % N 12.80. Therefore, the elemental formula is $C_{20}H_{15}N_3O_2Cu•2CH_3CN•5H_2O$.

5.3.2 Voltammetric analysis during ERC using complex 1 electrocatalyst

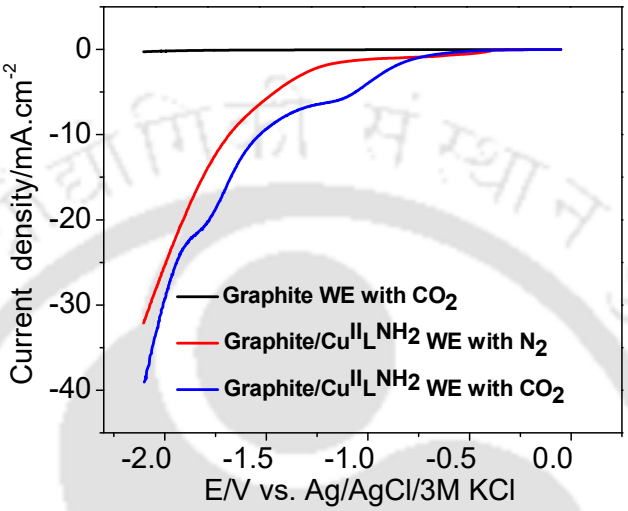

Figure 5.5: LSV analysis at bare and complex **1**/graphite WEs during ERC under inert and CO_2 environment with 30 $mV.s^{-1}$ scan rate. Experimental condition: Electrolyte 0.5 M $KHCO_3$, catholyte, and anolyte 120 mL each, pH 7.0, and CO_2 bubbling rate 10 $mL.min^{-1}$ during ~45 min initial pre-saturation time.

In examining the metal complex **1** as a catalyst in ERC, the electrochemical measurements were performed in a bicarbonate solution at neutral pH. Bicarbonates suppress the H_2 evolution reaction, and the cationic species effect H_2 release with the increasing order as $Li^+>Na^+>Cs^+>K^+$ (Murata and Hori, 1991). On the other hand, CO_2 (ad) and H_2CO_3 species prevail in an acidic catholyte pH which could enhance H_2 evolution. Therefore, the catholyte was neutralized at pH 7.0 by continuous CO_2 bubbling for about 45 mins in 0.5 M $KHCO_3$ electrolyte. LSV scanning was conducted under 0 to −2.10 V vs. Ag/AgCl. One control LSV scanning was performed in an inert environment keeping the other experimental condition the same as that of the CO_2 system. No reduction peak was

observed. Two reduction peaks were found to appear with the CO_2 system (Fig. 5.5). As the onset potential of HER is at −0.70 V vs. SHE, it can be said that the peak observed at E_{cat} = −1.14 V was for the H_2 evolution reaction (HER) (Uchida et al., 2017). The peak observed at E_{cat} = −1.80 V was for ERC with an onset potential of −1.20 V at complex **1**/graphite WE (Fig. 5.6). This observation was further confirmed with chronoamperometry analysis. To note, Cu porphyrin complex coated over carbon fibre also exhibited a close reduction potential (−0.98 V vs. RHE) in 0.5 M $KHCO_3$ media producing C_2H_4, CH_4, and CO with FE of 54% in ERC (Weng et al., 2016). Complex **1** showed a notable peak separation of ERC and HER, which is considered as one of the primary shortcomings of many metals, and metal oxides catalyzed ERC systems (Hara et al., 1995; Schouten et al., 2011). No reduction peak was observed with the inert environment at complex **1**/graphite and graphite WEs, respectively. Nevertheless, the current density was lower in the inert environment than the carbonated media.

5.3.3 Products formation and FE during ERC using complex 1 electrocatalysts

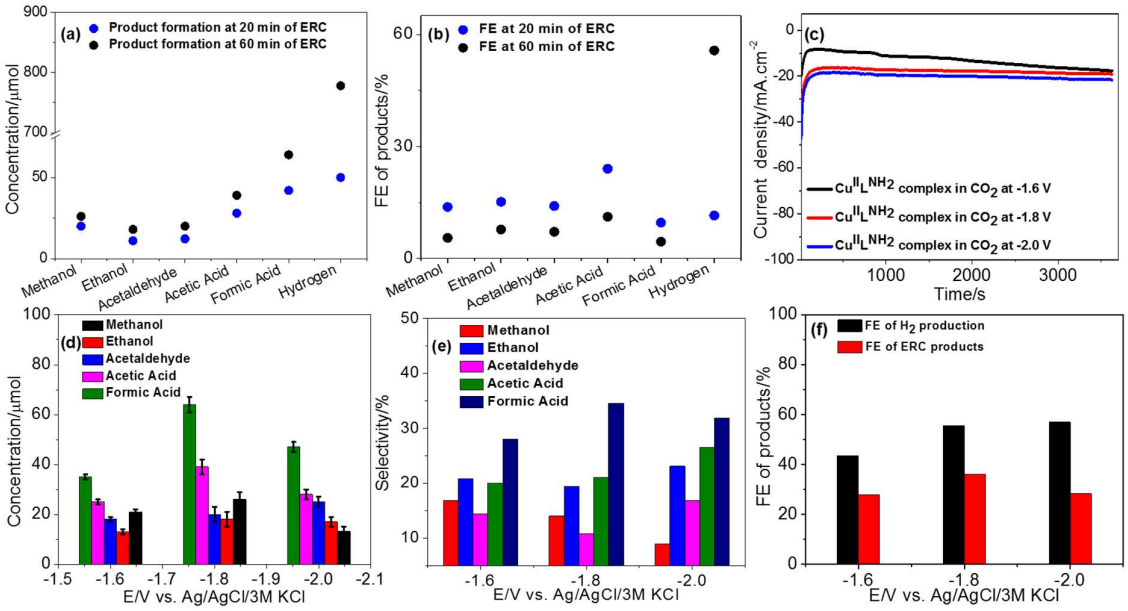

Figure 5.6: (a) Products formation during ERC for complex **1**/graphite WE at peak potential, (b) FE of the reduced products formed as shown in Fig. 5.6a, (c) constant potential analysis with time, (d) Product distributions and FE of reduced products within three different potentials, (e) Selectivity of reduced products formed for the half-cell potentials as shown in Fig. 5.6d and (f) FE of hydrogen production during ERC for complex **1**/graphite WE at 60 min. Experimental condition: Electrolyte 0.5 M $KHCO_3$, catholyte, and anolyte 120 mL each, pH 7.0, and CO_2 bubbling rate 10 mL.min^{-1} during ~45 min initial pre-saturation time.

The constant potential analysis was conducted at six different potentials. The potentials are referenced vs. Ag/AgCl. The product formation and corresponding total FE in six different electrode potentials are depicted in Table 5.1. At −1.10 V, no CO_2-reduced products were detected. H_2 was the only reduced product. Formic acid (21.20 μmol/FE 2.14%) was detected as the sole product at −1.20 V. In addition to the production of formic

acid (28.5 µmol; FE of 2%), the C_2 products; acetic acid (16.70 µmol; FE 5.96%) and acetaldehyde (13.9 µmol; FE 6.20%) formed at −1.40 V. The five different CO_2-reduced products; acetic acid, formic acid, methanol, ethanol, and acetaldehyde were detected at E_{cat} = −1.60 V. The results are summarized in Fig. 5.6a, Fig. 5.6b, and Fig. 5.6d. The formation of formic acid further increased at E_{cat} = −1.80 V (Fig. 5.6). The production was of 42 µmol at 20 min of ERC which reached 64 µmol after 60 mins, and FE was decreased from 9.6% to 4.5% at −1.80 V (5.6b). The acetic acid formation was 28 µmol (FE 24%) and 39 µmol (FE 11.14%) at 20 and 60 mins of ERC. The production of formic and acetic acid was notably higher than methanol, ethanol, and acetaldehyde. Nevertheless, their FE was very close irrespective of the time of reaction (Fig. 5.6b). The amount of production of methanol/ethanol/acetaldehyde production of 20/11/12.20 µmol was increased to 26/18/20 µmol with the progress of the reductive reaction from 20 to 60 min. The corresponding FE of Methanol/ethanol/acetaldehyde was 13.80/15.20/14 and 5.50/7.70/7.10% at 20 and 60 mins, respectively. Total FE of 76.50% for the formation of reduction products at 20 min of ERC decreased to 36.12% at 60 min at E_{cat} = −1.80 V. The decrease was due to the escalation of H_2 formation from an FE of 11.50% at 20 min to 55.50% at 60 min (Figs. 5.6a and 5.6b). The transfer of protons to the working electrode side from the counter electrode side during the entire constant-potential analysis was faster with the decrease in solution pH. So, more H_2 was evolved resulting in the fall of product formation (Kyriacou and Anagnostopoulos, 1992). The constant potential analysis is shown in Fig. 5.6c. At −2.00 V, the rate of CO_2-reduced product formation and corresponding FE decreased. The cumulative production was 112 µmol (FE 27.92%), 167 µmol (36%), and 130 µmol (FE 28.29%) at 60 min at −1.60 V, −1.80 V and −2.00 V, respectively, for the complex **1**/graphite WE (Fig. 5.7d). The hydrogen production was 569 µmol (FE 43.57%)

and 896 µmol (FE 56.5%) at −1.60 V and −1.80 V, respectively (Fig. 5.6f). The hydrogen production remained almost the same at −2.00 V as that of −1.80V.

Table 5.1: ERC Product formation and corresponding total FE at six different applied potentials with complex **1** as electrocatalyst in ERC.

Reduction potential (E_{cat}, V vs. Ag/AgCl)	**CO_2 reduction products**	**Cumulative Amount of reduction products**	**Total FE (%)**
−1.10	No products were detected	-	-
−1.20	HCOOH	21	2
−1.40	HCOOH, CH_3COOH, CH_3CHO	59	14
−1.60	HCOOH, CH_3COOH, CH_3CHO, CH_3OH, C_2H_5OH	112	28
−1.80	HCOOH, CH_3COOH, CH_3CHO, CH_3OH, C_2H_5OH	167	36
−2.00	HCOOH, CH_3COOH, CH_3CHO, CH_3OH, C_2H_5OH	130	28

SE of HCOOH formation was the highest (SE 35%) followed by acetic acid (SE 21 %), ethanol (SE 19.45%), methanol (SE 14%), and acetaldehyde (SE 11%) at E_{cat} = −1.80 V after 60 min of ERC. A similar trend was found both at E_{cat} = −1.60 V and −2.00 V except methanol and acetaldehyde. It can be seen from Fig. 5.7d that the variation of E_{cat} has a significant effect on the product yield (formic acid: 64, acetic acid: 39, methanol: 26, acetaldehyde: 20, and ethanol: 18 µmol). Nevertheless, the change in SE with the variation of E_{cat} was relatively less (Fig. 5.7e). It signifies that the catalytic activity of complex **1** on the selective formation of CO_2-reduced products is not affected much with the change of E_{cat}.

The maximum TON was obtained for CH_3COOH production (2852 with TOF 0.8 s^{-1}, followed by C_2H_5OH (TON 1986 with TOF 0.6 s^{-1}) at peak potential. TON was found to be 1151 (TOF 0.3 s^{-1}) for the HCOOH production and CH_3OH, TON reached 1405 (TOF 0.4 s^{-1}). The total TON and TOF of the catalyst were calculated to be 9230 and 2.6 s^{-1}, respectively Table 5.2. The larger the value of TOF of a catalyst, the more active is the catalyst (Shen et al., 2015). Thus, complex **1** as a catalyst is capable of producing C_2 products by ERC.

Table 5.2: Calculated TON and TOF of the formation of ERC products using complex **1** in ERC at −1.80 V vs. Ag/AgCl.

Product	V vs. Ag/AgCl	TOF (S^{-1})	TON
CH_3COOH	−1.80	0.80	2852
C_2H_5OH	−1.80	0.60	1986
HCOOH	−1.80	0.30	1151
CH_3CHO	−1.80	0.50	1836
CH_3OH	−1.80	0.40	1405

Employing a Cu salen complex, $[Cu^{II}(L^{NO2})]$, with $-NO_2$ anchoring group at the ligand backbone, a total 25% FE was achieved at E_{cat} = −1.80 V vs. Ag/AgCl during ERC forming CH_4, C_2H_4, and C_2H_6 (Singh et al., 2015). Cu-phthalocyanine catalyst was also reported to form CH_4, C_2H_4, and CO in ERC. At lower potential (−0.76 V vs. RHE) only CO was formed, while, mixture products HCOOH (FE 25%), CO (FE 6%) and C_2H_4 (13%) formation start at a higher potential of −0.86 V vs. RHE (Weng et al., 2018). In another study, Co-phthalocyanine molecules modified carbon nanotubes in a 0.5 M $KHCO_3$ solution exhibited a higher FE (>95%) but the product was only C_1 (CO) and not C_2 (Zhang et al., 2017). These reports consolidate the ability of the Cu-based catalysts to form the C-C bond (C_2) during ERC. In the present study, FE was about 26% for the formation of C_2

products using the synthesized metal complex **1** as the catalyst. Thus, subtle improvement in the C_2 product formation by ERC is achieved using complex **1**.

5.3.4 Cyclic voltammograms of complex 1

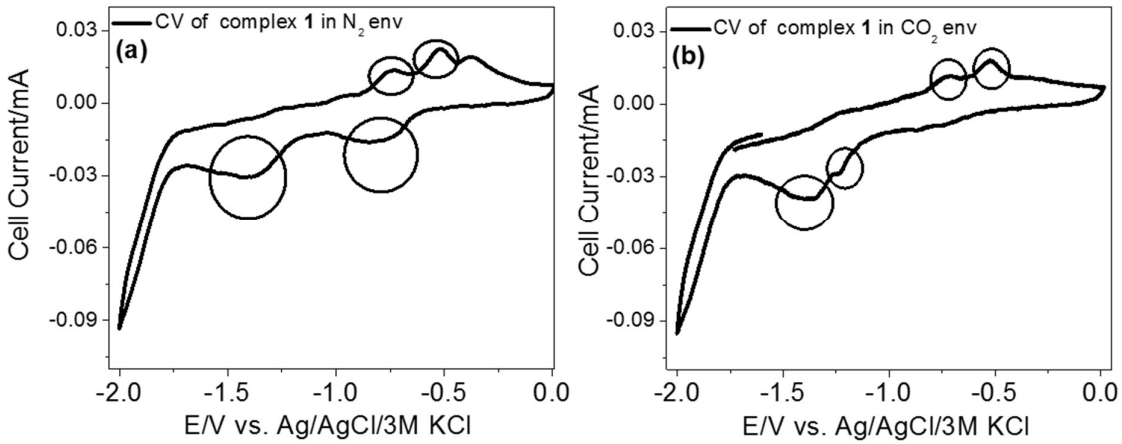

Figure 5.7: CV curves at a scan rate of 100 $mV.s^{-1}$ at glassy carbon WE in1 mM complex **1** as analyte at (a) N_2 saturation and (b) CO_2 saturated environment. Experimental condition: Electrolyte 0.1 M $TBAPF_6$ in CH_3CN solution, Pt wire as CE, and Ag/AgCl as RE.

Complex **1** was then subjected to CV analysis in an inert and carbonated environment where 0.1 M $TBAPF_6$ in ACN solution was used as an electrolyte. Glassy carbon was used as the WE, CE was Pt wire, and RE was Ag/AgCl (3 M KCl). At first, complex **1** was mixed properly with DMF, and then 1 mM of it was mixed with 0.1 M $TBAPF_6$ prepared in CH_3CN solution. Then, N_2 gas was purged for 15 minutes, and CV data was taken, and the same procedure was repeated for the CV analysis in a CO_2 environment. In CV analysis in an inert environment, Cu(II)/Cu(I) redox pair appeared at −0.81/−0.52 V, and then Cu(I)/Cu(0) redox pair observed at −1.38/−0.74V in an inert environment. In the carbonated environment, Cu(II)/Cu(I) and Cu(I)/Cu(0) redox pair observed at −1.24/0.53 V and −1.38/−0.74 V (Fig 5.7) (Kang et al., 2015).

5.4 Electrode Characterization

5.4.1 EDX analysis of complex 1 coated electrode

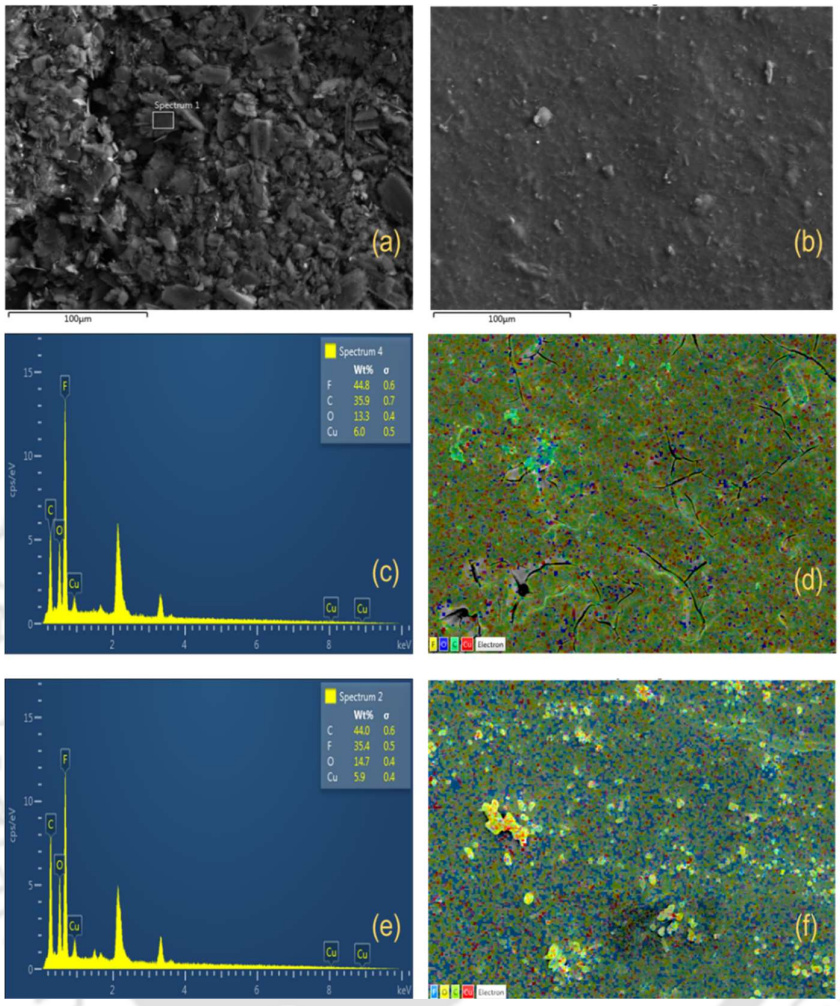

Figure 5.8: FESEM image of (a) graphite plate before coating, (b) WE after complex **1** coating, (c) EDX micrograph of the WE after complex **1** coating: Elemental distribution, (b) Corresponding image mapping showing Cu surface coverage on the WE (red dots) before ERC reaction, (d) EDX micrograph of the WE after complex **1** coating: Elemental distribution, (f) Corresponding image mapping showing Cu surface coverage on the WE (red dots) after ERC reaction.

The FESEM micrographs of graphite plates before and after the surface modifications are depicted in Figs. 5.8a and 5.8b. The elemental distribution of the surface of the modified WE was recorded before and after the ERC reaction and is shown in Fig. 5.8c and Fig. 5.8e. The dispersion of Cu (complex **1**) on the WE before and after the ERC reaction is illustrated in Fig. 5.8d and Fig. 5.8f respectively. The percentage of Cu in the coated electrodes is almost similar even after the electrolysis which confirms electrode stability. There is no change is observed in the complex which confirms the reusability of the metal complex too.

5.4.2 XRD analysis of complex 1 coated electrode

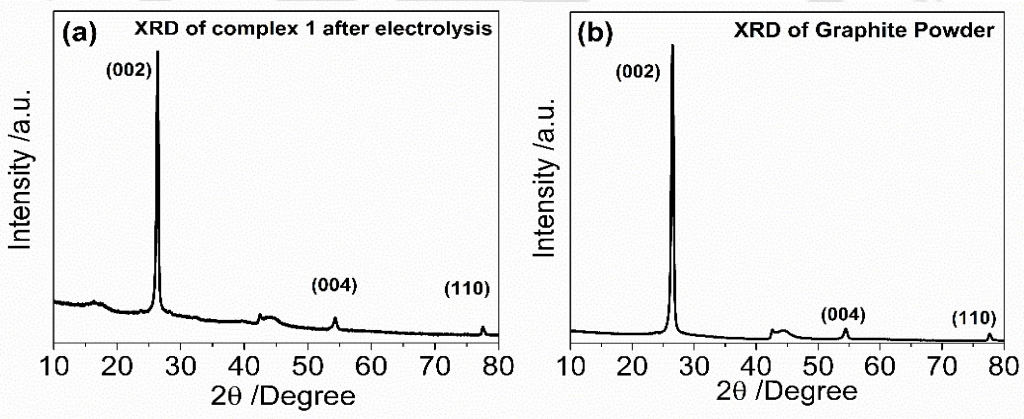

Figure 5.9: XRD patterns of complex **1** after ERC of CO_2 (a) and graphite powder (b).

The post electrolysis characterization was pursued by collecting the sample from the electrode surface and thereafter, XRD analysis. The peaks were obtained in the XRD analysis was for graphite powder of electrode (002), (004), (110) and no peak was observed due to the Cu or its oxides (Fig 5.10a). A reference scan was also added using only graphite powder of electrode surface (Fig 5.10b) (Li et al., 2007). This study confirms the absence of Cu nanoparticle formation after the ERC reaction.

5.4.3 GC analysis of products formation

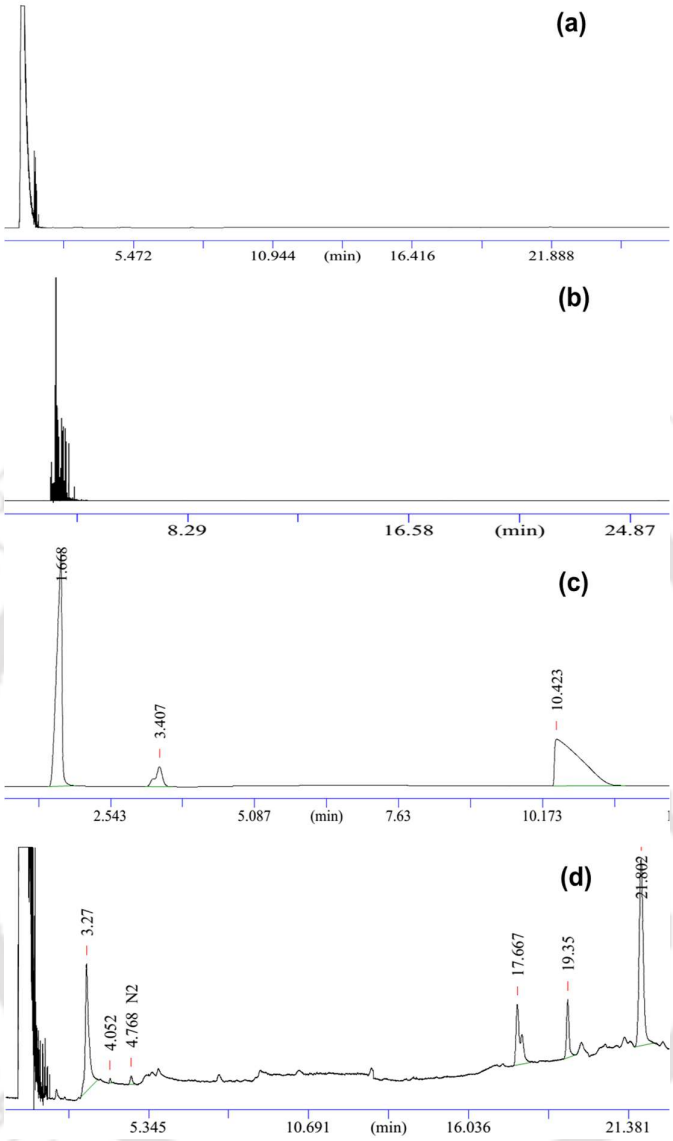

Figure 5.10: Gas chromatograms showing product formation during ERC (a) chromatograph of the liquid sample only with graphite electrode without the catalyst, (b) chromatograph of the liquid sample using complex **1** in an inert atmosphere, (c) chromatograph of the gaseous sample using complex **1** in the CO_2 atmosphere, and (d) chromatograph of the liquid sample using complex **1** with CO_2 atmosphere after 1 h of electrolysis at −1.80 V vs. Ag/AgCl. RT= 3.27 min for CH_3CHO, RT = 4.05 for CH_3OH, RT= 4.70 for C_2H_5OH, RT= 19.35 is for HCOOH and RT= 21.80 is for CH_3COOH using complex **1** WE in Fig. 5.10b. RT = 1.60 min is for H_2 and RT = 3.40 min is for N_2 in Fig. 5.10d.

A reference voltammetric scan was first performed for ERC only with the support-electrode (without catalyst) and it was then compared with ERC using the catalyst coated electrode (Fig 5.10). In the reference experiment, no product formation was observed without catalyst along with continuous CO_2 bubbling (Fig. 5.10a). It confirms that the carbon source of the reduction of products is not the electrode material itself. Further with N_2 bubbling, no reduced product was noted at −1.80 V vs. Ag/AgCl (Fig. 5.10b). Therefore, it can be affirmed that the carbon source of the reduction products was neither the electrode material (graphite) nor the breaking of the catalyst. To support this observation, the gas chromatogram for the formation of different ERC and proton reduction products at complex **1** WE during ERC reaction are shown (Figs. 5.10c and 5.10d). The chromatographs were matched with authentic samples showed in Fig. 5.11.

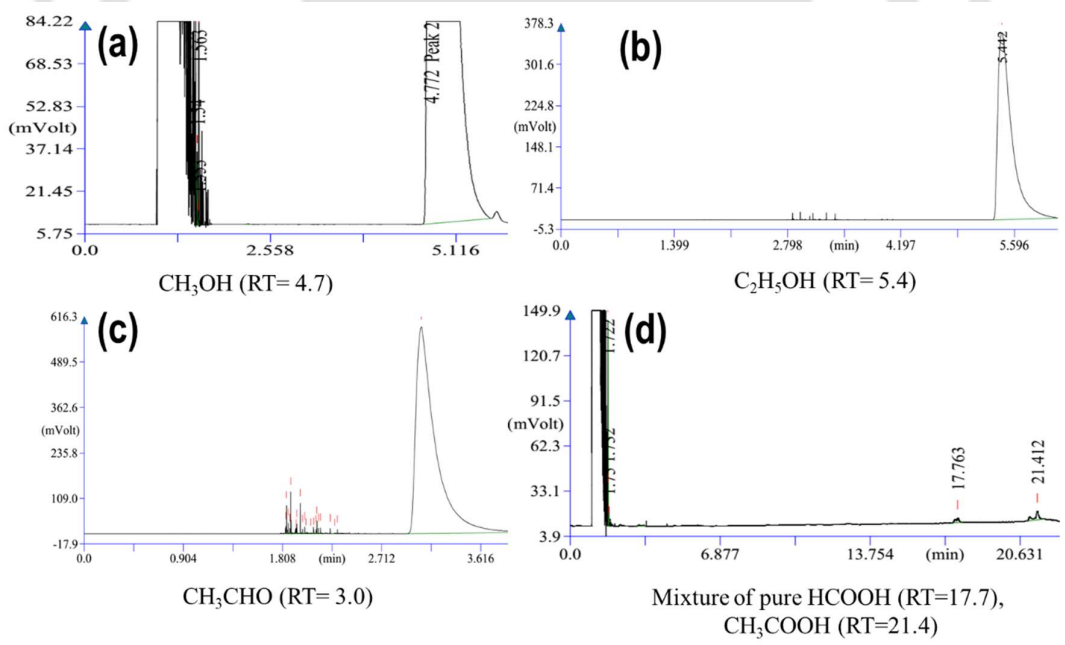

Figure 5.11: Gas chromatograms of pure samples: (a) CH_3OH, (b) C_2H_5OH, (c) CH_3CHO and (d) mixture of HCOOH and CH_3COOH.

5.5 Effect of anchoring group (-NH_2) in ERC

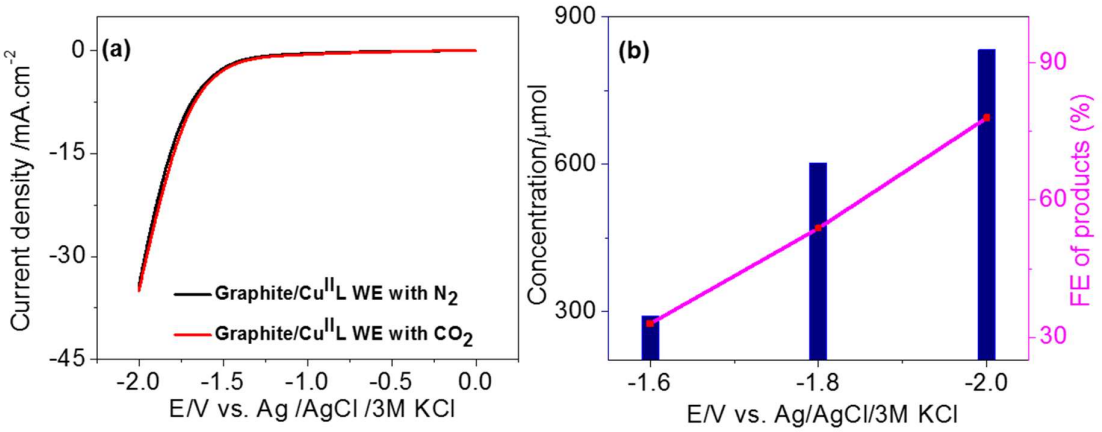

Figure 5.12: Hydrogen formation and corresponding FE (a) and constant potential analysis with time at different half-cell potentials (b) for [Cu^{II}(L)] complex WE. Experimental condition: Electrolyte 0.5 M $KHCO_3$, catholyte, and anolyte 120 mL each, pH 7.0, and CO_2 bubbling rate 10 $mL.min^{-1}$ during ~45 min initial pre-saturation time.

The electrode provides electrons to the catalyst to initiate the reaction. The faster is the electron transfer, the more active is the catalyst towards CO_2 electroreduction. The attached anchoring group in the ligand backbone provides a better interaction between the electrode material and metal complex that facilitates the electron transfers and enhances the reactivity. The attached anchoring -NH_2 group facilitated the electron transfer from the electrode to the metal ions (Cu(II) by holding the catalyst tightly and firmly to the electrode in the presence of Nafion binder, which is a sulfonic acid group-containing polymer. Thus, to investigate the role of the anchoring -NH_2 group, present in the ligand backbone of [$Cu^{II}(L^{NH_2})$] complex (**1**), towards the betterment of the catalytic performance, parent salen ligand (H_2L) without the anchoring-group and, correspondingly, [Cu^{II}(L)] complex was synthesized as per the previously reported procedures (Barboza et al., 2015). After that, the

LSV and constant-potential analysis were conducted between the same potential ranges and compared its role with complex **1**.

The LSV profiles in [Cu^{II}(L)] complex catalyzed ERC in the case of both inert and CO_2 environments (scan rate 30 $mV.s^{-1}$) are illustrated in Fig. 5.12a. Unlike complex **1**, [Cu^{II}(L)] complex didn't show the reduction peaks for both ERC and HER (Fig. 5.12b). The current density observed with these control systems were for the HER, which is discussed later. The current density was 15.42 $mA.cm^{-2}$ in CO_2 saturated system against 14.17 $mA.cm^{-2}$ in the inert environment (N_2) at −1.80 V vs. Ag/AgCl with 30 $mV.s^{-1}$ scan rate using [Cu^{II}(L)] complex. That means that the current density increased very marginally in the presence of CO_2 compared to the inert environment (Fig. 5.12a). This trend of current density is contrary to the complex **1**/graphite WE. A current density of 20.80 and 14.51 $mA.cm^{-2}$ was noted during ERC for the carbonated and inert systems at −1.80 V vs. Ag/AgCl using complex **1**/graphite WE at that potential (Fig. 5.6). In most of the findings, the ERC peak does not appear, and the higher current density is considered as the preliminary observation of a catalyst to be active. Thus, it can be argued that complex **1** was catalytically active for ERC, while, [Cu^{II}(L)] complex was not.

Furthermore, no CO_2-reduced products were identified during the chronoamperometry analysis in the potential range of −1.60 to −2.00 V vs. Ag/AgCl in the carbonated system using [Cu^{II}(L)] complex WE, and only H_2 gas was evolved during this process (Fig. 5.12b). H_2 production was 603 μmol (FE 53.87%) at 60 min of HER at −1.80 V for the carbonated system with CO_2 saturated environment at [Cu^{II}(L)] complex WE (Fig. 5.12b). H_2 production was 291 and 834 μmol at −1.60 V and −2.00 V vs. Ag/AgCl, respectively, under the same experimental conditions (Fig. 5.12b). Thus, this analysis confirmed that the anchoring group (-NH_2 group) present in complex **1** [$Cu^{II}(L^{NH_2})$] plays

an important role in the ERC. The previous report by Singh et. al. suggested that a -NO_2 anchoring group attached with the salen ligand helps the corresponding Ni(II) and Cu(II) complexes to interact with the electrode material with better efficacy (Singh et al., 2015). In another study, a Cu-porphyrin (PorCu) complex with a built-in -OH group was reported to exhibit better catalytic activity compared to its -OH free PorCH_3Cu complex congener in ERC in $KHCO_3$ electrolyte at various applied potentials (Weng et al., 2016).

Herein, the attached anchoring -NH_2 group facilitated the electron transfer from the electrode to the metal ion Cu(II) by holding the catalyst tightly and firmly to the electrode in the presence of Nafion binder, which is a sulfonic acid group-containing polymer. This can happen due to the protonation of the -NH_2 group by the polymer creates an ammonium cation and a sulfonate anion. Thus, coulombic interactions between the catalyst-molecules and the polymer occur.

5.6 Reaction kinetics in ERC using metal complexes

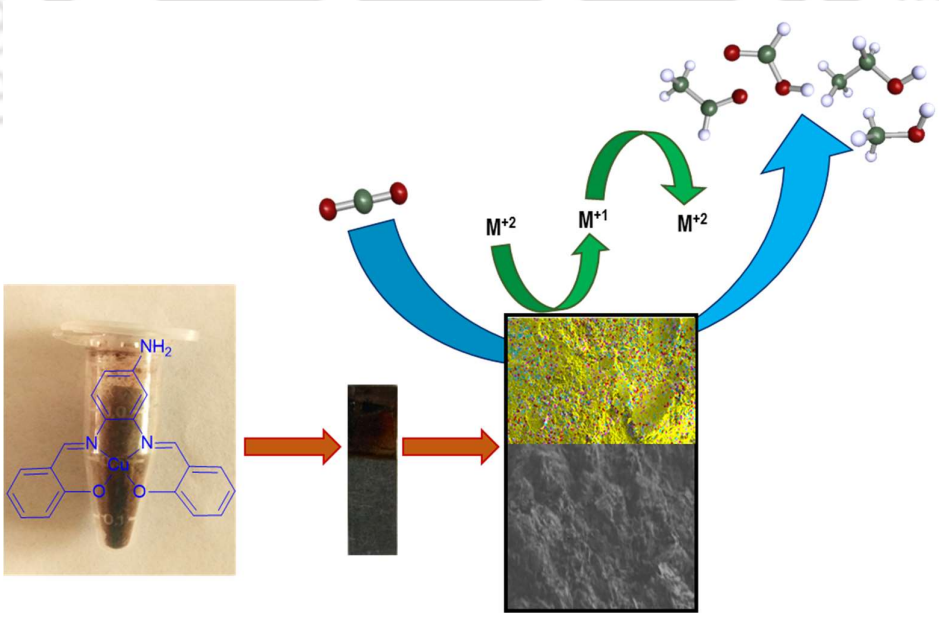

Figure 5.13: A schematic representation of the redox behaviour of salen metal complexes.

Heterogeneous catalysis using molecular complexes with metal centre has been studied by many groups of scientists. Zhu and his co-workers (2019) stated that three main steps are involved in CO_2-reduced product formation. The first step is the activation of the CO_2 molecule, and the second step is the C_1 product formation. The last step is the dimerization of CO, which leads to C_2 product formation. The first intermediate for the reduction of CO_2 using those metal complexes is $CO_2^{\bullet-}$ bound to the metal centre. Thus, in presence of a water molecule, it produces M-COOH intermediate first (Kortlever et al., 2015). According to Shen et al. (2015), the active state of CO_2 reduction is through the formation of the M^{+1} state (Cu(I)). The onset potential of the CO_2 reduction thus depends upon the conversion between the M^{+2} to the M^{+1} state. Cu(II) first converts into Cu(I) intermediates by taking an electron from the electrode and coordinates with CO_2 at the WE side. The CO_2 is then converted into other products (in presence of H^+) and again Cu(I) converts into its previous state Cu(II) (Figure 5.13). The stability of the intermediate affects product distribution (Singh et al., 2015). The rate-determining step of CO_2 reduction using metal complexes is the generation of M-COOH intermediate. Further, the selectivity of the intermediate towards either CO or $HCOO^-$ production via $2e^-$ transfer reaction depends on the nature of the metal complex. First, the M-COOH intermediate produces formate (or HCOOH), and this finally resulted in methanol formation. The C-C bond formation also can occur by producing oxalate type intermediate at the beginning, and then further reduction leads to acetate (or CH_3COOH) production (Boutin et al., 2019; De et al., 2020; Göttle and Koper, 2018). Total 6 and 8 electrons are required to produce methanol and acetate, respectively from CO_2. C_2H_5OH production can occur by the reaction of CH_3CHO intermediate (which requires a total of 12 e^- transfer) (Scheme 2.1 in Chapter 2) (Ma et al., 2016; Ren et al., 2018; Zheng et al., 2019; Zhu et al., 2019). In this way, CO_2 can be

electrochemically converted into various by-products. A mechanistic pathway is described in Scheme 2.1 in chapter 2 describing the reaction kinetics and probable mechanism for the various products formation and electrons involved in it.

5.7 Copper complex vs. Cu oxide

The newly introduced Cu(II) complex (**1**) from salen ligand ($H_2L^{NH_2}$) through a metalation reaction in the presence of Et_3N was successful in reducing CO_2. The WE was modified with that metal complex for the electrocatalytic scissoring of the C-O bond to convert CO_2 to value-added products. The best experimental condition for ERC at complex **1**/graphite WE in an H-type divided cell was identified at $E_{cat} = -1.80$ V vs. Ag/AgCl at pH 7.0, WE area of 4 cm^2 and CO_2 bubbling rate of 10 $mL.min^{-1}$. The CO_2 reduced products were obtained as HCOOH>CH_3COOH>CH_3OH>C_2H_5OH, which were formed through multiple electrons transfer (2 e^- to 12 e^-) proton-insertion reactions. The highest FE for HCOOH, CH_3COOH, CH_3OH, and C_2H_5OH production was found to be 36% for 60 min of reaction. The highest selectivity was achieved for the formation of non-alcoholic CO_2 reduced products such as CH_3COOH (SE 21%) and HCOOH (SE 35%). Whereas, in the same experimental conditions Cu_2O was able to produce mainly HCOOH (FE 22%). The trace amount of CH_3OH (3.5%) was detected at higher potential (−2.20 V vs. Ag/AgCl). The redox behaviour of the central metal atom is the key reason for the better performance of the metal complex. However, the catalytic activity of the Cu(II) complex was enhanced by the presence of the terminal -NH_2 anchoring-group in the ligand backbone. In general, Cu(II)-based catalysts are known to convert CO_2 to preferably C_2H_4 over CH_3COOH, and EtOH in ERC (Han et al., 2020). Alcohols are produced only in the presence of a high concentration of CO. Herein, the reported catalyst is selective towards acids (CH_3COOH and HCOOH) production than the alcohols in ERC.

References

Barboza, C. A., Germino, J. C., Santana, A. M., Quites, F. J., Vazquez, P. A. M., and Atvars, T. D. Z., 2015. "Structural Correlations between Luminescent Properties and Excited State Internal Proton Transfer in Some zinc(II) N, N'-bis(salicylidenes)." *Journal of Physical Chemistry C*, *119*, 6152-6163.

Bennur, T. H., Srinivas, D., and Ratnasamy, P., 2001. "EPR spectroscopy of copper and manganese complexes encapsulated in zeolites." *Microporous and Mesoporous Materials*, *48*, 111-118.

Boutin, E., Wang, M., Lin, J. C., Mesnage, M., Mendoza, D., Lassalle-Kaiser, B., Hahn, C., Jaramillo, T. F., and Robert, M., 2019. "Aqueous Electrochemical Reduction of Carbon Dioxide and Carbon Monoxide into Methanol with Cobalt Phthalocyanine." *Angewandte Chemie-International Edition*, *58*, 16172-16176.

Cohen, C. T., and Coates, G. W., 2006. "Alternating Copolymerization of Propylene Oxide and Carbon Dioxide with Highly Efficient and Selective (Salen)Co(III) Catalysts: Effect of Ligand and Cocatalyst Variation." *Journal Of Polymer Science: Part A: Polymer Chemistry*, *44*, 5182-5191.

Cozzi, P. G., 2004. "Metal-Salen Schiff Base Complexes in Catalysis: Practical Aspects." *Chemical Society Reviews*, *33*, 410-421.

De, R., Gonglach, S., Paul, S., Haas, M., Sreejith, S. S., Gerschel, P., Apfel, U-P., Vuong, T. H., Rabeah, J., Roy, S., Schöfberger, W., 2020. "Electrocatalytic Reduction of CO_2 to Acetic Acid by a Molecular Manganese Corrole Complex." *Angewandte Chemie-International Edition*, *59*, 10527-10534.

Gambarotta, S., Arena, F., Floriani, C., and Zanazzi, P. F., 1982. "Carbon Dioxide Fixation: Bifunctional Complexes Containing Acidic and Basic Sites Working as Reversible

Carriers." *Journal of the American Chemical Society*, *104*, 5082-5092.

Göttle, A. J., and Koper, M. T. M., 2018. "Determinant Role of Electrogenerated Reactive Nucleophilic Species on Selectivity during Reduction of CO_2 Catalyzed by Metalloporphyrins." *Journal of the American Chemical Society*, *140*, 4826-4834.

Han, H., Noh, Y., Kim, Y., Park, S., Yoon, W., Jang, D., Choi, S. M., and Kim, W. B., 2020. "Selective Electrochemical CO_2 Conversion to Multicarbon Alcohols on Highly Efficient N-doped Porous Carbon-supported Cu Catalysts." *Green Chemistry*, *22*, 71-84.

Hara, K., Kudo, A., and Sakata, T., 1995. "Electrochemical Reduction of Carbon Dioxide under High Pressure on Various Electrodes in an Aqueous Electrolyte." *Journal of Electroanalytical Chemistry*, *391*, 141-147.

Kang, S., Dale, A., Sarkar, S., Yoo, J., and Lee, H., 2015. "Electrocatalytic Reduction of CO_2 by Copper (II) Cyclam Derivatives." *Journal of Electrochemical Science and Technology*, *6*, 106-110.

Kortlever, R., Shen, J., Schouten, K. J. P., Calle-Vallejo, F., and Koper, M. T. M., 2015. "Catalysts and Reaction Pathways for the Electrochemical Reduction of Carbon Dioxide." *Journal of Physical Chemistry Letters*, *6*, 4073-4082.

Kyriacou, G., and Anagnostopoulos, A., 1992. "Electroreduction of CO_2 on Differently Prepared Copper Electrodes. The Influence of Electrode Treatment on the Current Efficiencies." *Journal of Electroanalytical Chemistry*, *322*, 233-246.

Li, Z. Q., Lu, C. J., Xia, Z. P., Zhou, Y., and Luo, Z., 2007. "X-ray Diffraction Patterns of Graphite and Turbostratic Carbon." *Carbon*, *45*, 1686-1695.

Ma, S., Sadakiyo, M., Luo, R., Heima, M., Yamauchi, M., and Kenis, P. J. A., 2016. "One-Step Electrosynthesis of Ethylene and Ethanol from CO_2 in an Alkaline Electrolyzer." *Journal of Power Sources*, *301*, 219-228.

Murata, A., and Hori, Y., 1991. "Product Selectivity Affected by Cationic Species in The Electrochemical Reduction of CO_2 and CO at a Cu Electrode." *Bulletin of the Chemical Society of Japan*, *64*, 123-127.

Ren, D., Fong, J., and Yeo, B. S., 2018. "The Effects of Currents and Potentials on the Selectivities of Copper Toward Carbon dioxide Electroreduction." *Nature Communications*, *9*, 1-8.

Schouten, K. J. P., Kwon, Y., Van Der Ham, C. J. M., Qin, Z., and Koper, M. T. M., 2011. "A New Mechanism for the Selectivity to C_1 and C_2 Species in the Electrochemical Reduction of Carbon Dioxide on Copper Electrodes." *Chemical Science*, *2*, 1902-1909.

Shen, J., Kortlever, R., Kas, R., Birdja, Y. Y., Diaz-morales, O., Kwon, Y., Ledezma-Yanez, I., Schouten, K. J. P., Mul, G., and Koper, M. T. M., 2015. "Electrocatalytic Reduction of Carbon Dioxide to Carbon Monoxide and Methane at an Immobilized Cobalt Protoporphyrin." *Nature Communications*, *6*, 1-8.

Singh, S., Phukan, B., and Verma, A., 2015. "Salen Ligand Complexes as Electrocatalysts for Direct Electrochemical Reduction of Gaseous Carbon Dioxide to Value Added Products." *RSC Advances*, *5*, 3581-3589.

Uchida, T., Sasaki, Y., Ikeshoji, T., and Osawa, M., 2017. "4, 4′-Bipyridine as a Molecular Catalyst for Electrochemical Hydrogen production." *Electrochimica Acta*, *248*, 585-592.

Weng, Z., Jiang, J., Wu, Y., Wu, Z., Guo, X., Materna, K. L., Liu, W., Batista, V. S., Brudvig, G. W., and Wang, H., 2016. "Electrochemical CO_2 Reduction to Hydrocarbons on a Heterogeneous Molecular Cu Catalyst in Aqueous Solution." *Journal of the American Chemical Society*, *138*, 8076-8079.

Weng, Z., Wu, Y., Wang, M., Jiang, J., Yang, K., Huo, S., Wang, X-F., Ma, Q., Brudvig, G. M., Batista, V. S., Liang, Y., Feng, Z., and Wang, H., 2018. "Active Sites of Copper-Complex Catalytic Materials for Electrochemical Carbon Dioxide Reduction." *Nature Communications*, *9*, 1-9.

Zhang, X., Wu, Z., Zhang, X., Li, L., Li, Y., Xu, H., Li, X., Yu, X., Zhang, Z., Liang, Y., and Wang, H., 2017. "Highly Selective and Active CO_2 Reduction Electrocatalysts Based on Cobalt Phthalocyanine/Carbon Nanotube Hybrid Structures." *Nature Communications*, *8*, 1-8.

Zheng, Y., Vasileff, A., Zhou, X., Jiao, Y., Jaroniec, M., and Qiao, S. Z., 2019. "Understanding the Roadmap for Electrochemical Reduction of CO_2 to Multi-Carbon Oxygenates and Hydrocarbons on Copper-Based Catalysts." *Journal of the American Chemical Society*, *141*, 7646-7659.

Zhu, Q., Sun, X., Yang, D., Ma, J., Kang, X., Zheng, L., Zhang, J., Wu, Z., and Han, B., 2019. "Carbon Dioxide Electroreduction to C_2 Products over Copper-Cuprous Oxide Derived from Electrosynthesized Copper Complex." *Nature Communications*, *10*. 1-11.

CHAPTER 6

Investigation on Ni(II)-Salen Complexes in Electrocatalysing CO_2 Conversion: role of Ligand-based Anchoring Groups

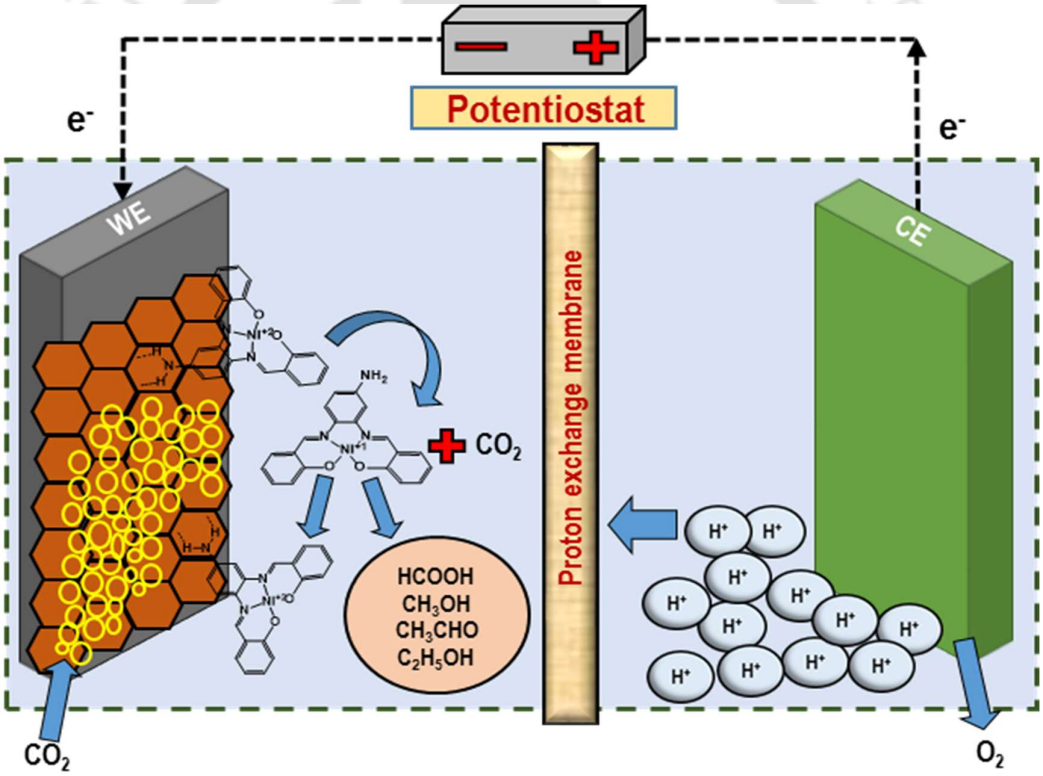

6.1 Background of the work

A newly synthesized Ni^{II} complex $[Ni^{II}L^{NH_2}]$ (**2**) of the tetradentate salen ligand ($H_2L^{NH_2}$) with an anchoring amine functional group in the ligand backbone was synthesized and characterized in this chapter. For better electronic-communications, i.e., electron transfer, between the graphite electrode and Ni(II) ion of the complex, an amine functional group was attached in the ligand backbone. The complex effectively reduced CO_2 to C_1 (HCOOH, CH_3OH) and C_2 (C_2H_5OH) products in a simple H-type reactor upon imbolilization on the graphite electrode. Initially, HCOOH was formed which was further reduced to CH_3OH and C_2H_5OH in a $4e^-$ and $10e^-$ transfer pathway. The overall current efficiency of 49% was recorded for the formation of alcohol at −1.80 V vs. Ag/AgCl in aqueous media (ERC time 1 h, pH 7.0, and $KHCO_3$ 0.5 M). Thus, the common limitation of the formation of deeply reduced C_2 products is being overcome. The effect of the anchoring free amine group was further established by examining the CO_2 reduction-efficiency of the similar Ni^{II} complex without having the tethered -NH_2 group. No alcohol production for this case buttressed the importance of the anchoring group with the electrodes during the electrochemical reduction.

6.2 Synthesis of complex 2: $[Ni^{II}(L^{NH_2})]$

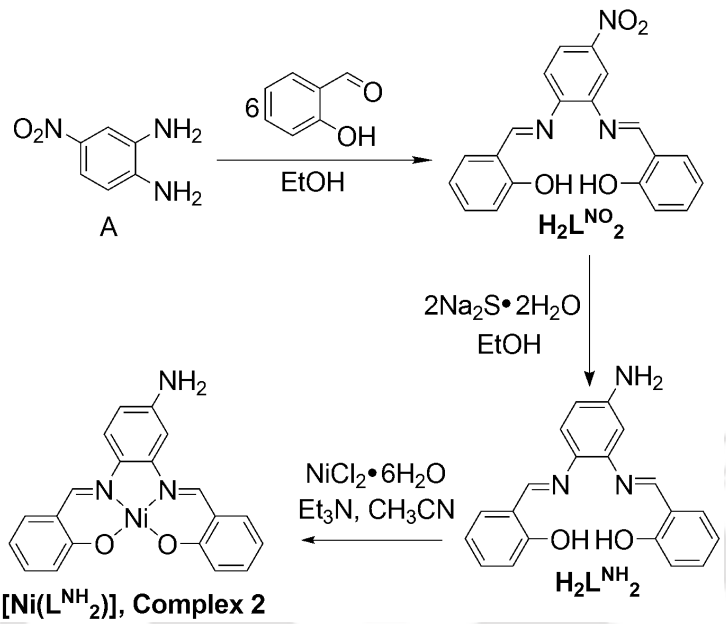

Scheme 6.1. Schematized steps for the synthesis route of Ni(II) complex (**2**).

Salen ligand $H_2L^{NH_2}$ was synthesized from the reaction of ligand $H_2L^{NO_2}$ (1.81 g; 5 mmol) and $Na_2S•H_2O$ (0.78 g; 10 mmol) in EtOH (15 mL) solution under refluxing condition. After that, in a CH_3CN solution (8 mL), $H_2L^{NH_2}$ (0.163 g, 0.5 mM) was mixed with $NiCl_2•6H_2O$ (0.119 g, 0.5 mM). To the reaction mixture in triethylamine (0.2 mL) was added dropwise and stirred the resulting solution for 6 h at 30°C. The colour of the suspension was changed from yellow to red in due course and finally, a red colour precipitate appeared. The precipitate was collected, washed thoroughly with CH_3CN, and air-dried to get the expected $Ni^{II}L^{NH_2}$ complex ($C_{20}H_{15}N_3O_2Ni$**; 2**) (Yield: 0.138 g, 71%) (Scheme 6.1).

6.3 Results and Discussion

6.3.1 Metal complex characterization

The metal complex was characterized by FTIR spectroscopy, Mass, and CHN analysis. All the electrochemical analysis was conducted using Potentiostat.

6.3.1.1 Mass analysis of complex 2

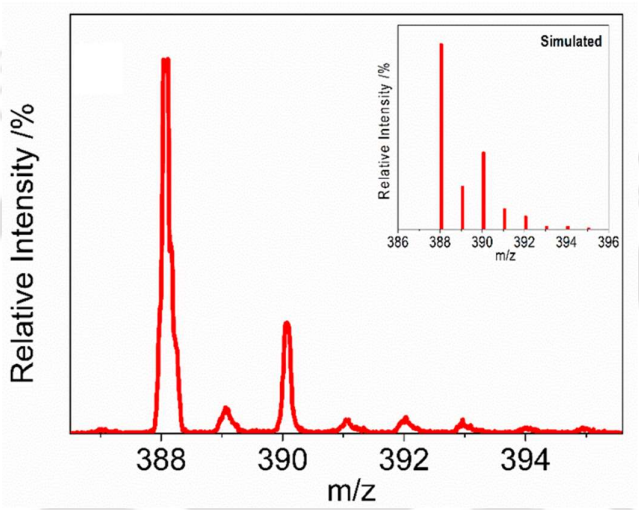

Figure 6.1: Experimental and simulated mass spectrum of synthesized complex **2** [$C_{20}H_{15}N_3O_2Ni$ + H].

Electrospray ionization mass spectrum (ESI-MS) analysis in positive mode on complex **2** appeared at 388.06 amu and the theoretically calculated values were 388.06 (Fig. 6.1). The peak corroborated to the composition $C_{20}H_{15}N_3O_2Ni$ was established by isotope pattern distribution. The composition corresponded to [M + H]; where M is the molecular composition of the expected complex **2**. Thus, mass spectrum analysis was congruous with the formation of the complex.

6.3.1.2 FTIR spectrum of complex 2

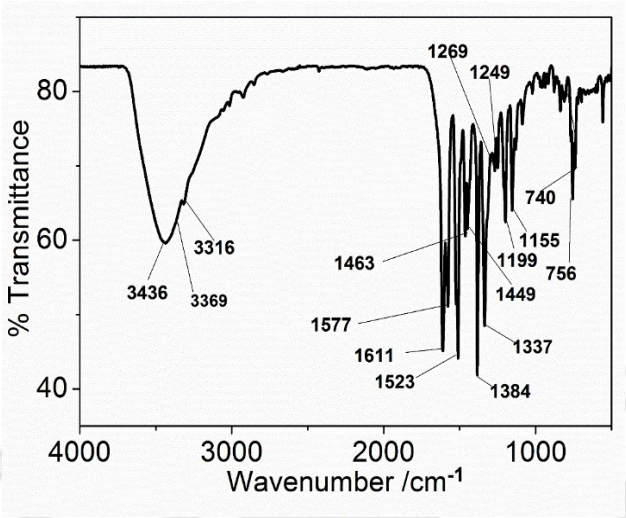

Figure 6.2: FTIR spectrum of complex **2**.

The FTIR spectrum of complex **2** was observed at characterized peaks at 3436, 3369, 3316, 1611, 1577, 1523, 1337, 1269, 1249, 1199, 1155, 756, 740 cm^{-1}. In complex **2**, a broad peak centered at 3436 cm^{-1} was present. The peak has been attributed to ν(O-H) stretch of moisture. In the FTIR spectrum of the corresponding Ni(II) complex, ν(N-H) stretches of the -NH_2 anchoring-group observed at 3369 and 3316 cm^{-1} (Fig. 6.2). A single-sharp band for the ν(C=N) stretch was found at 1611 cm^{-1}. The decrease in the band-position relative to the position found in the corresponding ligand confirmed the complex formation.

6.3.1.3 CHN analysis of complex 2

The elemental analysis (CHN) of complex **2** was conducted to establish the elemental formula. The theoretically calculated percentage of C, H, and N were 51, 5.19, and 8.9%. The experimental composition was found is % C 50.81; % H 5.39; % N 9.35. 4.6 molecules of lattice bound water were found in the experimentally calculated values of complex **2**. Therefore, the elemental formula is $C_{20}H_{15}N_3O_2Ni•4.6H_2O$.

6.3.1.4 Voltammetric analysis during ERC using complex 2 electrocatalyst

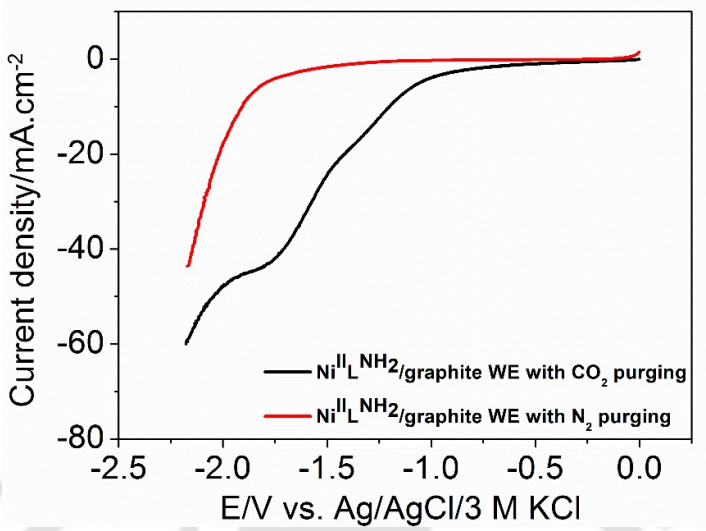

Figure 6.3: (a) LSV curves at a scan rate of 30 $mV.s^{-1}$ during ERC at bare and complex **2**/graphite WEs with N_2 and CO_2 saturation, Experimental condition: Electrolyte 0.5 M $KHCO_3$, catholyte, and anolyte 120 mL each, pH 7.0, and CO_2 bubbling rate 10 $mL.min^{-1}$ during ~45 min initial pre-saturation time.

In this study, CO_2 was bubbled into the aqueous bicarbonate solution and saturated at a fixed reaction pH of 7.0. In water, CO_2 can exist in three different forms based on the pH of the solution. The most electroactive species CO_2 (ad)/H_2CO_3 are abundant in between pH 2 to 8.5. HCO_3^- (H^+ aq + CO_3^{2-}) is present between pH 4.5 and 8.5. Above pH 8.5, only CO_3^{2-} is present (Tan et al., 1995). Lowering the pH of the electrolyte solution could dissolve more electroactive species (CO_2 (ad)/H_2CO_3), but a low pH (<4.5) increases H_2 evolution reaction (HER). Thus, the final pH of this experiment was set to be neutral. In the aqueous medium, the reduction potential of CO_2 reduction and hydrogen evolution is almost similar. The onset potential of HER is −0.70 V vs. SHE (Uchida et al., 2017). Thus, in the aqueous medium, the cell current observed in the ERC of CO_2 was not only for the ERC but also for H_2 gas generation. Therefore, it is really difficult to distinguish from the

LSV whether the peak observed is for the ERC or for the HER (−1.00 V vs. Ag/AgCl saturated with 3 M KCl). In this study, one pair of weak and broad peaks were observed at E_{cat} = −1.80 V and at E_{cat} = −1.30 V vs. Ag/AgCl for complex **2** in the CO_2 saturated media which was for ERC and HER reactions, respectively. It was further confirmed from the constant potential analysis. The onset potential for the HER and ERC starts at −0.95 V vs. Ag/AgCl in the CO_2 saturated media. With N_2 purging, the reduction peak did not appear in the LSV, but in the absence of CO_2, a significant amount of current was observed (Fig. 6.3) which was due to the HER. According to the previous researches, the current observed in the ERC was the sum of HER and ERC. The current observed in the N_2 saturated environment has the same value as the HER current (Hori, 2008). Thus, a higher current density observed in the CO_2 saturated environment (Fig. 6.3) than the N_2 environment (Fig. 6.3) also confirmed the CO_2 reduction reaction (Fig. 6.3). The change in electrochemical performances specifies that the Ni- complex **2** helped in the conversion of CO_2 and its intermediate species, which leads to an increase in current density with CO_2 bubbling. Though only LSV data is not adequate to evaluate the catalytic activity of the complex and it is mandatory to quantitatively investigate (Jia et al., 2014).

6.3.1.5 Products formation and FE during ERC using complex 2 electrocatalyst

After the successful completion of voltammetric analysis, the electrode potential was varied (−1.60 to −2.00 V vs. Ag/AgCl) and the corresponding FE was calculated (Fig. 6.4c and 6.4d). The formation of ERC products was started at $E_{cat} \leq -1.60$ V and the maximum amount of product formation was found at E_{cat} = −1.80 V (Fig. 6.4c). At −1.60 V, the production of C_2H_5OH was maximum (63 µmol) followed by HCOOH (59 µmol). The selectivity of the C_2H_5OH formation was 52.5% at this potential (Fig. 6.4f). The production of methanol was reached to 44 µmol and the CH_3CHO production was reached up to 11.2 µmol at this potential. The selectivity of HCOOH was the highest at −1.60 V as

its formation was favorable over other products. However, the formation of C_2H_5OH (selectivity 54%) was favorable at −2.00 V. The production of CH_3OH and CH_3CHO was 51.00 µmol and 13.16 µmol with a selectivity of 20.0% and 5.1%, respectively, at this potential. At lower potential ($E_{cat} \leq -2.00$ V), hardly any product was formed. The rate of hydrogen production increases with the increase in potential. During the constant potential analysis, the cell current was high at the very beginning due to the non-faradaic current. After some time, the non-faradaic current is neutralized and the faradaic current is recorded thereafter (>2 s) (Fig. 6.4e) (Yuan et al., 2004).

In this study, the newly synthesized Ni complex **2** showed an improved performance reducing CO_2 into C_2H_5OH in a 12 e^- pathway. Therefore, this study is compared to some recently reported catalysts. A nitrogen-doped nanodiamond electrode (NDD/Si RA) in $NaHCO_3$ electrolyte rapidly converted CO_2 to acetate over formate with an onset potential of −0.36 V vs. RHE with FE above 90.0% (Liu et al., 2015). Cave and his coworkers reported that the surface of Au foil catalysts is not favorable for C-O scission and thus produces CH_3OH over CH_4. At lower negative potential (−0.96 V vs. RHE), the Au foil catalyst produces CH_3OH with a low FE of 0.01%. At −0.68 V vs. RHE, the Au foil catalyst produces CO with a FE of 97% (Cave et al., 2017). Usually, a nickel catalyst is selective for the formation of CO. In 1990, Azuma and coworkers used Ni metal as electrocatalyst in 0.05 M $KHCO_3$, and CO (FE 21%) and HCOOH (13.7%) were the only products (Azuma, 1990). A dinuclear Ni complex in acetonitrile solution at $E_{cat} = -1.16$ V vs. NHE reduces CO_2 to only CO with FE of 95% (Zhong and Lu 2018). $[M^{n+}(cyclam)Cl_n]$ (M = Ni^{2+} and Co^{3+}) complexes as electrocatalyst in ionic liquids electrolyte produces only CO as with a FE of 95.2 and 85.9%, respectively, at −1.40 V vs. Ag/AgCl. $[Ni(cyclam)Cl_2]$ shows a better efficiency for reducing CO_2 than $[Co(cyclam)Cl_3]$ (Honores et al., 2017).

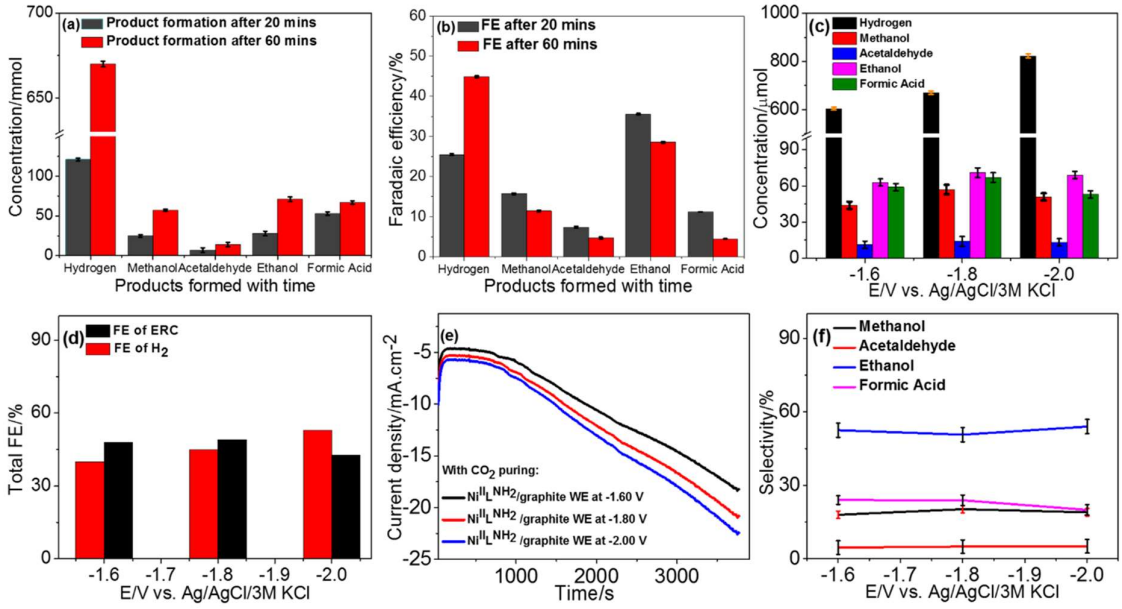

Figure 6.4: (a) Formation of products during ERC of CO_2 at complex **2**/graphite WE, (b) FE of the products formed at $E_{cat} = -1.80$ V, (c) Distribution of products in the liquid phase at various electrode potentials at complex **2**/graphite WE, (d) FE of CO_2 reduction at different potentials, (e) Cell current vs. time plot at different half-cell potentials vs. Ag/AgCl, and (f) Selectivity of products formed. Experimental condition: Electrolyte 0.5 M $KHCO_3$, catholyte, and anolyte 120 mL each, pH 7.0, and CO_2 bubbling rate 10 $mL.min^{-1}$ during ~45 min initial pre-saturation time.

A molecular polypyridyl Ni complex was used in ERC in MeCN solution with 0.1 M $TBAPF_6$ and it can reduce CO_2 into CO at $E_{cat} = -1.86$ V vs. Ag/AgCl. Achieving high efficiency is one of the major challenges in ERC (Lieske et al., 2018). In the present study employing Ni-salen complex (**2**), the product formation and efficiency were more selective towards the formation of C_2H_5OH with a decreased ERC potential (theoretical potential is −1.90 V vs. SHE). The present work using complex **2**/graphite WE exhibited a similar total FE for the ERC forming value-added chemicals. The C_2H_5OH production efficiency was the highest with a selectivity of 50.7% at −1.60 V vs. SHE. HCOOH was formed with a selectivity of 23.9% at the same potential. The highest TON was found to be 7560 (TOF

2.1 s^{-1}, Table 6.1) for the formation of C_2H_5OH followed by CH_3OH (TON 3060 and TOF 0.8 s^{-1}) at −1.80 V vs. Ag/AgCl (Table 6.1). Both HCOOH and CH_3CHO exhibited close TON and TOF. This implies that complex **2** is more active towards the formation of alcoholic products.

Table 6.1: Calculated TON and TOF of the formation of ERC products using Ni complex **2** in ERC.

Product	V vs. Ag/AgCl	TOF (S^{-1})	TON
C_2H_5OH	−1.80	2.1	7560
HCOOH	−1.80	0.33	1214
CH_3CHO	−1.80	0.3	1270
CH_3OH	−1.80	0.8	3060

6.3.2 Cyclic voltammograms of complex 2

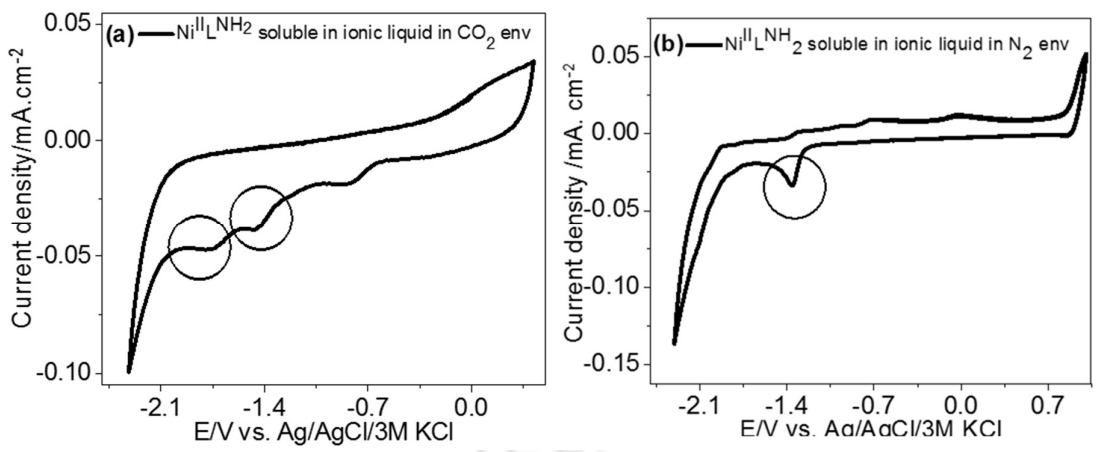

Figure 6.5: CV curves at a scan rate of 100 $mV.s^{-1}$ at glassy carbon WE in1 mM complex **2** as analyte at (a) CO_2 saturation and (b) N_2 saturation. Experimental condition: Electrolyte 0.1 M $TBAPF_6$ in CH_3CN solution, Pt wire as CE, and Ag/AgCl as RE.

Besides, complex **2** was also analyzed by dissolving it in an ionic liquid, tetrabutylammonium hexafluorophosphate ($TBAPF_6$). First, 0.1 M $TBAPF_6$ solution was prepared in CH_3CN in which 1 mM of the catalyst was mixed, and after that, the electrochemical analysis was performed. The experiment was conducted both with N_2 and CO_2 bubbling by using glassy carbon as the WE, Pt wire as the CE, and Ag/AgCl (3 M KCl) as the RE. With N_2 bubbling, an Ni(II)/Ni(I) redox pair was observed at −1.45/−1.32 V vs. Ag/AgCl (Fig.6.5a) (Froehlich and Kubiak 2015; Zhong and Lu 2018). With CO_2 saturation/bubbling, a distinct ERC peak was noted at −1.80 V vs. Ag/AgCl along with a Ni(II)/Ni(I) redox pair (Fig.6.5b). This indicates that the complex **2** redox system exhibits a significant peak separation with ERC (Lieske et al., 2018).

6.4 Electrode Characterization

6.4.1 CV analysis of catalysts coated WE after ERC reaction

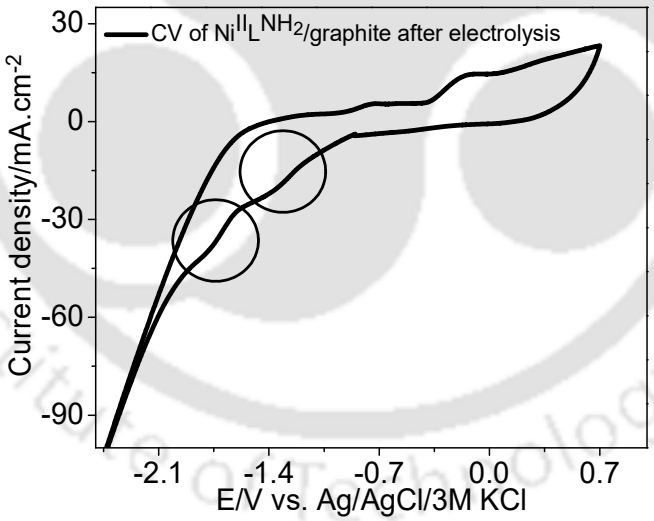

Figure 6.6: CV curves at a scan rate of 30 mV.s^{-1} during ERC at complex **2**/graphite WEs CO_2 saturation after 1 hour of electrolysis. Experimental condition: Electrolyte 0.5 M $KHCO_3$, catholyte, and anolyte 120 mL each and ~45 min initial pre-saturation time.

It is important to mention here that whether the catalyst changes its real active species or not was checked by conducting a cyclic voltammetric (CV) test in 0.5 M $KHCO_3$ solution after 1 h of electrolysis (Fig. 6.6). At first, the electrolysis was complete after 1 h and then CO_2 was again bubbled for about 45 minutes and the voltammogram was recorded by maintaining the same conditions as in Fig. 6.3 for the LSV analysis. There was no specific change observed either in the redox potential (no variation) or in the peak current density (3% variation). This confirms that the catalyst maintained its actual structure even after electrolysis and is reusable.

6.4.2 EDX analysis of complex 2 coated electrode

The FE-SEM and EDX analysis were conducted to know the surface morphology and the elemental distribution of the coating layer of the electrode. The EDX micrograph and FE-SEM spectrum of the electrocatalysts were recorded by simply scratching a small thin (~0.1 mm) layer from the electrode surface. Elemental mapping and percentage analysis were done to measure the distribution of elements over the electrode surface. In the Figs. 6.7a and 6.7c, the FE-SEM micrographs of the bare and complex **2**/graphite WEs are depicted. The corresponding elemental abundances are illustrated in Figs. 6.7b and 6.7d. A high dispersity of C, O, and Ni was also evident from the elemental analysis with a sufficient amount of Ni concentration over the electrode material. Ni, C, and O elements are present both in the ligand and the electrode material, and the presence of F is from the Nafion binder. The elemental analysis confirms the homogeneous distribution and successful coating of the catalyst over the graphite surface (Fig. 6.7e).

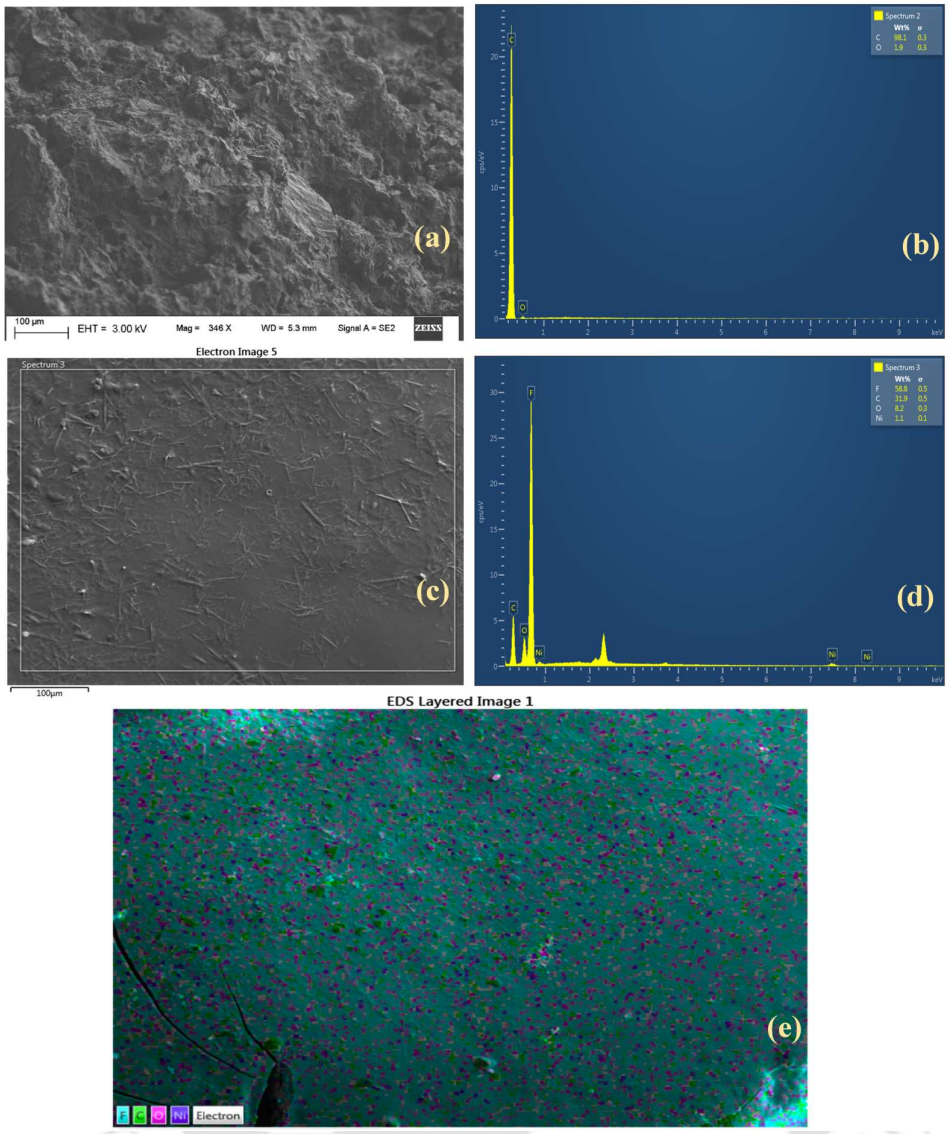

Figure 6.7: Morphology and EDX analysis of complex **2**/graphite WE. (a) FE-SEM micrograph of bare graphite WE surface before catalyst coating, (b) Elemental abundance of the bare graphite WE (Fig. 6.7a), (c) FE-SEM micrograph of a fresh surface of complex **2**/graphite WE, (d) Elemental abundance of complex **2**/graphite WE and (e) Elemental distribution of complex **2**/graphite WE.

6.4.3 GC analysis of products formation

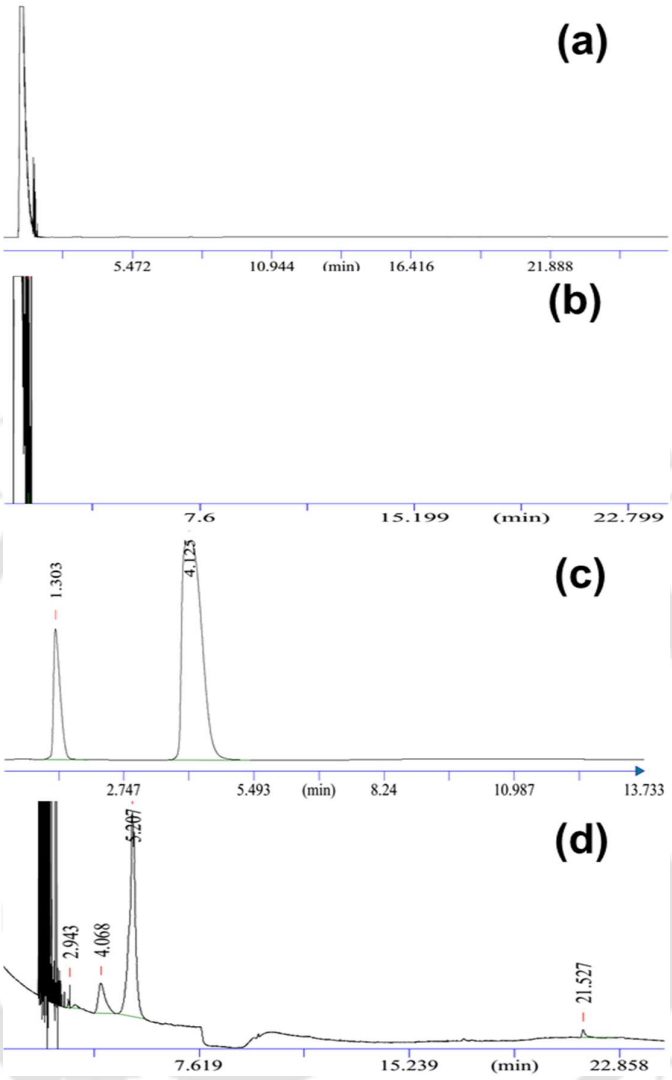

Figure 6.8: Gas chromatograms showing product formation during ERC using (a) chromatograph of the liquid sample only with graphite electrode without the catalyst, (b) chromatograph of the liquid sample using complex **2**/graphite electrode in N_2 atmosphere, (c) chromatograph of the gaseous sample using complex **2**/graphite electrode in N_2 atmosphere, and (d) chromatograph of the liquid sample using complex **2**/graphite electrode with CO_2 atmosphere after 1 h of electrolysis at −1.80 V vs. Ag/AgCl. RT= 2.94 min for CH_3CHO, RT = 4.068 for CH_3OH, RT= 5.2 for C_2H_5OH and RT= 21.5 is for

HCOOH using complex **2**/graphite WE in Fig. 6.8b. RT = 1.3 min is for H_2 and RT = 4.125 min is for N_2 in Fig. 6.8d.

In Fig. 6.8, the GC chromatographs of the reduction products are shown. With N_2 bubbling, H_2 was formed as the only product, and its formation was increased with the progress of the reaction. H_2 production was 603 μmol (FE 65%) due to water splitting at the same electrode potential at complex **2**/graphite WE after 60 mins of reaction. The gas chromatograms recorded during ERC with only the support electrode (the graphite plate without a catalyst) were compared with ERC using the catalyst-coated electrode with continuous CO_2 bubbling in both the conditions (Fig. 6.8). In the reference experiment, no product formation was observed without a catalyst along with continuous CO_2 bubbling (Fig. 6.8a). This confirms that the carbon source of the products observed was the CO_2 itself and not the electrode material. Further with N_2 bubbling, only H_2 formation was noted at −1.80 V vs. Ag/AgCl with the complex **2** coated electrode (Fig. 6.8b and 6.8c). Therefore, it can be confirmed that the carbon source of the products is neither the electrode materials nor the catalyst. Thus, there is no possibility of the breaking of the catalyst during the ERC reaction and this confirms the catalyst stability. To support this observation, the gas chromatograms for the formation of different ERC products at the complex **2**/graphite WE are shown in Fig. 6.8d.

6.5 Effect of anchoring group (-NH_2) in ERC

To discern the role of anchoring -NH_2 to the catalytic efficiency of the Ni(II) complexes (complex **2**) in ERC, the investigation on another Ni complex having no anchoring group ($Ni^{II}L$) was pursued in the inert as well as CO_2 saturated 0.5 M $KHCO_3$ system. An LSV scan was performed between 0 and −2.10 V vs. Ag/AgCl (Fig. 6.9a). A high current density was found in the CO_2 saturated media than the inert gas condition at lower electrode potential (<−0.90 V vs. Ag/AgCl). It indicated that HER was significant at

a higher potential in the inert gas environment, i.e., in the absence of CO_2. $Ni^{II}L$ complex didn't show any ERC peak and current density was higher in N_2 saturated media under the reported potential range. It implies its non or weak catalytic activity towards ERC (Fig. 6.9a). The constant potential analysis was done in a CO_2 saturated environment at different electrode potentials where the only product detected was H_2 (Fig. 6.9b). The FE of H_2 production was 52.2% with the production of 589 µmol at $E_{cat} = -1.60$ V vs. Ag/AgCl. The production was increased to 794 µmol at −1.80 V and 903 µmol at −2.00 V. The FE of H_2 production reached up to 45.27 and 37.23% at −1.80 and −2.00 V vs. Ag/AgCl, respectively (Fig. 6.9b). This confirms that the anchoring group of the $Ni^{II}L^{NH2}$ complex (complex **2**) played an important role in ERC for reducing the energy required and the formation of mostly HCOOH, CH_3OH, and C_2H_5OH.

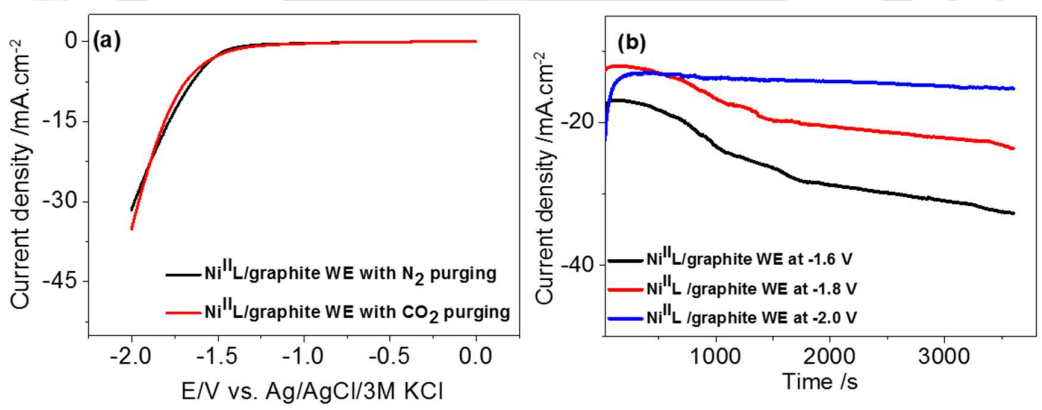

Figure 6.9: (a) LSV curves at a scan rate of 30 $mV.s^{-1}$ in ERC at $Ni^{II}L$/graphite WE with N_2 and CO_2 saturation, and (b) Cell current vs. time plot at different half-cell potentials vs. Ag/AgCl. Experimental condition: Electrolyte 0.5 M $KHCO_3$, catholyte, and anolyte 120 mL each, pH 7.0, and CO_2 bubbling rate 10 $mL.min^{-1}$ during ~45 min initial pre-saturation time.

6.6 Role of synthesized Ni metal complex in ERC and a comparison with NiO electrocatalyst

Complex **2** was being tested for the electrocatalytic reduction of CO_2. The catalyst was able to break the centrosymmetric CO_2 molecule, construct the C-C bond, and produces a mixture of C_2 products in a simple H-type electrolyzer. Noteworthy, complex **2** can successfully reduce CO_2 to C_2H_5OH through 12 electrons transfer reaction per molecule of CO_2 with a selectivity of 49%. The peak potential of ERC catalyzed by complex **2** was identified at $E_{cat} = -1.80$ V vs. Ag/AgCl from LSV. The abundance of the product formation was found in the order as C_2H_5OH>HCOOH>CH_3OH in terms of FE after 60 mins of ERC ($KHCO_3$ 0.5 M, pH 7.0, CO_2 saturation for ~45 min at 10 mL.min^{-1} and room temperature). The catalyst catalyzed ERC with FE of 70% at 20 mins of reaction but FE decreases with the progress of reaction due to the rise in HER. Whereas, in the same experimental conditions NiO was active towards the formation of any CO_2 reduced product. NiO coated electrode surface is more favourable for proton adsorption than gaseous CO_2. Thus, the Ni and NiO catalysts mostly produce either CO, HCOOH with low FE, or hardly produce any value-added products from CO_2 (Karamad et al., 2015; Nakagawa et al., 1991; Pérez-Rodríguez et al., 2011). NiO was very efficient for hydrogen evolution only (FE 79%) (Chapter 4).

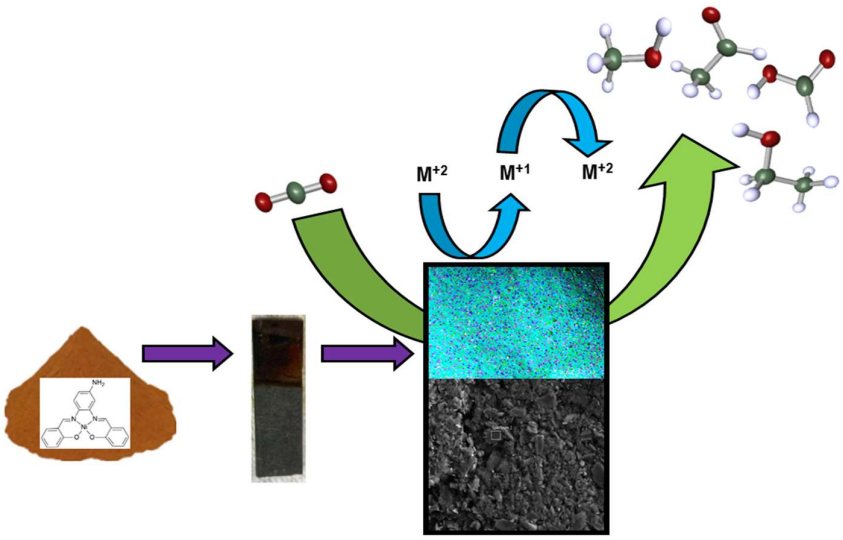

Scheme 6.2: Schematic diagrams of the representation of redox character of the salen metal complex during electrolysis of CO_2.

The improved performance of the Ni metal complex than its oxide can be beautifully explained with Scheme 6.2. The attached anchoring -NH_2 group facilitates the electron transfer from the electrode to the metal ion Ni(II) and finally to the substrate CO_2 by improving the interaction between the electrocatalysts and the electrode material. In this study, complex **2** acted nicely in the reduction of CO_2 and participated in multi-electron transfer processes resulting in the formation of a mixture of liquid fuels. Moreover, the catalytically active state for proton reduction in the M^{+1} state. The onset potential for the reduction of CO_2 thus depends upon the M^{+2}/M^{+1} redox potential. The lower the redox potential for the formation of M^{+1} from the M^{+2} state, the lesser is the energy required to reduce CO_2 (Shen et al., 2015). Thus, it is implied that the metal complexes undergo redox reaction from M^{+2} to M^{+1} and vice versa and help in the formation of a variety of products after multi-electron reduction (Scheme 6.2) (Cao et al., 2018).

The binding of the center metal atom with the CO_2 molecule is very important as the strong metal-CO_2 complex may affect in reducing the reactivity. However, the weak metal-

CO_2 bonding results in increasing the overpotential. During the electrolysis, Ni(II) centre at first transformed to Ni(I) intermediate and then again into the +II state. Intermediate Ni(I) is not thermodynamically that much stable and thus transfers an electron to the weakly interacting CO_2 molecule and develops stable Ni(II)-$CO_2^{\bullet-}$ complex upon binding, which induces multi-electron reduction of CO_2 (Singh et al., 2015). Therefore, the Ni complex produces not only previously reported C_1 products but also the C_2 products acting as a redox species. Thus, the redox behavior of complex **2**, the oxidation state of Ni metal-center, and the built-in -NH_2 group were recognized for an improved catalytic performance towards the formation of alcohols, and the formation of the products was likely initiated through the formation of metal-bound $CO_2^{\bullet-}$ radical. The production of alcohols using Ni complexes is new in this field of ERC. Thus, this work opens up an opportunity to develop new heterogeneous catalysts and therefore unlocks enormous scopes for further research in this area.

References

Azuma, M., Hashimoto, K., and Hiramoto, M., 1990. "Electrochemical Reduction of Carbon Dioxide on Various Metal Electrodes in Low-Temperature Aqueous $KHCO_3$ Media." *Journal of The Electrochemical Society*, 137, 1772.

Cao, Y., He, X., Wang, N., Li, H., and He, L., 2018. "Photochemical and Electrochemical Carbon Dioxide Utilization with Organic Compounds." *Chinese Journal of Chemistry*, 36, 644-659.

Cave, E. R., Montoya, J. H., Kuhl, K. P., Abram, D. N., Hatsukade, T., Shi, C., Hahn, C., Nørskov, J. K., and Jaramillo, T. F., 2017. "Electrochemical CO_2 Reduction on Au Surfaces: Mechanistic Aspects Regarding the Formation of Major and Minor Products." *Phys. Chem. Chem. Phys*., 19, 15856-15863.

Engelbrecht, A., Uhlig, C., Stark, O., Hämmerle, M., Schmid, G., Magori, E., Wiesner-Fleischer, K., Fleischer, M., and Moos, R., 2018. "On the Electrochemical CO_2 Reduction at Copper Sheet Electrodes with Enhanced Long-Term Stability by Pulsed Electrolysis." *Journal of The Electrochemical Society*, 165, J3059-J3068.

Froehlich, J. D., and Kubiak, C. P., 2015. "The Homogeneous Reduction of CO_2 by $[Ni(cyclam)]^+$: Increased Catalytic Rates with the Addition of a CO Scavenger." *Journal of the American Chemical Society*, 137, 3565-3573.

Honores, J., Quezada, D., García, M., Calfumán, K., Muena, J. P., Aguirre, M. J., Arévalo, M. C., and Isaacs, M., 2017. "Carbon Neutral Electrochemical Conversion of Carbon Dioxide Mediated by $[M^{n+}(cyclam)Cln]$ (M = Ni^{2+} and Co^{3+}) on Mercury free Electrodes and Ionic Liquids as Reaction Media." *Green Chem*., 19, 1155-1162.

Hori, Y., 2008. "Electrochemical CO_2 reduction on metal electrodes," In Vayenas et al. (ed.) '*Modern Aspects of Electrochemistry*', No. 42, Ch. 3, Springer, New York, pp. 89-189.

Jia, F., Yu, X., and Zhang, L., 2014. "Enhanced Selectivity for The Electrochemical Reduction of CO_2 to Alcohols in Aqueous Solution with Nanostructured Cu and Au Alloy as the Catalyst." *Journal of Power Sources*, 252, 85-89.

Karamad, M., Hansen, H. A., Rossmeisl, J., and Nørskov, J. K., 2015. "Mechanistic Pathway in the Electrochemical Reduction of CO_2 on RuO_2." *ACS Catalysis*, *5*, 4075-4081.

Kyriacou, G., and Anagnostopoulos, A., 1992. "Electroreduction of CO_2 on Differently Prepared Copper Electrodes. The Influence of Electrode Treatment on the Current Efficiencies." *Journal of Electroanalytical Chemistry*, 322, 233-246.

Lieske, L. E., Rheingold, A. L., and Machan, C. W., 2018. "Electrochemical Reduction of Carbon Dioxide with a Molecular Polypyridyl Nickel Complex." *Sustainable Energy and Fuels*, 2, 1269-1277.

Liu, Y., Chen, S., Quan, X., and Yu, H., 2015. "Efficient Electrochemical Reduction of Carbon Dioxide to Acetate on Nitrogen-Doped Nanodiamond." *Journal of the American Chemical Society*, 137, 11631-11636.

Nakagawa, S., Kudo, A., Azuma, M., and Sakata, T., 1991. "Effect of Pressure on the Electrochemical Reduction of CO_2 on Group VIII metal electrodes." *Journal of Electroanalytical Chemistry*, *308*, 339-343.

Ooka, H., Figueiredo, M. C., and Koper, M. T. M., 2017. "Competition between Hydrogen Evolution and Carbon Dioxide Reduction on Copper Electrodes in Mildly Acidic Media." *Langmuir*, 33, 9307-9313.

Pérez-Rodríguez, S., García, G., Calvillo, L., Celorrio, V., Pastor, E., and Lázaro, M. J., 2011. "Carbon-Supported Fe Catalysts for CO_2 Electroreduction to High-Added Value Products: A DEMS Study: Effect of the Functionalization of the Support." *International Journal of Electrochemistry*, *2011*, 1-13.

Shen, J., Kortlever, R., Kas, R., Birdja, Y. Y., Diaz-morales, O., Kwon, Y., Ledezma-yanez, I., Schouten, K. J. P., Mul, G., and Koper, M. T. M., 2015. "Electrocatalytic Reduction of Carbon Dioxide to Carbon Monoxide and Methane at an Immobilized Cobalt Protoporphyrin." *Nature Communications*, 6, 1-8.

Singh, S., Phukan, B., Mukherjee, C., and Verma, A., 2015. "Salen Ligand Complexes as Electrocatalysts for Direct Electrochemical Reduction of Gaseous Carbon Dioxide to Value-added Products." *RSC Advances*, *5*, 3581-3589.

Tan, T. A., Yusuf, S. Y., and Fazara, M. A. U., 1995. "Electrochemical Reduction of Carbon Dioxide into Formate." *Journal of Engineering Science and Technology*, 36, 625-628.

Uchida, T., Sasaki, Y., Ikeshoji, T., and Osawa, M., 2017. "4, 4′-Bipyridine as a Molecular Catalyst for Electrochemical Hydrogen Production." *Electrochimica Acta*, *248*, 585-592.

Yuan, Y., Wang, L., and Amemiya, S., 2004. "Chronoamperometry at Micropipette Electrodes for Determination of Diffusion Coefficients and Transferred Charges at Liquid/Liquid Interfaces." *Analytical Chemistry*, 76, 5570-5578.

Zhong, D., and Lu, T., 2018. "The Synergistic Catalysis Effect within a Dinuclear Nickel Complex for Efficient and Selective Electrocatalytic Reduction of CO_2 to CO." *Green Chemistry*, 20, 798-803.

This page is intentionally left blank

CHAPTER 7

Anchoring Groups guided Various Value-added Products Formation from Electrochemical Reduction of CO_2 by Pb(II)-Salen Complexes: Role of Ligand Framework

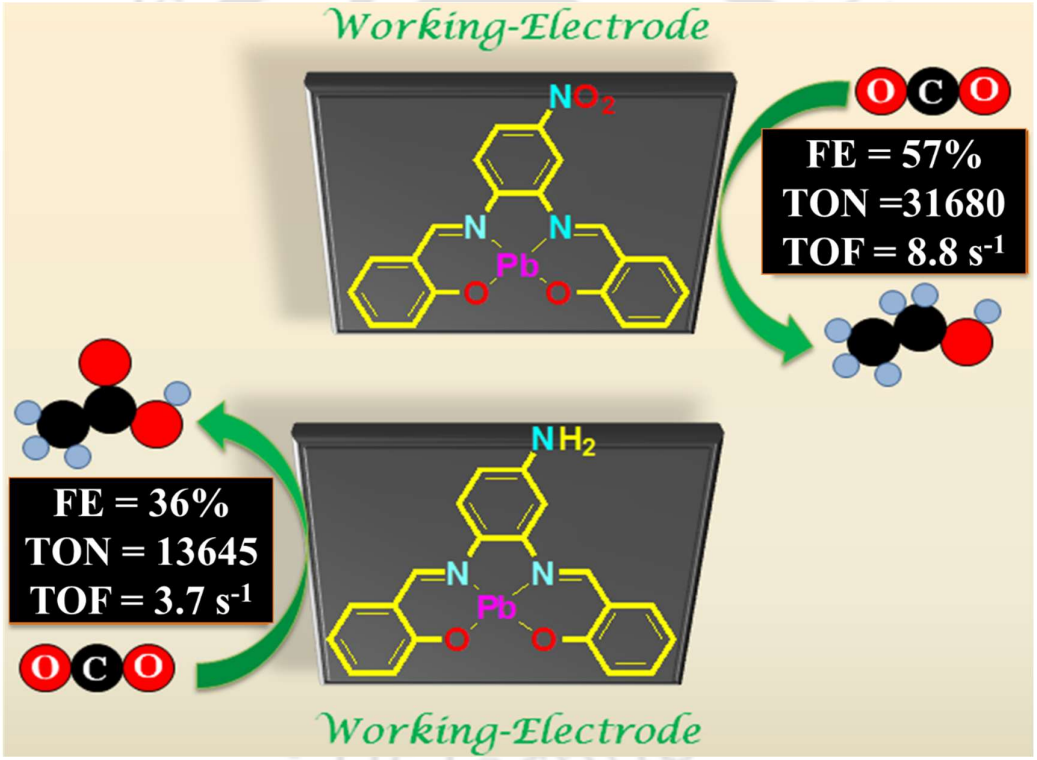

7.1 Background of the work

In the previous chapters, the role of various metal oxides and their corresponding metal complexes in ERC was already elaborated. The role of main group metal complexes is still unknown. Oxide-derived-Pb as catalysts have been reported for converting CO_2 molecules to C_1 product (C_1 stands for the molecule with one carbon atom), $HCOO^-$, in an aqueous electrolyte with a maximum FE of 95% (Lee and Kanan 2015). In 2020, Shi et al. reported the formation of $HCOO^-$ with FE of 96% in an ERC by using pre-catalyst, Pb(II)-tanin complex, which is converted to $PbCO_3$ and thereafter catalyst $[Pb_3(CO_3)_2(OH)_2]$ during the ERC (Shi et al., 2020). Although the successful and selective conversion of CO_2 to C_1 products in an aqueous electrolyte has been realized, the catalytic systems with the efficiency of producing highly desirable C_1^+ products (C_1^+ stands for the molecule with more than one carbon atom) using metallic lead/lead oxides or lead complexes are not familiar. Thus in this chapter two lead complexes $Pb^{II}(L^{NO_2})$] complex (**3**) and $[Pb^{II}(L^{NH_2})]$ complex (**4**); respectively were introduced in ERC (scheme 7.1). In this study, a $-NO_2$ functional group and an $-NH_2$ functional group been incorporated in the backbones of parent ligand H_2L to obtain ligand $H_2L^{NO_2}$ and ligand $H_2L^{NH_2}$, respectively.

It was envisaged that ligand-appended functional groups would involve in H-bonding and quadrupole-interactions with CO_2 molecules as well as the generated key intermediates species *CO and/or *CHO during the ERC. Thus, the concentration of CO_2 close to the catalyst-active sites would be high which would enhance the rare of ERC. Besides, the intermediate species would also be in close proximity on to the working electrode to facilitate the crucial intra-species C-C couplings in resulting C_1^+ products formation. Indeed, ERC in the presence of complex **3** and complex **4** as electrocatalysts provided majorly C_2 products at pH ~ 7.0. While, C_2H_5OH was produced with FE = 57% and SE = 66% at −1.80 V vs. Ag/AgCl by complex **3**, a mixture of acetic acid (CH_3COOH,

FE = 36%), acetaldehyde (CH_3CHO, FE = 12%) and CH_3OH (FE = 14%) with total FE = 68% at −1.80 V vs. Ag/AgCl was realized employing complex **4**. Conversely, another electrocatalyst having no anchoring group provided only C_1 products, formic acid (HCOOH, FE = 7%) and methanol (CH_3OH, FE = 27%) at −1.40 to −1.80 V vs. Ag/AgCl.

7.2 Synthesis of complex 3 [$Pb^{II}(L^{NO_2})$] and 4 [$Pb^{II}(L^{NH_2})$]

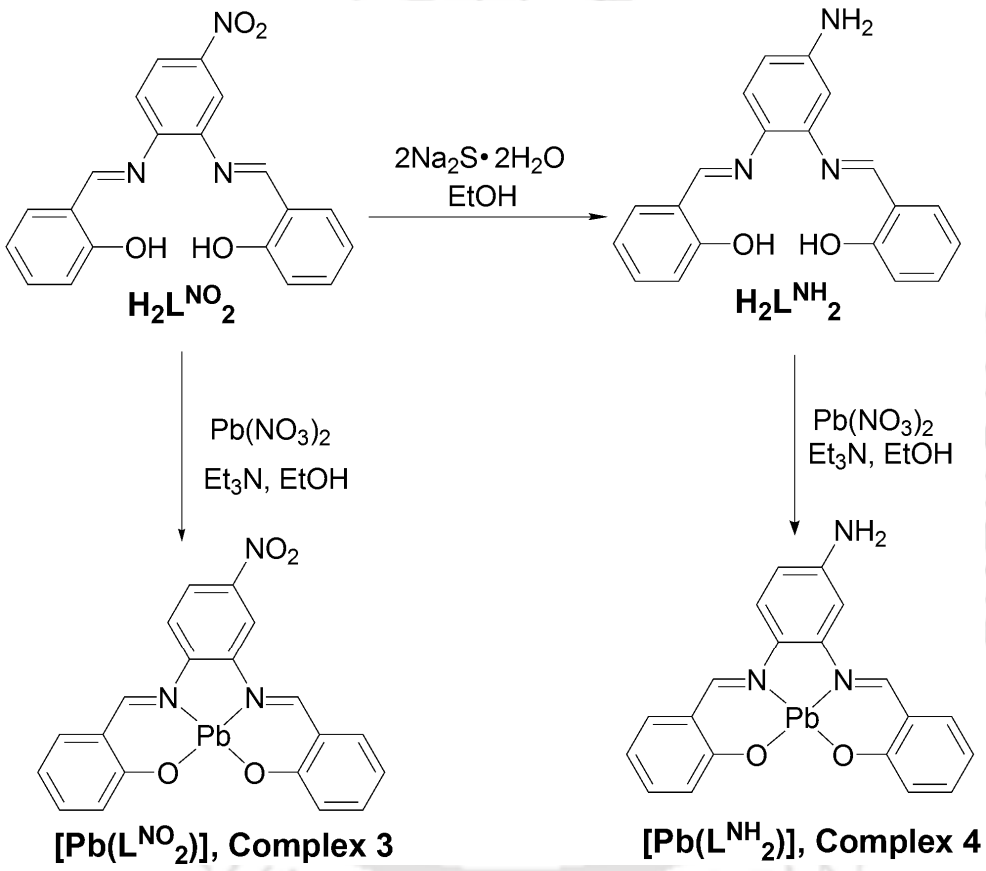

Scheme 7.1: Schematized steps for the synthesis route of Pb complexes (**3** and **4**).

Salen ligand $H_2L^{NO_2}$ was synthesized from the reaction of compound A (1.53 g; 10 mmol) and salicyldehyde (7.32 g; 60 mmol) in a 1:6 ratio (w/w), as reported previously (Singh, et al., 2015). $H_2L^{NO_2}$ ligand (0.5 mmol, 0.180 gm) was added to a stirring ethanolic (9 mL) solution of $Pb(NO_3)_2$ (0.5 mmol, 0.165 gm). To the suspension, Et_3N (0.2 mL) was added dropwise and the resulted mixture was refluxed for 7 h during which the color of the

solution changed from yellow to reddish-orange. The mixture was allowed to cool down at room temperature (25°C) and then the precipitate was collected by filtration. The precipitate was washed thoroughly with ethanol to avoid impurities and finally air-dried to get $[Pb^{II}(L^{NO_2})]$ complex ($C_{20}H_{13}N_3O_4Pb$; **3**), Yield: 0.204 g, 69% (Scheme 7.1). The synthesis procedure for the preparation of $H_2L^{NH_2}$ is described in Chapter 5. Then, to prepare complex **4**, $H_2L^{NH_2}$ ligand (0.5 mmol, 0.165 g) and $Pb(NO_3)_2$ (0.5 mmol, 0.165 g) were mixed in EtOH (9 mL) at first. To the stirred solution, Et_3N (0.2 mL) was added. The resulted reaction solution was then continued to stir under the refluxing condition for 7 h during which an orange-brown color solid appeared. The mixture was allowed to cool down at room temperature and the precipitate was filtered and washed with ethanol. Finally dried over air to get $[Pb^{II}(L^{NH_2})]$ complex ($C_{20}H_{15}N_3O_2Pb$; **4**), Yield: 0.188 g, 70% (Scheme 7.1).

7.3 Results and discussion

7.3.1 Metal complex characterization

The metal complexes were characterized by FTIR spectroscopy, Mass and CHN analysis. All the electrochemical analysis was conducted using Potentiostat.

7.3.1.1 Mass analysis of complex 3 and 4

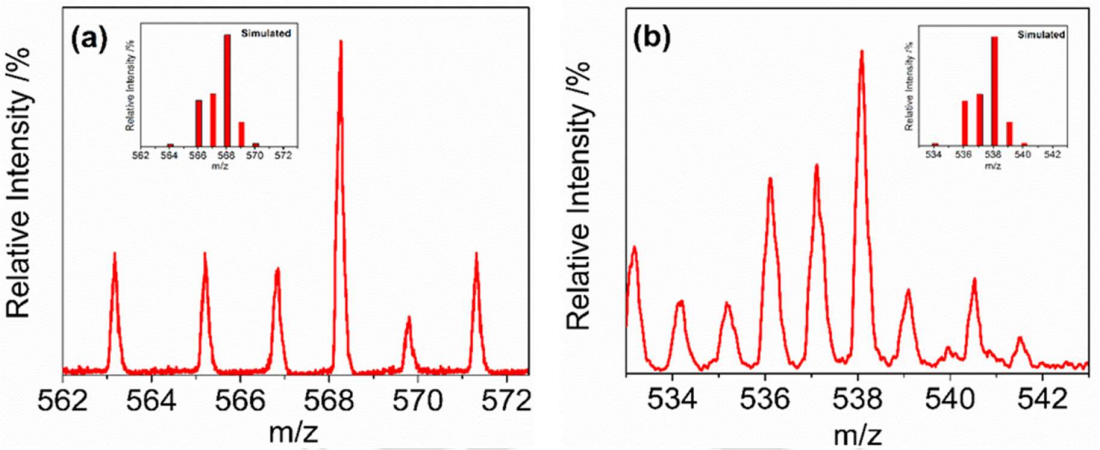

Figure 7.1: Experimental and simulated mass spectrum of synthesized complex **3** [$C_{20}H_{13}N_3O_4Pb$ + H] and **4** [$C_{20}H_{15}N_3O_2Pb$ + H].

Electrospray ionization mass spectra (ESI-MS) of complexes **3** and **4** in the positive mode in DMF: CH_3CN (1:25) solvent mixture provided 100% molecular ion peaks at 568.24, and 538.14 amu, respectively. The observed-peaks corresponded to the expected [M + H] (M is the molecular mass) compositions for the neutral complexes and confirmed the successful syntheses of $C_{20}H_{13}N_3O_4Pb$ (**3**) and $C_{20}H_{15}N_3O_2Pb$ (**4**) complexes (Figs. 7.1a and 7.1b). The molecular-compositions were further supported by microanalyses (elemental C, H, and N).

7.3.1.2 FTIR spectra of $H_2L^{NH_2}$ ligand and corresponding complex 3 and 4

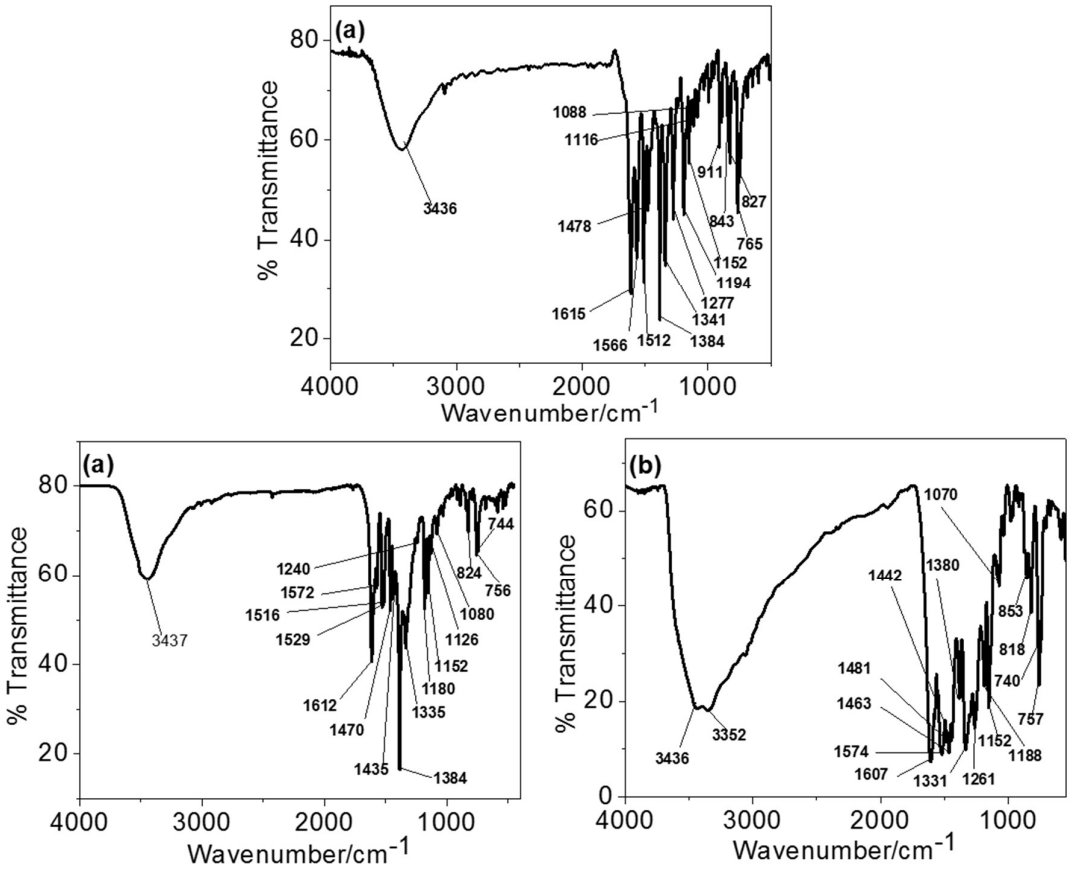

Figure 7.2: FTIR spectrum of (a) $H_2L^{NO_2}$ ligand, (b) complex **3** and (c) complex **4**.

In the FTIR spectrum of ligand $H_2L^{NO_2}$, the band for ν(O-H) stretch appeared at 3437 cm^{-1} (Fig. 7.2a). The existence of bands at 1341 and 1512 cm^{-1} confirms the presence of the -NO_2 group. The asymmetric (C=C) stretching band and the phenolic stretching band appeared at 1566 and 1277 cm^{-1} respectively. In complex **3**, the aldamine C=N stretch shifted slightly to a lower value and appeared at 1612 cm^{-1} (Fig 7.2b). After complexation, asymmetric (C=C) stretching band for phenyl ring appeared at 1572 cm^{-1}. This indicated a more aromatic character inside the phenyl rings in the complexes compared to the ligand. Additionally, a lower phenolic stretching value in the complexes (1240 cm^{-1}) was observed. In complex **4**, the Phenolic stretching (C-O) stretching band appeared at, 1240 cm^{-1}. The FTIR analysis of $H_2L^{NH_2}$ ligand is described in chapter 5 in Fig. 5.3a. In the FTIR

analysis of complex **4**, aldamine C=N stretch appeared at 1607 cm^{-1}. A broad band observed at 3436 cm^{-1} was due to the ν(O-H) stretch of moisture. The -NH_2 group refrained from deprotonation and metal coordination as evident by the appearance of two ν(N-H) stretches at 3352 cm^{-1} (Fig. 7.2c). The shift in the peaks in the complexes than the parent ligand confirms the successful synthesis of metal complexes.

7.3.1.3 CHN analysis of complex 3 and 4

The elemental analysis (CHN) of complex **3** and **4** were conducted to establish the elemental formula. The theoretically calculated percentage of C, H and N were 40.71, 2.65 and 7.12%. A very low amount of lattice bound water molecule was found in the experimentally calculated value of complex **3**. Thus, the experimental composition was found is % C 40.44; % H 2.34; % N 6.96. Thus, the elemental formula is $C_{20}H_{13}N_3O_4Pb•1.25H_2O$. Whereas the experimental composition of complex **4** was theoretically calculated as % C, 44.68; % H 2.81; % N 7.82. The experimentally observed values of C, H and N was 44.15%, 2.70% and 7.54% respectively. These values are well-matched with the theoretically calculated values and thus the elemental formula will be $C_{20}H_{15}N_3O_2Pb$.

7.3.2 Voltammetric analysis during ERC using complex 3 and 4 electrocatalysts

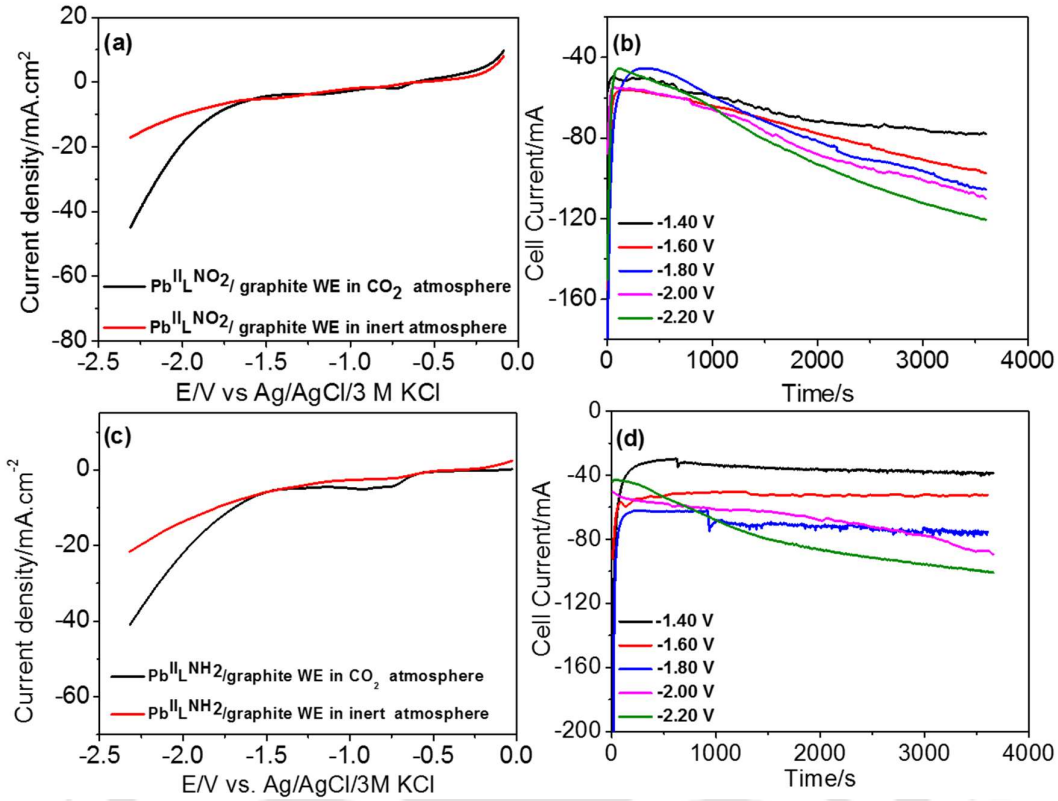

Figure 7.3: Linear sweep voltammetry of reduction of CO_2 by sweeping from 0.05 V to −2.30 V vs. Ag/AgCl at inert and at CO_2 saturated environment using (a) complex **3**, and (c) complex **4** as electrocatalysts at a scan rate of 30 mV.s^{-1}, constant-potential analysis during the electrochemical reduction of CO_2 at five different electrode potentials (−1.40 to 2.20 V) with (b) complex **3**, and (d) complex **4** as electrocatalysts. Experimental condition: Electrolyte 0.5 M $KHCO_3$, catholyte and analyte 120 mL each, pH 7.0 and CO_2 bubbling rate 10 mL.min^{-1} with ~45 min initial pre-saturation time.

The performance of the catalysts for ERC was confirmed by conducting chronoamperometry analysis in CO_2 saturated 0.5 M $KHCO_3$ solution at pH = 7.0. The electrocatalytic CO_2 reduction by the electrodes was carried out at five different electrode-potentials of the two complexes (**3** and **4**) and the constant-potential curves are depicted in

Figs. 7.3b, and 7.3d respectively. The potentials are reported vs. Ag/AgCl. At each potential, the electrochemical reduction was conducted for 1 h and the products were analyzed by gas chromatography and subsequently, the FE of the products was calculated.

7.3.3 Products formation and FE during ERC using complex 3 and 4 electrocatalysts

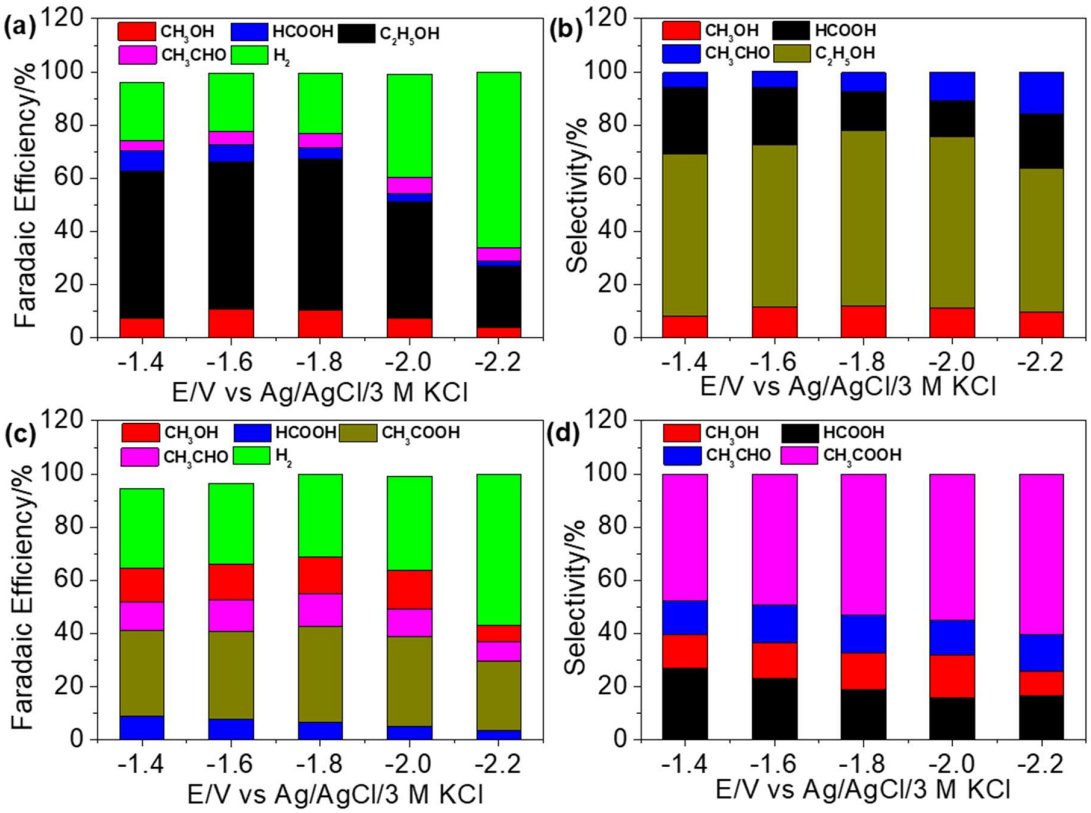

Figure 7.4: (a) FE of products formation, and (b) corresponding SE of products formation using complex **3** as electrocatalyst, (c) FE of products formation, and (d) corresponding SE of products formation using complex **4** as an electrocatalyst. Electrolyte 0.5 M $KHCO_3$, catholyte and anolyte 120 mL each, pH 7.0 and CO_2 bubbling rate 10 mL.min^{-1} with ~45 min initial pre-saturation time.

In the case of complex **3** as the catalyst-material, at −1.40 V, the rates of formations of C_1 product HCOOH and C_2 product C_2H_5OH were almost equal. The productions of HCOOH/CH_3OH/C_2H_5OH/CH_3CHO were 111/35/134/12 µmol, respectively. At −1.60 V,

elevations in the productions of C_2H_5OH (167 μmol, FE 55.3%) and CH_3OH (64 μmol, FE 10.6%) were observed (Fig. 7.4a), while, the formation of HCOOH and CH_3CHO remained almost uncharged, 118 μmol (FE 7.7%) and 18 μmol (FE 4.9%). The maximum C_2H_5OH production with 186 μmol (FE 57.0%) was achieved at −1.80 V. At this potential, the formation of HCOOH, CH_3CHO and CH_3OH were 81 (FE = 4.13%), 21 (FE = 5.3%) and 68 μmol (FE = 10.4%), respectively. The highest FE = 76.7% to the generation of C_1 (14.5%) and C_2 (62.26%) products were also recorded at this potential. At higher potentials, *i.e.*, above −2.00 V, HER dominated substantially that suppressed the electrochemical reduction of CO_2. At −2.00 V, % FEs to the formations of HCOOH/CH_3OH/C_2H_5OH/CH_3CHO were 3.0/7.4/43.5/6.09%, respectively, whereas % FE for H_2 production reached 39% compared to 22.5% at −1.80 V. The total % of FE of the formation of HCOOH, CH_3OH and C_2H_5OH diminished further to 33.8% at −2.20 V. In this ERC process, C_2H_5OH was the major product and was also the solo C_2 product. The selectivity of the ethanol formation increased slightly from 61% to above 64% with the increasing of the electrode potential from −1.40 to −2.20 V (Fig. 7.4b).

During the ERC using complex **4**-coated graphite electrode as the electrocatalysts, HCOOH and CH_3OH was formed as the C_1 products at all the applied electrode potentials. C_2 products, acetic acid (CH_3COOH), and acetaldehyde (CH_3CHO) were detected. At −1.40 V, HCOOH and CH_3COOH formed majorly almost at the same rate. The productions of HCOOH/CH_3COOH/CH_3CHO/CH_3OH were 64/60/15/30 μmol, respectively (Fig. 7.4c). FE for HCOOH production was highest at that potential (Fig. 7.4c). With increasing the electrode potential, % FE to the formation of HCOOH decreased slightly, while, % FE to the generation of major product CH_3COOH increased marginally (Fig. 7.4c). At −1.80 V, the total % FE for the ERC to the formation of C_1 and C_2 products was 68%. The respective % FE for CH_3COOH/CH_3CHO/CH_3OH were 36.3/11.9/14.1%. The production

of CH_3COOH was found to be improved with increasing the electrode potential to −2.00 V., the production was highest with 138 μmol at that potential, however, HER prevailed with FE = 35%.

ERC with complex **4** as the catalyst-material was more selective towards HCOOH and CH_3COOH productions compared to CH_3CHO and CH_3OH at any potential. The product selectivity of HCOOH was the highest (SE = 26.8%) at −1.40 V. With the increase in the electrode potential, % SE to HCOOH production decreased, while, an improvement in % SE (48% at −1.40 V, 60% at −2.20 V) to the formation of CH_3COOH was realized (Fig. 7.4d). To note, % SEs to the generation of CH_3CHO and CH_3OH were almost the same in all the applied electrode potentials (Fig. 7.4d).

The calculated TOF and TON of complex **3,** and **4** are given in table 7.1 and 7.2. Using complex **3** as the catalyst-material, at −1.80 V, TON = 2268/5760 and TOF 0.63/1.60 s^{-1} for HCOOH/CH_3OH products were found. The maximum TON = 31680 with TOF = 8.8 s^{-1} (Table 7.1) was obtained for C_2H_5OH production employing complex **3**-containing graphite plate as the electrocatalyst at −1.80 V. The maximum TON for complex **4**-coated electrocatalyst was realized for CH_3COOH production (13644 with TOF 3.79 s^{-1}) followed by CH_3OH (TON 5292 with TOF 1.47 s^{-1}) at −1.80 V (Table 7.2). Hence, it is clear that both complex **3** and complex **4** were efficient catalysts for the conversion of CO_2 to value-added C_2 products.

Table 7.1: Calculated TON and TOF of the formation of ERC products using complex **3** in ERC.

Product	**V vs. Ag/AgCl**	**TOF (S^{-1})**	**TON**
HCOOH	−1.80	0.63	2268
CH_3OH	−1.80	1.60	5760
C_2H_5OH	−1.80	8.80	31680
CH_3CHO	−1.80	0.81	2916

Table 7.2: Calculated TON and TOF of the formation of ERC products using complex **4** in ERC.

Product	**V vs. Ag/AgCl**	**TOF (S^{-1})**	**TON**
HCOOH	−1.80	0.67	2412
CH_3COOH	−1.80	3.79	13644
CH_3CHO	−1.80	1.25	4500
CH_3OH	−1.80	1.47	5292

7.3.4 Cyclic voltammograms of complexes 3 and 4

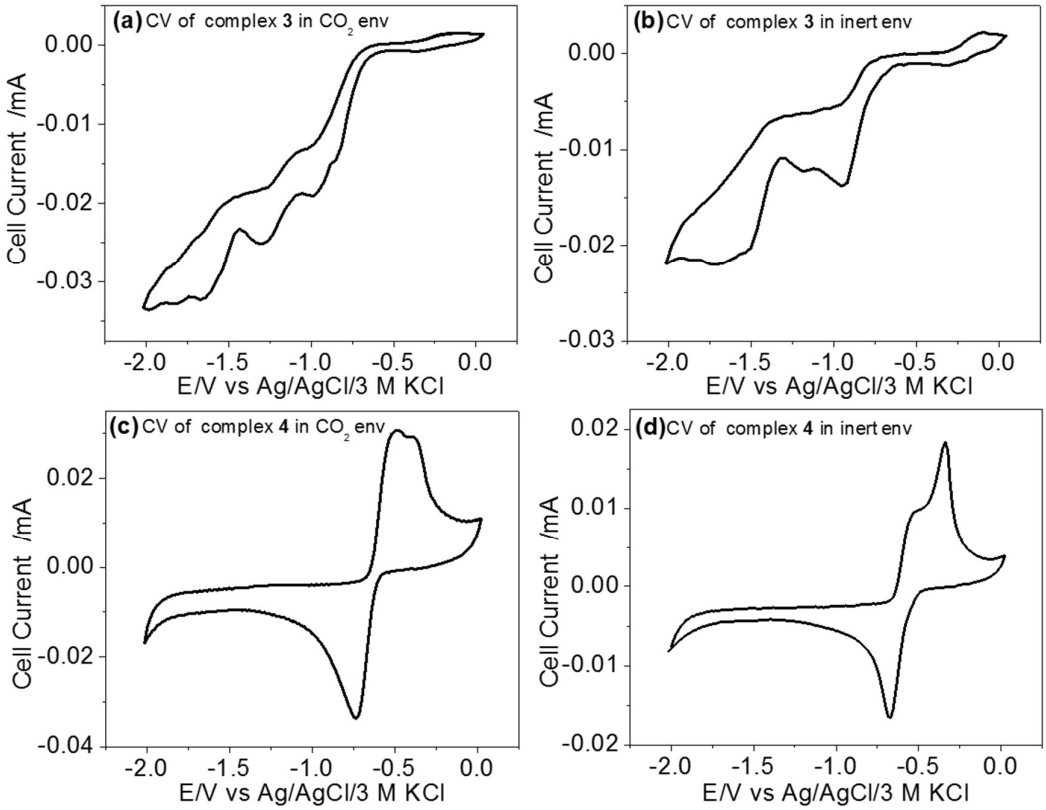

Figure 7.5: CV curves at a scan rate of 100 $mV.s^{-1}$ at glassy carbon WE in1 mM complex **3** as analyte (a) in CO_2 and (b) in inert and complex **4** as analyte (c) in CO_2 and (d) in an inert environment. Experimental condition: Electrolyte 0.1 M $TBAPF_6$ in CH_3CN solution, Pt wire as CE and Ag/AgCl as RE.

The CV of complex **3** and **4** was also analysed by dissolving it in an ionic liquid, tetrabutylammonium hexafluorophosphate ($TBAPF_6$). First, 0.1 M $TBAPF_6$ solution was prepared in CH_3CN in which 1 mM of the catalyst was mixed, and after that, the electrochemical analysis was performed. The experiment was conducted both with N_2 and CO_2 bubbling by using glassy carbon as the WE, Pt wire as the CE and Ag/AgCl (3 M KCl) as the RE. In inert environment, an Pb(II)/Pb(0) redox pair was observed at −0.95/−1.32 V vs. Ag/AgCl using complex **3** (Fig. 7.5a.). With CO_2 saturation/bubbling, and Pb(II)/Pb(0)

redox pair was observed at −0.98/−1.12 V vs. Ag/AgCl using complex **3** (Fig. 7.5b.). Using complex **4** as an electrolyte, Pb(II)/Pb(0) redox pair was observed at −0.68/−0.33 V vs. Ag/AgCl in an inert atmosphere (Fig. 7.5c.). With CO_2 saturation/bubbling, and Pb(II)/Pb(0) redox pair was observed at −0.73/−0.48 V vs. Ag/AgCl using complex **4** (Fig. 7.5d.) (Abbasi et al., 2009; Liu et al., 2019; Marken et al., 1997).

In the field of ERC, most of the metals were reported either CO or methane. However, the catalytic systems with the efficiency of producing highly desirable C_2 products are quite rare (Bushuyev et al., 2018; Fan et al., 2020; Song et al., 2017; Sun et al., 2017). Some Cu-based materials are reported for the generation of C_2 products. For instances; Mougel, Fontecave and coworkers have shown that Cu-N-doped carbon catalyst can generate ethanol (C_2H_5OH) with FE = 55% at −1.20 V vs. RHE (Karapinar et al., 2019). Zhuang and coworkers have employed polyaniline-coated Cu nanoparticles as catalysts to achieve C_2 products with FE = 66% (FE = 44% for C_2H_4 and FE = 22% for C_2H_5OH) at −1.08 V vs. RHE (Wei et al., 2020). $Cu_{1.8}Se$ nanowires have been utilized as a catalyst to generate C_2H_4 (FE = 55%) and EtOH (FE = 24%) at −1.10 V vs. RHE (Mi et al., 2018). Yeo and coworkers have reported Cu_2O films of various thickness to successful conversion of CO_2 to C_2H_5OH with a FE of 9-16% (Ren et al., 2015). By incorporating Fe-porphyrin derivatives on Cu surface, CO_2 has been converted to the acetate (CH_3COO^-) and C_2H_5OH with FE = 38%, and FE = 27% at −0.45 V vs. RHE (Gong et al., 2017). These catalysts can produce ethanol which requires 12 electrons to produce. Complex **3** is selective towards the formation of ethanol whereas complex **4** is selective for the production of acetic acid.

7.4 Electrode characterization

7.4.1 EDX analysis of complexes 3 and 4 coated electrode

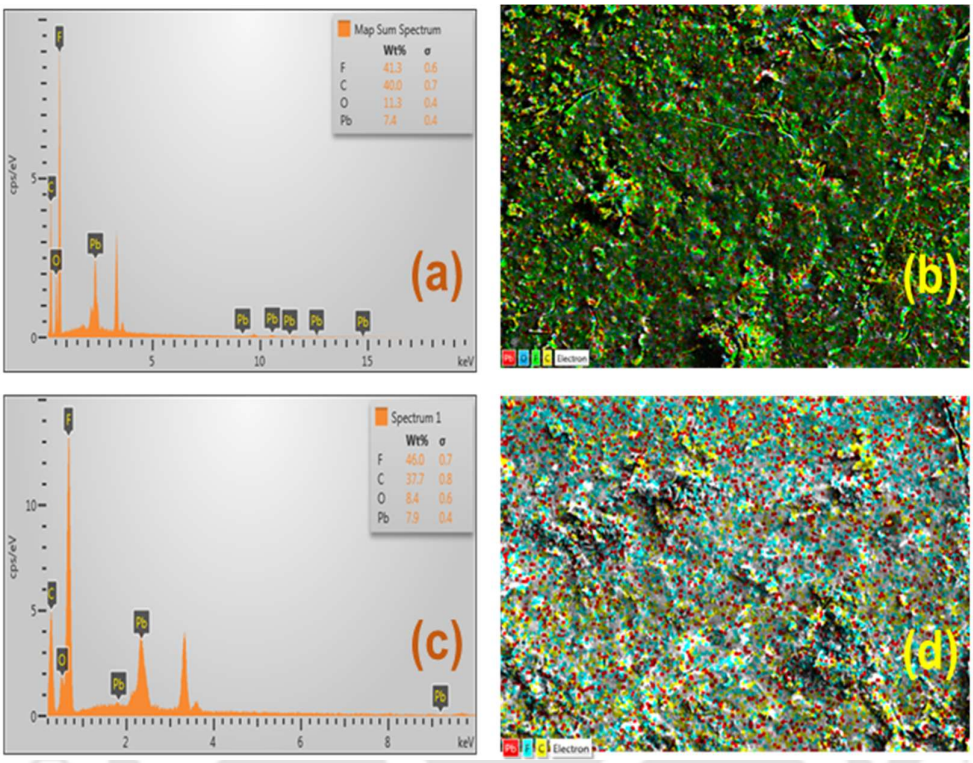

Figure 7.6: (a) EDX micrograph of the WE after complex **3** coatings: elemental distribution, (b) corresponding image mapping showing Pb surface coverage on the WE (red dots), (c) EDX micrograph of the WE after complex **4** coatings: elemental distribution and (d) corresponding image mapping showing Pb surface coverage on the WE (red dots).

To prepare catalysts-coated electrodes, the catalysts, complexes **3** and **4**, were initially dissolved in N, N-dimethylformamide (DMF) and mixed with Nafion dispersion (5 wt%) solution. Each resulted solution mixture was then brushed onto a graphite plate to finally fabricate a catalyst-coated electrode of 4 cm^2 size. A thin layer (about 0.1 mm width) from the surface of each prepared electrode was collected and subjected to FESEM-EDX micrographs and elemental mapping analyses. The elemental distribution and

corresponding mapping is described in Figs. 7.6a and 7.6b using complex **3**. Similarly, in the Figs. 7.6c and 7.6d the mapping of the elements over the WE and the elemental distribution of complex **4** coatings are shown. A high amount of C, O, F and Pb were found from the elemental analysis. The C, O and the Pb ions are present in the metal complexes and the F ion is present in the Nafion binder. The images and elemental mapping indicated that the coatings were homogeneous and the distribution of the Pb-catalysts was uniform over the basal graphite plates (Fig. 7.6).

7.5 Effect of ligand-framework to ERC

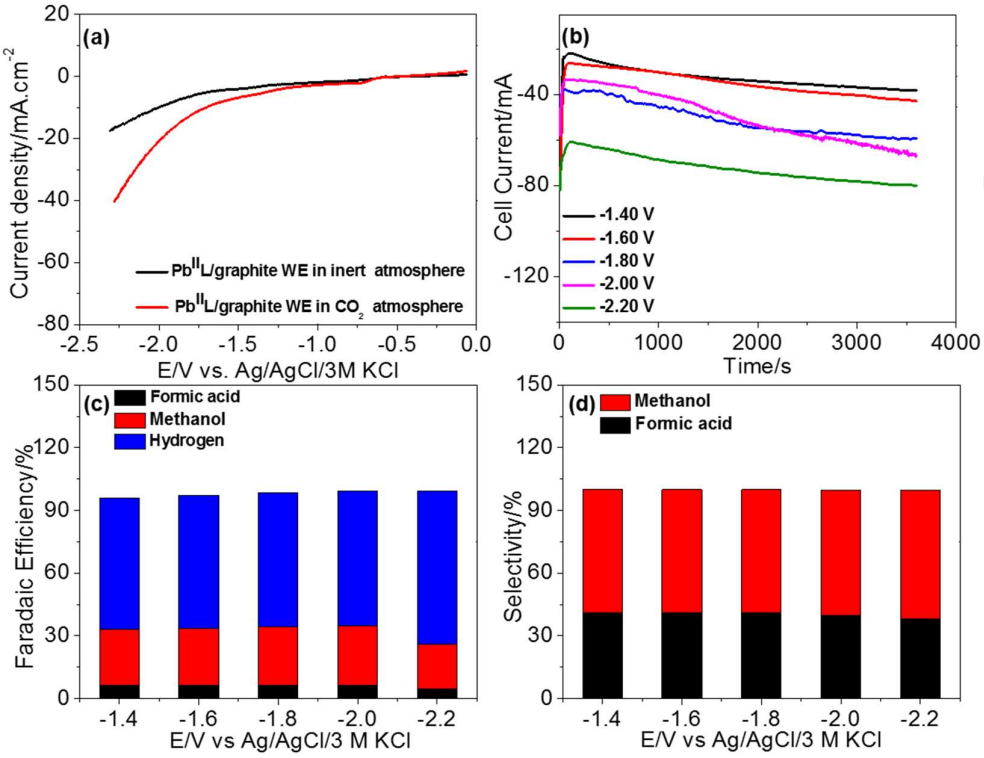

Figure 7.7: (a) Linear sweep voltammetry of reduction of CO_2 by sweeping from 0 to −2.30 V vs. Ag/AgCl at inert and CO_2 saturated environment at a scan rate of 30 mV.S^{-1}, (b) constant-potential analysis during electrochemical reduction of CO_2 at five different electrode potentials (−1.40 to 2.20 V), (c) FE of products formation, and (d) corresponding SE of products formation using [Pb^{II}(L)] complex WE. Experimental condition: Electrolyte

0.5 M $KHCO_3$, catholyte and anolyte 120 mL each, pH 7.0 and CO_2 bubbling rate 10 $mL.min^{-1}$ during ~45 min initial pre-saturation time.

From the preliminary analysis (LSV data) the activity of the two complexes (**3** and **4**) in the field of ERC was confirmed. The performance of the catalysts for ERC was further confirmed by conducting chronoamperometry analysis in CO_2 saturated $KHCO_3$ solution using them. The constant-potential analysis was conducted using the $[Pb^{II}(L)]$ complex as an electrocatalyst in the same potential range same as the other two complexes (**3** and **4**). Initially, in the LSV analysis, the higher current density in the CO_2 saturated atmosphere confirms the activity of the catalyst in ERC. Further, in a control experiment, the NH_2 and NO_2 free Pb complex was used as an electrocatalyst and after 1 h of ERC reaction, CH_3OH and HCOOH was the only product observed (total FE 35%). At five different potentials, the complex produced HCOOH and CH_3OH mainly. At lower potentials, HCOOH production prevails. The FE of HCOOH production was highest at −1.80 V vs. Ag/AgCl with 6.45% (71 μmol). Whereas, the CH_3OH production rate increases with an increase in potential and highest at −2.00 V vs. Ag/AgCl (112 μmol, 28.56% FE) (Fig. 7.7a). At lower potential, the catalyst was selective towards HCOOH production and the product selectivity is almost similar up to potential −1.80 V (41%). The rate of CH_3OH production increases at higher potentials. The selectivity for CH_3OH production was 60% and 61.7% at −2.00 and −2.20 V respectively (Fig. 7.7b). Herein, HER predominated with FE = 62% to 72%. This study proves that the anchoring group has a crucial role in felicitating in electron transfer and thus helps the metal complex in CO_2 electroreduction.

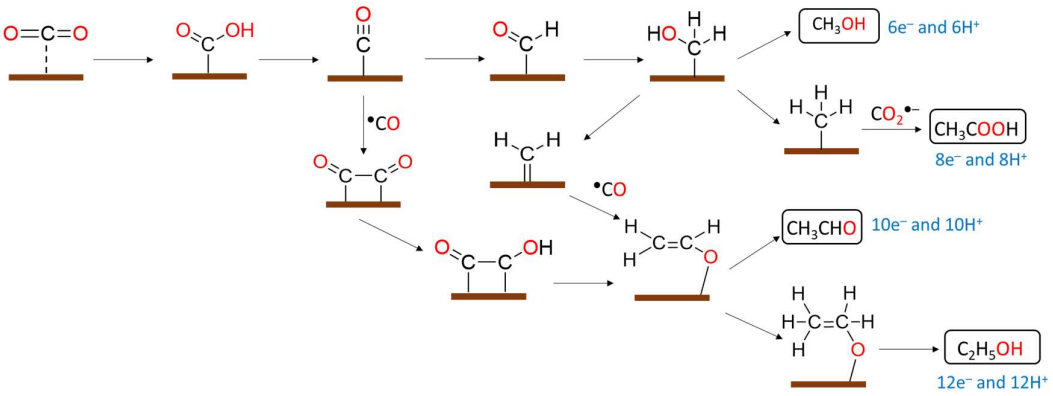

Scheme 7.2: Showing some selective important intermediates to the formation of CH_3OH, CH_3COOH and C_2H_5OH by the electrochemical CO_2 reduction in the presence of protons.

To discern the effect of ligand backbones and the attached substituents, electrocatalysis was performed using PbO as the catalyst. In the catalysis, irrespective to the applied potentials, *i.e.*, −1.40 to −2.20 V, HCOOH was formed as the solo product with FE ~23% (Chapter 4, Fig 4.10)**.** This observation indicated that the ligands have profound effect to the further reduction of HCOOH. In the complexes, the central Pb^{2+} was coordinated by two imine sp^2 N atoms and two phenolate sp^3 O atoms. All the coordinating atoms are highly electronegative in nature and can attract protons (H^+). Thus, in the electrocatalysis using [Pb^{II}(L)] complex coated graphite, the sufficient availability of protons in the vicinity of the active-site [Pb(II)] led to the further reduction of HCOOH to six-electron-six-proton coupled product CH_3OH *via* *CO (* refers the atom of the species bonded to the catalysts-surfaces) intermediate pathway (Hasani et al., 2020; Ma et al., 2016; Nitopi et al., 2019; Ren et al., 2018; Zheng et al., 2019).

The presence of electron-donating -NH_2 substituent in the ligand backbone of complex **4** increased electron-density and consequently basicity of the imine N atoms compared to that in [Pb^{II}(L)] complex. Hence, further reduction of *CH_2OH

to $*CH_3$ species would be favorable and postulated, herein (Scheme 7.2). The presence of basic $-NH_2$ group (aniline unit) can form strong interactions with acidic CO_2 molecules. Therefore, the concentration of CO_2 molecules is expected to be high in the proximity of the reaction centre in complex **4**. The insertion of $*CH_3$ into an adjacent CO_2 molecule, followed by reduction of the formed species provided eight-electron-eight-proton coupled major product CH_3COOH (Scheme 7.2). The formation of $*CH_2$ intermediate followed by CO insertion and subsequent reductions could be the path to the formation of minor product such as CH_3CHO (Hasani et al., 2020; Ma et al., 2016; Nitopi et al., 2019; Ren et al., 2018; Zheng et al., 2019). Nevertheless, the path is expected to be less favorable as the high electron-density on the N atoms would diminish the electropositive nature of Pb^{2+} reaction centre and accordingly the stability of $*CH_2$ species with the high electron density on *C atom would be low.

In complex **3**, the ligand backbone comprised of a strong electron-withdrawing $-NO_2$ substituent. The effect of the substituent would decrease the electron density on the N atoms greatly. Thus, the availability of protons surrounding the electrode surface would be low and consequently, a C-C coupling between the *CO molecules would be favoured to produce C_2 products than the hydrogenation of C_1 intermediate *CO or *CHO to render C_1 products. Indeed, C_2H_5OH was detected as the major product.

7.6 Lead metal complexes vs. lead metal oxide

The aim of introducing various metal complexes in ERC was to enhance the catalytic activity with high FE. In this chapter, two lead complexes of different anchoring group were synthesized and demonstrated as catalysts to the electrochemical reduction of CO_2 to various value-added C_1 and C_2 products. PbO as the electrocatalyst, irrespective of the

applied potentials, *i.e.*, −1.40 to −2.20 V, only HCOOH was detected as the reduction product. The FE of HCOOH production was also very low (FE = 23%) and the description is given in chapter 4. Whereas, the incubation of Pb^{2+} within the organic frameworks, [Pb^{II}(L)] complex, favored further reduction of HCOOH to CH_3OH with enhanced efficiency (FE = 27%, SE = 59%). Not only that, the incorporation of the anchoring group in the parent ligand [Pb^{II}(L)], have improved the efficiency of the catalysts enhancing the electron transfer rate between the catalyst and the electrode material.

At −1.80 V vs. Ag/AgCl at pH = 7.0, complex **3** ($Pb^{II}(L^{NO2})$] derived C_2H_5OH with = 57% and SE = 66%, whereas CH_3COOH was obtained with FE = 36% and SE = 53% employing complex **4** ($Pb^{II}(L^{NO2})$]. Thus, the incorporation of electron-withdrawing -NO_2 or electron-donating-basic -NH_2 functional group in the backbone of the parent ligand preferentially generated multiple-electrons-multiple-protons reduced C_2 products by stabilizing *CO, *CHO/*CH_3 intermediates and increasing the availability of CO_2/CO near the electrode surface. However, the complicated reactions that proceed *via* the generation of several intermediates need detailed theoretical studies to apprehend the possible mechanism and will be pursued in the near future. Nevertheless, this study consolidated that the introduction of different substituents could lead to highly desirable C_2 products by modifying the substrate or proton concentration over the electrode surfaces.

7.7 Metal complexes vs. metal oxides

A thorough literature survey showed the uses of transition metal catalysts for the CO_2 reduction reactions. The majority of the studies were performed using the oxides of Cu, Ni and Pb in ERC. The Cu_2O electrocatalyst was active for the formation of primarily HCOOH with a trace amount of CH_3OH at the higher potential. 22% FE was found at −1.80 V vs. Ag/AgCl, for HCOOH production with a small amount of CH_3OH (3.5% of FE) at −2.00 V vs. Ag/AgCl. NiO as an electrocatalyst produced only H_2 and was inactive in reducing

CO_2 products also in that same system. The PbO electrocatalysts were able to produce HCOOH from CO_2 and a maximum of 23% FE was achieved (Chapter 4). The production of HCOOH requires only $2e^-$ from CO_2. The first step is to absorb the gaseous CO_2 molecule onto the catalysts (metal and metal oxides) surface. The second step is activating the CO_2 molecule followed by proton and electron insertion processes (thus produces various reaction products). The last step is the desorption of the CO_2 molecule (Scheme 4.4 in Chapter 4) from the catalyst surface. The inefficient desorption of the CO_2 molecule from the metal oxide surface adversely affects the reduction reaction. Also, there is a competition between H_2 and CO_2 molecules (to adsorb on the surface) at the catalyst surface. Thus, a continuous hydrogen evolution reaction also decreases the CO_2 reduction reaction. To overcome the above demerit, salen metal complexes (Cu, Ni and Pb complexes) were explored as potential electrocatalysts which were expected to enhance the CO_2 reduction reaction. It was observed that the FE of products was increased using all of the metal complexes in this study.

In Table 7.3, a comparison of products formation and corresponding FE is provided. Using $Cu^{II}L^{NH_2}$ complex (**1**), a maximum amount of 36% FE was achieved at −1.80 V vs. Ag/AgCl after 60 mins of reaction (Chapter 5). The production of HCOOH was 4.5%, and the acetic acid formation FE was 11.14%. $Ni^{II}L^{NH_2}$ complex (**2**) effectively reduced CO_2 to C_1 (HCOOH, CH_3OH) and C_2 (C_2H_5OH). The overall current efficiency of 49% was recorded to form alcohols at −1.80 V vs. Ag/AgCl in aqueous media (Chapter 6). The presence of electron-donating anchoring group $-NH_2$, helps in increasing the electron density and thus the basicity of the imine N atoms. Thus, the concentration of acidic CO_2 increases at the vicinity of the electrode surface. The Pb complexes were also reported for various C_1 and C_2 products, which could be due to the attached anchoring group. The catalytic activity of the metal complexes was enhanced by the terminal $-NH_2$ and $-NO_2$

anchoring groups in the ligand backbone. Thus, the used salen metal complexes showed a better product profile than the metal oxides and increased the product FE in this study. The H_2 production also decreased using the metal complexes due to the improved adsorption of CO_2 on the catalyst surface, directing the electron transfer kinetics towards CO_2 reduction reactions. The enhanced performance of the metal complexes is due to the initial reduction of the central metal atom and subsequent reduction reaction of CO_2 (Scheme 5.12 in Chapter 5). Thus, the metal complexes were performed better than the corresponding metal oxides in terms of FE and SE of product formation."

Table 7.3: Product profile of different ERC catalysts used in this study.

Catalysts	FE (%)				
	Methanol	**Ethanol**	**Acetic acid**	**Formic acid**	**Acetaldehyde**
Cu_2O powder	3.5	--	--	22	--
$Cu^{II}L^{NH_2}$ Complex	5.5	7.70	11.14	4.5	7.10
NiO Powder	--	--	--	--	--
$Ni^{II}L^{NH_2}$ complex	11.4	28.6	--	4	4.7
PbO powder	--	--	--	23	--
$Pb^{II}L^{NH_2}$ complex	14.15	--	36.3	6.4	12
$Pb^{II}L^{NO_2}$ complex	10.4	57	--	4.13	5.3

References

Abbasi, S., Allahyari, M., Co, A., and Nematollahi, D., 2009. "New Determination of Lead in Edible Oil and Water Samples by High Selective New Determination of Lead in Edible Oil and Water Samples by High Selective Adsorptive Stripping Voltammetry with Spadns." *International Journal of electrochemical science*, *4*, 602-613.

Bushuyev, O. S., De Luna, P., Dinh, C. T., Tao, L., Saur, G., van de Lagemaat, J., Kelley, S. O., and Sargent, E. H., 2018. "What Should We Make with CO_2 and How Can We Make It?." *Joule*, *2*, 825-832.

Fan, L., Xia, C., Yang, F., Wang, J., Wang, H., and Lu, Y., 2020. "Strategies in Catalysts and Electrolyzer Design for Electrochemical CO_2 Reduction Toward C_{2+} Products." *Science Advances*, *6*, 1-18.

Gong, M., Cao, Z., Liu, W., Nichols, E. M., Smith, P. T., Derrick, J. S., Liu, Y-S., Wen, X., and Chang, C. J., 2017. "Supramolecular Porphyrin Cages Assembled at Molecular-Materials Interfaces for Electrocatalytic CO Reduction." *ACS Central Science*, *3*, 1032-1040.

Hasani, A., Teklagne, M. A., Do, H. H., Hong, S. H., Van Le, Q., Ahn, S. H., & Kim, S. Y., 2020. "Graphene-based Catalysts for Electrochemical Carbon Dioxide Reduction." *Carbon Energy*, *2*, 158-175.

Hori, Y., 2008. "Electrochemical CO_2 reduction on metal electrodes", In Vayenas et al. (ed.) 'Modern Aspects of Electrochemistry', No. 42, Ch. 3, Springer, New York, pp. 89-189.

Karapinar, D., Huan, N. T., Ranjbar Sahraie, N., Li, J., Wakerley, D., Touati, N., Zanna, S., Taverna, D., Tizei, L. H. G., Zitolo, A., Jaouen, F., Mougel, V., and Fontecave, M., 2019. "Electroreduction of CO_2 on Single-Site Copper-Nitrogen-Doped Carbon Material: Selective Formation of Ethanol and Reversible Restructuration of the Metal

Sites." *Angewandte Chemie-International Edition*, *58*, 15098-15103.

Lee, C. H., and Kanan, M. W., 2015. "Controlling H^+ vs. CO_2 Reduction Selectivity on Pb Electrodes." *ACS Catalysis*, *5*, 465-469.

Lei, Liu., Ke, Zhang., and Yumin, W., 2019. "A Simple Strategy for the Detection of Cu(II), Cd(II) and Pb(II) in Water by a Voltammetric Sensor on a TC4A Modified Electrode." *New Journal of Chemistry*, *43*, 1544-1550.

Ma, S., Sadakiyo, M., Luo, R., Heima, M., Yamauchi, M., and Kenis, P. J. A., 2016. "One-Ztep Electrosynthesis of Ethylene and Ethanol from CO_2 in an Alkaline Electrolyzer." *Journal of Power Sources*, *301*, 219-228.

Marken, F., Leslie, W. M., Compton, R. G., Moloney, M. G., Sanders, E., Davies, S. G., and Bull, S. D., 1997. "Homogeneous and Heterogeneous Catalytic Redox Processes: Solution and Solid-state Voltammetry of Lead Complexes at Carbon Electrodes." *Journal of Electroanalytical Chemistry*, *424*, 25-34.

Mi, Y., Peng, X., Liu, X., and Luo, J., 2018. "Selective Formation of C_2 Products from Electrochemical CO_2 Reduction over $Cu_{1.8}Se$ Nanowires." *ACS Applied Energy Materials*, *1*, 5119-5123.

Nitopi, S., Bertheussen, E., Scott, S. B., Liu, X., Engstfeld, A. K., Horch, S., Seger, B., Stephens, I. E. L., Chan, K., Hahn, C., Nørskov, J. K., Jaramillo, T. F., and Chorkendorff, I., 2019. "Progress and Perspectives of Electrochemical CO_2 Reduction on Copper in Aqueous Electrolyte." *Chemical Reviews*, *119*, 7610-7672.

Ren, D., Deng, Y., Handoko, A. D., Chen, C. S., Malkhandi, S., and Yeo, B. S., 2015. "Selective Electrochemical Reduction of Carbon Dioxide to Ethylene and Ethanol on Copper(I) oxide Catalysts." *ACS Catalysis*, *5*, 2814-2821.

Ren, D., Fong, J., and Yeo, B. S., 2018. "The Effects of Currents and Potentials on the Selectivities of Copper toward Carbon Dioxide Electroreduction." *Nature*

Communications, *9*, 1-8.

Shi, Y., Ji, Y., Long, J., Liang, Y., Liu, Y., Yu, Y., Xiao, J., and Zhang, B., 2020. "Unveiling Hydrocerussite as an Electrochemically Stable Active Phase for Efficient Carbon Dioxide Electroreduction to Formate." *Nature Communications*, *11*, 1-10.

Singh, S., Phukan, B., and Verma, A., 2015. "Salen Ligand Complexes as Electrocatalysts for Direct Electrochemical Reduction of Gaseous Carbon Dioxide to Value Added Products." *RSC Advances*, *5*, 3581-3589.

Song, Y., Chen, W., Zhao, C., Li, S., Wei, W., and Sun, Y., 2017. "Metal-Free Nitrogen-Doped Mesoporous Carbon for Electroreduction of CO_2 to Ethanol." *Angewande Chemie*, *56*, 10840-10844.

Sun, Z., Ma, T., Tao, H., Fan, Q., and Han, B., 2017. "Fundamentals and Challenges of Electrochemical CO_2 Reduction Using Two-Dimensional Materials." *Chem*, *3*, 560-587.

Uchida, T., Sasaki, Y., Ikeshoji, T., and Osawa, M., 2017. "4, 4′-Bipyridine as a molecular catalyst for electrochemical hydrogen production." *Electrochimica Acta*, *248*, 585-592.

Wei, X., Yin, Z., Lyu, K., Li, Z., Gong, J., Wang, G., Xiao, L., Lu, J., and Zhuang, L., 2020. "Highly Selective Reduction of CO_2 to C_{2+} Hydrocarbons at Copper/Polyaniline Interfaces." *ACS Catalysis*, *10*, 4103-4111.

Zheng, Y., Vasileff, A., Zhou, X., Jiao, Y., Jaroniec, M., and Qiao, S. Z., 2019. "Understanding the Roadmap for Electrochemical Reduction of CO_2 to Multi-Carbon Oxygenates and Hydrocarbons on Copper-Based Catalysts." *Journal of the American Chemical Society*, *141*, 7646–7659.

CHAPTER 8

Thesis conclusions and future work directions

8.1 Overall conclusions

In this study, a variety of metal oxide and metal complex electrocatalysts were synthesized and they were introduced in ERC. At first, an electrochemical reactor was prepared of 150 mL volume of each electrolyte chamber. A proton exchange membrane (Nafion-117) was sandwiched between the two electrolyte chambers. The synthesized electrocatalysts were coated on the graphite plate and used as the WE. In the beginning, the metal oxide electrocatalysts were synthesized. The Cu_2O and NiO were synthesized through a chemical route in which ascorbic acid was used as the reducing agent. Then PbO was synthesized using urea as a reducing agent. Then the nanoparticles were used as the electrocatalysts in ERC in 0.5 M $KHCO_3$ saturated with gaseous CO_2 at pH 7.0. CV and LSV analysis was conducted where no reduction peak was observed. Using Cu_2O and PbO as electrocatalysts a higher current density was observed in the CO_2 saturated medium than the inert atmosphere. Whereas using NiO nanocatalyst there was no change was detected in the current density in the CO_2 environment also. These preliminary studies confirm that the Cu_2O and PbO are active whereas NiO was inactive in reducing CO_2. In the constant-potential analysis also NiO was failed to produce any product other than H_2. Cu_2O and PbO mostly produce HCOOH at various electrode potentials. At higher potential (−2.00 V vs. Ag/AgCl), a very little amount of CH_3OH (FE 3.5%) was detected as the reduction product using Cu_2O electrocatalyst. Other than that, the oxides were unsuccessful to produce any other hydrocarbons and alcohols. Moreover, the FE of ERC products was ≤25% and the hydrogen evolution was very high using all the metal oxides. During ERC in metal oxide surfaces, the first step is the adsorption of CO_2 and the last step is the desorption of products. The metal and metal oxide surface can be easily get contaminated by the adsorbed CO_2. Another possible reason for the decreased performance of the metal oxides in this study was the continuous H_2 evolution (HER) with progress in time.

With this context, the metal complexes were synthesized from salen ligand **1** and **2**, through a metalation reaction in the presence of Et_3N (complexes **1**, **2**, **3**, and **4**). The Cu complex (**1**) was selective towards acids formation (HCOOH and CH_3COOH). An improvement of FE (36%) was found after 1 h of ERC reaction in the same experimental condition as the Cu_2O. The total TON and TOF of the catalyst were calculated to be 9230 and 2.6 s^{-1}, respectively using complex **1**. Whereas, the total TON was calculated to be 2707 at the same experimental conditions using Cu_2O. The Ni complex (**2**) showed a very better performance than its oxides. Complex **2** can successfully reduce CO_2 to C_2H_5OH through 12 electrons transfer reaction per molecule of CO_2 with a selectivity of 49%. The peak potential of ERC catalyzed by $Ni^{II}L^{NH_2}$ complex was identified at Ecat = −1.80 V vs. Ag/AgCl from LSV. The abundance of the product formation was found in the order as C_2H_5OH>HCOOH>CH_3OH in terms of FE after 60 mins of ERC using Ni complex (**2**). The catalyst catalyzed ERC with FE of 70% at 20 mins of reaction but FE decreases with the progress of reaction due to the rise in HER. According to the researchers, the active state of CO_2 reduction is the M^{+1} state. Thus the onset potential of the CO_2 reduction solely dependent on the conversion between the M^{+2} to the M^{+1} state. During the electrolysis, M(II) centre at first transformed to M(I) intermediate and then again into the +II state. Intermediate Ni(I) is less stable than the Cu(I) and thus transfers an electron to the weakly interacting CO_2 molecule and develops stable Ni(II)-$CO_2^{\bullet-}$ complex upon binding, which induces multi-electron reduction of CO_2. This can be the possible reason for the Ni complex (**2**) can act better than the synthesized Cu complex (**1**). The redox behaviour of the metal complexes can reduce the problem of the surface poisoning of the electrode and thus shows better FE than the metal oxides also.

Two post-transition metal complexes were synthesized and their role in CO_2 reduction was determined in these experiments. Complex **3** [$Pb^{II}L^{NO_2}$] was selective

towards the formation of ethanol whereas complex **4** [$Pb^{II}L^{NH_2}$] preferentially produces acetic acid the most in the same experimental conditions. Complex **3** and **4** have performed nicely after 1 h of CO_2 electroreduction process. The anchoring NH_2 and NO_2 played an important role in terms of inducing the multi-electron reduction process. These confirm that the catalysts (complex **3** and **4**) can easily break the centrosymmetric CO_2 molecule and is eligible for the formation of C_2 products also. Using complex **3** as electrocatalyst ethanol production was highest at −1.80 V vs. Ag/AgCl with FE of 57% and 66% of selectivity. Using complex **3** as electrocatalyst a total of 76.7% FE was achieved for the production of CH_3OH, C_2H_5OH, CH_3CHO and HCOOH. Complex **4** achieved 53% selectivity and 36% FE for the acetic acid production at −1.80 V vs. Ag/AgCl. During the process of these constant-potential electrolysis and HCOOH, CH_3COOH, CH_3OH, and CH_3CHO were detected as the main products using complex **4** as electrocatalyst (total 68% FE). Whereas, the NH_2 and NO_2 free [Pb^{II}(L)] complex, favoured reduction of CO_2 to HCOOH and CH_3OH mainly (FE = 27%, SE = 59%). PbO was only able to produce HCOOH (FE 23%) at the same experimental conditions. The results also confirm that the presence of the anchoring groups in the complexes initiates the multielectron reduction and thus enhances the reactivity. It was envisaged that ligand-appended functional groups would involve in H-bonding interactions with the generated key intermediates *CO and/or *CHO and/or CH_2 species during the ERC. Thus, the intermediate species would be close to facilitate intra-species C-C coupling and thus helped in the C_2 product formation during the ERC reactions. Thus, the newly synthesized metal complexes (M = Cu, Ni, and Pb) were successful in reducing CO_2 with increased FE and also able to construct the C-C coupling towards the generation of C_{1^+} products. Not only that, but the competitive hydrogen evolution was also reduced, and thus the aim of the thesis was fulfilled. Still there are several limitations of this work which were not possible to be conducted

experimentally. As the complexes are newly synthesized, the exact electrokinetics and mechanism of its action are still unknown and thus some recommendation of the future work is describing in section 8.2.

8.2 Recommendations for future work

- These complexes were newly synthesized and were introduced in ERC for the first time and have shown a very excellent performance in this thesis. These complexes produce C_2 products by scissoring the C-O bond with greater efficiency than the corresponding metal oxides. Mostly a lab-scale batch analysis was conducted and it is important to perform pilot-scale continuous studies that can further clarify the stability of the catalysts
- This thesis focuses on the production of acids and alcohols. Further, the production of hydrocarbons for the synthesized catalysts can be tested in the future. The pilot-scale studies in ERC using the synthesized electrocatalysts also can be done in the future
- More studies and optimization of experimental parameters need to be oriented towards a single production formation (C_2) to make the system industrially viable
- Further modifications can be done to reduce hydrogen production and increase the formation of ERC products. Tuning various factors such as modification in the reactor, introduction of direct gaseous CO_2 in the reactor (DERC), changing the electrolyte solution and anode material, etc. also can help to address these objectives in near future

- A continuous and long term study can be done for the catalysts. The study on the deactivation of the catalyst needs to be done in the future so that the reusability of them can be explored

- The detailed electro-kinetics study and the mechanism of action for the metal-salen complexes can be further explored. $^{13}CO_2$ can be introduced to the system to identify the exact mechanism of ERC reactions. The mass transfer limitations of the gaseous CO_2 into the surface of the catalyst need to be studied in the future

- Ligand-based functional groups would involve in H-bonding and quadrupole-interactions with CO_2 molecules and intermediates formed during the ERC. However, the ligand is quite away from the active site. DFT calculations could be performed to unravel reaction insights during ERC

This page is intentionally left blank

Research Outcomes

PUBLICATIONS

Journal publications

1. P. Bose, C. Mukherjee and A.K. Golder, A Ni^{II} complex of the tetradentate salen ligand $H_2L^{NH_2}$ comprising an anchoring $-NH_2$ group: synthesis, characterization and electrocatalytic CO_2 reduction to alcohols, ***Inorg. Chem. Front***. 2019 (6), 1721-1728 (RSC).

2. P. Bose, C. Mukherjee, and A. K. Golder, Reduction of CO_2 to Value-Added Products on a Cu(II)-Salen Complex Coated Graphite Electrocatalyst, ***Chem. Select***. 2020 (5), 9281-*9287 (Wiley).*

3. P. Bose, C. Mukherjee, and A. K. Golder, Electrochemical Conversion of CO_2 to C_2 Oxygenates with High Faradaic Efficiency and Product Selectivity on Pb(II)-Salen Catalysts-Coated Graphite Electrodes: Role of Ligand-Bound Functional Groups (Manuscript communicated).

International conferences

1. P. Bose, A.K. Golder and C. Mukherjee, Electrochemical reduction of CO_2 on Cu and Cu_2O catalysts towards fuels generation, 12^{th} International Symposium on Advances in Electrochemical Science and Technology, Jan 8-10, 2019, SAEST and CSIR-CECRI, Chennai, India.

2. P. Bose, C. Mukherjee, and A. K. Golder, Ni salen metal complex and NiO catalyst for Electrocatalytic CO_2 Reduction to fuels, CHEMCON-2019, December 16-19, IIT Delhi, Delhi, India.

National conferences/ symposiums

1. P. Bose, A.K. Golder and C. Mukherjee, Electrochemical reduction of carbon dioxide: Effect of metal complexes, Reflux 2017, March 24-26, Indian Institute of Technology Guwahati, Guwahati, India.

2. P. Bose, C. Mukherjee, and A. K. Golder, Metal salen complex catalyzed electrochemical reduction of CO_2 to value-added products, Research Conclave, 2019, March 14-17, Indian Institute of Technology Guwahati, Guwahati, India.

3. P. Bose, C. Mukherjee, and A. K. Golder, "Electrocatalytic reduction of CO_2 to Value–Added Products using oxide of metals (M= Pb and Ni)". Bio-inspired Nano materials for Environmental Applications 2020, February 12-13, IIT-Guwahati, Guwahati, India.

Awards

1. 1st Prize for presenting the paper entitled, "Metal salen complex catalyzed electrochemical reduction of CO_2 to value-added products" organized by Research Conclave, 2019, March 14-17, Indian Institute of Technology Guwahati, Guwahati, India.

Curriculum vitae

Dr. PAULOMI BOSE
PhD (Environment, IIT Guwahati)
M.Tech (Environment, University of Kalyani)
B.Tech (Biotechnology, Haldia Institute of Technology)
Phone : 9831317363, 7503702440
E-mail: bose.paulomi0621@gmail.com, paulomi@iitg.ac.in
Google Schloar Link :
https://scholar.google.com/citations?user=gpYMbZQAAAAJ&hl=en

ACADEMICS.....

YEAR	NAME OF THE UNIVERSITY/ COLLEGE /SCHOOL	QUALIFICATION	MARKS/ SGPA OBTAINED
April 2021	IIT Guwahati	**Ph.D.** (Electrocatalysing CO_2 conversion to value-added products using metal oxides and metal-salen complexes)	Completed
2013	University of kalyani	**M.Tech in Environmental Management** Principle courses taken: • Air, Water, Land & Noise Pollution Control • Environmental Biotechnology • Environmental Impact Assessment and Solid Waste Management	8.00
2011	Haldia Institute of Technology, Haldia (WBUT)	**B.Tech in Biotechnology** Principle courses taken: • Environmental Biotechnology • Biochemistry, Immunology • Principles of Molecular Genetics • Ethics and IPR in Biotechnology • Human Genomics • Plant and Animal Biotechnology	7.41

YEAR	NAME OF THE SCHOOL	EXAMINATION	MARKS/ SGPA OBTAINED
2007	Tarasundari balika vidyabhaban (WBBHSE)	12^{th} Subjects taken: • English • Science • Mathematics	79.5 %
2005	Tarasundari balika vidyabhaban (WBBSE)	10^{th} Subjects taken: • English • Science • Mathematics	77.5 %

PUBLICATIONS……

Journal publications:

1. **P. Bose**, C. Mukherjee and A.K. Golder, A Ni^{II} complex of the tetradentate salen ligand $H_2L^{NH_2}$ comprising an anchoring -NH_2 group: synthesis, characterization and electrocatalytic CO_2 reduction to alcohols, ***Inorg. Chem. Front***. 2019 (6), 1721-1728 (RSC).
2. **P. Bose**, C. Mukherjee, and A. K. Golder, Reduction of CO_2 to Value–Added Products on a Cu(II)–Salen Complex Coated Graphite Electrocatalyst, ***Chem. Select***. 2020 (5), 9281-9287 (Wiley).
3. Shreya Medda, Amita Hajra, Uttiya Dey, **Paulomi Bose** and Naba Kumar Mondal Biosynthesis of silver nanoparticles from Aloe vera leaf extract and antifungal activity against Rhizopus sp. and Aspergillus sp. Applied Nanoscience, 2015 (5), 875-880.

International conferences:

1. P. Bose, A.K. Golder and C. Mukherjee, Electrochemical reduction of CO_2 on Cu and Cu_2O catalysts towards fuels generation, 12^{th} International Symposium on Advances in Electrochemical Science and Technology, Jan 8-10, 2019, SAEST and CSIR-CECRI, Chennai, India.
2. P. Bose, C. Mukherjee, and A. K. Golder, Ni salen metal complex and NiO catalyst for Electrocatalytic CO_2 Reduction to fuels, CHEMCON-2019, December 16-19, IIT Delhi, Delhi, India.

National conferences/ symposiums:

1. P. Bose, A.K. Golder and C. Mukherjee, Electrochemical reduction of carbon dioxide: Effect of metal complexes, Reflux 2017, March 24-26, Indian Institute of Technology Guwahati, Guwahati, India.
2. P. Bose, C. Mukherjee, and A. K. Golder, Metal salen complex catalyzed electrochemical reduction of CO_2 to value-added products, Research Conclave, 2019, March 14-17, Indian Institute of Technology Guwahati, Guwahati, India.

3. P. Bose, C. Mukherjee, and A. K. Golder, "Electrocatalytic reduction of CO_2 to Value–Added Products using oxide of metals (M= Pb and Ni)". Bio-inspired Nano materials for Environmental Applications 2020, February 12-13, IIT-Guwahati, Guwahati, India.

WORK EXPERIENCE……

Worked as lecturer in Afflatus Institute of Engineering and Technology (Kalyani). January 2014 to December 2014, was engaged in Teaching.

Ph.D. Research Thesis: Electrocatalysing CO_2 conversion to value-added products using metal oxides and metal-salen complexes.

M.Tech Research Thesis: A study on nutrient recycling and phytoremediation of nutrients by Chlorella from Municipal Waste Water.

B.Tech Research Thesis: Partial Purification of a LAB Originated Lantibiotic and Demonstration of its antimicrobial activity.

TRAINING & WORKSHOPS……

- Underwent a Vocational Training for one month during 4th semester at **Bose institute, Maniktola**
- Attended two days' international workshop on Low Carbon Development: Carbon Capture and Carbon Sequestration Technology Route at **MCKV Institute of Engineering (Feb 2014)**
- Successfully completed a short-term continuing education course on Vermicompost Production at **the University of Kalyani (2011)**

RESEARCH INTERESTS ……

- Electrochemical and photochemical CO_2 reduction and CO_2 sequestration
- Biofuel production
- Biological wastewater treatment
- Nanoparticle synthesis
- Domestic & industrial wastewater treatment
- Environmental biotechnology

INSTRUMENT & ANALYTICAL TECHNIQUE EXPERTISE……

- UV-Visible Spectrophotometer
- Gas Chromatography
- HPLC
- Potentiostat
- Water quality analysis
- Electrochemical techniques (CV, LSV, Chronoamperometry)

PROJECTS.....

Ph.D.: Electrocatalysing CO_2 conversion to value-added products using metal oxides and metal-salen complexes:

Carbon dioxide (CO_2) is essential for the survival of living organisms. It exists as a tiny fraction of the total carbon inventory in the atmosphere and the continuous industrial development primarily has increased the level of CO_2 in the atmospheric gases. The rise in CO_2 causes an increase in global temperature by 1-2°C. With this context, the Ph.D. thesis focuses to look for a suitable technology to convert CO_2 into valuable products. Electrochemical reduction of CO_2 (ERC) is an alternative to the other methods of carbon dioxide reuse which converts CO_2 to useful chemicals within a very short time. Electrochemical reduction of CO_2 is carried out either in aqueous or non-aqueous electrolyte solutions saturated with CO_2 or directly as a gas at different metal or metal derivative catalysts. Metals and their derivatives can gain or lose electrons easily and thus, act as electrocatalysts during the conversion process. Thus, various metal oxides and metal complexes were used as catalysts to reduce CO_2 to other alcohols, acids, hydrocarbons, etc.

M.Tech: A study on nutrient recycling and phytoremediation of nutrients by Chlorella sp. From municipal wastewater:

Wastewater is the spent or used water containing dissolved and suspended solids such as pollutants and microbes, including nutrients. The wastewater discharged into the water bodies is hazardous to the environment and causes various health problems in human beings. Eutrophication is one of such major environmental problems caused due to the discharge of nutrient-rich wastewater into the nearby water bodies. There are various methods for the removal of those pollutants but their high cost and huge sludge production are the main drawbacks of those methods. Thus, this thesis aimed to find a suitable low-cost method which not only reduces the pollutants but also can reuse the sludge after treatment. Thus, microalgae were chosen to remove those pollutants. They have great potential for the removal of nitrogen and phosphorus from wastewater. They also can capture carbon dioxide thereby reducing the CO_2 as well as converts algal biomass into energy. The used microalgae (*Chlorella Vulgaris*) reduced the amount of phosphate, nitrate, etc. present in the municipal wastewater and also efficiently reduced the other parameters.

B.Tech: Partial Purification of a LAB Originated Lantibiotic and Demonstration of its antimicrobial activity:

Lactic Acid Bacteria (LAB) have been reported to be widely used as probiotics. Several mechanisms have been put forth on the mechanism of probiotics and how the bacterial population causes health benefits. One of the most recently reported mechanisms of such beneficial action is said to be by the secretion of Lantibiotics. Lantibiotics are small molecular peptides with similar action to that of the bacteriocins (Colicins). We focused on one of such Probiotic LAB cultures isolated from the local niche. The LAB has shown beneficial effects in aquaculture systems. Several potent enteric and non-enteric pathogens were subjected to the presence of the Lantibiotic. Potent pathogens like *Proteus Vulgaris*, *Vibrio Paraheamilyticus* and *Pseudomonad* Species had shown to be inhibited by the lantibiotic.

PERSONAL INFORMATION……

Name	PAULOMI BOSE
Date of birth	21st April,1989
Father's Name	Mr. TAPAN KUMAR BOSE
Sex	Female
Languages known	English, Hindi, Bengali.
Nationality	Indian
Present Address	Nabanagar, Po: Duilya, Po: Sankrail, Dist: Howrah, Pin: 711302

VOLUNTEERSHIPS ……

Volunteered at IIT Guwahati from January 2015
Registrations
Convocations
Conferences & Workshops

PERSONAL TRAITS……

Good Communication Skills, Competitive and Participating, Ability to change and self-analysis, Team working spirit.

I declare that all the information furnished above is correct.

Date: 30th June 2021

Place: IIT Guwahati

Paulomi Bose